Calculating and Assessing Mobile Mapping System Point Density for Roadside Infrastructure Surveys

by

Conor Cahalane BSc., MSc.

NUI MAYNOOTH

Ollscoil na hÉireann Má Nuad

A thesis presented in fulfilment of the requirements for the Degree of Doctor of Philosophy

Supervisors: Dr. Tim McCarthy, Dr. Conor P. McElhinney

National Centre for Geocomputation

Faculty of Science

National University of Ireland Maynooth,

Maynooth, Co.Kildare, Ireland

October, 2012

To Eimear, my family and friends.

Declaration

This thesis has not been submitted in whole or in part to this or any other university for any other degree and is, except where otherwise stated, the original work of the author.

Signed: _____

Conor Cahalane BSc., MSc.

Acknowledgments

I would like to thank my supervisors and supervisory team, Tim, Conor and Paul. Their advice made this thesis better in every way and I am grateful for it. Thanks to Martin and Juha Hyyppä for agreeing to examine my thesis and for making the viva enjoyable. I would also like to thank Jan for forwarding my CV to Tim after I first enquired about the PhD and then in helping me to apply. I would like to thank Kieran Feighan from PMS for agreeing to co-fund this thesis and for giving some valuable input at StratAG meetings which formed the motivation for work in later chapters and Will Tompkinson from Optech who provided data for testing.

More thanks for the people at the very start - Maryam, Wenbai, Tommy and Sandra - all since moved on and missed. It would have been great to finish up together. Thanks to Pamela, Pankaj, BinBin and Ishwari who I sat with in Iontas, to Carson who helped me learn latex but who left before I could bug him to show me Python, to Fergal, Cathal and Felix who then had that unenviable role, to Ishtiak, Rory, Byrcin and Helen and to Ronnie who is the only one who helps me with the plants. To everyone else at the NCG and NIRSA and to the one or two other people who might read this thesis someday, thanks to you too.

Thanks to my mam and dad for helping me to get this far. Thanks to Sarah and Tom for providing me with the best distractions possible, my niece and nephew, Emma and Liam. Finally, but most importantly, thanks to Eimear, my bride-to-be. I couldn't have done it without you and I mean that.

Research presented in this thesis was funded by the the Irish Research Council and the Enterprise Partner, Pavement Management Services Ltd. Pavement Management Services are an industry partner in StratAG, which is funded by a Strategic Research Cluster grant (07/SRC/I1168) from Science Foundation Ireland.

Abstract

The current generation of Mobile Mapping Systems (MMSs) capture increasingly larger amounts of data in a short time frame. Due to the relative novelty of this technology there is no concrete understanding of the point density that different scanner configurations and scanner hardware settings will exhibit on objects at specific distances. Depending on the project requirements, obtaining the required point density impacts on survey time, processing time, data storage and is the underlying limit of automated algorithms. Insufficient knowledge of the factors influencing MMS point density means that defining point density in project specifications is a complicated process. The objectives of this thesis are to calculate point density, to assess MMS laser scanner configuration and hardware settings and to benchmark a selection of MMSs in terms of their point density. The calculation methods involve a combination of algorithms applying 3D surface normals and 2D geometric formulae and outputs profile angle, profile spacing, point spacing and point density. Each of these elements are a major factor in calculating point density on arbitrary objects, such as road signs, poles or buildings - all important features in asset management surveys. These algorithms are combined in a system called the Mobile Mapping Point Density Calculator (MIMIC). MIMIC is then applied in a series of tests identifying the recommended MMS laser scanner configuration and scanner hardware settings for near side infrastructure. The influence that the scanner orientation and location on the MMS has on point density is quantified, resulting in a recommended MMS laser scanner configuration. A series of benchmarking tests assess the performance of one commercial and two theoretical MMSs in terms of their point density. The recommended configuration identified in the previous tests al-

lows a low specification MMS to increase its performance in relation to a higher specification MMS. The benchmarking tests also highlight that a high pulse repetition rate is preferable to a high mirror frequency for maximising point density. The findings in this thesis enable a MMS to be configured to maximise point density for specific targets. Researchers can utilise MIMIC to tailor their automated algorithm's point density requirements for specific targets.

Contents

List of Figures

List of Tables

Acronyms

ASW	Angular Step Width
CAD	Computer Aided Design
DMI	Distance Measurement Instrument
DOD	Department of Defence
DOT	Department of Transport
FOV	Field of View
GLONASS	Globalnaya Navigatsionnaya Sputnikovaya Sistema
GNSS	Global Navigation Satellite System
GPS	Global Positioning System
INS	Inertial Navigation System
LiDAR	Light Detection and Ranging
MIMIC	Mobile Mapping Point Density Calculator
MMS	Mobile Mapping System
NCG	National Centre for Geocomputation
NRA	National Roads Authority
OSi	Ordnance Survey Ireland
PRR	Pulse Repetition Rate
StratAG	Strategic Research into Advanced Geotechnologies
TLS	Terrestrial Laser Scanner
TOF	Time of Flight
VISAT	Video Inertial Satellite
XP1	Experimental Platform 1

Chapter 1

Introduction

A mobile mapping system (MMS) combines navigation sensors and spatial measurement sensors on a moving platform and this sensor combination enables rapid, high density spatial data collection. In this chapter the reader is introduced to the fields of laser scanning, MMSs and MMS performance assessment. The aim of this chapter is to provide a general overview of these fields. This chapter identifies the contributions to knowledge which are made in the field of MMS performance assesment in this thesis. An introduction to the operational and technical details of a MMS is required to allow the reader to appreciate the importance of MMSs as a survey technology. The three core contributions of this thesis are then detailed. Firstly, a method of calculating point density for MMSs operating a laser scanner(s) is designed. Secondly, this method is used to assess MMS configurations. In the third contribution, a benchmarking process is applied to a selection of MMSs. By completing these three objectives it is now possible to calculate what performance to expect from a MMS, to assess MMS configurations and to compare the quality of a MMS in relation to alternative models. The list of publica-

tions arising from work carried out in this thesis is also presented. The MMSs that are used for validation of the methodology in this thesis are introduced. This chapter closes by explaining the assumptions made in this research and outlining the thesis structure.

1.1 Mobile Mapping Systems

MMSs equipped with laser scanners enable high density spatial data collection along road networks, in a rapid and efficient manner. Although early MMSs were predominantly image based [Goad, 1991, Schwarz et al., 1993], this thesis will deal with MMSs operating laser scanners only. Laser scanners are an optical remote sensing technology capable of measuring the distance to a target. Laser scanners operate on the principle of Light Detection and Ranging, or LiDAR. Although Airborne Topographic LiDAR is a well established survey technology [Lillesand et al., 2008, Tuck et al., 2012, Vosselman and Maas, 2010], this thesis will deal with terrestrial MMSs only. On a terrestrial MMS, navigation sensors are combined with spatial measurement sensors to facilitate rapid, efficient and accurate spatial data collection.

In their recent study on 'LiDAR for data efficiency', the Washington State Department of Transport (WSDOT) [Yen and T.A., 2011] identified that MMSs decrease staff exposure to traffic and other hazards and decrease personnel, equipment and travel costs. MMSs also enable unnecessary traffic delays for the travelling public to be avoided. This study shows that over a total of six years, the WSDOT could save up to $6,140,100 by purchasing a MMS, a saving of over $1,000,000 per annum. MMSs can acquire data at typical driving speeds under normal traffic conditions and thereby

avoiding expensive overhead costs arising from road closures. This MMS capability is important for Departments of Transport and National Road Authorities. For example, the Irish National Roads Authority (NRA) have included a requirement for MMS surveys in their topographic survey specifications [O Cathain, 2011] because, MMSs "minimise disruption and expense associated with Traffic Management". Work on MMS topographic survey specifications is ongoing [California Department of Transport, 2012, Florida Department of Transport, 2012].

Terrestrial MMSs complement aerial topographic surveys in a number of ways. For example, large scale information such as road signs or detailed infrastructure condition can be recorded [Huang et al., 2008, Shi et al., 2008, Toth and Grejner-brzezinska, 2004]. Extensive ground control is not essential, however limited ground control improves the accuracy of the surveyed points in planimetry and elevation [Graefe, 2007b, Miller and Mills, 2008]. Additionally, MMSs can survey features that are occluded from aerial platforms, i.e. roads that pass through tunnels or under bridges [Hunter et al., 2006, Kremer and Hunter, 2007].

1.2 MMS Data Processing and Applications

A MMS requires a high accuracy navigation solution to accurately georeference individual laser returns. State of the art MMSs incorporate a Global Navigation Satellite System (GNSS) receiver, an Inertial Navigation System (INS) and a Distance Measurement Instrument (DMI) and when combined enable accurate positioning. Post processing the outputs from these positioning and navigation sensors provides accurate latitude, longitude and elevation

together with information on the vehicle orientation such as pitch, roll and yaw. MMSs are a versatile surveying technology, and although originally designed for route corridor surveys, the number of potential applications of MMSs are increasing.

1.2.1 Data Processing

The orientation and positioning sensors on the MMS are used to convert the laser scan data into the correct coordinate system. This involves three key stages. Firstly, the GNSS measurements recorded by the MMS are corrected for any external error sources that may have influenced them. For a MMS survey in Ireland, this is achieved by comparing the GNSS data with local base stations maintained by Ordnance Survey Ireland (OSi). The base stations have been surveyed to a high degree of accuracy (better than 1mm) and any errors in the GNSS signal arising from atmospheric interference or satellite problems are identified and quantified. These corrections are then made freely available from the OSi's website [Ordnance Survey Ireland, 2012] in a Receiver Independent Exchange Format (RINEX) to download. The RINEX files are combined with the GNSS data from the MMS resulting in a more accurate GNSS navigation solution. Best practice guidelines for GNSS surveying in Ireland are detailed in [Prendergast, 2004, Prendergast et al., 2008]. The post-processed GNSS solution is then combined with the INS data and the DMI data for the survey. These data are then combined in an algorithm designed to provide a statistically optimal estimate of the underlying navigation solution [Grewal et al., 2007], commonly referred to as a Kalman Filter. Application of the Kalman Filter results in an optimised navigation solution.

The final navigation solution is combined with the laser scan data to produce a fully georeferenced point cloud in the desired mapping coordinate system. Figure 1.1 illustrates this workflow.

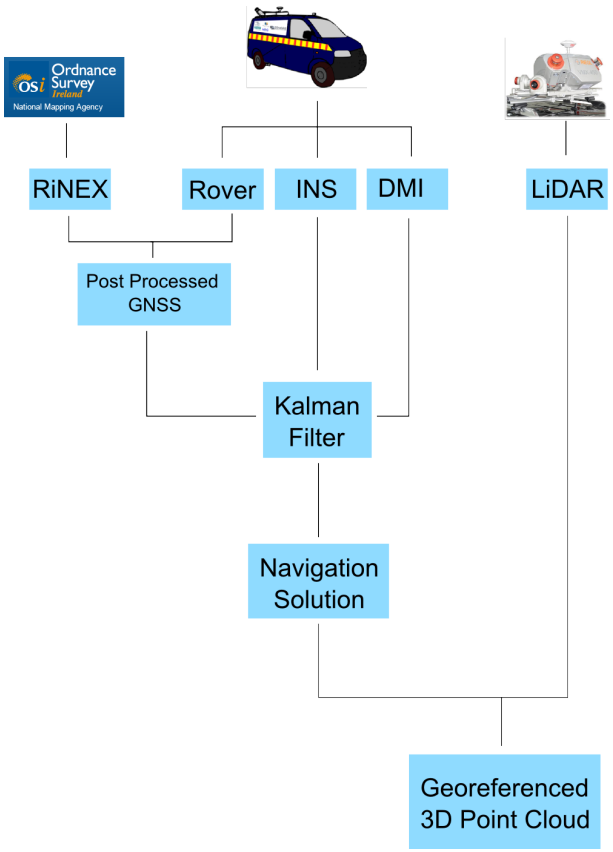

Figure 1.1: MMS Positional and Spatial Data Processing

1.2.2 MMS Applications

MMS are not just designed to record information about the elevation, dimensions and geometry of the road. Numerous other MMS applications exist. MMS surveys can target road markings [Jaakkola et al., 2008, Kim et al., 2006, Kumar et al., 2010, Kumar et al., 2011, Kumar, 2012], or be designed to assess earthen bank slope assessment on route corridors [Miller and Mills,

2008]. Alternatively, the target of the survey can be power lines or telegraph poles [Kim et al., 2006]. MMSs can survey the dimensions of buildings and record high density spatial measurements on the building facades, facilitating creation of 3D city models [Becker and Haala, 2009, Graefe, 2007b]. MMSs can be used for map updating and change detection [Hyyppä et al., 2009]. Coastal Surveys [Kremer and Hunter, 2007] can be carried out rapidly in areas of high tidal change. MMSs can be used in research on forestry [Lin et al., 2012]. MMSs are not limited to land based vehicles, but have been installed on boats, trolleys and backpack mounted [Kukko et al., 2012]. The summarised work is only a limited sample of the potential applications of MMSs, numerous others exist.

1.3 Positioning and Navigation

To understand the complexities of a MMS as a survey technology and to appreciate the importance of further research into MMS performance, MMS calibration and hardware issues must first be investigated. An MMS combines three navigation sensors: a GNSS, an INS and a DMI. These three sensors require calibration. Successful calibration enables high accuracy positional measurements. The first step in the claibration process is the measurement of the position of each of these sensors relative to a fixed point on the MMS. This fixed point is generally the sensor datum point of the INS.

1.3.1 Lever Arm Offsets

An issue that influences the accuracy of the MMS positioning is the quality of the MMS hardware calibration. This issue is not specific to the position-

ing and orientation component but also influences the accuracy of the spatial measurements. The GNSS receiver(s), INS, DMI and Laser Scanner(s) must all be located in the same vehicle coordinate reference system. The distance offset from each sensor datum point to a point of reference in the vehicle coordinate system must be specified. This point of reference is usually the sensor datum point of the INS. These offsets are termed the 'lever arm offsets' and must be measured accurately to minimise errors when surveying. The contribution of lever arm offsets to absolute accuracy has been the subject of previous work by [Betaille et al., 2007, Hong et al., 2006, Seo et al., 2005]. Traditional surveying methods like a tripod mounted laser scanner can be used to survey the entire MMS hardware configuration. This laser scan survey can then be used to identify the location of the centre of measurement of each piece of hardware. Alternatively a CAD model can be used to measure each lever arm offset if it is available. An example of a CAD model used to measure lever arm offsets can be seen in Figure 1.2.

1.3.2 Global Navigation Satellite Systems

The GNSS is the term given to the rapidly expanding collection of satellites available for navigation and surveying purposes [Bevley and Cobb, 2010, Grewal et al., 2007]. The forerunner of the GNSS is the Global Positioning System (GPS), designed by the U.S. Department of Defense (DOD). The Russian Globalnaya Navigatsionnaya Sputnikovaya Sistema (GLONASS) joined the GPS as a functioning satellite constellation in 1995. The Chinese Beidou 2 (COMPASS) system and the European GALILEO system are both currently at the development stage. The GNSS is a space based navigation system that

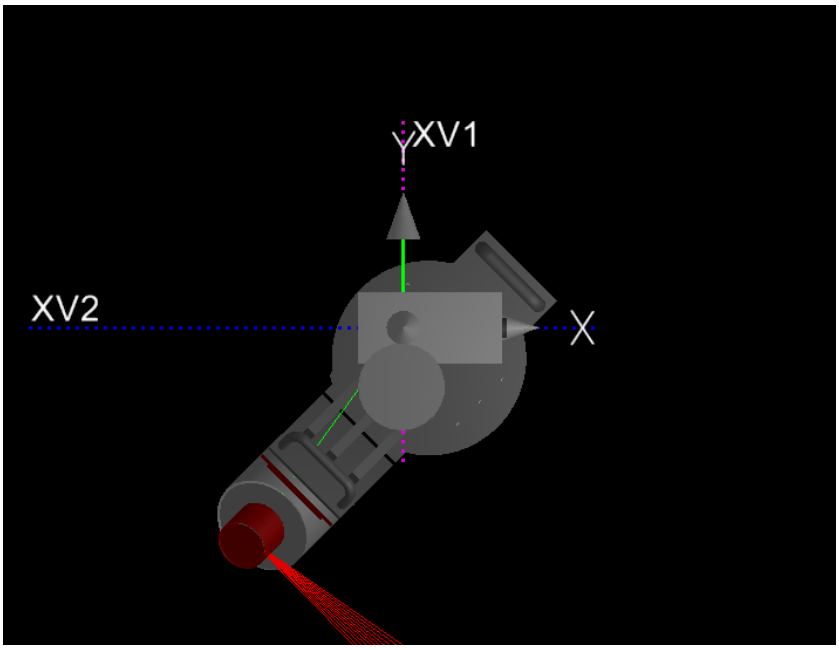

Figure 1.2: 3D CAD Design Drawing Being Used to Measure Lever Arm Offsets. Offsets are Defined in Terms of the Vehicle Axes, XV1 and XV2 and XV3

uses satellites to provide receivers on earth with an accurate positional fix, as illustrated in Figure 1.3. The basic operational procedure is as follows:

- The satellite emits a signal. Each signal is timestamped.
- Using accurate satellite orbital data the receiver on earth can then use this information to determine the length of time that the satellite signal took to reach it.
- Combining the signal travel time information with the satellites orbital position the receiver can therefore calculate its distance from the satellite.
- By cross-checking with more satellites the receiver's global reference

coordinates can be found. These 3D coordinates provide the latitude/longitude and elevation of the receiver.

A minimum of four satellites are required to provide a 3D positional fix. The GNSS provides a MMS with the positional data required to register all spatial measurements to a coordinate reference system.

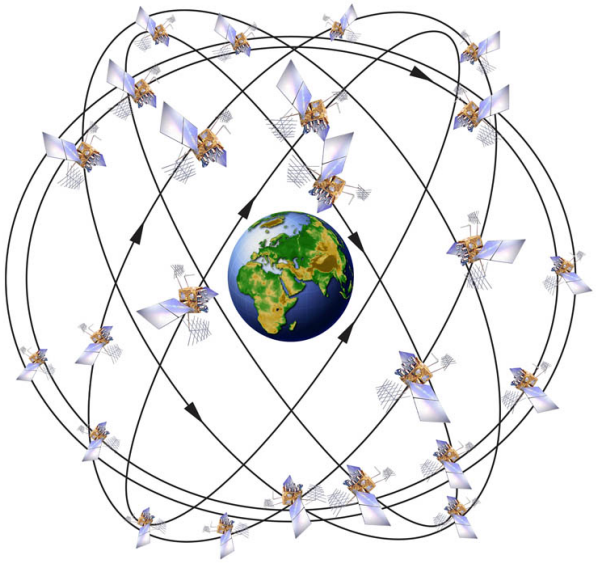

Figure 1.3: A Minimum of Four Satellites are Required for Positioning in Three Dimensions [GPS.gov, 2012]

Although a GNSS receiver provides accurate positional data to the MMS, these receivers are incapable of operating at the required frequency to register every spatial measurement. For instance, a vehicle travelling at 100km/h travels 27m between each positional fix for a GNSS receiver operating at 1Hz. A modern MMS equipped with two laser scanners is capable of recording one million points per second. If relying on a 1Hz positional update, the first and last laser points only would be surveyed from an accurate X,Y,Z coordinate. The point of origin for the remaining 999,998 points would have

to be interpolated and this could introduce errors. Additionally, a single GNSS receiver can not provide information on the orientation of the MMS. [Alamús et al., 2004, Geng et al., 2006, Graefe et al., 2001, Talaya et al., 2000] have attempted to incorporate multiple GNSS receivers to provide information on the orientation of the MMS. However, the most common solution is for a MMS to incorporate an INS. INSs provide position and orientation information at a higher frequency than GNSS receivers. INSs can operate in areas of limited satellite visibility. Figure 1.4 illustrates the principle of an urban canyon. In this example a MMS is surveying an urban area. The structures on either side of the MMS have obstructed the GNSS signal to the receiver. GNSS signal can also be obstructed by foliage or when driving through tunnels.

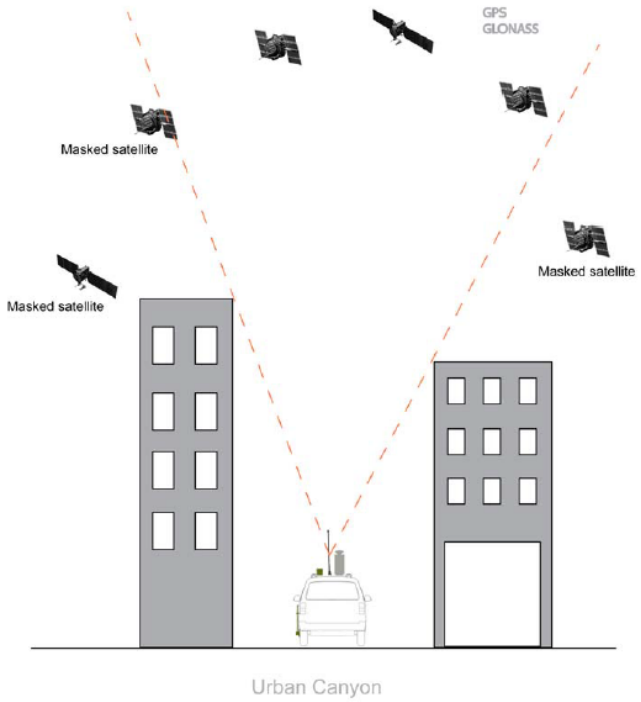

Figure 1.4: Loss of GNSS Lock in Urban Canyons ([IXSEA, 2009])

1.3.3 Inertial Navigation Systems

An INS is a navigation sensor which can calculate the orientation and acceleration of a moving platform. An INS uses an accelerometer to measure the acceleration of the vehicle whereas the orientation of the vehicle is measured using a gyroscope [Bevley and Cobb, 2010, Grewal et al., 2007]. This sensor combination enables an INS to calculate the direction, motion and acceleration of the vehicle in any direction. When supplied with an initial positional fix, an INS can continuously estimate the current position of the vehicle. INSs and GNSS receivers have complementary error characteristics [Chiang and Huang, 2008, Schwarz and El-Sheimy, 2004]. For example, INSs are accurate over the short term but experience errors that accumulate over time, even when the vehicle is stationary. Under the right conditions, a GNSS receiver is consistently accurate and can be used to provide a positional fix to the INS. However, an INS is capable of higher frequency positional updates than a GNSS receiver and is therefore better suited to aid in the positioning of a mobile platform moving at high velocities [Grewal et al., 2007, Titterton and Weston, 2004].

An INS can help compensate for positional error in areas of limited satellite visibility. While the MMS is experiencing zero satellite visibility, the INS will provide positional updates [IXSEA, 2009]. Figure 1.5(a) illustrates a plot of a survey route where the GNSS receiver experienced poor satellite visibility. The gaps in the data represent areas of limited or zero GNSS signal. Figure 1.5(b) displays the completed navigation solution for the survey. In this image, gaps in the GNSS navigation solution have been augmented with INS positional data. However, errors increase over time and the INS

requires GNSS positional updates to control these errors. For example, state of the art INSs such as the IXSEA LandINS experience a decrease in X,Y positional accuracy of 0.6m after 300 seconds [IXSEA, 2009] of zero satellite visibility. The IXSEA LandINS is the GNSS/INS combination installed on the XP1, one of the MMSs used for validation in this thesis.

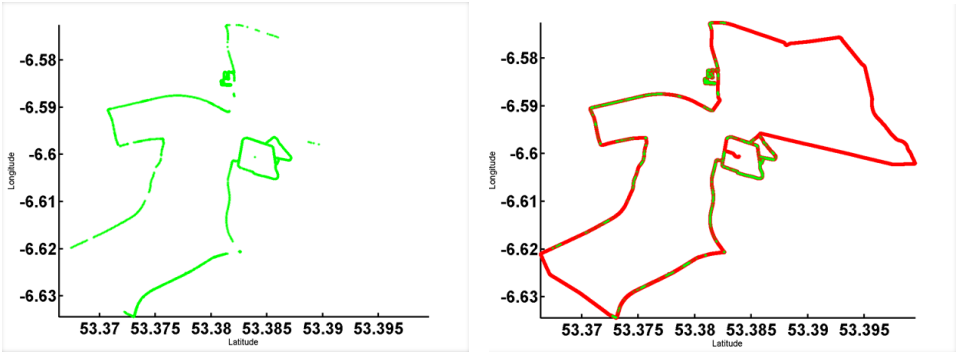

(a) (b)

Figure 1.5: INS compensates for loss of GNSS lock (a) Track with GNSS only (b) completed track with INS and GNSS)

1.3.4 Distance Measurement Instrument

A DMI is a survey grade odometer that is attached to the wheel of a MMS and is illustrated in Figure 1.6. DMIs provide an additional check on the navigation solution of the MMS during processing. Additionally, DMIs are particularly useful for controlling errors in the INS at times of zero velocity. INS accelerometers experience an error known as 'drift'. Due to drift in the INS accelerometer the INS registers vehicle motion although the vehicle is actually stationary. The solution supplied by the DMI is a, 'zero velocity update' or ZUPT. ZUPTs are an important addition to the quality of the navigation solution [Aggarwal et al., 2009, Toth and Grejner-brzezinska,

2004]. The DMI identifies when the vehicle velocity is zero, and then this provides an additional calibration for the INS.

Figure 1.6: DMI Attached to Wheel of Survey Vehicle

1.4 Spatial Measurement

MMSs combine navigation sensors and spatial measurement sensors on a moving platform. A state of the art MMS can incorporate multiple spatial measurement sensors such as laser scanners. Similarly to the position and navigation sensors, a calibration process is required to ensure no orientation errors exist for the laser scanner(s). The calibration process is introduced in this section. Descriptions of the three different laser scanning principles are provided. The distinction between current tripod mounted laser scanners and scanners specifically designed for MMSs is made. Three different elements of laser scanning are introduced. These are the size of the laser footprint, the intensity of the return, and the principle of multiple returns.

1.4.1 Boresight Alignment

After the lever arm offset for the laser scanner is quantified, an additional calibration process known as the boresight alignment is also required. This minimises orientation errors between the laser scanner and the INS. Figure 1.7 illustrates a boresight misalignment on a dual scanner MMS. Although the two scanners have surveyed the same area of road, the individual scanners have recorded a road surface with different orientations. Calibration can be carried out to eliminate boresight errors using dedicated software applications like TerraMatch [TerraSolid, 2012a]. Studies [Glennie, 2007, Glennie and Lichti, 2010, Madeira et al., 2012, Pothoua et al., 2006, Schaer et al., 2007] have investigated the influence of boresight misalignments on laser data captured by aerial survey platforms. The impact of satellite visibility on MMS survey accuracy has also been investigated in the work by [Barber et al., 2008, Haala et al., 2008].

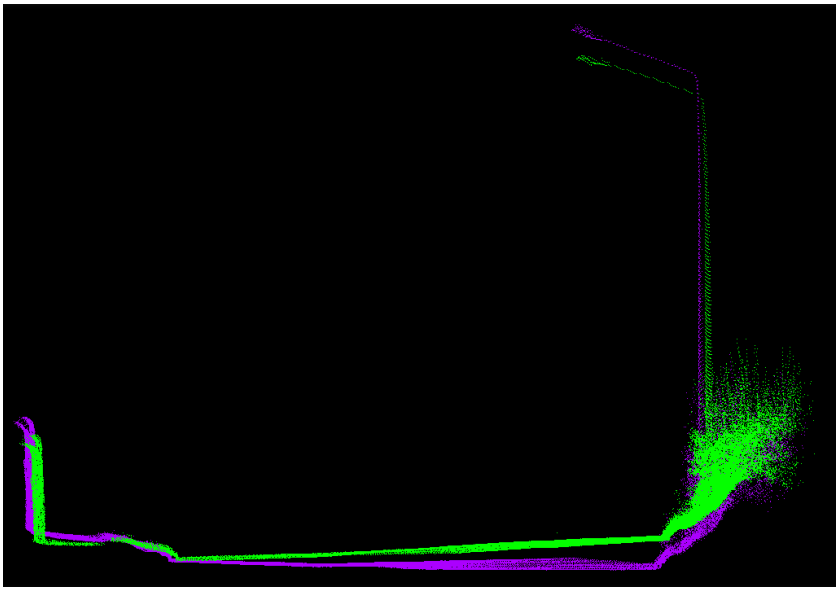

Figure 1.7: Cross section of a Road Surface Highlighting a Boresight Misalignment from a Dual Scanner MMS

1.4.2 Laser Scanning

Laser scanners measure the distance to a target from the sensor head. Each point is recorded with an X,Y,Z coordinate. Figure 1.8 illustrates a typical output from a laser scan survey of building facades in an urban environment. There are three distinct categories of laser scanner: Time of Flight, Phase Based and Triangulation Based. Each has a different principle of operation and is suitable for specific projects. This thesis will focus on Time of Flight scanners only, however a summary of the three types is provided here to identify the different principles of operation. Scanner types are covered in detail in [Petrie and Toth, 2009].

Figure 1.8: Laser Scanner Survey of Building Facades in an Urban Environment [Graefe, 2007b]

- Time of Flight (TOF): TOF laser scanners operate by measuring the length of time it takes a laser pulse to reach a target and then return to the scanner. TOF scanners are capable of very long range measurements and a high measurement rate. For instance, the new Riegl

VZ-6000 [RIEGL, 2012b] displayed in Figure 1.9(a) is capable of measurement ranges up to 6,000m and measurement rates up to 220,000 points per second. The strength of TOF scanners is their long-range measurement capabilities. TOF scanners have lower measurement rates than phase based scanners and lower accuracy than triangulation based scanners. TOF scanners are common on MMSs [Optech, 2012, RIEGL, 2011b, RIEGL, 2009b].

- Phase Based: Phase based scanners operate by concentrating a continuous laser beam on the target. The received signal is phase shifted because it is a time delayed version of the original signal. The phase distance between the transmitted laser beam and the reflected laser beam represents the distance to the target. Phase based scanners are capable of medium measurement ranges and very high measurement rates. The Leica HDS7000 phase based scanner displayed in Figure 1.9(b) [Leica, 2012] is capable of over 1 million points per second and a 200m measurement range. The strength of phase based scanners is their high measurement rate. Phase based scanners have a lower measurement range than TOF scanners and a lower accuracy than triangulation based scanners. To the best of the authors knowledge, scanners designed by FARO [Faro, 2012] are the only phase based scanner to have been installed on a MMS.

- Triangulation: Triangulation based scanners operate by focussing a laser pulse on the target. By offseting a camera at a known distance from the scanners center of measurement, they measure the location of the laser footprint. Triangulation scanners are used for short range, high accuracy surveys. They are capable of very high accuracy [Boehler

(a) (b) (c)

Figure 1.9: Scanner Types (a) Riegl VZ-6000 [RIEGL, 2012b] (b) Leica HDS 7000 [Leica, 2012] (c) Konica Minolta VI9i [Konica, 2012]

et al., 2003], medium measurement rate and low range. The Konica Minolta VI9i displayed in Figure 1.9(c) [Konica, 2012] has a maximum range of 2.5m but is capable of an extremely high accuracy 0.1mm. The strength of triangulation scanners is their high accuracy. They have a short measurement range and a low measurement rate. Due to this short measurement range (approximately 3m), these scanners are unsuitable for MMS surveys.

1.4.3 MMS Specific Laser Scanners

Terrestrial laser scanners (TLS) are predominantly tripod mounted. The three scanners listed in the previous section are all tripod mounted scanners. Tripod mounted scanners have servo-motors which are used to rotate the scanner 360^o. These motors enable a 360^o survey to be carried out around the scanner. Although certain research MMSs have been designed mounting TLSs on moving platforms [Kukko et al., 2007, Talaya et al., 2000], the scanners installed on commercial MMSs are specifically designed to be mounted

on moving platforms. MMS specific scanners survey in a 2D plane. The forward motion of the vehicle provides the third dimension for the data. MMS specific scanners will be covered in greater detail in Section 1.6.4 and in Chapter 2.

1.4.4 Intensity

As well as X,Y,Z coordinates for the location of the target, a TOF laser scanner also returns a value measuring the intensity of the returned pulse from the target surface. The intensity of a return is a measurement of the recorded energy of that returned pulse. Brightly coloured or highly reflective surfaces result in a high intensity return. The intensity of the return can assist in object classification. For example, a high intensity return on the road surface could be a road marking while a low intensity return could be tarmac. Figure 1.10 illustrates points coloured by intensity for a road surface. The brighter points are the high intensity points. These higher intensity points have been returned from the road marking. This is not always a reliable classification method as the intensity can vary across a surface. The intensity varies across a surface because the angle of incidence between the laser pulse and the surface also influences the amount of energy recorded and therefore the intensity value for that point. A laser return from a surface perpendicular to the pulse will result in a higher return than for any other orientation of that target. Recent studies by [Kaasalainen et al., 2011, Soudarissanane et al., 2011] have investigated the influence of the angle of incidence on laser scan quality.

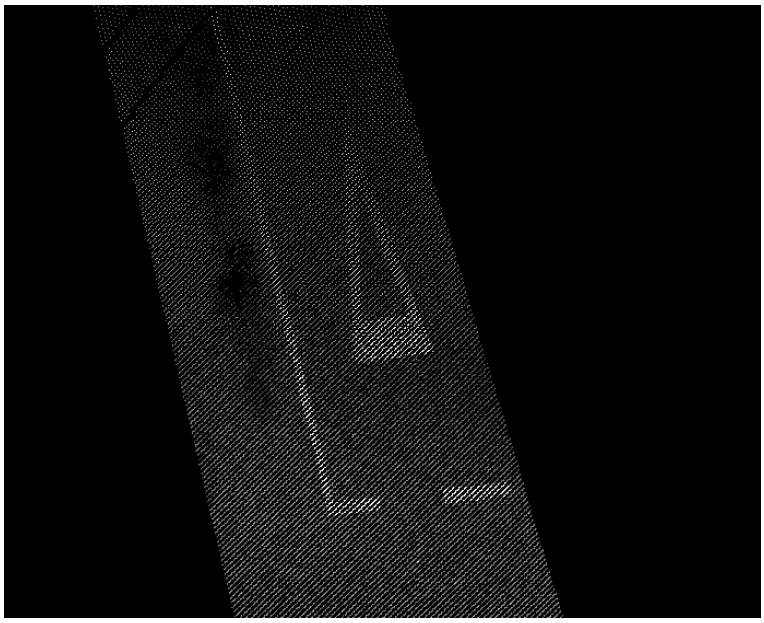

Figure 1.10: High Intensity Returns Identify Road Markings

1.4.5 Multiple Returns

Certain laser scanners are capable of recording multiple returns from a single laser pulse. This information can also be used to classify objects. A laser pulse that results in a single return has passed unobstructed to a solid object. Multiple returns are an indicator of obstructions between the scanner and the target which are not larger than the laser pulse, i.e it's footprint. The laser footprint is the size of the laser pulse on the surface it is measuring. A laser beam expands as it leaves the scanner and this value is known as the beam divergence. The higher the beam divergence, the larger the footprint. The longer the range to the target, the larger the footprint. The most common example of the type of obstruction that results in multiple returns is vegetation. Figure 1.11 illustrates the principle of multiple returns. Figure 1.12 illustrates the measured signal. The first pulses corresponds to the reference pulse. The echoes from the tree and the final return from the roof can be

seen in this pulse. The time difference between the reference and each of the returns allows calculation of the distance to the target.

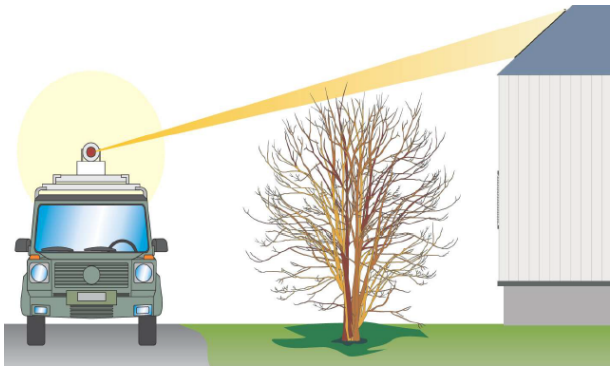

Figure 1.11: Laser Pulse Passing Through Vegetation and Striking a Solid Structure [RIEGL, 2009b]

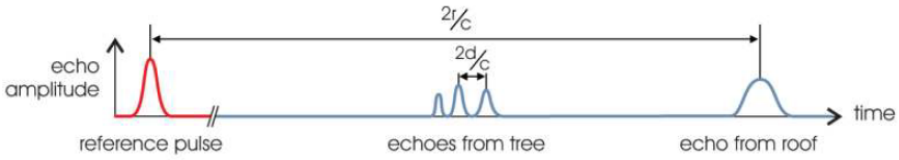

Figure 1.12: Example of Laser Pulse Exhbiting Multiple Returns [RIEGL, 2009b]

1.4.6 Data Volumes and Automated Algorithms

MMS produce high density spatial data, however this also has its disadvantages. High density spatial data results in high data volumes and also increased processing times. The Riegl VQ250 [RIEGL, 2009b] laser scanner produces in excess of 20GB of point cloud data per hour. The Riegl VQ250 is the laser scanner installed on the XP1, one of the MMSs used for validation in this thesis. The current generation of commercial MMSs employ 2 x Riegl VQ250 [RIEGL, 2009a]. This results in a possible 40GB of data per hour.

For large surveys, processing this data and creating 3D CAD models is time consuming. This is because every relevant piece of infrastructure and all road surfaces along with their geometry must be manually identified, defined and measured. Section 1.4.2 described the different scanner types and the number of points that each scanner type is capable of recording each second. Manually interrogating this data to identify every object is extremely time consuming and therefore automated algorithms play an important role in the processing workflow. These algorithms are being developed to automatically recognise features in laser scan data, thus eliminating or reducing the amount of manual interrogation of the data.

Figure 1.13 displays an example of the results from three automated algorithms [McElhinney et al., 2010]. These algorithms have identified trees, poles and the road edge. Automated algorithms assist in processing the large point clouds captured by modern MMSs [Becker and Haala, 2009, Hammoudi et al., 2009, Kumar, 2012, Pu and Vosselman, 2007]. For example, cylindrical objects require a minimum number of points on each profile to recognise a curved shape. Work documented by [Brenner, 2009, Kukko et al., 2009, Lehtomäki et al., 2010] require a minimum number of points or profiles on pole shaped objects to enable their algorithm to recognise those features. Laser profiles and points will be explored in greater detail in Chapter 2. From [Kaartinen et al., 2005] it can be seen that point density directly impacts on the accuracy of the resulting extracted model. Although [Kaartinen et al., 2005] investigated the link between point density, automated algorithms and aerial LiDAR data, the principle is still valid when designing automated algorithms for terrestrial MMSs.

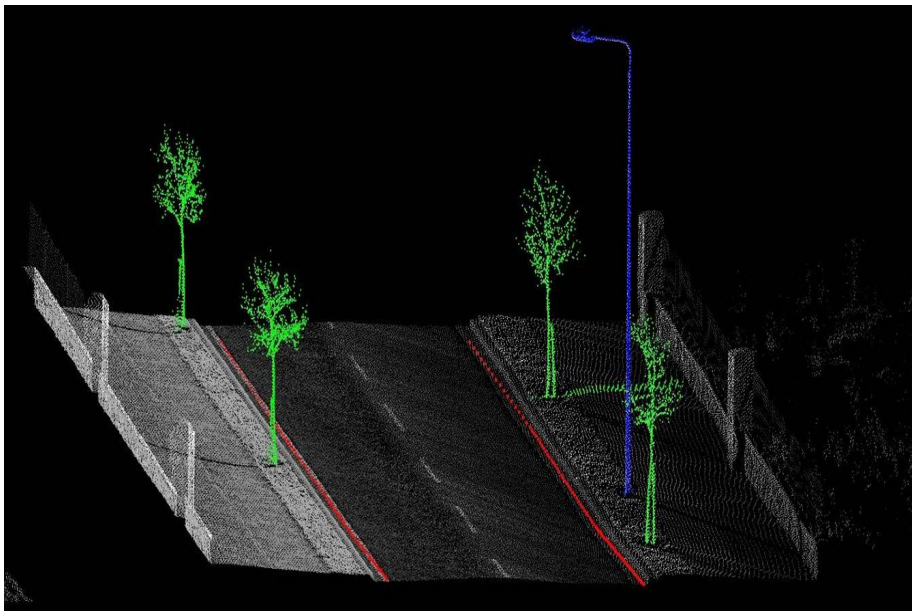

Figure 1.13: An Example of an the Results of an Automated Algoritm Applied to Laser Scan Data - Note Identification of Trees, Poles and the Road Edge

Understanding point density is key to accurately and effectively calculating real-world objects using a MMS. This motivates an investigation into a method capable of determining point density pre-survey. Identifying what MMS configuration and hardware settings will result in the required point density makes efficient use of data storage and increases the potential accuracy of the automated algorithms.

1.5 MMS Performance

Despite a MMSs ability to decrease survey times and also avoid road closures, if a MMS cannot compete with traditional survey methods in three key areas of performance they will not be adopted as a technology. Three areas of

MMS performance are discussed in this section. These areas are absolute and relative accuracy - combined as one area, repeat survey accuracy and point density. Absolute, relative and repeat survey accuracy are all investigated as influencing the accuracy of the MMS data. Point density, which is the focus of this thesis, is dealt with separately. This section provides background information to each area of MMS performance.

1.5.1 Accuracy

Two areas of MMS performance can be categorised using the term, 'accuracy'. These are absolute and relative accuracy, combined into one category, and repeat survey accuracy. Absolute and relative accuracy refer to data resulting from a single survey, whereas in this context, repeat survey accuracy can be defined as a measure of the correlation between two or more laser scan surveys captured at different times over the same environment.

1.5.1.1 Absolute and Relative Accuracy

The absolute accuracy of a point refers to its accuracy when compared to the true location of the point as referenced on a pre-defined geodetic framework. There have been a number of papers published assessing the absolute accuracy of a MMS survey when compared with a reliable source of survey control. For instance, [Barber et al., 2008] surveyed road markings using traditional surveying techniques and used these as survey control for comparison with MMS data. In another study, [Haala et al., 2008] assessed the absolute accuracy of a MMS using an existing 3D city model and cadastral footprints. These studies identified that MMSs are capable of accuracies in the region of 0.03m in planimetry and 0.05m in elevation in good GNSS conditions.

These studies identified that the GNSS is potentially the largest contributor to accuracy errors. In their recent benchmarking tests, [Kaartinen et al., 2012] identified that with properly calibrated high-end MMSs, planimetric accuracies of approximately 0.02m were achievable.

Relative accuracy is the accuracy of a surveyed point relative to a subsequent point under the same test conditions. Due to the high rate of measurement of a laser scanner, the relative accuracy of a MMS is hardware dependant and the quoted precision of an instrument typically defines this. For example, the precision of the Riegl VQ-250 is quoted at 0.01m [RIEGL, 2009b]. Figure 1.14 illustrates the principles of absolute and relative accuracy. In Figure 1.14(a), the measurements in red do not match the true value in green. Additionally, there is a significant deviation between the measurements. The absolute accuracy and relative accuracy is poor in both cases in this test. In Figure 1.14(b), the measurements do not match the true value, however the measurements are consistent. In Figure 1.14(c), the measurements do match the true value and the measurements are also consistent. Both the absolute and relative accuracy in this test are high. Relative and absolute accuracy are important performance issues, however they are not the focus of this thesis.

1.5.1.2 Repeat Survey Accuracy

Repeat survey accuracy is a term applied in this thesis for defining the accuracy of two surveys in relation to each other when the test conditions have changed. In Section 1.3 the process for calibrating the MMS and computing the navigation solution is explained. A number of issues are highlighted that

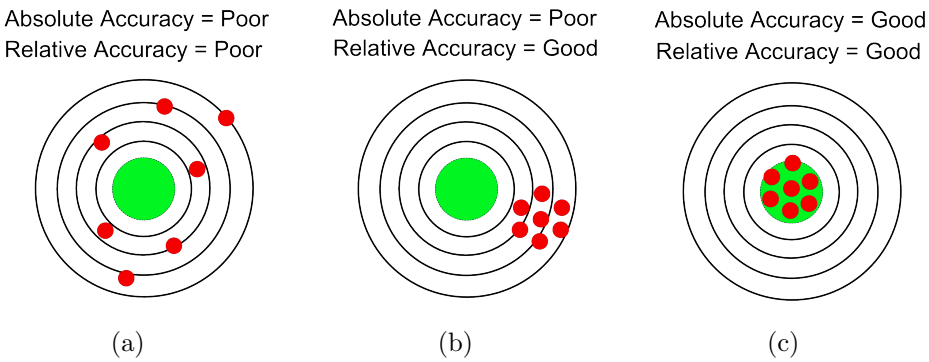

Figure 1.14: Distinction Between Relative and Absolute Accuracy for a Circular Target

could potentially influence the accuracy of the point cloud. These include satellite configuration, system lever-arm offsets and boresight misalignments. Each of these contribute to the repeat survey accuracy of a MMS.

A MMS may carry out a survey on the same stretch of road on two different days. The GNSS constellation overhead and the atmospheric conditions will be different for the second survey. A comparison of the known control points in the resulting point clouds is a measure of the repeat survey accuracy. Additionally, it is common practice for a MMS to drive a route in both directions to ensure full coverage of the surrounding environment. Even in this short time, the GNSS coverage will have changed. The atmospheric conditions may also have changed.

1.5.2 Point Density

This thesis focuses on point density. The term 'point density' is generally applied for the number of pulses striking a target per unit^2. In this thesis the term point density refers to the total number of pulses striking the tar-

get. Point density is important when trying to manually or automatically recognise structures in laser scan data. Understanding the factors influencing point density is also important for MMS design and also for system configuration prior to a survey. This area of MMS performance has largely been unexplored to date. It will be investigated in greater detail in Chapter 2 but is introduced in this section.

Point density is an important part of a laser scan survey yet there are unanswered research questions in this area, particularly for MMSs. This is in part due to the fact that there is no requirement for a high point density with existing topographic survey methods such as total stations. A total station is a surveying instrument that measures angles and the distance from the instrument to a reflective prism. If a measurement of an object is required, a surveyor will manually identify the points on the target that define it properly. Figure 1.15 illustrates a two man survey crew surveying a road edge. This survey method is time consuming but has the advantage that the position and dimensions of every feature are measured and identified at the survey stage while the surveyor is still in the field. Survey codes [Trimble, 2012] are used for classification of every feature and are applied at the time of measurement by the surveyor. Therefore, assuming the surveyor can visually identify the object, an incorrect classification is unlikely.

This situation is more complicated when working with MMS data. With certain exceptions where research groups have attempted real-time data processing [Brun and Deschaud, 2007, Toth and Grejner-Brzezinska, 2001], this stage is conducted post survey. Clarification or confirmation of an object

Figure 1.15: Two Man Survey Crew Operating a Total Station [Ohio Land Surveys, 2012]

type cannot be carried out until after processing. In the event of a mis-classification of an object, clarification requires an additional site visit. Automated algorithms improve on manual classification by identifying and measuring structures and infrastructure at higher speeds than a human operator is capable of. Entrusting an automated algorithm with object classification can result in errors if the point density of the target is insufficient, as identified in Section 1.4.6. Prior knowledge of the MMS configuration and operational settings that return a required point density for a specific target on a survey could minimise the risk of mis-classifications. It could also increase the accuracy of the automated algorithms [Kaartinen et al., 2005].

Traditional survey specifications define the required number of measurements for any ground type. This requirement may be that a road cross sec-

tion is to be surveyed at 10m intervals on roads. The specification could then stipulate that a height measurement is recorded at any significant change of elevation along that cross section [O Cathain, 2011]. Specifically defining the location for each measurement facilitates an accurate definition of the surface. Defining the location for measurements during a MMS survey is impossible as the operator has no control over where each measurement is taken. Laser scanners compensate for the lack of control by surveying a target with high density measurements. Currently, MMS configuration, hardware and operating parameters have unpredictable results on point density. This thesis will quantify these effects and therefore potentially improve survey, storage and processing efficiency.

Point density is traditionally quoted in points per m^2, yet objects are 3D. Defining the point density of a cylinder in 3D is difficult. In their work on simulation based analysis of point density, [Yoo et al., 2009] projected all 3D neighbour points per m^3 onto a 2D surface circle. However, point density is not uniform across a surface, and therefore quoting point density is not that straight forward. Further research is required to calculate what point density different MMSs are capable of. For example, one MMS survey specification [Florida Department of Transport, 2012] states that, 'the point density should be sufficient to identify and extract physical detail to the accuracy specified for the project' but does not specify what point density will permit that accuracy, or what MMS configuration will facilitate that point density. One set of LiDAR guidelines [Yen and T.A., 2011] informs that clients requesting LiDAR surveys must carefully specify 'the point-cloud point density' but links this to the speed of vehicle only. Neither of these

guidelines specify what a suitable point density is. At present there is no method of quantifying or assessing the point density of a MMSs and it is these questions that this thesis will address.

1.6 Research Objectives

The aim of this thesis is to investigate MMS point density. To achieve this aim this thesis incorporates three objectives that further the body of knowledge in the field of quantifying MMS point density. This section summarises these three objectives. Each objective will be explored in greater detail in Chapter 2.

1.6.1 Objective 1

No satisfactory method for calculating MMS point density exists. The first objective of this thesis is to design a method that is capable of calculating the point density recorded by MMSs from generic targets. This method incorporates MMS configurations, different hardware settings and different MMS operating parameters. This objective will be investigated in greater detail in Chapters 2 and 3 and will be implemented and validated in Chapters 4 and 5.

1.6.2 Objective 2

The second objective of this thesis is to assess different MMS configurations and to quantify what influence these configurations have on point density. A recommended configuration for different survey targets is presented. This

objective will be investigated in greater detail in Chapter 2 and will be implemented in Chapter 6.

1.6.3 Objective 3

The final step of this thesis applies the method designed after completion of Objective 1 to a selection of hypothetical and existing MMSs to benchmark their point density performance. The recommended configuration identified after successful completion of Objective 2 is employed in the benchmarking tests. This objective will be investigated in greater detail in Chapter 2 and the methods employed to achieve it will be discussed in Chapter 7.

1.6.4 Test Systems

The algorithms, methods and conclusions resulting from the completion of Objectives 1, 2 and 3 will require verification. Laser scanner data from two MMS will be used to test and validate each of the findings. The first MMS that is used for validation is a research platform called the XP1. The second MMS used for validation is a commercial MMS. The commercial system is the Optech Lynx [Optech, 2012] and it provides the opportunity for further validation with different hardware and a different system configuration.

The multi-disciplinary research group, StratAG [Stratag, 2012], established to research advanced geotechnologies at the National Centre for Geocomputation (NCG), NUI Maynooth have designed and developed a multi-purpose, state of the art, land based experimental platform MMS, the XP1. The component of this MMS most relevant to this thesis is the Riegl VQ-250 laser scanner. This scanner is specifically designed for MMS surveys. Table

1.1 details the relevant information for the laser scanner that is required for this research. The Optech Lynx MMS is a commercial MMS, designed by the Canadian firm Optech. The Optech Lynx incorporates two laser scanners. The scanners on the Lynx are the M1 scanner type. Data from this system was provided as an extra validation source. Table 1.2 lists the relevant parameters of this scanner. The scanner attributes and their importance will be discussed in greater detail in Chapters 2 and 3.

Table 1.1: Riegl VQ250 Laser Scanner [RIEGL, 2009b]

Category	Value
Min Range	1.5m
Max Range @ 300kHz (m)	200m
Pulse Repetition Rate	300kHz
Mirror Frequency	100Hz
FOV	360^o

Table 1.2: Optech M1 Laser Scanner [Optech, 2012]

Category	Value
Max Range @ 200kHz (m)	200m
Pulse Repetition Rate	500kHz
Mirror Frequency	200Hz
FOV	360^o

1.6.5 Publications

The following papers have been published arising from work on MMSs. The first paper [McElhinney et al., 2010] focusses on the benefits of employing a MMS for route safety inspections on rural roads. The remaining four papers

[Cahalane et al., 2010a, Cahalane et al., 2010b, Cahalane et al., 2011, Cahalane et al., 2012] are steps in the implementation of a method to calculate point density and are therefore work carried out to complete Objective 1.

Conor P. Mc Elhinney, Pankaj Kumar, Conor Cahalane, Timothy McCarthy (2010) *Initial results from European Road Safety Inspection (EURSI) mobile mapping project*, 440-445. In ISPRS Commission V Technical Symposium.

C. Cahalane, T. McCarthy, and C. McElhinney. *Mobile mapping system performance : An initial investigation into the effect of vehicle speed on laser scan lines*. In Remote Sensing and Photogrammety Society Annual Conference From the sea-bed to the cloudtops, September 2010, Cork, Ireland, 2010.

C. Cahalane, C. McElhinney, and T. McCarthy. *Mobile mapping system performance : An analysis of the effect of laser scanner configuration and vehicle velocity on scan profiles*. In European Laser Mapping Forum ELMF 2010, November 2010, The Hague, Holland, 2010.

C. Cahalane, C. McElhinney, and T. McCarthy. *Calculating the Effect of Dual-Axis Scanner Rotations and Surface Orientation on Scan Profiles*. In 7th International Symposium on Mobile Mapping Technology, June 2011, Krakaw, Poland, 2011.

C. Cahalane, T. McCarthy, and C. McElhinney. *MIMIC: Mobile Mapping*

Point Density Calculator. In Proceedings of the 3rd International Conference on Computing for Geospatial Research and Applications (COM.Geo), July 2012, Washington D.C, U.S.A, 2012.

1.7 Research Assumptions

A number of assumptions have been made in this thesis to facilitate work on the Objectives listed in Section 1.6. These are;

- The aim of Objective 1 is to calculate point density - i.e. the number of pulses returning from an object. An assumption is made that there is a return from every pulse, one return only per pulse and also a smooth surface. In practice this will not always be the case, but the majority of man-made roadside infrastructure is solid and if unobstructed will therefore provide a return for each pulse.

- Time of Flight scanners are the most common type of laser scanner on commercial MSSs, and therefore these are the only type that are investigated in this thesis. To the best of the authors knowledge, only one phase based scanner [Faro, 2012] has been used on a MMS, a FARO scanner.

- Point density is assessed for different MMS configurations, in a standardised testing process. Point density is not assessed for every eventuality. Therefore it is assumed that there is a constant vehicle velocity, no course deviation and no pitch or roll of the MMS when surveying a target. Although this will not be the case in a real world setting these

parameters are identified as a possible error source in the validation tests.

- When calculating point density, it is assumed that high accuracy, properly calibrated positioning and spatial measurement sensors are employed on the MMS and that there will not be significant errors between subsequent scan lines or scan points.
- Vehicles in Ireland drive on the left hand side of the road. The XP1 is a single scanner system. Therefore the VQ-250 on the XP1 is fixed on the left hand side of the vehicle. The work in this thesis is targeted at near-side infrastructure only. Objects on the right hand side of the vehicle are a potential topic for future work.
- It is assumed that there are no obstructions present between the scanner and the target. Again, the reason for this is that point density is assessed for different MMS configurations in a standardised testing process and not for every eventuality.

1.8 Thesis Structure

This thesis consists of a further seven chapters structured and detailed as follows.

Chapter 2 introduces the field of point density in more detail and investigates the work to date in this area. The three research objectives listed in Section 1.6 are investigated. The solutions proposed in each objective are presented and justified in reference to existing work.

Chapter 3 discusses the MMS configuration, MMS hardware and target variables that must be incorporated in an algorithm for calculating point density. The changes in MMS configuration, vehicle behaviour and target parameters that impact on point density are identified and their impact on point spacing illustrated.

Chapter 4 details the initial components of the point density calculation algorithm. In this chapter the interaction of the individual scan pulses and targets are calculated and validated using the two test systems introduced in Section 1.6.4.

Chapter 5 completes the point density calculation algorithm. The findings from the calculations in the previous chapters are combined to calculate point density for an entire target. A series of targets are employed to validate these calculations using data from both test MMSs.

Chapter 6 applies the point density calculation algorithm to assess the impact of MMS configurations on point density. By changing the hardware and configuration parameters and assessing these changes with the point density calculation algorithm, the recommended MMS configuration for specific targets can be identified. The tests in this chapter are theoretical and no validation is carried out.

Chapter 7 uses the point density calculation algorithm to benchmark a selection of MMSs in terms of their point density performance. The parameters for a commercial MMS and two theoretical MMSs are entered into the

algorithm to identify strengths and weaknesses of each for different target and operating parameters. This chapter is also theoretical and therefore no validation is carried out.

Chapter 8 discusses the main conclusions of this research by summarising the work completed, introducing work in progress and identifies potential future work. It concludes with some final remarks.

Chapter 2

Point Density

The previous chapter identified the three fundamental elements in the field of MMS performance: absolute and relative accuracy, repeat survey accuracy and point density. Point density was identified as the subject matter of this thesis and provides the underlying motivation for carrying out this research. This chapter investigates point density in greater detail and identifies the areas where research has been carried out. This chapter also outlines the proposed solution to achieve each research objective and provides justifications for adopting these approaches.

2.1 Introduction

The first objective of this thesis is to design an algorithm to calculate the point density of a target prior to performing a MMS survey. There are three primary inputs to this algorithm and each input contains multiple parameters. These inputs are the scanner, the target and the vehicle parameters. Although previous studies have investigated point density, these studies were limited to manual measurements, LiDAR simulations or limited geometric

formulae. The influence of a number of parameters on point density has been ignored. Section 2.2 identifies these parameters and the related studies.

The second objective of this thesis is to apply the point density calculation algorithm, designed in the previous objective, to assess various system configurations. There are multiple hardware and operational parameters to consider when constructing a MMS. The effect of these parameters are assessed for different types of target to identify the optimum configuration for each survey scenario. Research in this area is limited. Objective 2 is explored in Section 2.3.

The third and final objective of this thesis is to benchmark a selection of MMSs in terms of their point density. The point density calculation algorithm facilitates these tests. To date, benchmarking of MMSs has been limited to accuracy tests or comparisons of manufacturers hardware specifications. This thesis proposes benchmarking one commercial and two hypothetical MMSs for a selection of targets. Objective 3 is investigated in more detail in Section 2.4.

2.2 Objective 1 - Point Density

MMSs equipped with a laser scanner are potentially capable of capturing hundreds of thousands of points per second. For example, the MMS designed at the NCG, the XP1 (Section 1.6.4), is equipped with a single Riegl VQ-250 scanner [RIEGL, 2009b] that is capable of emitting up to 300,000 laser pulses per second. The current generation of MMSs are often equipped with multiple laser scanners. Commercial systems like Riegl's VMX250 [RIEGL,

Figure 2.1: An Example of a Point Cloud Collected by the Single VQ-250 Scanner on the XP1

2009a] operate dual scanners (2 x VQ-250), which are therefore capable of capturing up to 600,000 points per second if they receive a return from each pulse. Riegl's latest dual scanner system, the VMX450 [RIEGL, 2011a] incorporates 2 x VQ-450 [RIEGL, 2011b] and is capable of emitting upwards of one million pulses per second.

Each laser return is then georeferenced and when viewed as a whole, comprise a 'cloud'. This collection of points is commonly referred to as a 'point cloud'. Figure 2.1 displays a sample point cloud captured by the XP1 MMS. The interaction between the vehicle, scanner and target dictate the number of laser pulses that strike a target. These factors must therefore be incorporated into any attempt to calculate the theoretical point density of a target.

2.2.1 Scanner Parameters

In general, terrestrial laser scanners (tripod or vehicle mounted) result in a higher point density than aerial scanning systems due to the shorter measurement range. A tripod mounted scanner benefits from its static set-up. Employing servo-motors to change the field of view enables 360^o scanning around the scanner from a single location. One consequence of tripod mounting is that the base of the scanner obstructs the field of view. For example, the Leica HDS7000 introduced in Section 1.4.2 has a 360^o x 320^o FOW, therefore it has a 40^o blind spot under the scanner.

It is possible to mount a TLS on a vehicle and use it in 'stop and go' mode. In 'stop and go' a tripod mounted scanner is placed on a moving platform and driven to a survey location. The vehicle stops at this location and the TLS scans the entire scene while the vehicle remains stationary. The vehicle then moves to the next survey point [Hesse and Kutterer, 2007] and this process is repeated. It is the author's opinion that this is technically not a MMS as a MMS must, by definition, be capable of mapping while mobile. MMSs like the XP1 operate a 2D, full-circle laser scanner specifically designed for mobile mapping surveys. This class of scanner utilises the forward motion of the vehicle to create the third dimension for the scanner and results in a corkscrew scanning pattern as the MMS travels along its route, as Figure 2.2 illustrates. To operate a TLS on a moving platform, the TLS can have one of its axes of rotation locked and can then operate in 'profile mode'. TLSs configured to operate in profile mode can then be used on a moving vehicle [Glennie, 2008, Kukko et al., 2007] rather than 'stop and go'. Any point cloud collected by a scanner specifically designed for MMS surveys or a

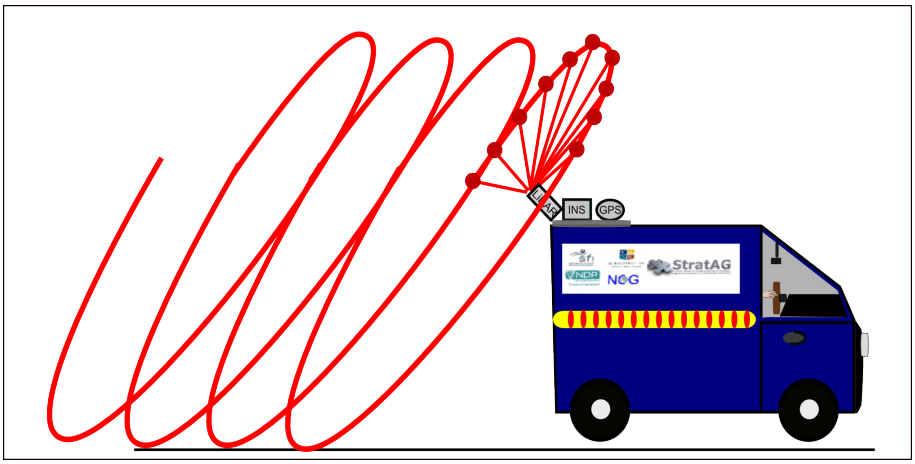

Figure 2.2: The Corkscrew Scanning Pattern Exhibited by a MMS Scanner

TLS operating in profile mode exhibits three very distinctive features. These are the profile spacing, the profile angle and the point spacing and these three scanning characteristics constitute the unknowns involved in the point density calculation.

2.2.1.1 Scan Profiles

The corkscrew scanning pattern of a MMS operating a 2D full circle laser scanner is illustrated in Figure 2.2. When this corkscrew scanning pattern intersects with a planar surface, the resulting laser points describe a linear pattern on that surface. These lines of points are termed 'scan profiles'. Gaps are formed between scan profiles for each mirror rotation. The distance between each scan profile is the profile spacing and this is illustrated in Figures 2.2 and 2.3. Vehicle velocity influences the distance between each scan profile. The angle of the scan profile in relation to the direction of travel of the vehicle is influenced by the rotation of the scanner. Figure 2.4 displays the horizontal and vertical rotation of the laser scanner on the XP1. Rotations of the scanner are important for maximising coverage of the environment. Scan

profiles that run perpendicular to the direction of travel will not intersect with objects whose sides are also perpendicular to the direction of travel, as illustrated in Figure 2.5(a). A horizontal rotation of the scanner solves this problem (Figure 2.5(b)). Scan profiles that are vertically perpendicular to the direction of travel are also problematic. These scan profiles will not intersect with some vertical structures such as the faces of road signs above motorways or bridge faces. This is demonstrated in Figure 2.6(a) and can be solved with a vertical rotation of the scanner as illustrated in Figure 2.6(b).

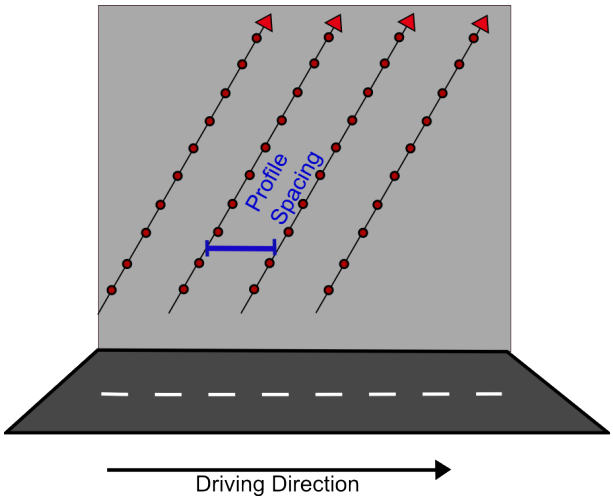

Figure 2.3: Profile Spacing on a Vertical Surface.

Rotations of the scanner or target in the horizontal or vertical plane alter the angle that scan profiles intersect with horizontal and vertical surfaces. This angle is termed the 'profile angle'. The profile angle on a vertical surface resulting from a scanner with a vertical rotation is illustrated in Figure 2.7. Designing a method for calculating both profile spacing and profile angle are essential for calculating point density. The vehicle speed, the rotation of the scanner(s), the scanner mirror frequency (how many profiles per second) and

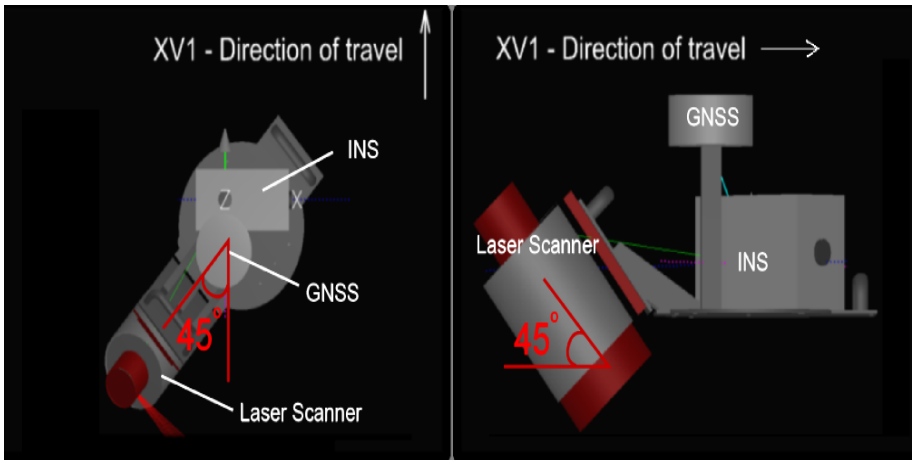

Figure 2.4: A 45^o Horizontal and 45^o Vertical Rotation of the Scanner on the XP1

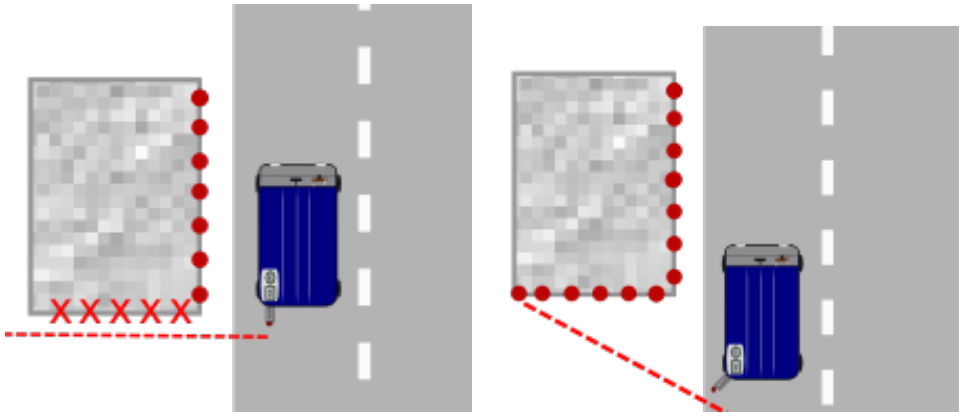

(a) (b)

Figure 2.5: Importance of a Horizontal Rotation of the Scanner - Top Down View (a) Without (b) With

the rotation of the object all influence scan profiles.

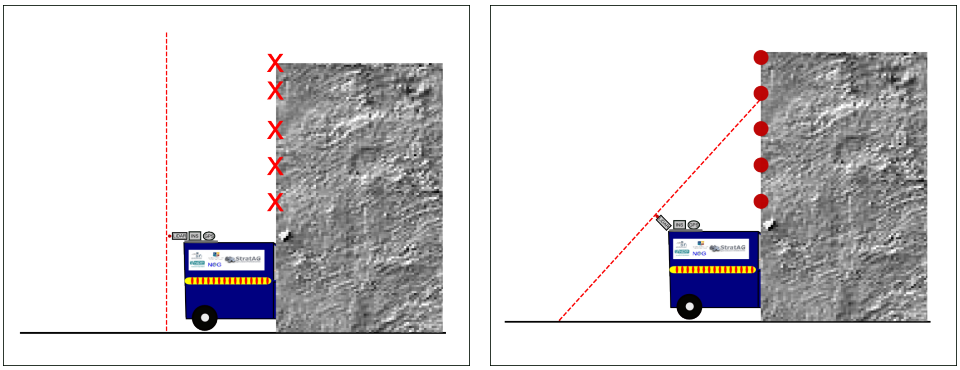

(a) (b)

Figure 2.6: Importance of a Vertical Rotation of the Scanner - Side View of a MMS Travelling Under a Bridge (a) Without (b) With

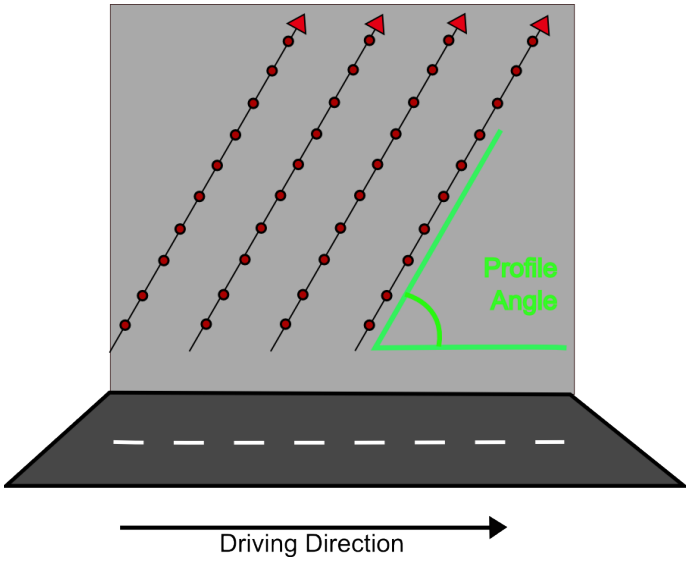

Figure 2.7: Profile Angle on a Vertical Surface.

2.2.1.2 Point Spacing

The distance between subsequent points along a single scan profile for a 2D scanner is known as the point spacing. Point spacing along a profile line is illustrated in Figure 2.8. Calculating point spacing requires multiple parameters. Point spacing is influenced by a number of factors, including: the pulse repetition rate (PRR), which is the number of pulses per second, the miror frequency, which controls the number of mirror rotations per second, the range to the target from the scanner, the field of view, the height difference between target and scanner, the orientation of the target and the orientation of the scanner. Each of these factors must be addressed when calculating point density.

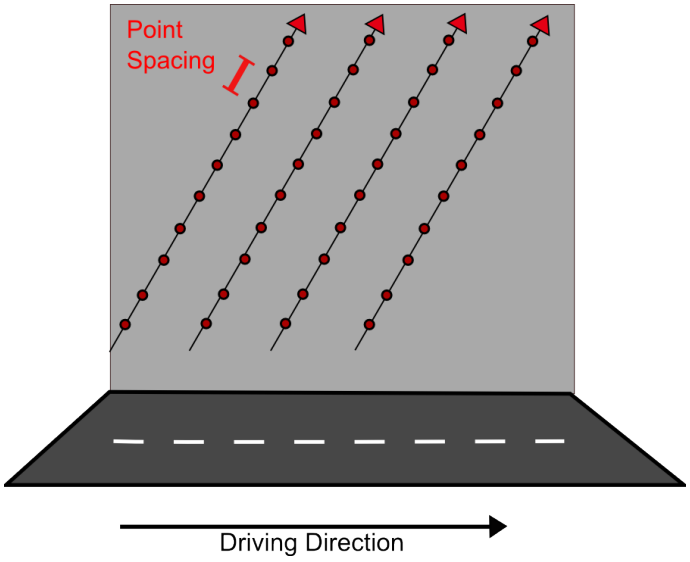

Figure 2.8: Point Spacing on a Vertical Surface.

2.2.2 Survey Vehicle Parameters

The vehicle also influences the number of laser pulses that strike a target. Vehicle parameters must be incorporated into the algorithm to accurately calculate the point density of a target. One example is the effect of the vehicle speed on profile spacing. Designing an algorithm to calculate point density is further complicated when the algorithm must accommodate a moving body, the vehicle, that is free to rotate in three dimensions. The three dimensions of rotation are termed pitch, roll and yaw. These rotations correspond to an inclined surface, a road cross-fall and a course change respectively and are illustrated in Figure 2.9. These rotations change the orientation of the scanner and therefore the geometry of how each profile intersects with the target. This will alter the profile angle. When calculating point density on a target surveyed by a moving vehicle, pitch, roll and yaw are potential error sources. These error sources are investigated in greater detail in Chapter 4.

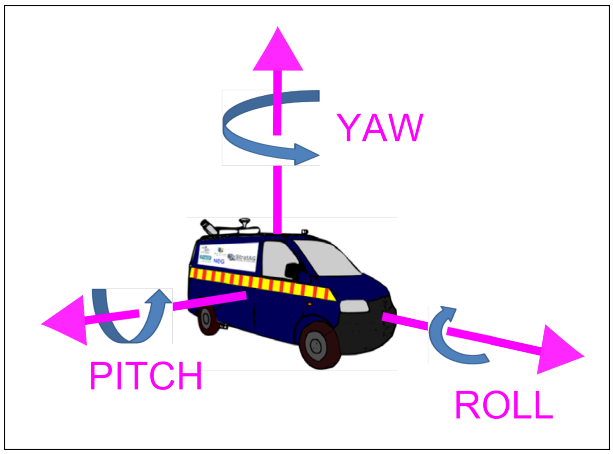

Figure 2.9: The Three Dimensions of Rotation of a MMS

2.2.3 Targets

The third and final element involved in calculating point density is the target. Both the size of the target and its range from the scanner impact on point density. Other target characteristics include the shape of the object and its orientation relative to the scanner. To illustrate the importance of the target shape on point density, Figure 2.10 displays the scan profiles resulting from a vertical scanner rotation which have altered the profile angle on a vertical surface. By introducing subsequent 15^o increments to the vertical rotation of the scanner the number of points striking the target are increased. Without a vertical rotation of the scanner, narrow vertical surfaces (e.g a signpost) are not captured sufficiently to resolve their shape and dimensions accurately from the point cloud. Good coverage of a target is a requirement from automated algorithms that aim to automatically identify structures from point clouds. To date, the recommended scanner orientation for targets of different dimensions has not been identified. Determining this orientation is one of the goals of this thesis.

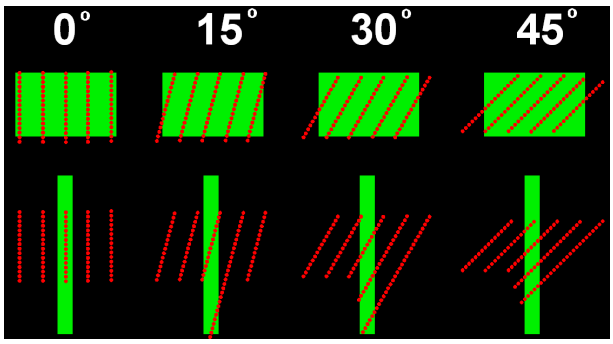

Figure 2.10: The Importance of Introducing a Vertical Rotation of the Scanner for Narrow Objects

2.2.4 Calculating Point Density

Assessing MMS performance and calculating point density are processes involving numerous factors and ones that warrant further study. Research and associated publications in this area are limited. There is at least one commercial software application that provides the ability to calculate basic point density information. There have also been studies investigating the point density displayed by a TLS.

2.2.4.1 Work to date

Research focussing on MMS point density is limited. By locking one rotation axis of a FARO TLS, [Kukko et al., 2007] operated the scanner in profile mode and then manually measured the profile and point spacing at different ranges, speeds and scan frequencies post mission on the road surface. It was then possible to plot these measurements and to approximate what point and profile spacing a user could expect from that specific MMS. Figure 2.11(a) illustrates the point spacing results at different ranges. This data could be used to estimate point spacing for subsequent surveys. This data was manually measured, and therefore it provides very accurate point and profile spacing for that MMS and that survey site. Similar tests have also been performed by [Hesse and Kutterer, 2007] with a Leica HDS 4500 locked in one axis and operating in profile mode. These tests were less comprehensive than [Kukko et al., 2007] and did not provide a plot of the measurements, but only a short table listing profile spacing at three vehicle speeds and three scanner mirror frequencies. Only [Kukko et al., 2007] incorporated scanner rotations. Unlike TLSs such as the Leica HDS 4500, vertical rotations of the scanner can be implemented with the FARO scanner. Neither study incorporated dual-axis

scanner rotations. The benefits of a dual-axis scanner rotation were outlined in Section 2.2.1.1. Neither study measured or provided a method to calculate point density.

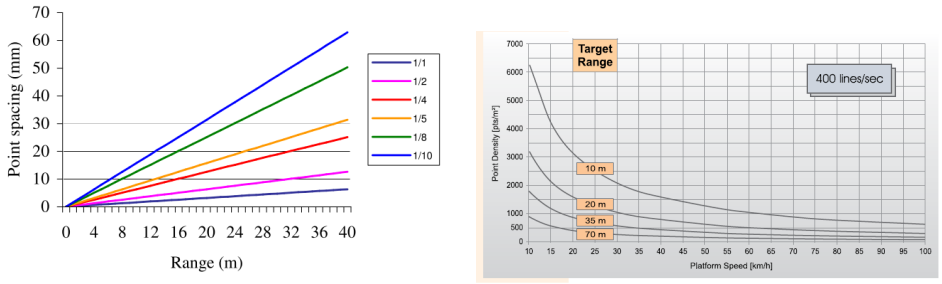

(a) (b)

Figure 2.11: Plotting Results (a) Point Spacing from FGI Roamer [Kukko et al., 2007] and (b) Point Density for Riegl's VMX450 [RIEGL, 2011a]

This thesis improves on these manual point and profile measurement methods by providing a generic formula that will calculate point spacing, profile angle, profile spacing and point density for any scanner settings and vehicle velocity. Additionally, it incorporates dual-axis scanner and target rotations into the algorithm. In their work on automated algorithms, [Hofmann and Brenner, 2009] have identified the effect that a change in vehicle direction and velocity has on scan profiles. Their work has focused on automatic detection of objects and the sole purpose of their basic point density calculation is to eliminate areas of low point density in point clouds. Eliminating these areas from the point cloud results in an improved performance of their automated algorithm.

Certain laser scanner manufacturers provide basic information on the point density that a user can expect from their scanner. For example, Riegl

provide graphs plotting the point density a user can expect at different vehicle velocities or from different scanner settings at different target ranges. An example of a point density graph for Riegl's VMX-450 is displayed in Figure 2.11(b). These graphs do not incorporate scanner rotations, target rotations or any height difference between the scanner or the target. These graphs are limited to specifying point density by calculating point spacing at a single target location, whereas point spacing varies over a target. Variations in point spacing across a target are particularly relevant for angled surfaces. Riegl also licence a software package called RiACQUIRE [RIEGL, 2012a] and one of its functions is to calculate point density pre-survey. Figure 2.12 displays RiACQUIRE's interface. In this example, RiACQUIRE has calculated profile spacing, point pacing and point density for a Riegl scanner on a specific target. RiACQUIRE does not recognise horizontal or vertical scanner rotations, horizontal or vertical target rotations, height difference between scanner and target or different types of target. Furthermore it specifies the point density by calculating point spacing at a single central target location and therefore the point density calculation does not represent the change in point spacing over a target.

Another alternative method for investigating point density is a LiDAR simulation. A LiDAR simulation models the real world interaction between a LiDAR system and the terrain. Simulations have been used for investigating aerial systems [Lohani and Mishra, 2007], but the viewing geometry is less complicated and the field of view is more restricted. Other simulators have been designed, such as that by [Kukko and Hyyppä, 2009] for assessing algorithm development, system validation and error assessment for aerial and

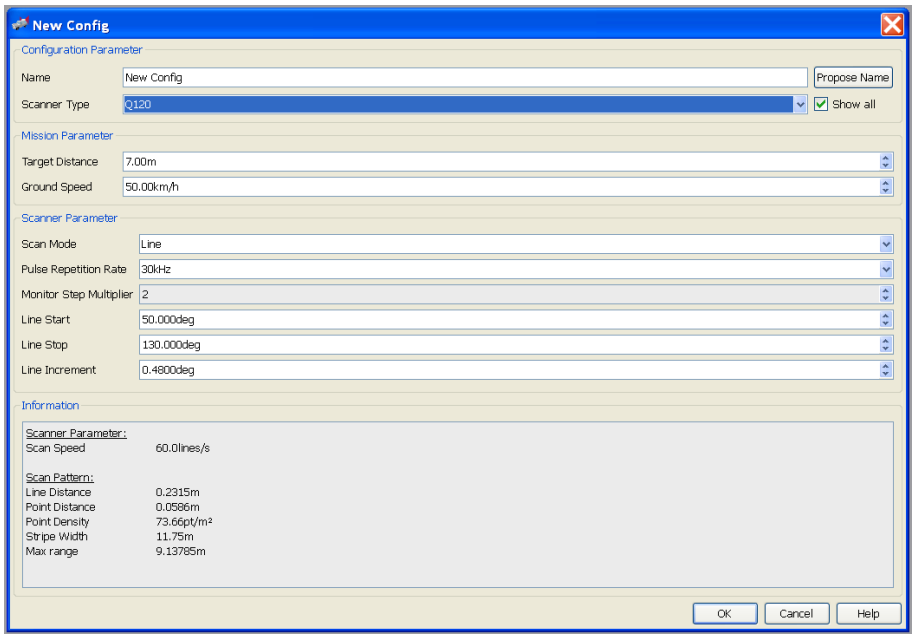

Figure 2.12: Mission Planning with Riegl's RiAcquire Software Package [RIEGL, 2012a]

terrestrial systems. Simulators are useful tools for assessing MMS coverage over wide areas, or for algorithm development, but do not provide a method for calculating point density. A MMS simulation was designed by [Yoo et al., 2009] to provide a method for measuring the mean point density for large areas of a scene. Figure 2.13 ilustrates the simulated point cloud. This study recommended specific MMS configurations to minimise data shadows for terrestrial MMS surveys. This study also included some important elements: dual-axis scanner rotations, variations in scanner location on the MMS, different PRRs and mirror frequencies, yet it did not provide a capability for pre-mission calculation of point density, profile spacing, profile angle or point spacing. After a simulation is complete, point and profile measurements are manual and localised to a single point on a target. Additionally, the simulated scanner was not the 2D circular scanner that the state of the art

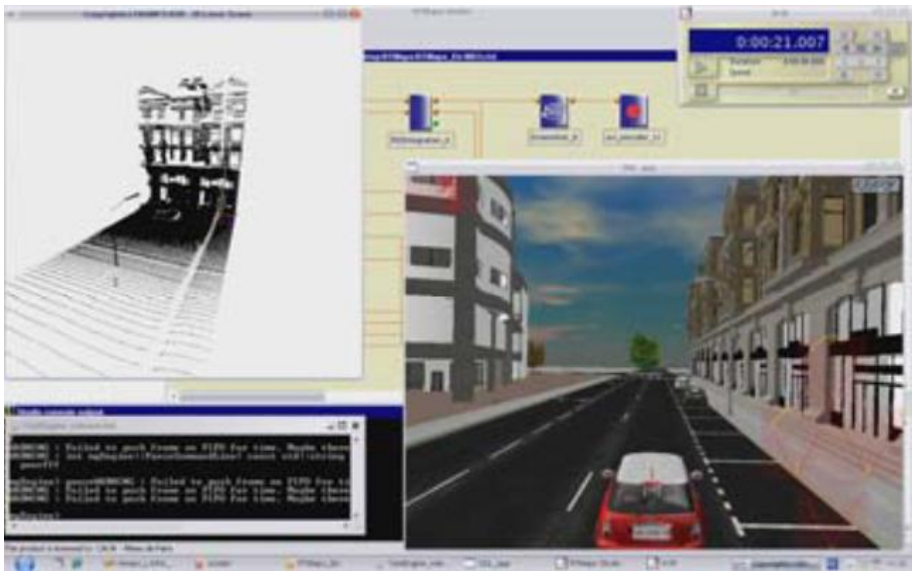

Figure 2.13: MMS LiDAR Simulator [Yoo et al., 2009]

MMSs employ but rather a lower specification 2D laser range sensor. The laser range scanner was a LD Automotive from IBEO and is capable of 1080 pulses per mirror rotation and ten mirror rotations per second [Yoo et al., 2009]. [Yoo et al., 2009] employed this scanner for the simulation as this scanner was incorporated in their LARA 3D MMS [Goulette et al., 2006]. This results in a low point density because the the LD IBEO is only capable of 10,800 pulses per second.

Point density is not only of interest to a new technology like MMSs. A recent study [Gonzlez-Jorge et al., 2011] testing the metrology specifications of TLSs investigated the resolution of TLS point clouds. In their work on TLS, [Lichti, 2004, Lichti and Jamtsho, 2006] have attempted to identify what was the smallest feature that can be recognised in a point cloud for different TLS hardware. This study was also concerned with identifying the effect of laser footprint size on the accuracy of individual points. These

studies are of benefit to TLS operators surveying fine detail like statues or paintings, but MMSs are not designed for such high resolution studies.

2.2.4.2 Proposed Solution

Profile spacing, profile angle and point spacing constitute the primary variables involved in the point density calculation algorithm. Point density is usually quoted in m^2, but point density per m^2 is an unsuitable metric for a large amount of roadside features as they are complex, non-planar objects whose dimensions are non regular - e.g a signpost and sign. Point density in this thesis refers to the total number of points recorded on the target. The method that is designed for calculating point density from this information utilises 3D surface normals, rotation matrices and 2D geometrical formulae.

2.2.4.3 Justification

The existing research can be divided into three distinct categories. These categories are: manual measurements, LiDAR simulations and geometric formulae. The geometric solution that is proposed in this thesis is an improvement on the existing work. The following justifications are given:

Automatic versus manual - Applying an algorithm is preferable to manual point cloud measurements for a number of reasons:

- *Easier to implement* - Running an algorithm is unquestionably easier to implement than carrying out a MMS survey, downloading, processing and manually interrogating the data.
- *Accuracy* - With the manual approach, there is no complete understanding of what factors contribute to point density. The results are

only measured. Additionally, there is no understanding of how many factors are involved. Conversely, for the area that particular survey was carried out in, the manual results are more accurate than the automated method due to the use of surveyed values.

- *More efficient* - Manual measurements are required for every relevant MMS configuration and for every target type. Every input parameter would have to be tested. To standardise this process, the tests would have to be performed on the same test-route. Point density measurements would then have to be carried out for each survey and if an automated method could not be designed, this would lead to a largely manual, time consuming process.

- *Measuring 2D point density* - Systems like TerraScan from TerraSolid [TerraSolid, 2012b] provide a simple point density measurement tool. The size of the tool can be adjusted ($1m^2$, $5m^2$, etc.) and this is useful for point density measurements on a planar surface. Figure 2.14(a) displays this tool being used on the road surface. For a vertical target this tool is not applicable, as all of the points under the cursor are included in the point density measurement, even though they belong to different object planes. Figure 2.14(b) displays this tool being used on a pillar.

Geometric formulae versus Simulation - Applying an automated algorithm is also different to the simulation approach for a number of reasons:

- *More rigorous* - The proposed geometric solution explores each factor in detail, designs a method for calculating their contribution to point

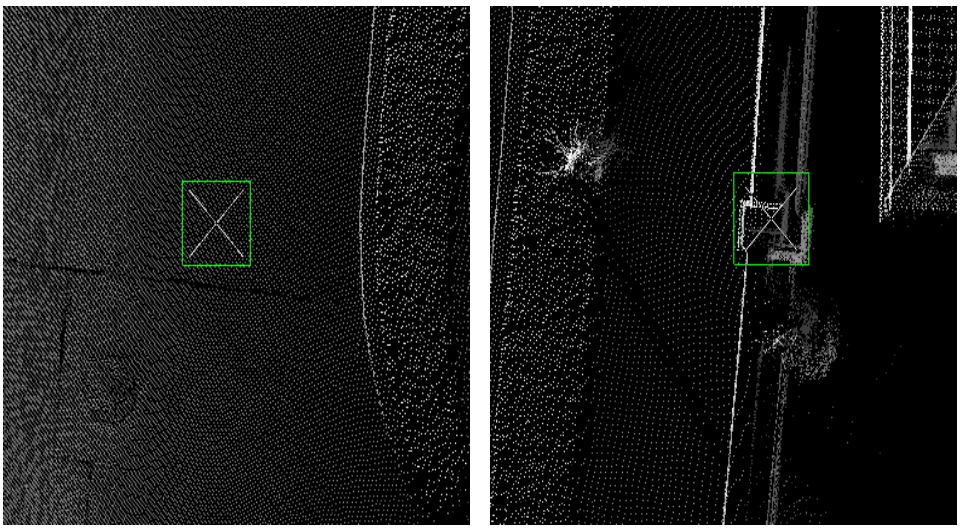

(a) (b)

Figure 2.14: TerraScan Point Density Calculation Tool (a) Flat Object - the Road (b) Vertical Object - a Pillar

density and then validates each in turn. Unlike a simulation, this ensures a thorough understanding of each factor rather than applying an iterative process and then measuring the variation.

- *Faster* - Simulators can be slow, although work is ongoing to improve the speed of these systems [Kim et al., 2011]. Once the simulation is finished, point density measurements are a manual process and are localised to one point on the target. Manual measurements have to be repeated for every area of interest. The solution proposed in this thesis provides measurements automatically across the entire target.

- *Obstructions* - By introducing objects that occlude other features into the simulator obstructions can be modelled. The calculation algorithm proposed in this thesis has not been designed to deal with obstructions.

- *Algorithm testing* - A simulator provides the user with a complete point

cloud for an area. This point cloud can be used to test automated extraction algorithms or object classification algorithms. This thesis is not designed to test algorithms but to provide information that should help tailor an algorithm in the early stages of development.

- *Optimised coverage* - Simulators model large areas whereas the focus of this thesis is on smaller objects, such as roadside infrastructure.

2.3 Objective 2 - Assessing MMS Parameters

The second objective of this thesis is to apply the point density calculation algorithm to assess the impact that the MMS parameters such as the scanner hardware settings and system configuration have on point density. Scanner hardware settings such as the PRR, mirror frequency and field of view (FOV) influence point density. The MMS configuration details the type, number, location and orientation of the scanner(s) on the vehicle. The tests developed to achieve this objective for both single scanner and dual scanner systems are explored in Chapter 6.

2.3.1 Type of scanner

MMS scanners have a variety of settings. Of these hardware settings, three have been identified as having a significant impact on point density. These are the scanners PRR, FOV and mirror frequency.

2.3.1.1 Pulse Repetition Rate

The first of the scanner parameters that must be incorporated is the PRR. PRR is a measure of how many pulses per second the scanner is capable of

emitting. In most scanners, the PRR is user selectable. Section 2.2 detailed the information for a Riegl scanner, but Riegl are only one scanner manufacturer and different scanners have different PRRs. This is an important factor for consideration when choosing the scanner for an MMS.

2.3.1.2 Mirror Frequency

The second scanner parameter which influences point density is the mirror frequency. Each mirror rotation creates a scan profile. The mirror frequency, in conjunction with the scanner rotations and the vehicle speed determine the profile spacing. Different scanners have different maximum mirror frequencies. It is important to identify whether it is better to have a high PRR or a high mirror speed. In other words - is it better to have a smaller spacing between profiles or between points? For example, Riegl's VQ250 has a higher PRR than its closest competitor, Optech's V200 (300kHz v 200kHz), but it has a lower mirror speed (100Hz v 200Hz). The trade-off between mirror frequency and PRR and the resulting impact on point density will be investigated in Chapter 7.

2.3.1.3 FOV

The final scanner parameter influencing the point density is the FOV. FOV impacts on the angular step width (ASW). The ASW of a scanner is the angular change between subsequent laser pulses. ASW is a programmable setting in laser scanners, but is dependant on the PRR, the mirror speed and the FOV of the scanner. The smaller the ASW, the smaller the point spacing and a smaller point spacing results in an increased point density. With certain scanners, the lowest ASW possible cannot be implemented if

the scanner is operating a full 360^o FOV.

2.3.2 Number of scanners

Multiple scanners result in a higher point density but they are costly not only in monetary terms but also in terms of data storage and processing time. Figure 2.15 displays Riegl's dual scanner VMX-450. An important research question that is answered in this thesis is whether it is possible to achieve a high level of detail with a single scanner, or one high quality scanner and one low quality scanner, or whether it is essential to use a high performance system similar to the one displayed in Figure 2.15.

Figure 2.15: Multiple Scanner - Riegl's VMX450 [RIEGL, 2011a]

2.3.3 Location of scanners

Commercial MMSs like StreetMapper [Hunter and Cox, 2010] and the Optech Lynx operate dual scanners. These scanners are genrally both located at the rear of the vehicle. One reason for picking this location is to ensure the body of the vehicle does not obstruct the scanners field of view. A series of tests

are designed to investigate whether placing both scanners on one side of the vehicle results in a higher point density than locating both at the rear of the vehicle. This thesis defines the recommended position for each scanner to maximise point density for near side infrastructure.

2.3.4 Orientation of scanners

Identifying the optimum scanner rotation is important, as systems like the XP1 that have a rigid mounting are not capable of introducing any change in scanner orientation. This also applies to systems like Riegl's VMX250 and VMX450 which are both housed in a rigid casing. This arrangement is not flexible and so companies like 3D Laser Mapping have designed a swivel mount, shown in Figure 2.16(a), which allows the surveyor to change the horizontal scanner rotation pre-survey. Alternatively a MMS using a TLS like the FARO scanner [Kukko et al., 2007] in profile mode can take advantage of the rotatable head to change the vertical angle of the scanner. Scanners on the Optech Lynx are also capable of changing their vertical orientation. This is due to another specially designed mount as displayed in Figure 2.16(b). The feature that facilitates the change in orientation is circled in red.

The scanner orientation on the XP1 is a 45^o horizontal and a 45^o vertical rotation. If the XP1 was a dual scanner system, one scanner would be rotated $+45^o$ horizontally to cover the left hand side of the vehicle, and the other rotated -45^o horizontally to cover the right hand side of the vehicle. This orientation also helps to capture the sides of objects that a single scanner system is unable to without multiple passes. This capability is one of the major benefits of a dual-scanner system. In Figure 2.10, the importance of a

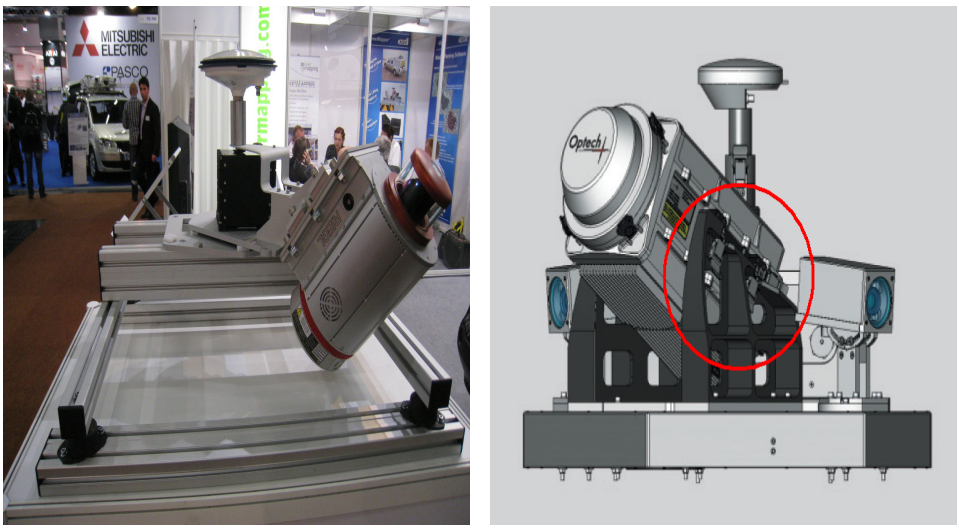

(a) (b)

Figure 2.16: Mounts Facilitating A Change in Scanner Orientation (a) 3D Laser Mapping - Mount Allows Change in Horizontal Orientation(b) Optech - Mount Allows Change in Vertical Orientation [Optech, 2012]

vertical rotation of the scanner for certain targets was illustrated. This thesis identifies the recommended scanner orientations for both single scanner and dual scanner systems when surveying roadside infrastructure.

2.3.5 Assessing MMS Parameters

The previous sections have identified the need for a series of tests to identify the recommended scanner configuration and scanner hardware settings when surveying specific targets. This section introduces the work to date, the proposed solution and provides justification for taking this approach.

2.3.5.1 Work to date

To date there has only been one study assessing MMS configuration in terms of its point density. [Yoo et al., 2009] applied their LiDAR simulation to iden-

tify the best scanner configuration to minimise occlusions and data shadows. In this simulation a multi-scanner MMS was modelled. [Yoo et al., 2009] investigated multiple configurations to minimise data shadows. Three laser scanners were modelled in this simulation. There does not appear to have been tests carried out to find the optimal configuration for a single scanner MMS. This simulation was limited to low-performance scanners. To date there has been no research carried out to identify the recommended configuration for a single scanner MMS. The current method for ensuring that a MMS produces a high point density is to overcompensate with scan hardware or to drive the route multiple times. This practice can result in more data being captured than necessary. This practice also results in increased survey and processing time and requires increased data storage space. Another popular method to ensure a high point density is for surveys to be carried out at a lower speed than is necessary [Goulette et al., 2006, Graefe, 2007a], which can impact on the productivity of a MMS. A third method is mission planning and Riegl's RiACQUIRE is an example of a software package that can be used for this.

2.3.5.2 Proposed Solution

This thesis applies a novel point density algorithm to a selection of scanner settings, orientations and locations. This algorithm identifies the optimum system configuration and hardware settings for specific targets. By focussing the work in this thesis on infrastructure on one side of the MMS only, the recommended configuration for a single scanner MMS is identified. Targets are represented by angled surfaces and cylinders. These tests are carried out for dual scanner and single scanner systems.

2.3.5.3 Justification

The proposed method for calculating point density allows for the contribution of each factor to be identified, modelled and a method of automatically calculating it to be designed. This facilitates a series of tests assessing system configuration. The previous tests carried out by [Yoo et al., 2009] employed a LiDAR simulation and were designed for large areas. The aim of these tests was primarily to assess the best configuration for minimising occlusions and data shadows. There was not a sufficient understanding of the effect of system configuration on point density. The point density tests carried out by [Yoo et al., 2009] were also limited to a general measure of point density for large areas. The tests in this thesis concentrated on calculating point density for features such as roadside infrastructure.

2.4 Objective 3 - Benchmarking MMS Point Density

The third and final objective of this thesis is to apply the point density calculation algorithm to benchmark a selection of MMSs. The systems chosen are a representative sample of scanner hardware currently on the market and this benchmarking process highlights each systems strengths and weaknesses for specific features. A selection of survey targets representing different types of infrastructure are selected and each MMS is tested against these targets.

2.4.1 Test Vehicles

The commercial MMS that is used for the benchmarking tests is the Lynx, designed by the Canadian firm Optech. This MMS was introduced in Section 1.6.4. Although there are numerous other commercial MMSs on the market that could be included in the benchmarking process, there are three reasons for limiting the benchmarking to this system:

- *Limited market* - Optech and Riegl are two of the most popular scanner manufacturers at the high end of the MMS market and are used in a wide range of MMSs. Trimble, a large survey manufacturer and potential competitor in the MMS market uses Riegl scanners in its MMS, the MX8 [Trimble, 2010].

- *Research limitations* - As explained in Section 1.7, this thesis does not incorporate absolute accuracy of the laser points. The navigation component of a MMS contributes greatly to the absolute accuracy of a survey and differs widely per system. However, it is not a major factor in calculating point density for MMSs. Therefore, there is no benefit in testing multiple systems if they all operate the same scanner.

- *Laser scanners only* - This thesis is limited to MMSs operating 2D circular TOF laser scanners and therefore image based MMSs are not included in the benchmarking test, thus eliminating a number of MMSs.

The remaining systems in the benchmarking tests are hypothetical versions of the XP1. The first MMS is designed to operate a single VQ-250 and a low performance scanner. It is referred to as the 'XP1+'. This facilitates comparison of a system like this against the best dual-scanner commercial

systems on the market. The other hypothetical MMS is the XP2. This MMS is designed with two VQ-250 scanners.

2.4.1.1 Optech Lynx

The dual scanner Optech Lynx, as shown in Figure 2.17, is a popular commercial MMS. There are a number of different versions of the Lynx. The version closest in performance to the dual scanner XP2 is the Optech Lynx operating two V200 scanners. This is the precursor of their latest system, the M1 [Optech, 2012]. The M1 is used in the validation tests in Objective 1.

Figure 2.17: Optech Lynx [Optech, 2012]

2.4.1.2 XP1+

The XP1+ is a hypothetical version of the XP1. It incorporates a high specification scanner, a Riegl VQ-250 [RIEGL, 2009b] and also a low specification scanner, a SICK LMS 221 [SICK, 2010]. The position and orientation of the scanners are determined using the recommended configuration identified in Objective 2. The extra SICK LMS 221 (Figure 2.18) is positioned in the recommended location and angled at the recommended horizontal and vertical

Figure 2.18: SICK LMS 221 [SICK, 2010]

rotation when surveying near side infrastructure.

2.4.1.3 XP2

The XP2 is also a hypothetical iteration of the XP1 and incorporates two Riegl VQ-250 scanners. Although similar to the Riegl VMX-250, there are distinct differences between the scanners in the VMX-250 and the two on-board the XP2. Firstly, the offset between the two scanners matches the offset between the scanners on the Optech Lynx. This ensures a standard location for each scanner in the benchmarking tests. Secondly, the orientation of the scanners adhere to the current XP1 orientation, rather than that of the VMX-250. Each configuration is explained in greater detail in Chapter 7.

2.4.2 Benchmarking

To the best of the author's knowledge, no study benchmarking the point density of different MMSs exists. Comparisons of MMSs have been limited to accuracy tests. This section details the relevant existing work and also the solution proposed in this thesis.

2.4.2.1 Work to Date

To date, comparison of different MMSs has been limited to tables listing MMS components [Barber et al., 2008, Ellum and El-Sheimy, 2002, Tao, 2000]. Alternatively, manufacturers specifications for a piece of hardware can be examined. There is no way to translate this information into an easily understandable comparison of different systems in terms of point density. Although manufacturers specifications give information on scanner hardware, the parameters detailed in Section 2.2 that impact on point density are not taken into account. The only concerted effort to benchmark MMSs has been in the field of accuracy. [Kaartinen et al., 2012] have undertaken benchmarking tests on four MMS to assess planimetric and elevation accuracy and have identified that with a properly calibrated high-end MMS, planimetric accuracies of approximately 0.02m are achievable. These tests did not investigate point density.

2.4.2.2 Proposed Solution

The proposed solution involves defining a number of targets representing real-world objects and calculating the point density for each MMS on those targets. The targets must correspond with valid input shapes to the point density calculation algorithm. Therefore the benchmarking tests are limited

to objects that can be constructed using multiple 2D planes.

2.4.2.3 Justification

Unlike Objectives 1 and 2, there has been no previous attempt at benchmarking a selection of MMSs in terms of their point density. Therefore it is not possible to demonstrate the advantages of the method proposed in this thesis over other methods. These benchmarking tests will be of benefit to the end user when purchasing a MMS and also to designers when assembling a MMS.

2.5 Conclusions

This chapter discussed and detailed point density for MMS surveys and the issues involved in calculating it. Point density was identified as an area of MMS performance that required further study. The existing work in this field was investigated and analysed and facilitated identification of the areas that require further study. This investigation provided the context for the three objectives described in this thesis.

The first objective is to design an efficient and accurate method to calculate point density. Current methods of calculating point density through surveys and manual measurements, limited geometric formulae or LiDAR simulations are not suitable. Manual measurements are difficult to implement and do not provide an understanding of the factors influencing point density. They are inefficient and also difficult to perform on 3D vertical features. Manual measurements do not enable a point density calculation. LiDAR simulations do not provide an understanding of the factors influenc-

ing point density and can be slow. LiDAR simulators do not enable a point density calculation. Existing geometric formulae for calculating point density are incomplete. Changes in scanner and target height or rotation are not incorporated. Point density is calculated at a single location on the target providing insufficient information on point spacing across a target. A novel solution to these problems involving 3D surface normals and 2D geometric formulae has been proposed and justified. The implementation and validation of this solution will be discussed in the following chapters.

The second objective of this thesis is to design a series of tests to assess MMS laser scanner configuration. There are many potential hardware configurations for MMSs. Further research is required to identify the recommended scanner position and orientation for single and dual scanner MMSs. These experiments require a method of calculating point density.

The final objective of this thesis is to benchmark a selection of MMSs in terms of their point density. No method exists for benchmarking the current generation of MMSs in terms of their point density. The development of a point density calculator enables the comparative assessment of MMSs in terms of their hardware settings and laser scanner configuration. These experiments also rely on the accurate calculation of point density.

In the next chapter the factors influencing point density will be investigated in greater detail. A methodology for calculating point density for a laser scanner on a MMS will be detailed.

Chapter 3

Mobile Mapping Point Density Calculator (MIMIC)

Calculating the point density of a target surveyed by a MMS equipped with a laser scanner is the first objective of this thesis. Section 2.2 investigated the fundamental elements influencing point density. This step is required before attempting to devise a comprehensive point density calculator. Contemporary research in the field of MMS point density was also explored in that section. Section 2.2.4.2 briefly introduced the solution proposed in this thesis. In this Chapter the challenges involved in calculating point density and the solutions will be explored in greater detail.

3.1 Introduction

This thesis proposes a new modelling approach to point density calculation. A prototpye system, the '**M**ob**I**le **M**apping point dens**I**ty **C**alculator' or 'MIMIC' is developed in the course of this thesis. Multiple variables

need to be considered when designing a system to calculate point density. MIMIC must be compatible with different scanner, vehicle and target variables. MIMIC comprises two main stages: variable input and point density calculation. Although the current version of MIMIC is limited to the input and point density calculation stages, data visualisation is a work in progress and is introduced in Section 8.3 as current work. The user input module and the calculation module are investigated in Section 3.3.

3.2 Point Density

The first objective of this thesis is to develop a methodology for determining the point density of point clouds collected by a MMS with respect to known objects at specified distances. In Section 2.2 the difficulty in calculating point density and the factors influencing it were introduced. In this section the three elements of the point density calculation are investigated. These three elements are the profile angle, the profile spacing and the point spacing. The vehicle, the scanner and the target all contribute to the resulting point density.

3.2.1 Overview

Calculating point density would be a trivial process if no external forces impacted on it. Figure 3.1(a) illustrates an example of a road sign and Figure 3.1(b) illustrates the resulting laser returns as the MMS passes it. In the hypothetical example illustrated in Figure 3.1(b), there is no change in profile angle (i.e. all profiles are vertical) and the point spacing and profile spacing are also constant. In this situation, calculating point density could

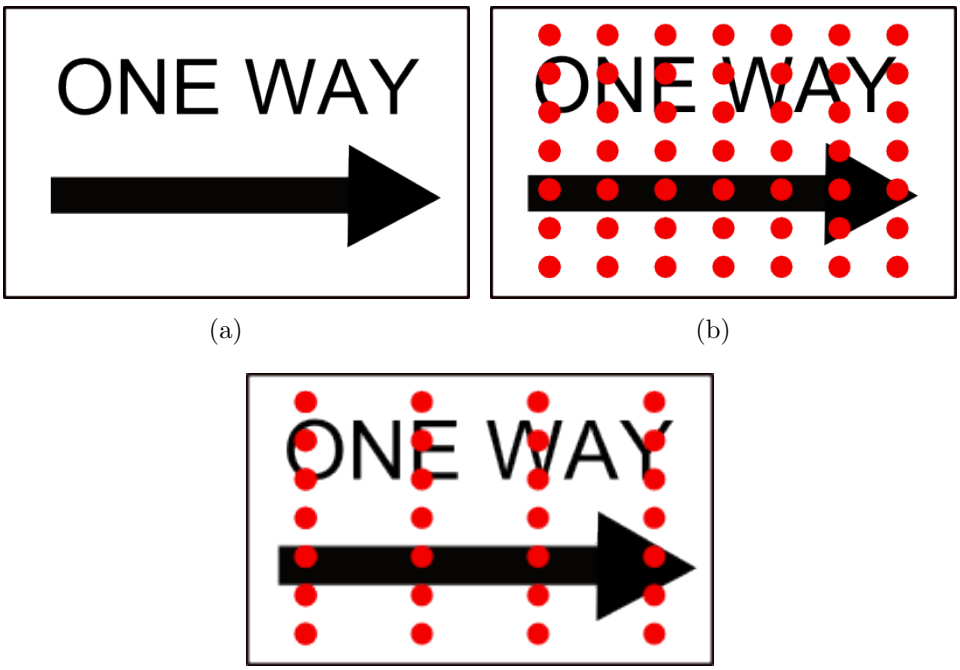

(a) (b)

(c)

Figure 3.1: Point Density (a) Sample Road Sign (b)Point Density Simplified and (c) Profile Spacing Increases with Vehicle Velocity

be found by simply dividing the target width by the profile spacing, and the target height by the point spacing. Then by multiplying these two values, the number of points on the target could be calculated. This situation is unlikely if not impossible in a real world scenario, as the properties of the vehicle, the scanner and the target all impact on the distribution of laser points.

3.2.2 Contributions of the Vehicle to Point Density

Two vehicle properties influence the point density of a target: the velocity of the vehicle and the rotational dynamics of the vehicle. Vehicle dynamics is the term applied in this thesis to refer to the roll, pitch and yaw of the vehicle

at one position. These three axes of rotation were illustrated in Figure 2.9. Vehicle velocity and dynamics contribute to the point density calculation in different ways. The elements of point density that are influenced by vehicle velocity and vehicle dynamics are shown in Table 3.1.

Table 3.1: Contribution of Vehicle Velocity and Dynamics

Attribute	Impacts on	Units
Vehicle velocity	Profile Spacing	m/s
Yaw	Profile Spacing	degrees
Roll	Profile Angle	degrees
Pitch	Profile Angle	degrees

3.2.2.1 Variations Arising from Vehicle Velocity

The velocity of the vehicle influences the distance between scan profiles, the profile spacing. An example of this effect can be seen in Figure 3.1(c) when it is compared to Figure 3.1(b). In this example the vehicle velocity has been increased. The resulting laser returns from the road sign are displayed in Figure 3.1(c). These examples demonstrate that a vehicle travelling at a higher velocity increases the spacing between scan profiles. Under normal survey conditions which exclude extreme vehicle vibrations, vehicle acceleration, deceleration or high vehicle velocity through road curves, the velocity of the vehicle does not have an impact on vehicle dynamics.

3.2.2.2 Variations Arising from Vehicle Dynamics

Roll, pitch and yaw are the three axes of movement of the vehicle. Figures 3.2 and 3.3 illustrate the effect of yaw on profile spacing. When the MMS turns towards a target, as illustrated in Figure 3.2(a), the profile spacing is decreased, as illustrated in Figure 3.2(b). When the MMS turns away from

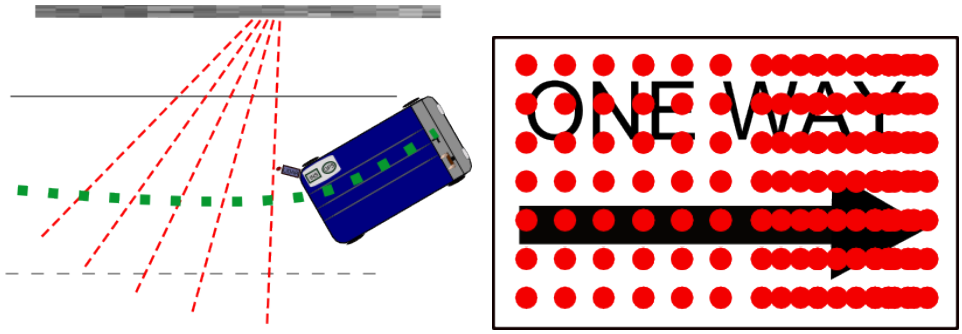

(a) (b)

Figure 3.2: Influence of Yaw on Profile Spacing (a) MMS Turning Towards the Target and (b) Profile Spacing Decreases

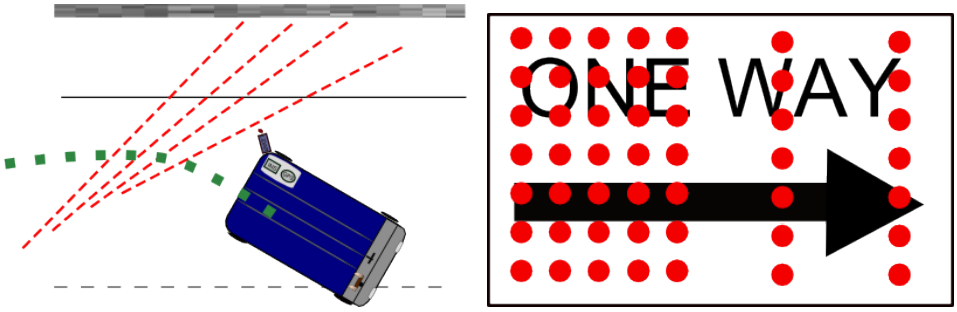

(a) (b)

Figure 3.3: Influence of Yaw on Profile Spacing (a) MMS Turning Away From the Target and (b) Profile Spacing Increases

a target, as illustrated in Figure 3.3(a), the profile spacing is increased, as illustrated in Figure 3.3(b). In this thesis one of the research assumptions is that there is zero course deviation while surveying a target. However, a vehicle will always display a slight heading deviation and therefore this is a potential error source when validating the calculated profile spacing with measurements from point clouds.

Roll is an action that occurs around the longitudinal axis of the vehicle and is the second axis of rotation of the vehicle. Roll is potentially the

most common error source that the vehicle dynamics contribute to the point density calculation. This is because roads are constructed with a cross-fall or gradient to allow for rain water to drain off their surface. This cross-fall means that in the majority of cases the MMS is not on a perfectly horizontal surface. Figure 3.4(a) illustrates the effect that any roll of the vehicle has on the the angle the scan plane intersects with the building. Roll is a potential error source in the profile angle calculations. Figure 3.4(c) illustrates the effect that roll has on subsequent scan profiles.

Pitch is an action that occurs around the lateral axis of the vehicle and is the final axis of rotation of the vehicle. The effect of pitch on point density is less common as the road surface is generally flat and the majority of roadside infrastructure are on the same plane as the vehicle. Therefore the pitch will not change in the short space of time it takes for the vehicle to pass the target. However, if pitch is present it will alter the profile angle as depicted in Figure 3.4(b) and would have the same effect as roll as illustrated in Figure 3.4(c). Pitch is a possible error source as any pitch of the vehicle will impact on profile angle and therefore point density.

One of the assumptions of this thesis is that there is no course deviation (i.e. yaw), or any variation in the roll and pitch of the vehicle while surveying a target. This is a limitation of MIMIC, as the algorithm is unable to predict the point density of objects in areas of road curvature, on road cross-falls or on road gradients accurately. This could potentially be applied in future work. Therefore in this thesis yaw, roll and pitch are not included in the calculations, but are noted and examined as possible error sources.

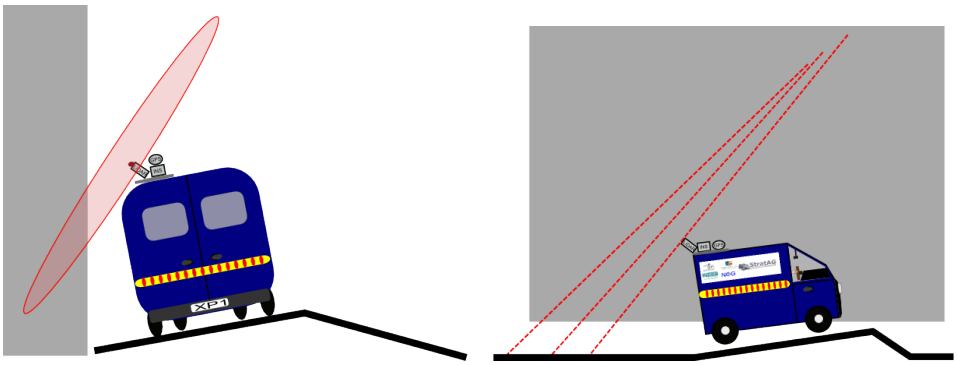

(a) (b)

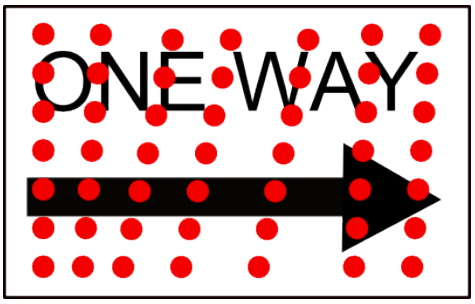

(c)

Figure 3.4: Change in Profile Angle (a) Roll (b) Pitch and (c) Example of Profile Angle Change Arising from Roll or Pitch

Table 3.2: Contribution of Scanner Properties

Attribute	Impacts on	Units
Field Of View	Profile/Point Spacing	degrees
Horizontal Rotation	Profile Angle/Point Spacing	degrees
Vertical Rotation	Profile Angle/Point Spacing	degrees
Pulse Repetition Rate	Point Spacing	kHz
Mirror Rotation velocity	Profile Spacing	Hz
Number Of Scanners	Point Density	n/a
Scanner Elevation	Point Spacing	m
Second Scanner Offset	Point Spacing	m

3.2.3 Contribution of Scanner Properties to Point Density

Of the three inputs into the MIMIC system, the laser scanner has the largest number of contributory elements that must be incorporated. These are: the FOV, the PRR, the mirror frequency, the scanners horizontal and vertical rotations, the number of scanners, the offset to any additional scanners and the scanner elevation. Table 3.2 lists each of these elements and defines which properties of point density they impact. As one of the objectives of this thesis is to calculate point density from 2D scanners (both full circle and limited FOV) the impact of the FOV is first explored.

3.2.3.1 Field of View

Incorporating a scanner with a wide FOV on a MMS is important in enabling the MMS to capture as much of the environment as possible. The scanner on the XP1 is a full-circle scanner (a 360 ^{o} FOV). However, this is user selectable and the FOV can be restricted for specialised surveys. For example, if the MMS was surveying a specific feature like road markings, the operators could restrict the FOV to a setting that captured the road surface

only. This would eliminate the points above and around the vehicle, reduce data volume and speed up the subsequent processing. It would also minimise file sizes, while maximising point density in the area of interest. A similar process could be applied for a survey concentrating on overhead power lines but with the FOV restricted to an arc over the vehicle.

Operating a scanner with a 360^o FOV has a number of drawbacks. It results in increased storage requirements and processing time. Allowing a scanner to operate in full circle mode also increases the ASW. ASW is the angular change between subsequent laser pulses and is one of the most significant factors in calculating point spacing. For example, if the VQ250 were to carry out a localised scan and operate with a restricted 30^o FOV, as illustrated in Figure 3.5(a), it could operate using the smallest ASW that this scanner is capable of, 0.018^o [RIEGL, 2009b]. This is not possible with the 360^o FOV, as illustrated in Figure 3.5(b) because the scanner is constrained by the PRR. The highest number of pulses possible from the VQ-250 is 300,000 points per second (300kHz). At 100 mirror rotations per second this is 3,000 pulses per mirror rotation. An ASW of 0.018^o for a 360^o scan would require a PRR of 2,000,000 points per second (2MHz). This highlights the trade off between FOV and ASW. The smallest ASW that the VQ-250 is capable of for a full 360^o scan at the highest mirror frequency and PRR is 0.12^o. The maximum FOV that can be employed using the smallest ASW of 0.018^o is 54^o. The minimum ASW is hardware specific.

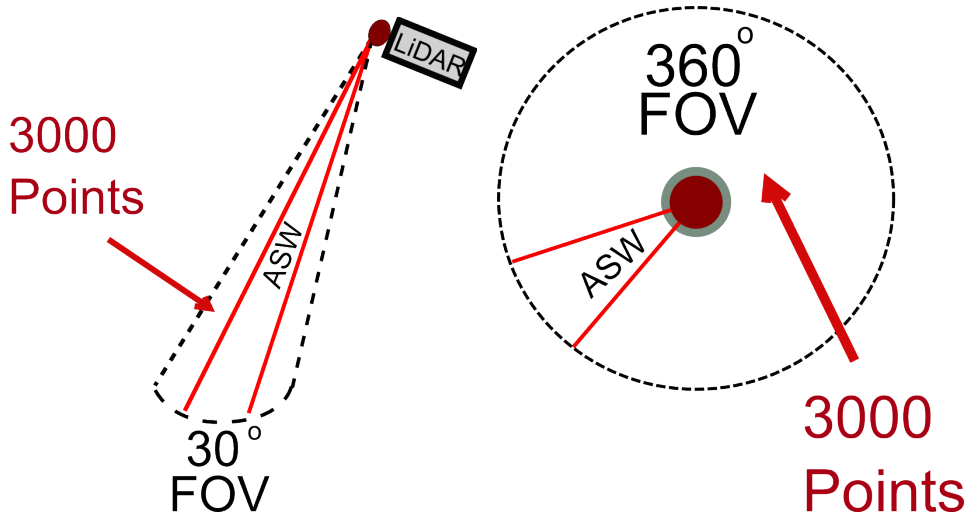

(a) (b)

Figure 3.5: Laser Scanner FOV (a) Limited to 30^o FOV and (b) Unlimited 360^o FOV

3.2.3.2 Pulse Repetition Rate

Another important factor in calculating point density is the PRR. There is a strong correlation between point density and PRR. The current generation of scanners are capable of PRRs in excess of 500kHz [RIEGL, 2011b]. MIMIC is designed to work with different scanner hardware and therefore incorporating PRR into the point density calculation is essential.

3.2.3.3 Mirror Frequency

Mirror frequency controls the number of profiles per second. This has a major impact on profile spacing as displayed for vehicle velocity in Figure 3.1(c). Section 3.2.3.1 demonstrated how mirror frequency also affects the ASW and therefore the point spacing. The mirror frequency and the number of pulses per mirror rotation are linked.

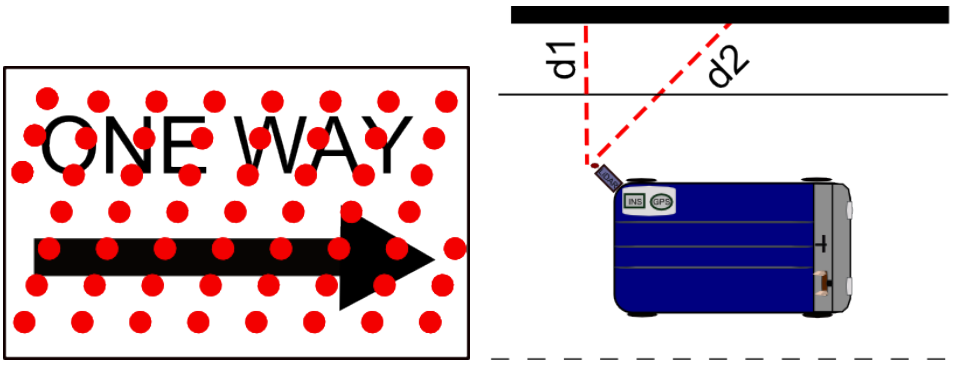

(a) (b)

Figure 3.6: Scanner Orientation (a) a Vertical Rotation of the Scanner Changes the Profile Angle and (b) a Horizontal Rotation Increases Measurement Range

3.2.3.4 Scanner Orientation

Scanner orientation affects point spacing, profile angle and profile spacing. It is therefore vital to include this in any point density calculation. Figure 3.6(a) is an example of a profile on a vertical surface after a vertical scanner rotation has been introduced. Introducing a horizontal rotation of the scanner into the system impacts on measurement range as displayed in Figure 3.6(b). In this scenario, an introduction of a horizontal rotation of the scanner results in an increased range to target (d1 before rotation, d2 after).

3.2.3.5 Number and Position of Scanners

Increasing the number of scanners increases the point density. It is not practical or desirable to have two scanners occupying the same position on a MMS or scanning the exact same area around the MMS. In practice a second scanner is employed to survey objects that are not visible to the first scanner. Figure 3.7(a) is an example of the scanning pattern that is popular amongst the majority of dual scanner MMSs on the market. The point spacing on

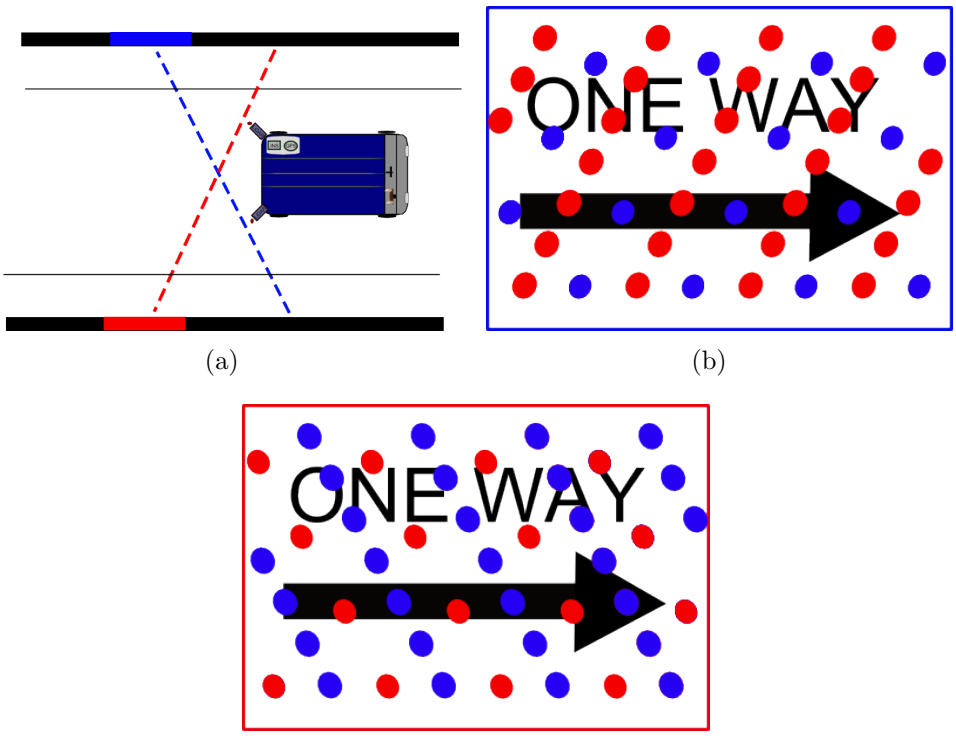

(a) (b)

(c)

Figure 3.7: Multiple Scanners (a) Dual Scanner System (b) Vertical Surface (Blue) (c) Vertical Surface (Red)

near side objects from the second scanner is significantly greater (blue points) than the first scanner (red points), leading to a reduced point density. Figure 3.7(b) illustrates this for near side objects and far side objects are displayed in Figure 3.7(c). The elevation of the scanner also effects point density. If an elevation difference exists between scanner and target this will result in an increased range from the scanner to the target. Point spacing increases as the range to the target increases.

3.2.4 Contribution of Target Parameters to Point Density

The target's range, dimensions, elevation and orientation all contribute to point density and must be included in the point density calculation. The calculations in this thesis utilise 2D geometric formulae, and therefore all targets in this thesis are represented by planar surfaces. Targets can be vertical surfaces such as walls or buildings and horizontal surfaces such as the road underneath the vehicle. Inclined structures represent road side embankments or rooftops. Targets can be rotated horizontally, inclined vertically or a combination of both. Curved or multi-faced targets that can be approximated using planes are also a valid type. Target types are discussed in greater detail in Section 3.3.2. Table 3.3 lists each of the target parameters involved in the point density calculation and what element of point density each impacts on.

Table 3.3: Contribution of Target Parameters

Attribute	Impacts on	Units
Horizontal Rotation	Profile/Point Spacing	degrees
Vertical Rotation	Point Spacing	degrees
Range	Point Spacing	m
Base Elevation	Point Spacing	m
Height	Point Spacing	m

3.2.4.1 Range to Target

The range to the target is an important factor in the point density calculations. Point spacing increases with range and therefore a target at 5m range exhibits a higher point density than one at 10m. Figure 3.8 illustrates the effect of range on point spacing for two laser pulses, p1 and p2. At range

r1, the point spacing (d1) on Target 1 is smaller than the point spacing (d2) on Target 2 at range r2. Scanner rotations and target rotations also alter the measurement range and therefore further influence variations in point spacing across the target.

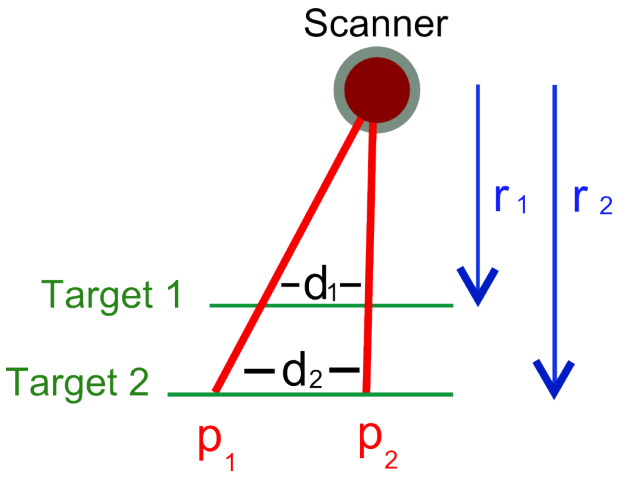

Figure 3.8: Effect of Range on Point Spacing for Two Subsequent Laser Pulses

3.2.4.2 Target Dimensions

The dimensions of the target influence the number of laser pulses striking it. The larger the target, the higher the point density, assuming the target is within the FOV of the scanner as the MMS passes by. However, the higher the target, the further the measurement range when it is first within the FOV of the scanner as Figure 3.9 illustrates. The range when the target is first surveyed by any of the laser pulses is shown as d1 in Figure 3.9. As the MMS approaches the target the range decreases (d2 - d4) and therefore the point spacing also decreases. This highlights one of the major shortcomings of existing methods that provide point density calculated from the centre of a target only as the point spacing varies over a target.

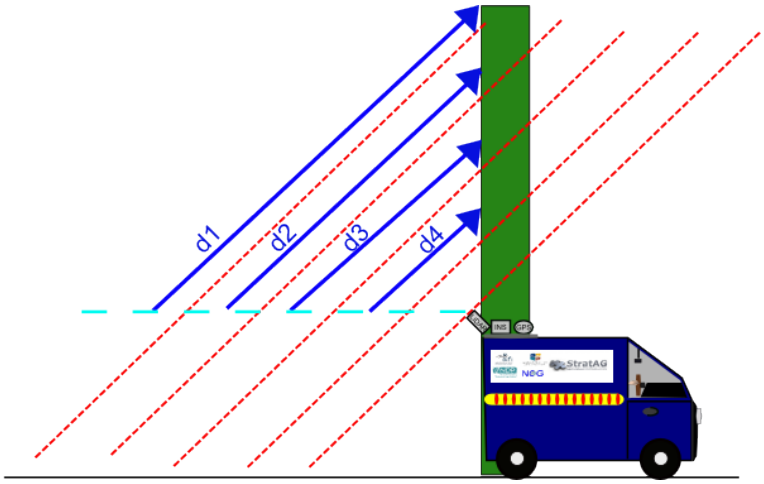

Figure 3.9: The Correlation Between Target Height and Range to the Target for a MMS Operating a 2D Laser Scanner

3.2.4.3 Target Orientation

The orientation of the target influences profile angle, profile spacing and point spacing. Real world features are rarely parallel with the direction of travel. A horizontal target rotation and a vertical target rotation are illustrated in Figures 3.10(a) and 3.11(a) respectively. The range is increased to one side of the target following a horizontal rotation of the target but decreased to the other. This results in an uneven point spacing on the target as shown in Figure 3.10(b). Similarly with a vertical rotation of the target there is a difference in point spacing between the bottom and the top of the target depending on which way it is rotated as illustrated in Figure 3.11(b).

3.2.4.4 Target Elevation

The base elevation of the target and the height of the target affect point spacing in a similar manner to the height of the scanner. A height difference

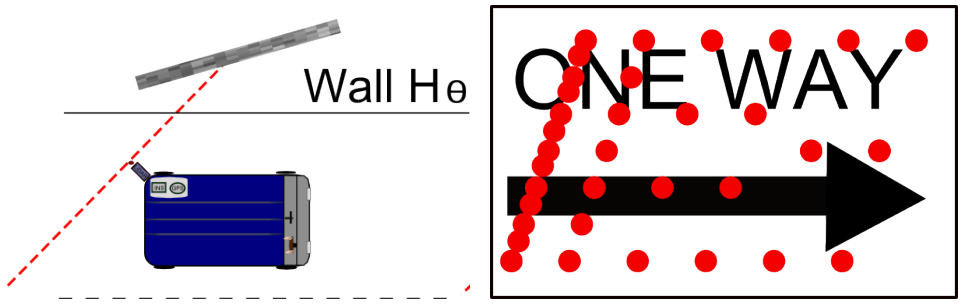

(a) (b)

Figure 3.10: Target Rotations (a) a Horizontal Target Rotation (b) Point Spacing Increases at Far End of the Target

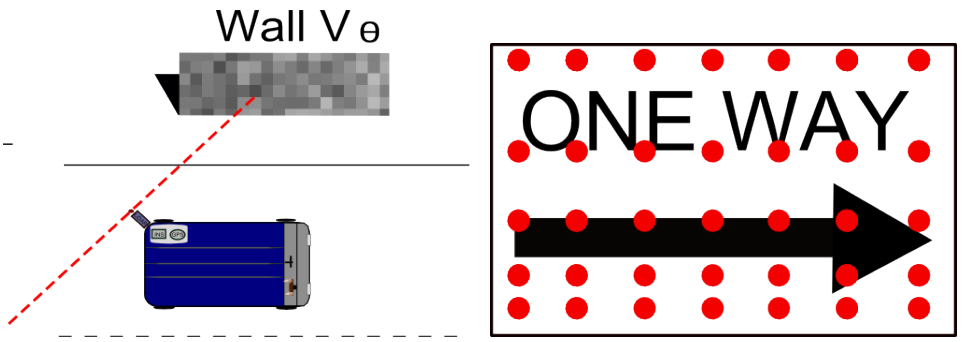

(a) (b)

Figure 3.11: Target Rotations (a) a Vertical Target Rotation (b) Point Spacing Increases at Top of the Target

between target and scanner increases or decreases point spacing depending on whether the range to the target increases or decreases and is included in the point density calculations.

3.3 Calculation Procedure

Section 3.2 explains the necessity for MIMIC to incorporate scanner, target and vehicle input parameters and to combine these to calculate point density. MIMIC requires the user to input these parameters. This section details the procedures that have been implemented in MIMIC in order to perform the point density calculations.

3.3.1 Input Module

MIMIC requires a user to provide details regarding the scanner hardware, the survey vehicle and the target parameters as illustrated in Figure 3.12. This section details the required information. This information is not required to be input in a particular order, however, adhering to the order that the topics were introduced in the previous sections the first set of input variables are the vehicle parameters.

3.3.1.1 Vehicle Parameters

To properly define the behaviour of a MMS, a number of attributes must be specified. These attributes are listed in Table 3.1. The first attribute is vehicle velocity and is entered as km/h. However, it is required in m/s in the calculation stage and therefore must be converted. As explained in Section 3.2.2.1 vehicle velocity is one of the major factors impacting on profile

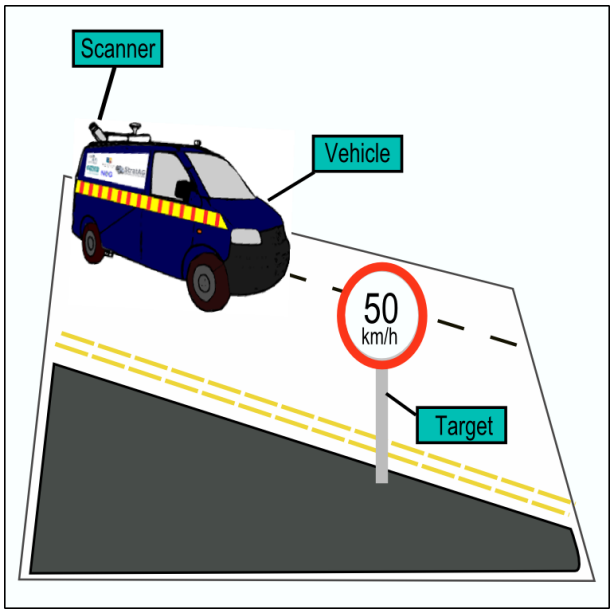

Figure 3.12: System Inputs

spacing.

3.3.1.2 Scanner Parameters

MIMIC is designed to function with any of the current generation of 2D TOF scanners. To calculate point density for this type of scanner a number of attributes must be specified by the user. MIMIC is also designed to incorporate horizontal and vertical rotations of the scanner. Calculating the ASW was explained in Section 3.2.3.3. To accommodate dual scanner systems such as Riegl's VMX-250, the number of scanners must also be specified. The offset to the second scanner from the first scanner and the scanner elevation must also be specified by the user. This offset is used is to quantify the range difference between the first and second scanner. These variables are required for each additional scanner on the MMS.

3.3.1.3 Target Parameters

A target has five definable attributes, as listed in Table 3.3, that influence point density. Horizontal and vertical target rotations allow for representation of angled surfaces. Combinations of horizontal and vertical target rotations can also be applied. In this thesis, the term 'angled surface' is used to refer to any surface that is not parallel with a face of the MMS. Horizontal range to the target from the scanner must be specified. This is then converted into the true range to the target and is dependant on the scanner's horizontal and vertical rotations. Using the offset to the second scanner, the range from the target to the second scanner is calculated. Section 5.2.2.1 will explain this in more detail. The height of the target and its base elevation are specified. Finally, the dimensions of the target are defined.

3.3.2 Calculation Module

The calculation module of MIMIC provides the user with three outputs for a 2D plane. These are: the point spacing, the profile angle and the profile spacing. However, as has already been stated in this thesis, calculating the point spacing at a single central target location does not provide an accurate representation of the point density, particularly on large, angled surfaces. To improve on existing methods MIMIC calculates point spacing at a number of locations across the target. These are then combined with the profile spacing and profile angle information that MIMIC calculates to provide a measure of the overall point density. The following sections detail these steps and Figure 3.13 illustrates this workflow.

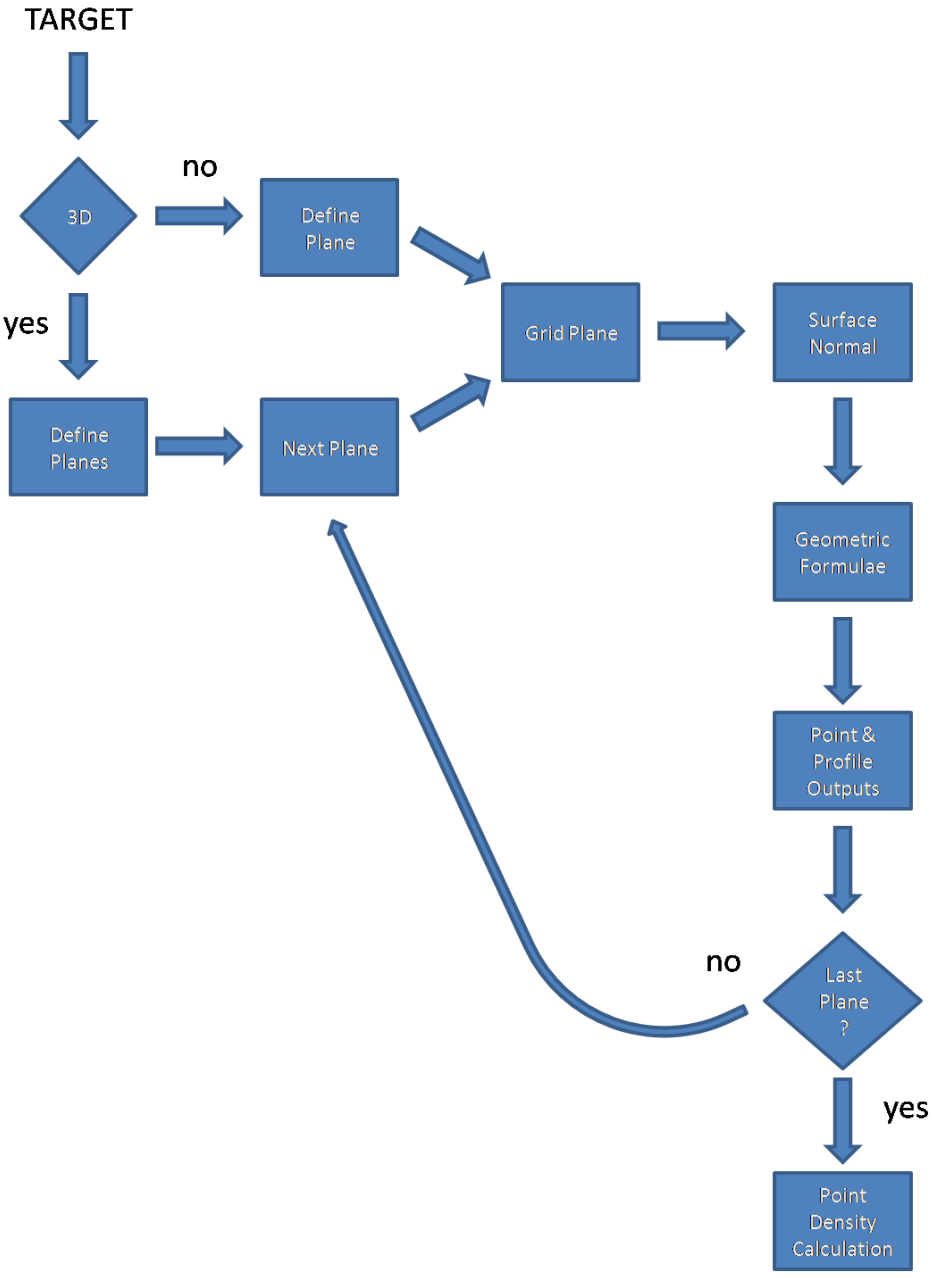

Figure 3.13: MIMIC Calculation Module Workflow

3.3.2.1 Planar Interaction

For MIMIC to calculate point density on a target it must be possible to approximate the target as a plane or as a series of planes. MIMIC only accepts 2D TOF scanners as a valid scanner input, due to their prevalence in commercial MMSs. MIMIC then treats each mirror rotation as a plane. This plane is referred to as the 'scan plane' in this thesis. Figure 3.14(a) illlustrates this in its most basic form. In this image the wall represents one plane and the 360^o scanner rotation represents another plane. One factor that influences planar interaction is the orientation of the target, as illustrated in Figure 3.14(b), which is free to rotate around three axes. This complicates the calculation procedure and additional information is therefore required for each plane to facilitate the point density calculation. MIMIC employs the principle of 3D surface normals to model these rotations. Surface normals are discussed in greater detail in Section 3.3.2.3.

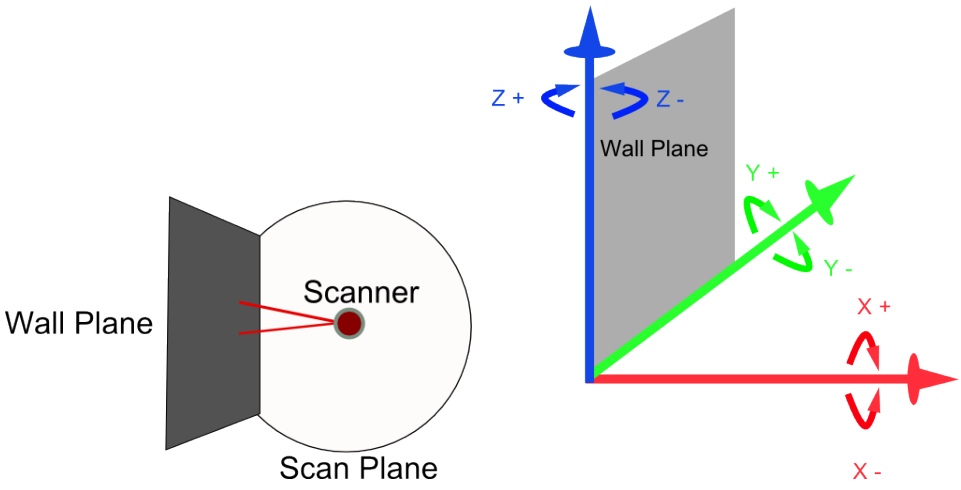

(a) (b)

Figure 3.14: Planar Interaction (a) Scan Plane Intersecting with Wall and Plane (b) All Planes are Free to Rotate Around their Axes

3.3.2.2 2D and 3D Objects

To simplify the point density calculations, MIMIC applies 3D surface normals and 2D geometrical formulae to 2D targets. MIMIC accepts 2D primitives as illustrated in Figure 3.15(a) as valid target types. Complicated objects like cylindrical targets are deconstructed into a series of 2D planes, as illustrated in Figure 3.15(b). In this image, a cross-section of a cylinder is shown. This cylinder is deconstructed into a series of 2D surfaces similar to the object shown on the right hand side of Figure 3.15(a). How point density is calculated for different target types is explained in greater detail in Section 5.3. It is important to note that the number of planes that are used in the calculation is dependant on the number of scanners and the scanner configuration. Depending on the scanner orientation, a single scanner system like the XP1 may only obtain laser returns from Faces (i) and (ii) of the cylinder illustrated in Figure 3.15(b). A dual-scanner system may obtain returns from Faces (i) to (iii) . It is impossible for any scanner configuration to capture Faces (i) - (vi) of a multi-faced object without driving 360^o around it.

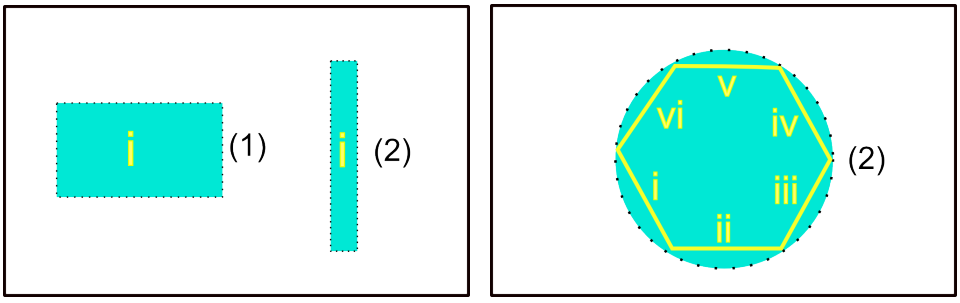

(a) (b)

Figure 3.15: Valid Targets (a) Planes (a single surface) and (b) A Cylinder Cross-Section (the Cylinder is Deconstructed into Multiple Planar Surfaces)

3.3.2.3 Surface Normals

Each target plane is free to rotate around three axes, although Chapter 4 will illustrate that defining only two rotations are required for 3D targets. The scanner is also free to rotate in three axes, but the full circle 2D plane is the third axis of rotation and therefore defining the rotation around this third axis is not required. To calculate the orientation of each plane the geometric principle of surface normals from computer graphics [Foley et al., 1995] is applied, whereby a surface normal is calculated for each plane. A plane's surface normal is the vector perpendicular to it. Figure 3.16 illustrates a surface normal for a vertical and horizontal surface respectively. Calculating point density on surfaces is further complicated as the surface is free to rotate around any axis (Figure 3.17(a)). This requires the inclusion of three-dimensional surface normals to take account of all potential plane orientations. Through application of 3D rotation matrices the surface normal for the rotated scan and target plane can be calculated.

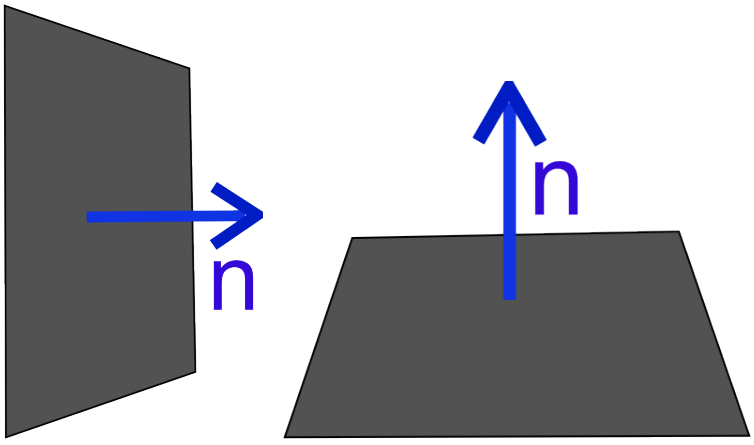

Figure 3.16: Surface Normals 'n' on (a) a Vertical Surface and (b) a Horizontal Surface

Figure 3.17(b) illustrates the 3D normals involved in the point density calculation. MIMIC represents each plane with a 1×3 matrix. For example, in the coordinate system displayed in Figure 3.17(b) the surface normal of the vertical wall (N_v) parallel to the direction of travel is directly to the right along the x axis, [1, 0, 0] and the road surface normal (N_h) is vertically upwards, along the z axis, [0, 0, 1]. The surface normal of a rotated scan plane or target plane is found by applying the user specified vertical and horizontal rotations of the scanner to the following rotation matrices

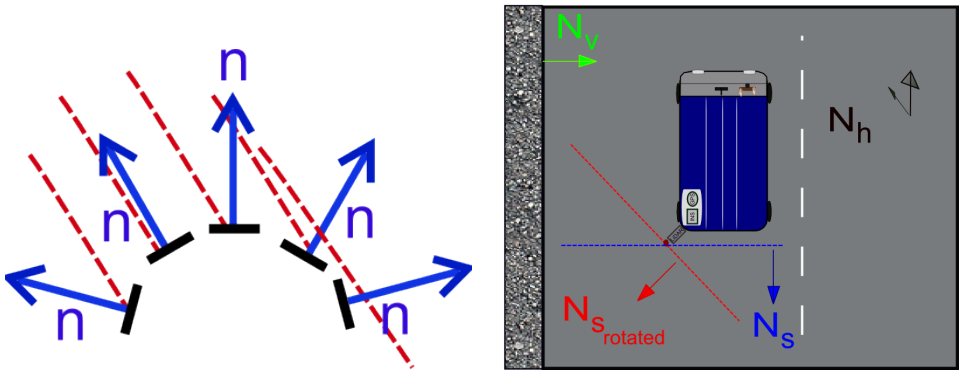

(a) (b)

Figure 3.17: Surface Normals (a) Surfaces are Free to Rotate (b) Normals Involved in Calculation

$$R_x(\theta) = \begin{bmatrix} 1 & 0 & 0 \\ 0 & \cos\theta & -\sin\theta \\ 0 & \sin\theta & \cos\theta \end{bmatrix} \tag{3.1}$$

$$R_y(\theta) = \begin{bmatrix} \cos\theta & 0 & \sin\theta \\ 0 & 1 & 0 \\ -\sin\theta & 0 & \cos\theta \end{bmatrix} \tag{3.2}$$

$$R_z(\theta) = \begin{bmatrix} \cos\theta & -\sin\theta & 0 \\ \sin\theta & \cos\theta & 0 \\ 0 & 0 & 1 \end{bmatrix} \tag{3.3}$$

Multiplying the three rotation matrices creates a 3D rotation matrix. By applying this rotation matrix to the scan plane, the surface normal of the rotated scan plane, $N_{S_{rotated}}$ can be calculated. This procedure will be discussed in greater detail in Chapter 4.

3.3.2.4 Grids

MIMICs calculation module returns a point spacing output for each input plane. As already identified in Section 2.2.4.1, one of the shortcomings of existing calculation methods is that point spacing is only calculated at a single target point. This is not an accurate approach to calculating point density, particularly when a rotation of the target can result in a wide variation in point spacing across the target. The solution proposed in this thesis is to apply a grid structure to the target. Point spacing is then calculated at each grid cell centre. The number of cells in the grid structure are user-specified at the input stage when defining the target. MIMIC currently operates a 4 cell grid (2x2), a 16 cell grid (4x4) and a 64 cell grid (8x8), as illustrated in Figure 3.18. The size of each grid cell varies by target size and also the number of grid cells. Increasing the number of grid cells increases the number of measurements and also increases the accuracy of the final result.

For small targets, there is no significant change in point spacing over the target and therefore increasing the number of grid cells offers little advan-

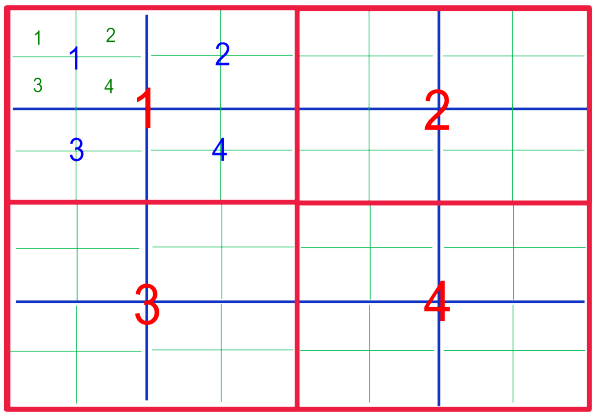

Figure 3.18: MIMIC's Grid Structure

tage. The correct selection of the number of grid cells is dependant on several factors, such as target size, range and rotation. The more grid cells, the more accurate the final result. After applying target rotations the range to each grid cell centre is found and the point spacing is then calculated for each grid cell centre.

MIMIC does not require square grid cells. Depending on the target dimensions the cells can be rectangular or stretched vertically or horizontally. Narrow vertical structures require a different grid structure than the structure displayed in Figure 3.18. This structure will be investigated in Chapter 5. The current version of MIMIC does not allow for user specified grid cell sizes however this could be explored for future work. Applying a grid structure to a target has the advantage of speeding up and simplifying the calculation process. This method is an improvement when compared to calculating the point spacing for every laser pulse individually or running a simulation (as mentioned in Section 2.2.4), but it is potentially not as accurate. The optimum number of grid cells necessary to provide an accurate representation of

the target will be dealt with in Section 5.4.1.

3.3.2.5 Application of Geometric Formulae

After the target is converted into a series of planes and surface normals, geometric formulae are used to calculate the angle of intersection between these planes. This angle of intersection is used to calculate the profile angle and profile spacing. Due to the research assumptions relating to vehicle velocity and vehicle dynamics listed in Chapter 1, profile angle and profile spacing do not vary over the target and are therefore only calculated once per plane. Combining these values with the point spacing for each grid cell on the target allows the point density to be calculated. The formulae employed in these calculations will be explained and verified in Chapter 4.

3.3.2.6 Calculating Point Density

To calculate point density for a gridded target, MIMIC takes the information on profile angle and profile spacing and traces scan profiles through each 2D grid cell in the form of 2D lines. It records every grid square that the scan profile passes through and calculates the length of the scan profile that has passed through that cell. Figure 3.19 illustrates this for a scan profile drawn in red on a rectangular target. Each blue rectangle represents a grid cell that the scan profile has passed through, even if only partially. The number of points can then be calculated for that scan profile using the grid cell's point spacing and the length of the scan profile inside that grid cell. The process is repeated for each scan profile, offset by the profile spacing, until the model is computed across the entire target surface. Point density is calculated using the point spacing for each grid square, the number of profiles passing through

that grid square and the length of each scan profile in that grid cell. Point density is then returned for each grid cell and summed to obtain the point density for the entire target.

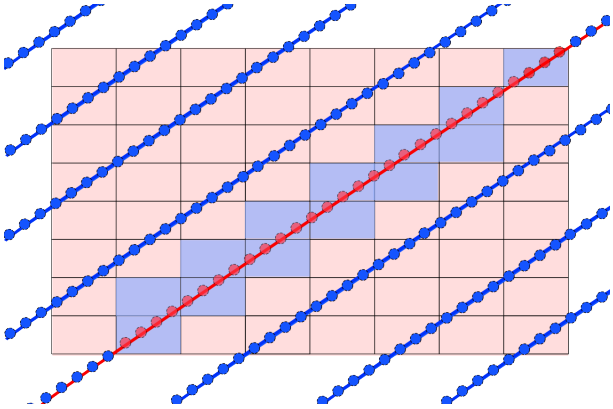

Figure 3.19: Calculating Point Density for Each Grid Cell

3.4 Conclusions

In this chapter each of the factors that influence point density have been identified and examined. Point density is influenced by the scanner, its hardware and configuration. The point density is also influenced by the target's position, orientation and dimensions. The final factor influencing point density is vehicle velocity and vehicle dynamics. The system for calculating point density, MIMIC, was introduced in this chapter. The current version of MIMIC comprises a data input stage and a calculation stage.

In the input stage, the user defines the scanner, target and vehicle parameters. This is followed by the calculation stage. MIMIC calculates three outputs using 3D surface normals and 2D geometric formulae. These outputs are defined as the profile angle, the profile spacing and the point spacing.

These three outputs describe and define the distribution of laser points on the target. Profile angle is the angle of the scan profile on the target in relation to the base of the target. Profile spacing relates to the distance between sequential scan profiles on the target. Point spacing refers to the distance between subsequent points on that scan profile. These outputs are then combined into a value for the total number of points on a target by gridding the target into cells and counting the number of scan profiles and points in each grid cell. The method for calculating point density will be detailed in Chapter 5.

In the next chapter the formula for calculating profile angle, profile spacing and point spacing for different target types will be detaild and validated using 3D models and point cloud data.

Chapter 4

Calculating Profile Information and Point Spacing

The first objective of this thesis is to design an algorithm for calculating the point density of a target surveyed using a MMS. This calculation requires multiple variables from the three components influencing point density; the vehicle, the target and the scanner. The method for calculating point density, MIMIC, was introduced in the previous chapter. This chapter explains the 3D surface normals and 2D geometric formulae that MIMIC employs to calculate profile information and point spacing. The tests applied to validate these formulae are described.

4.1 Introduction

MIMIC applies a combination of 3D surface normals and 2D geometric formulae to calculate the point density of an object. This process was introduced in Section 3.3.2. The outputs from these formulae were profile spacing, profile

angle and point spacing. The method for calculating these values for horizontal, vertical and angled surfaces is detailed in this chapter. The formulae for calculating profile angle are discussed in Section 4.2.1, for calculating profile spacing in Section 4.2.2 and for point spacing in Section 4.3. Testing and validation are detailed in Section 4.4 and the results are discussed. Potential error sources are identified in Section 4.4.

4.2 Calculating Profile Information

The profile angle and profile spacing are required to calculated point density. The profile angle and profile spacing are influenced by the scanner orientation, the target orientation, the mirror frequency and the vehicle velocity. In the following sections the methods for calculating profile angle and profile spacing are explained.

4.2.1 Profile Angle

When a laser scanner operating a rotating mirror is mounted on a moving platform, the forward motion of that platform creates individual scan profiles for each mirror rotation. Rotations of the scanner in the horizontal or vertical axis change the angle of the scan profiles on horizontal and vertical surfaces. These rotations alter the profile spacing and ultimately point density. In this section the method for calculating the angular effect that dual axis scanner rotations and angled surfaces have on sequential profiles is detailed. This angle is termed the profile angle, and is referred to in this chapter as $\theta_{Pr\mathrm{A}}$. $\theta_{Pr\mathrm{A}}$ is an important factor in calculating the profile spacing and hence the point density for all objects.

4.2.1.1 Horizontal Surface

Assuming the ground is a planar horizontal surface relative to the vehicle, the calculation of $\theta_{P_r\mathrm{A}}$ is trivial, as explained in Chapter 3. In this scenario, $\theta_{P_r\mathrm{A}}$ is equal to the horizontal rotation of the laser scanner on the MMS. However, both vehicle dynamics and the cross-fall of the road influence $\theta_{P_r\mathrm{A}}$, but as explained in Section 3.2.2.2, these two factors have not been included in this thesis. The correlation between the horizontal scanner rotation and $\theta_{P_r\mathrm{A}}$ is investigated in Section 4.4.1.2.

4.2.1.2 Vertical Plane

$\theta_{P_r\mathrm{A}}$ on vertical structures is important for two reasons. The first reason is ensuring optimal scan profile coverage on narrow vertical structures, as illustrated in Figure 2.10. The second reason is its significance in the calculation of point density on real world objects. To calculate $\theta_{P_r\mathrm{A}}$ for vertical surfaces MIMIC employs 3D rotation matrices and 2D geometric formulae. Section 3.3.2.3 introduced the three rotation matrices, R_x, R_y and R_z which are applied to rotate objects around the x, y and z axes. Figure 4.1 displays the three planes and the two vectors involved in calculating $\theta_{P_r\mathrm{A}}$. H represents a horizontal plane (the ground), V a vertical plane (a wall/building face) and S_{rotated} represents the rotated scan plane.

$\theta_{P_r\mathrm{A}}$ is the angle between the vectors t and u on plane V. The calculation of $\theta_{P_r\mathrm{A}}$ requires first calculating the two vectors t and u. Vector u is the vector created by the intersection of the planes V and S_{rotated}. Vector t is the vector created by the intersection of the planes V and H. To calculate these vectors, the first step is to calculate the surface normals of the three planes,

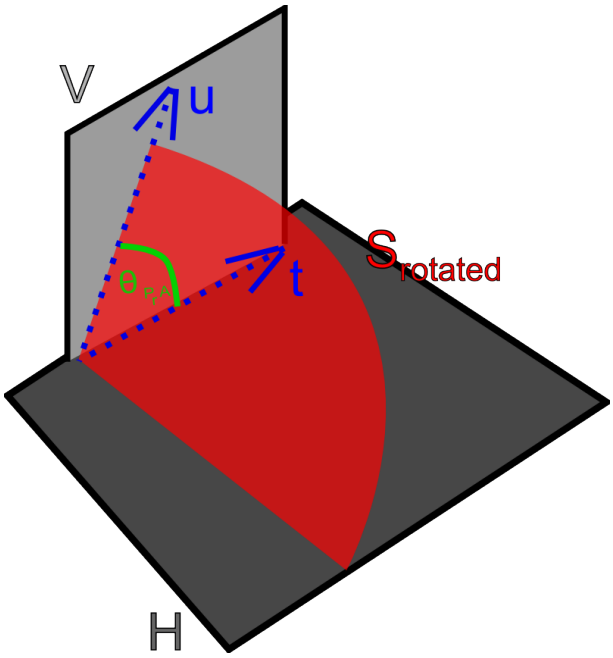

Figure 4.1: Planes and Vectors Involved in the Calculation of $\theta_{P_r\mathrm{A}}$

H, V and S_{rotated}. Each plane has a surface normal vector, which as explained in Section 3.3.2.3, is a vector perpendicular to the plane. For example, the procedure for calculating the surface normal for S_{rotated}, $N_{S_{\text{rotated}}}$, involves defining the rotation matrix for the laser scanner using

$$\text{Rotation Matrix}(S_{\text{rotated}}) = R_x(\gamma_{\text{scan}})R_y(\beta_{\text{scan}})R_z(\alpha_{\text{scan}}), \tag{4.1}$$

where γ, β and α are the vertical, axial and horizontal rotation angles of the scanner. Figure 4.2 illustrates the surface normals for a selection of vertical surfaces. A scanner at the rear of the vehicle facing backwards has an initial scan plane surface normal of [0, -1, 0]. To find the rotation matrix for the scanner on the XP1, $\gamma = 45^o$ (a vertical rotation around the x axis) , $\beta = 0^o$ and $\alpha = 45^o$ (a horizontal rotation around the z axis) are input into Equation 4.1. This returns the rotation matrix for S_{rotated}. The surface

normal for S_{rotated} is calculated by multiplying the initial scan plane surface normal by the rotation matrix. This returns a rotated surface normal of [-0.5, -0.5, 0.7071] for the XP1 scan plane.

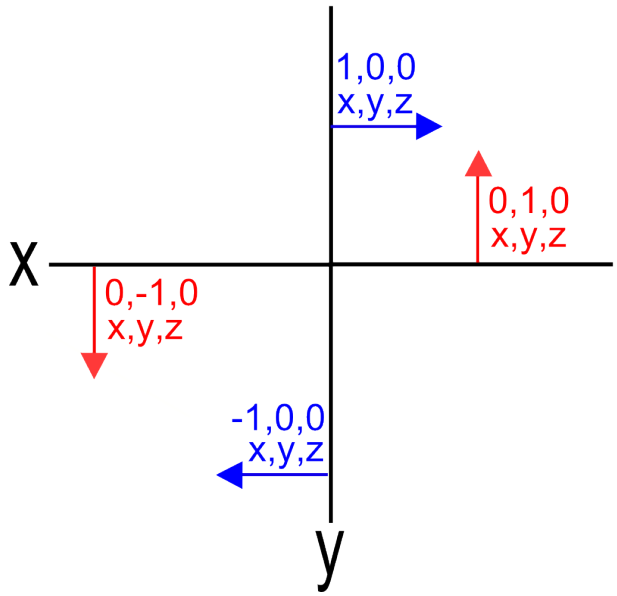

Figure 4.2: Top-Down View Illustrating Surface Normals for Vertical Planes

For ease of reference in the following formulae, the surface normal of vertical plane V becomes lower-case v and the ground surface normal becomes lower-case h, differing from the upper-case letters assigned to the planes in Figure 4.1. The surface normal for the scan plane can be defined for the scan plane where x is a vector parallel to the surface of the plane by

$$x.N_{S_{\text{rotated}}} = 0 \quad S = \{x | x \perp \text{scan normal}\}, \tag{4.2}$$

where '.' is the dot product and $N_{S_{\text{rotated}}}$ is the surface normal of the plane S_{rotated}. The surface normal of H can be defined for the horizontal plane by

$$x.N_h = 0 \quad H = \{x | x \perp \text{horizontal normal}\}, \tag{4.3}$$

where N_h is the horizontal surface normal. Finally the surface normal for the vertical plane can be defined with

$$x.N_v = 0 \quad V = \{x | x \perp \text{vertical normal}\}. \tag{4.4}$$

As shown in Figure 4.1, the scan plane intersects the building plane and creates a vector u defined as

$$\{\lambda u | \lambda \varepsilon \mathbb{R}\} = S \cap V = \{x | x \perp N_{S_{\text{rotated}}}, x \perp N_v\}, \tag{4.5}$$

where λ is a vector of real numbers and $\cap$ defines the intersection of two planes. The horizontal and building planes intersect and form vector t

$$\{\lambda t | \lambda \varepsilon \mathbb{R}\} = H \cap V = \{x | x \perp N_h, x \perp N_v\}. \tag{4.6}$$

The angle formed between vectors t and u is the profile angle, $\theta_{P_r\text{A}}$, one of the outputs required for the point density calculation. Vector u is a unit vector perpendicular to the scan plane surface normal, $N_{S_{\text{rotated}}}$ and also to the building surface normal, N_v

$$u \perp N_{S_{\text{rotated}}}, u \perp N_v, \|u\| = 1. \tag{4.7}$$

It can be calculated where $\times$ is the cross product with

$$u = \frac{N_{S_{\text{rotated}}} \times N_v}{|N_{S_{\text{rotated}}} \times N_v|}. \tag{4.8}$$

Vector t is a unit vector perpendicular to the horizontal surface normal,

N_h, and also to the building surface normal N_v

$$t \perp N_h,\ t \perp N_v,\ \|t\| = 1. \tag{4.9}$$

It can be calculated with

$$t = \frac{N_h \times N_v}{|N_h \times N_v|}. \tag{4.10}$$

To calculate $\theta_{P_r\mathrm{A}}$, the angle ($\sphericalangle$) between two vectors is required. This angle can be found using

$$\cos \sphericalangle(u, t) = u.t, \tag{4.11}$$

and as vectors u and t are also a product of two vectors, this is then expanded, where '$\cdot$' is the dot product to

$$\cos \sphericalangle(u, v) = \frac{(N_{S_{\text{rotated}}} \times N_v) \cdot (N_h \times N_v)}{|N_{S_{\text{rotated}}} \times N_v||N_h \times N_v|} = \theta_{P_r\mathrm{A}}. \tag{4.12}$$

This process can be repeated to calculate $\theta_{P_r\mathrm{A}}$ for any combination of scanner rotations by varying $N_{S_{\text{rotated}}}$. The limitation in this process is the reliance on vertical structures parallel to the vehicle and parallel to the ground. Therefore this process must be expanded to include angled planes.

4.2.1.3 Angled Planes

Real world objects are rarely perfectly parallel or perfectly horizontal to one face of the MMS. For this reason it is necessary to develop a method for calculating $\theta_{P_r\mathrm{A}}$ for angled surfaces. Although any surface can be rotated around three axes (R_x, R_y or R_z) only two of the axes will impact on the profile angle. The two axes that influence profile angle vary depending on

what type of surface is being rotated, i.e a horizontal or a vertical. For a vertical surface, rotations around R_x are not implemented in MIMIC. For instance, if a vertical surface is rotated around R_x it will not change the profile angle. Figure 4.3(a) illustrates a vertical target before it is rotated around R_x. A rotation of the target around R_x is illustrated in Figure 4.3(b). This rotation does not alter the profile angle.

MIMIC treats complex objects as a series of individual planes and does not deal with irregular shapes such as circles, triangles or diamonds. Therefore an angled surface can be represented by a horizontal and vertical rotation around R_z and R_y. As described in Section 4.2.1.2, the rotation matrices are applied to the standard surface normals for vertical and horizontal surfaces [1, 0, 0] and [0, 0, 1] respectively. The vertical surface is rotated horizontally by using the rotation matrix R_z (to represent surfaces converging with/diverging from the direction of travel), and vertically (to represent sloped surfaces such as embankments and roof tops) by using the rotation matrix R_y. These amended surface normals are then substituted into Equation 4.12, and $\theta_{P_r\mathrm{A}}$ for an arbitrary scanner rotation and surface rotation is calculated in this way.

4.2.2 Profile Spacing

A separate set of formulae are required for calculating the profile spacing, $d_{P_r\mathrm{S}}$. The larger the $d_{P_r\mathrm{S}}$, the less profiles that intersect with an object. Less profiles intersecting with a target results in a lower point density. The effect of vehicle speed on point density was illustrated in Figure 3.1. The factors involved in calculating $d_{P_r\mathrm{S}}$ are detailed in this chapter. Profile spacing is

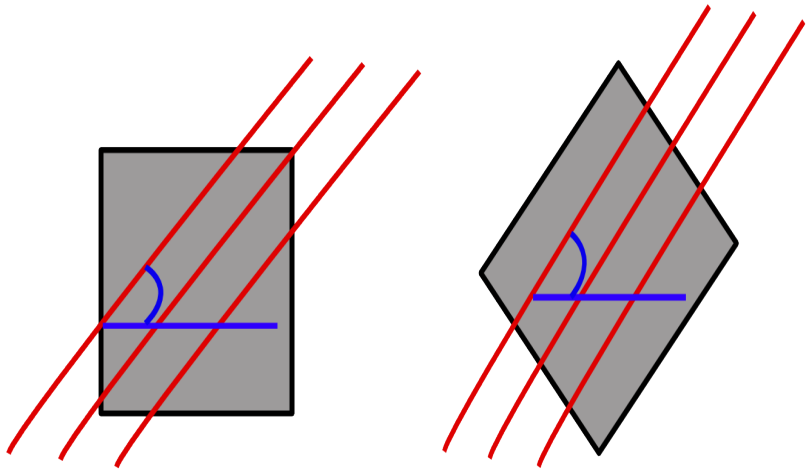

(a) (b)

Figure 4.3: Rotations Around R_x do not Effect Profile Angle in MIMIC(a) Profile Angle on a Rectangle and (b) a Rotated Rectangle - Identical Profile Angle

defined in terms of the horizontal and vertical spacing between scan profiles. The methods for calculating $d_{P_r\mathrm{S}}$ will be defined for a horizontal, vertical and an angled plane.

4.2.2.1 Horizontal Plane

Three factors influence $d_{P_r\mathrm{S}}$ on a horizontal plane: the vehicle velocity, the scanner mirror frequency and the horizontal scanner rotation. These factors are listed in Table 4.1. The mirror frequency and the vehicle velocity have the biggest impact on $d_{P_r\mathrm{S}}$. An illustration of sequential scan profiles on a horizontal surface is shown in Figure 4.4(a). The process for calculating the horizontal profile spacing, $d_{P_r\mathrm{SH}}$ is described in this section. The first step is to calculate the distance travelled in one mirror rotation by dividing the distance travelled in one second, v by the mirror frequency, M_f

$$d = v/M_f. \tag{4.13}$$

Once d has been calculated, $d_{P_r\mathrm{SH}}$ can be calculated using

$$d_{P_r\mathrm{SH}} = \frac{d}{\sin \alpha_{\mathrm{scan}}}, \tag{4.14}$$

where α_{scan} is the horizontal scanner rotation.

Table 4.1: Factors Influencing Profile Spacing on a Planar Horizontal Surface

Vehicle Velocity	v
Scan Mirror Frequency	M_f
Horizontal Scanner Rotation	α_{scan}

4.2.2.2 Vertical Plane

Calculating profile spacing on a parallel, vertical planar surface requires an additional variable, the vertical scanner rotation. This facilitates the profile angle calculation ($\theta_{P_r\mathrm{A}}$) detailed in Section 4.2.1. The profile angle is required to calculate the vertical profile spacing, $d_{P_r\mathrm{SV}}$. Figure 4.4(b) illustrates $d_{P_r\mathrm{SV}}$ and Table 4.2 lists the each of the factors that influence $d_{P_r\mathrm{SV}}$. For a vertical surface, the horizontal profile spacing is the distance travelled in one mirror rotation, d, as illustrated in Figure 4.4(b). $d_{P_r\mathrm{SV}}$ can be calculated using

$$d_{P_r\mathrm{SV}} = \frac{d * \sin \theta_{P_r\mathrm{A}}}{Sin(90 - \theta_{P_r\mathrm{A}})}. \tag{4.15}$$

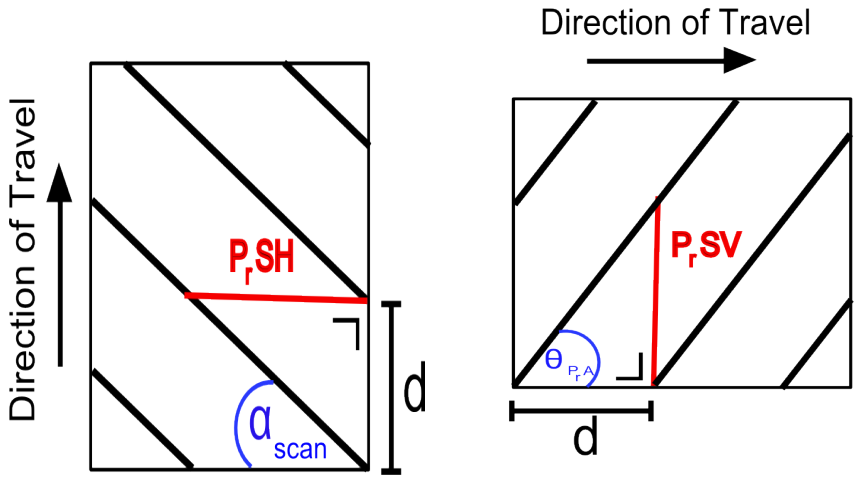

(a) (b)

Figure 4.4: Horizontal and Vertical Profile Spacing on (a) the Ground (top down view) and (b) a Vertical Surface (side view)

Table 4.2: Factors Influencing Profile Spacing on a Planar Vertical Surface

Vehicle Velocity (m/s)	v
Scan Mirror Frequency	M_f
Horizontal Scanner Rotation	α_{scan}
Vertical Scanner Rotation	γ_{scan}

4.2.2.3 Angled Plane

A horizontal rotation of the target alters the profile angle and profile spacing. Target rotations can be positive or negative. A positive rotation decreases the profile spacing on a target and a negative rotation increases it. A positive rotation of target, t, to the new orientation, $t+$, is illustrated in Figure 4.5(a). The distance travelled in one mirror rotation, d, is the vertical profile spacing on the horizontal plane. However, the horizontal rotation of the target, α_{targ}, results in a smaller horizontal profile spacing on the vertical surface, $d-$. A negative rotation of the target is illustrated in Figure 4.5(b). The negative horizontal rotation of target, t, to the new orientation, $t-$, results

in an increased profile spacing, $d+$, on the vertical target.

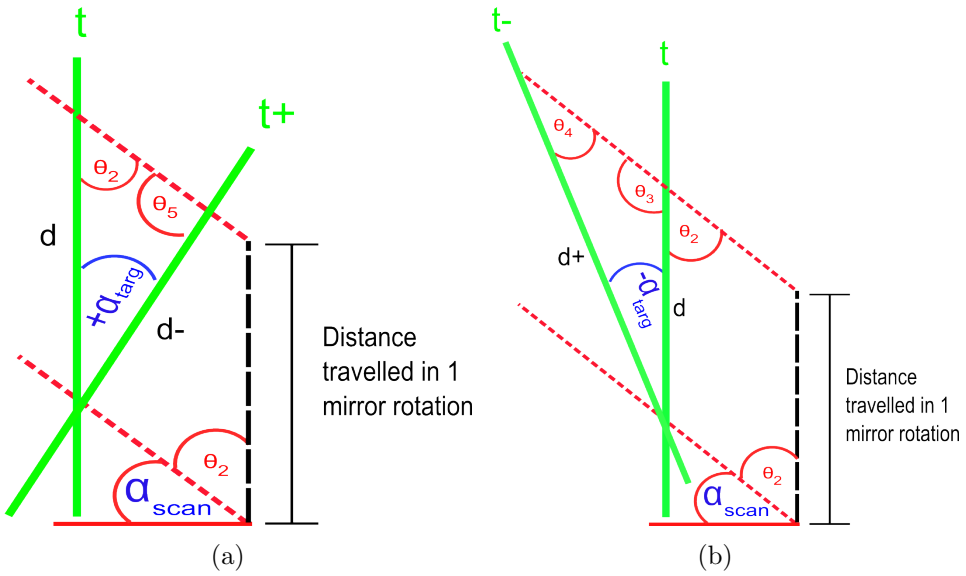

Figure 4.5: Profile Spacing on an Angled Plane Top Down View (a) Positive Rotation (b) Negative Rotation

The variables required to calculate $d-$ are illustrated in Figure 4.5(a). The angles θ_2 and θ_5 must first be found

$$\theta_2 = 90^o - \alpha_{\text{scan}}, \tag{4.16}$$

$$\theta_5 = 180^o - (\theta_2 + \alpha_{\text{targ}}). \tag{4.17}$$

$d-$ can then be calculated using

$$d- = \frac{d * \sin\theta_2}{\sin\theta_5}. \tag{4.18}$$

To calculate $d+$, angles θ_3 and θ_4 must first be computed, these can be calculated with

$$\theta_3 = 180^o - \theta_2, \tag{4.19}$$

and

$$\theta_4 = 180^o - (\theta_3 + \alpha_{\text{targ}}). \tag{4.20}$$

$d+$ can then be found using

$$d+ = \frac{d * \sin\theta_3}{\sin\theta_4}. \tag{4.21}$$

4.3 Calculating Point Spacing

This section details the methods employed by MIMIC to calculate point spacing. These methods are illustrated for horizontal and angled planes and the formulae used to calculate point spacing on each are explained.

4.3.1 Horizontal Plane

The point density on a surface is a product of the number of profiles and the number of points along each scan profile. Calculating the number of points along a scan profile requires knowledge of the point spacing and the target. The point spacing, d_{PS}, is the relative distance between successive points on a profile. d_{PS} is influenced by a number of factors. These factors are listed in Table 4.3. d_{PS} increases as the range from the scanner increases. The ASW, referred to as θ_A in these equations, is the angle between successive laser pulses, and an increase in θ_A results in an increase in d_{PS}. The PRR impacts θ_A which in turn impacts d_{PS}. A vertical rotation of the scanner increases

the range to the target surface, also increasing d_{PS}. The FOV determines θ_A, and therefore also influences d_{PS}.

Table 4.3: Factors Influencing Point Spacing on a Planar Horizontal Surface

Pulse Repetition Rate	PRR
Scan Mirror Frequency	M_f
Angular Step Width	θ_A
Points per Mirror Rotation	PpM
Field of View	FOV
Horizontal Range	H_r
Vertical Scanner Rotation	γ_{scan}
Height of Scanner	h_{scan}

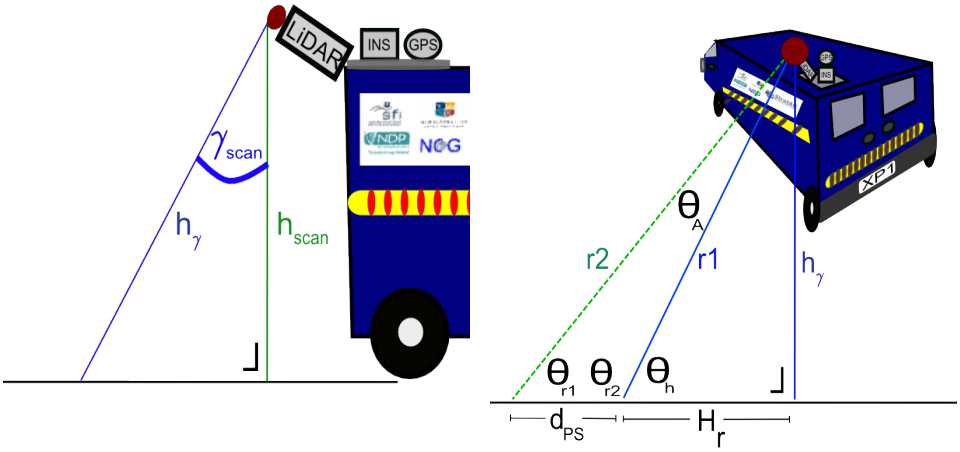

(a) (b)

Figure 4.6: Point spacing (a) Incorporating Vertical Scanner Rotation (b) Method for Calculating Point Spacing.

h_γ and θ_A are required for calculating d_{PS}. Figure 4.6(b) illustrates this process. A combination of trigonometric formulae and user input are required. The first step in computing d_{PS} is calculating the ASW, θ_A. To find

θ_A, the number of points per mirror rotation must first be calculated. This value can be calculated with

$$\text{PpM} = \frac{\text{PRR}}{M_f}. \tag{4.22}$$

Following this, θ_A can be found using

$$\theta_A = \frac{\text{FOV}}{\text{PpM}}. \tag{4.23}$$

The next step is to identify h_{scan}, which is the distance from the centre of measurement of the scanner to the ground. If a vertical rotation of the scanner is introduced in the system configuration, the distance from the scanner to the road surface is altered, as Figure 4.6(a) demonstrates. The amended vertical height can be calculated using

$$h_\gamma = \frac{h_{\text{scan}}}{\sin 90\,^\circ - \gamma_{\text{scan}}}. \tag{4.24}$$

The range from the scanner to the point of interest, $r1$, is calculated next. This is achieved by applying the user specified horizontal distance, H_r

$$r1 = \sqrt{h_\gamma^2 + H_r^2}. \tag{4.25}$$

To find θ_h, $r1$ and h_γ are used in the following equation

$$\theta_h = \sin^{-1}\left(\frac{h_\gamma}{r1}\right). \tag{4.26}$$

θ_{r2} can now be found by subtracting θ_h from 180^o

$$\theta_{r2} = 180\,^\circ - \theta_h. \tag{4.27}$$

The final unknown required to calculate d_{PS} is θ_{r1}, which can be calculated using

$$\theta_{r1} = (180^\circ - \theta_{r2}) - \theta_A. \tag{4.28}$$

Each of the required angles have now been identified, and therefore d_{PS} can be calculated with

$$d_{\mathrm{PS}} = \frac{(\sin\theta_A)(r1)}{\sin\theta_{r1}}. \tag{4.29}$$

4.3.2 Angled Plane

The method for calculating point spacing on angled planes differs from the method for calculating point spacing on the road surface. A methodology is required which accepts variations in target height, orientation and range. Figure 4.7 is a graphical aid illustrating each of the angles and variables required for calculating the point spacing, d_{PS}, for angled planes. Four variables are required for this calculation: the ASW, the height difference between target and scanner, the horizontal range to target and the scan angle. To calculate these four variables, twelve additional variables are required. Table 4.4 lists these twelve variables.

The ASW (θ_A) is required. By substituting the PRR, M_f and the FOV into Equations 4.22 and 4.23, θ_A can be calculated. The horizontal range to the target, H_r, must be specified by the user. For this part of the calculation, the target is simulated at the same height as the scanner. Therefore the range from the scanner to the target is $r1$. $r1$ is dependant on the scanner horizontal rotation, α_{scan}. $r1$ can be calculated with

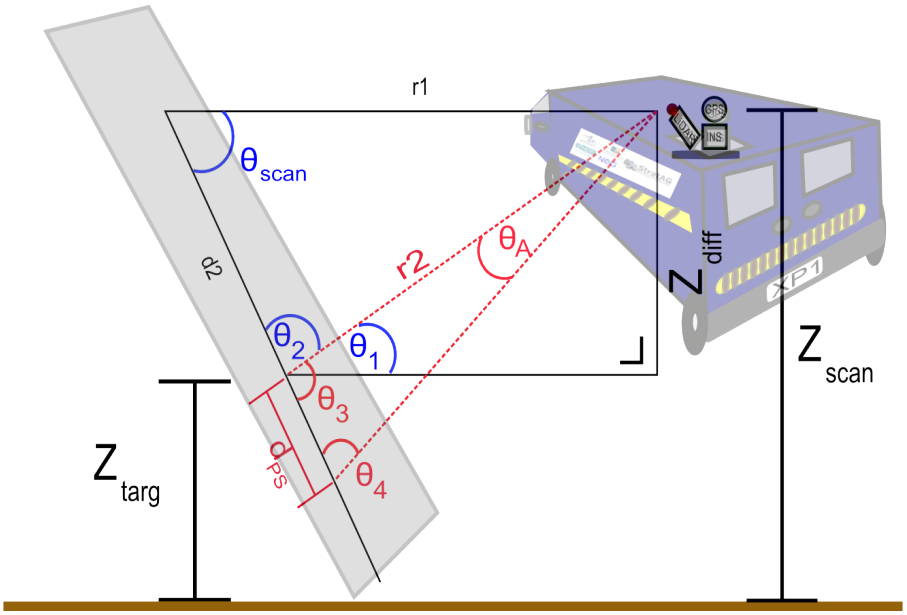

Figure 4.7: Values Required for Calculating d_{PS} on an Angled Plane

Table 4.4: Factors Influencing Point Spacing on an Angled Plane

Pulse Repetition Rate	PRR
Scan Mirror Frequency	M_f
Angular Step Width	θ_A
Points per Mirror Rotation	PpM
Field of View	FOV
Horizontal Range	H_r
Vertical Scanner Rotation	γ_{scan}
Horizontal Scanner Rotation	α_{scan}
Vertical Target Rotation	β_{targ}
Horizontal Target Rotation	α_{targ}
Height of Scanner	h_{scan}
Height of Target	h_{targ}

$$r1 = \frac{H_r}{\sin(90^o - \alpha_{\text{scan}})}. \tag{4.30}$$

MIMIC calculates d_{PS} through the application of 2D geometric formulae to identify the location of individual laser pulses on the angled surface. A horizontal and vertical rotation of the scanner alters the orientation of the scan plane in relation to the target and the scanner. This alters the viewing geometry for the 2D plane and therefore the height of the scanner and the target must be adjusted accordingly. This principle is illustrated in Figure 4.8. Z_{scan} and Z_{targ} represent these adjusted heights in Figure 4.7. The amended heights can be calculated using the original target and scanner heights (h_{targ}, h_{scan})and the vertical scanner rotation, β_{targ}, with

$$Z_{\text{targ}} = \frac{h_{\text{targ}}}{\sin(90 - \gamma_{\text{scan}})}, \tag{4.31}$$

and

$$Z_{\text{scan}} = \frac{h_{\text{scan}}}{\sin(90 - \gamma_{\text{scan}})}. \tag{4.32}$$

The height difference between the scanner and the target, (Z_{diff}), is required for these calculations on the 2D plane. MIMIC can calculate point spacing for targets above or below the scanner. Z_{diff} can be calculated using

$$Z_{\text{diff}} = Z_{\text{scan}} - Z_{\text{targ}}. \tag{4.33}$$

Additional variables are required for calculating d_{PS}. The next value that is required is the scan angle, θ_{scan}. This is the angle formed between $r1$ and scan profile on the angled surface, $d2$. This is calculated in a similar manner to the profile angle calculation, although for this calculation the vector u

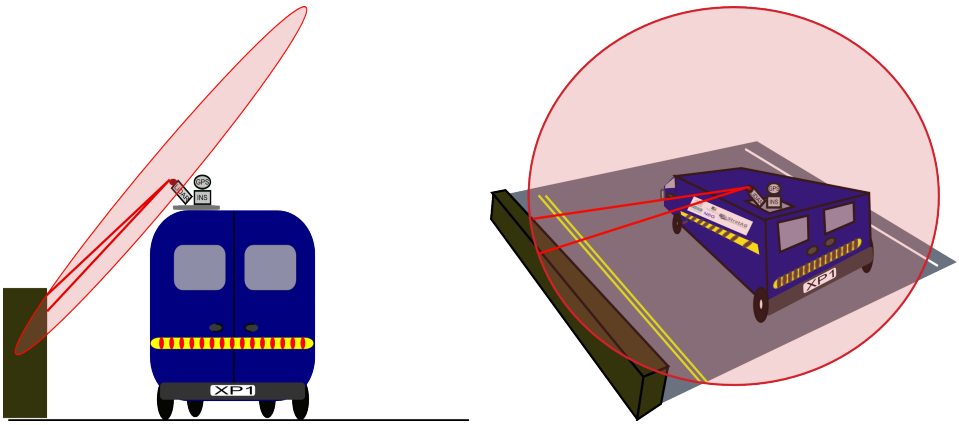

(a) (b)

Figure 4.8: Viewing Geometry (a) Orthogonal View does not Facilitate Calculation (b) Isometric View Required

represents the laser pulse, $r1$, and the vector t represents the vector formed by the intersection of the rotated scan plane and the vertical plane. This is illustrated in Figure 4.9 and the process and formulae involved in the calculation were detailed in Section 4.2.1.2.

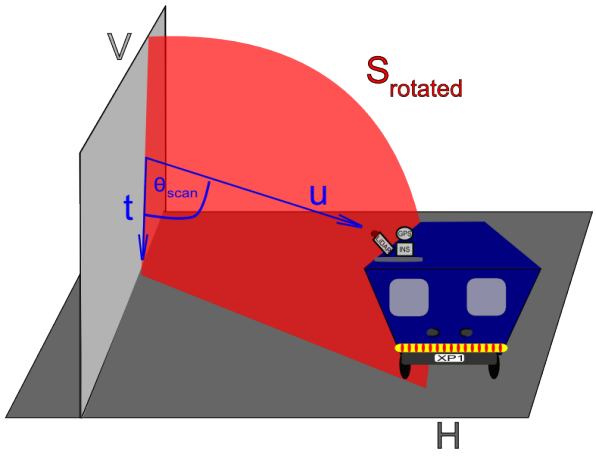

Figure 4.9: Scan Planes and Vectors Involved in Calculating Scan Angle Calculation

The method of calculating point spacing on angled surfaces incorporates different horizontal ranges to the target. This method also incorporates different target heights, the lack of which was identified in Section 2.2.4.1 as a shortcoming of existing point density calculators. Once MIMIC has calculated θ_A, $r1$, $scan\theta$ and Z_{diff}, it can calculate $r2$. Unlike the horizontal range, H_r, or the simulated range at $r1$, $r2$ is the actual range to the target along the scan plane. $d2$ is required to calculate $r2$. $d2$ is the portion of the scan plane that has intersected with the angled plane between $r1$ and h_{targ}. Calculating $d2$ does not require the same rotated perspective that the previous calculation did, but rather one with that is adjusted for the vertical rotation of the target. Therefore ht_{scan} and ht_{targ} are used. Figure 4.10 illustrates this principle. $d2$ can be calculated using

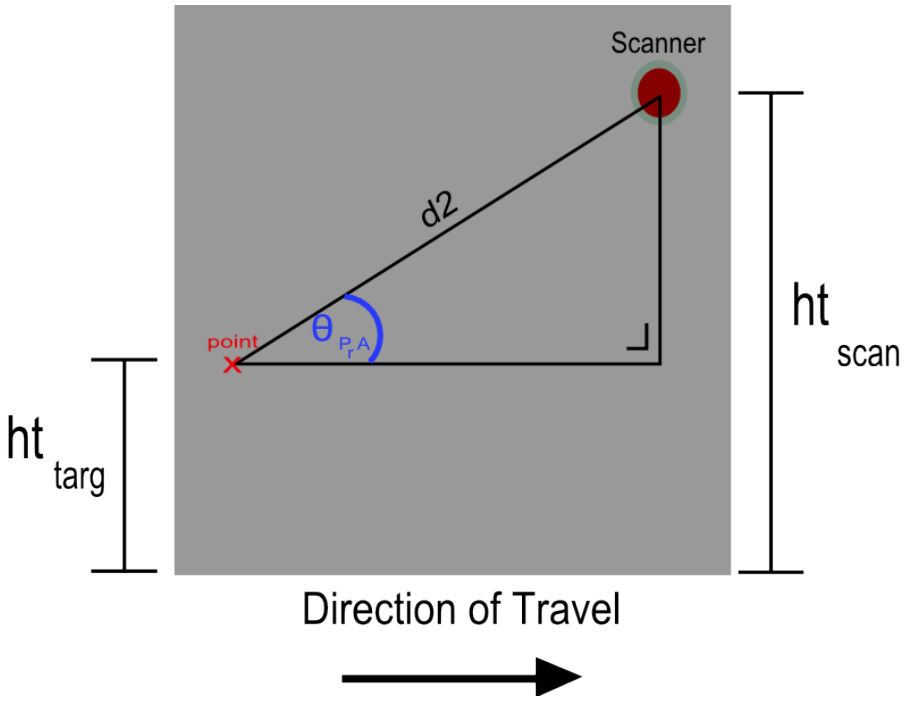

Figure 4.10: Values Required for Calculating d2

$$d2 = \frac{ht_{\text{scan}} - ht_{\text{targ}}}{\sin\theta_{P_r\text{A}}}, \tag{4.34}$$

Once $d2$ has been calculated the actual range to the target ($r2$) can be calculated with the cosine rule

$$r2 = \sqrt{d2^2 + r1^2 - 2((d2 * r1)(\cos(\theta_{\text{scan}}))}. \tag{4.35}$$

Once r2 has been calculated, the next step is to calculate θ_1, and this can be done using

$$\theta_1 = \sin^{-1}(\frac{Z_{\text{diff}}}{r2}). \tag{4.36}$$

θ_2 must then be found and this can be calculated using

$$\theta_2 = 180^o - (\theta_1 + \theta_{\text{scan}}). \tag{4.37}$$

Using θ_2, θ_3 can be calculated with

$$\theta_3 = 180^o - \theta_2. \tag{4.38}$$

The point spacing, d_{PS}, cannot be found using the sine rule with θ_3 as it is not the angle opposite the side r1, and therefore θ_4 must also be calculated. This can be calculated using

$$\theta_4 = 180^o - (\theta_3 + \theta_A). \tag{4.39}$$

The point spacing, d_{PS}, at that target height can then be found using

$$d_{\text{PS}} = \frac{(r1)(\sin\theta_A)}{\sin\theta_4}. \tag{4.40}$$

4.4 Results and Analysis

Two scenarios involving three datasets are analysed to verify the calculations of profile spacing, profile angle and point spacing in MIMIC. These three datasets are a constructed 3D CAD dataset, a point cloud from the XP1 and additional point cloud from the Optech Lynx. The constructed 3D CAD data is used as the control dataset. The XP1 and Optech Lynx point cloud data are used to experimentally validate MIMIC's calculations. Real world features such as walls, buildings and planar targets are used for experimental validation.

The Optech Lynx data facilitates system verification in a number of ways. Firstly, the Optech Lynx is a dual scanner system and this is used to verify that MIMIC can cater for dual scanner MMSs. The second scanner is assessed in Chapter 5 as it impacts on point density. The variations in scanner orientation between the Optech Lynx and the XP1 further verify MIMIC's profile angle calculations for different system configurations. Finally, the Optech M1 scanner is capable of operating at a higher mirror speed than the Riegl VQ-250 onboard the XP1, providing further test data for the profile spacing experiments. For each dataset a number of suitable areas for tests are identified and a series of sample measurements are recorded at each location. In each test area the profile spacing, profile angle and point spacing are manually measured and then compared to the predicted values from MIMIC. As it is difficult to find real world surfaces that are perfectly parallel and vertical to the vehicle, the point cloud tests are not applied to vertical surfaces but to angled surfaces.

4.4.1 Profile Angle

This section validates the methods for calculating profile angle on a horizontal plane, on a vertical plane and on an angled plane. CAD models are employed as a scientific control to validate MIMIC. MIMIC is then experimentally validated using data from the XP1 and Optech Lynx. The variations in scanner rotation between the Optech Lynx and the XP1 enable robust testing of MIMIC's profile angle calculations.

4.4.1.1 Measuring Profile Angles

There is the potential for error in the manual measurement of profile angles from the point cloud data. To demonstrate this, two sections of point cloud are chosen from two areas of point cloud. The first section has an irregular point distribution and therefore manual interpretation of scan profiles is difficult and may result in errors. The second section has a regular point distribution and therefore manual interpretation of scan profiles is simplified. The profile angle in relation to the direction of travel for the two scanners is measured at both locations. To provide an estimate of the quality of the manual process, five measurements are recorded for each scan profile and the average is then calculated. Figure 4.11 illustrates some of the issues involved when manually interpreting scan profiles for both profile spacing and profile angle measurements. In Figure 4.11(a) the point distribution exhibits irregularities. These irregularities are potentially due to vibrations of the vehicle or imperfections on the target surface. The scan profiles in Figure 4.11(a) exhibit visible differences in angle and spacing. In Figure 4.11(b) the point distribution is far more regular and the manual interpretation of the lines are a better approximation of the profile.

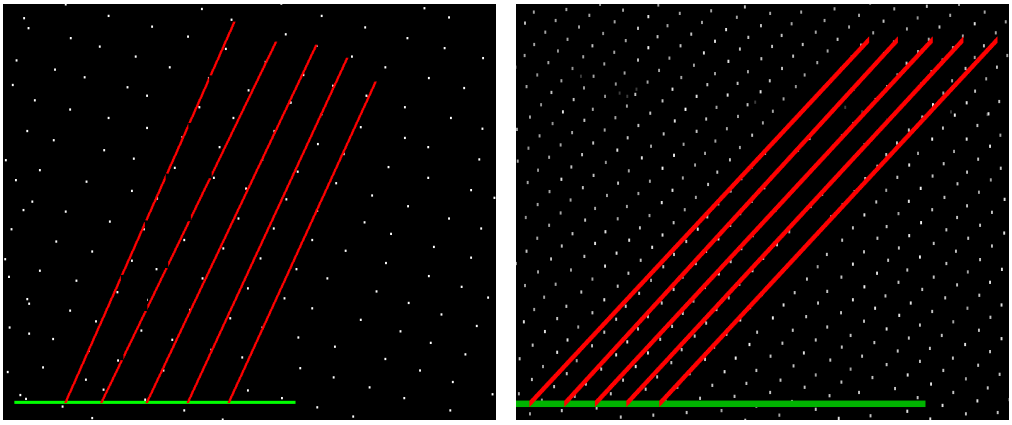

(a) (b)

Figure 4.11: Effect of Manual Interpretation of Scan Profiles on Profile Angle Measurements (a) Bad (b) Good

To quantify this effect, Table 4.5 lists a set of 5 measurements for the two cases displayed in Figure 4.11. A single scan profile is measured five times in each case. The standard deviation is calculated to quantify the variation in profile angle between measurements. 'Profile Angle 1' is measured from scan profiles in Figure 4.11(a) and 'Profile Angle 2' is measured from scan profiles in Figure 4.11(b). The standard deviation, σ is over an order of magnitude higher in the first case than in the second. This implies more variation in the measurements. To see how this can potentially effect the accuracy of the measurement, Table 4.6 lists the error for each of the measurements when compared to the value from MIMIC. The error is higher in the case with the higher σ. This may not always be the case, but is an important factor to consider when measuring the profile angle. Therefore the quality of the data used for validating MIMIC's calculations is dependant on the quality of the data in that location. In the validation tests in this thesis, where possible test data is selected from areas with a regular point distribution. These sites

are manually identified.

Table 4.5: Profile Angle - Manual Measurement

No.	Profile Angle 1	Profile Angle 2
1	59.412^o	35.355^o
2	59.571^o	35.323^o
3	59.51^o	35.343^o
4	59.257^o	35.325^o
5	59.25^o	35.333^o
σ	0.145^o	0.0133^o

Table 4.6: Profile Angle - Manual Measurement and Error

Result	Profile Angle 1	Profile Angle 2
Measured (Average)	59.40^o	35.323^o
MIMIC	59.175^o	35.264^o
Error	0.225^o	0.059^o

4.4.1.2 Horizontal Plane

As explained in Section 4.2.1.1, because the road underneath the vehicle is generally parallel to the direction of travel, the profile angle resulting from the intersection of the scan plane and the horizontal plane is entirely dependant on the horizontal scanner rotation. It is not affected by the vertical scanner rotation. Although the cross-fall of the road will effect this for point cloud tests, it is initially validated using a CAD model. Figure 4.12 illustrates these CAD tests. A plane representing the ground and a separate plane representing the scan plane are created. A selection of different scan rotations are applied, altering the horizontal and vertical scanner rotation

in turn by 15^o for each test. The profile angle on the horizontal plane is measured manually in CAD. Table 4.7 displays these results. For each scanner configuration it is possible to see that the measured profile angle on the ground plane corresponds exactly with the horizontal rotation of the scanner, regardless of what vertical rotation has been applied.

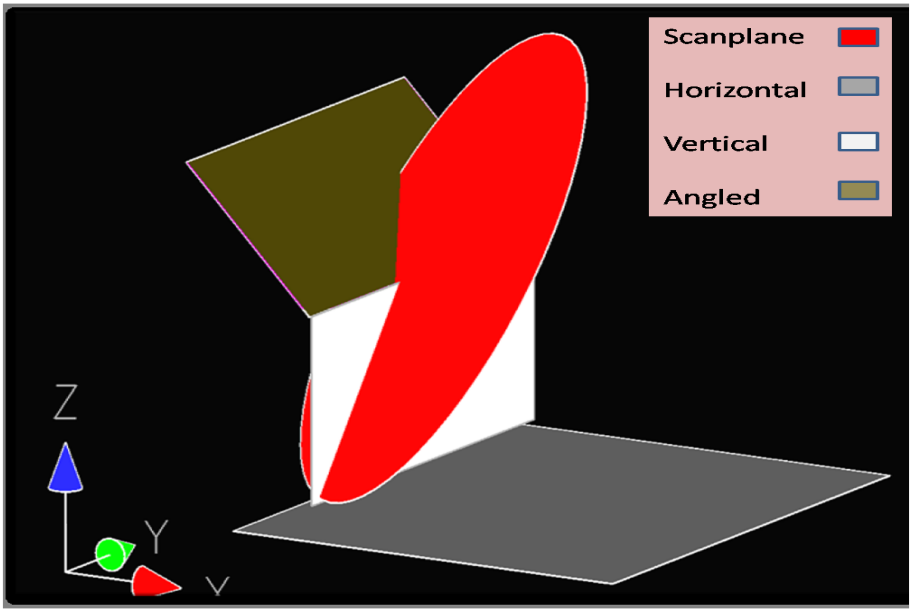

Figure 4.12: Profile Angle Verification in a CAD Environment.

Table 4.7: CAD Tests Ground Profile Angle

No.	α_{scan}	γ_{scan}	CAD
1	45^o	45^o	45^o
2	45^o	30^o	45^o
3	30^o	30^o	30^o
4	30^o	15^o	30^o
5	15^o	15^o	15^o

As road surfaces are generally non-planar and road cross-fall and vehi-

cle dynamics may impact on the profile angle, experimental verification is required. The profile angle is measured at three surface locations for each MMS dataset. Each profile is measured five times and the standard deviation, σ, is calculated to provide an indication of the reliability of the measurement. Table 4.8 illustrates the results for these profile angle tests on the road surface. The curvature of the road and the manual nature of the measurements results in a maximum standard deviation of approximately 0.5^o. The five measurements are then averaged and the difference between the measured value and MIMIC's value is calculated. The maximum error is approximately 0.1^o. The full results are available in Tables 1 and 2 in Appendix .1. The highest σ value, 0.537^o corresponds with the highest error, 0.102^o. The lowest σ value, 0.169^o corresponds with the lowest error, 0.002^o. These errors are due to the difficulty involved in measuring the profile angle on a road surface with a cross-fall. Profile angle errors will be discussed in greater detail in Section 4.4.1.5.

Table 4.8: Road Surface Profile Angle Tests - XP1 and Optech Lynx Data

No.	α_{scan}	γ_{scan}	σ	Error	MMS
1	37.48^o	29.6^o	0.352^o	0.079^o	Lynx
2	37.48^o	29.6^o	0.197^o	0.028^o	Lynx
3	37.48^o	29.6^o	0.203^o	0.062^o	Lynx
4	45^o	45^o	0.537^o	0.102^o	XP1
5	45^o	45^o	0.273^o	0.007^o	XP1
6	45^o	45^o	0.169^o	0.002^o	XP1

4.4.1.3 Vertical Plane

Unlike the profile angle on the road surface, the profile angle recorded on a perfectly parallel, vertical surface varies depending on both the horizontal and vertical rotation of the scanner. As explained in Section 4.4, the profile angle tests for a vertical plane have been restricted to CAD tests only. Different scanner rotations are selected and each profile angle is measured on the vertical surface. The scanner rotations are decreased in turn by 15^o for each test. The results for the profile angle calculated by MIMIC and the measured profile angle are displayed in Table 4.9. The errors are once again low, with the largest error being 0.067^o.

There are differences between the measured vales and the predicted values from MIMIC. These arise from the manual measurement process of profile angles in CAD packages. The profile angle is measured at the intersection between two planes. This requires manually drawing 3D lines and this manual component introduces errors to the CAD measurement. This manual error will not occur in the CAD tests for profile spacing and point spacing as the CAD package provides a 'snap' facility, whereby the end of a line or a point can be selected precisely. These tests demonstrate MIMIC's ability to calculate the profile angle for a vertical plane.

4.4.1.4 Angled Planes

A series of tests were designed to verify the profile angle calculations for an angled plane. The CAD tests consist of forty measurements, comprising four horizontal surface rotations and four vertical surface rotations for five differ-

Table 4.9: Profile Angle on a Vertical Plane - CAD Measurements Compared to MIMIC

No.	α_{scan}	γ_{scan}	MIMIC	CAD	Error
1	45^o	45^o	35.264^o	35.271^o	0.0075^o
2	45^o	30^o	56.768^o	50.784^o	0.0155^o
3	30^o	30^o	56.309^o	56.243^o	0.0669^o
4	30^o	15^o	72.807^o	72.810^o	0.0028^o
5	15^o	15^o	74.495^o	74.461^o	0.0349^o

ent dual axis scanner rotations. The profile angle is manually measured on each surface for each dual axis scanner rotation in the CAD environment. A representative subset of these results is displayed in Tables 4.10 and 4.11. The complete set of results can be seen in Tables 3 and 4 in Appendix .1. Table 4.10 illustrates the predicted and measured values for a horizontal rotation of a vertical surface and Table 4.11 illustrates the results for a vertical rotation of a vertical surface. The errors are small in the CAD tests, validating MIMIC's profile angle calculations. The errors that are present arise from the difficulties involved with the manual measurement process explained in Section 4.4.1.3.

Table 4.10: Profile Angle CAD Tests on an Angled Plane - Horizontal Target Rotation

No.	α_{scan}	γ_{scan}	α_{targ}	MIMIC	CAD	Error
1	45^o	45^o	15^o	40.893^o	40.840^o	0.0533^o
2	45^o	30^o	30^o	59.132^o	59.108^o	0.0245^o
3	30^o	30^o	45^o	59.132^o	59.097^o	0.0355^o
4	30^o	15^o	60^o	72.807^o	72.720^o	0.0878^o
5	15^o	15^o	60^o	69.246^o	69.290^o	0.0435^o

Table 4.11: Profile Angle CAD Tests on an Angled Plane - Vertical Target Rotation

No.	α_{scan}	γ_{scan}	β_{targ}	MIMIC	CAD	Error
1	45^o	45^o	75^o	31.27^o	31.209^o	0.0600^o
2	45^o	30^o	60^o	39.65^o	39.639^o	0.0107^o
3	30^o	30^o	45^o	49.02^o	48.963^o	0.0565^o
4	30^o	15^o	30^o	56.91^o	56.887^o	0.0227^o
5	15^o	15^o	30^o	69.67^o	69.657^o	0.0123^o

To experimentally validate MIMIC's profile angle calculations, seventeen surfaces with varying horizontal and vertical rotations are selected from a survey carried out by the XP1 system. The horizontal and vertical rotations of the target are measured. The accuracy of these measurements depend on the quality of the navigation solution, the manual interpretation of the orientation of the target and the calibration of the scanner. As explained in Section 1.7, assessing the absolute and relative accuracy of the MMS is not the focus of this thesis, and therefore the measured target orientation is assumed to be a reasonable representation of the real world feature. This is a potential error source. Ten manual measurements of the profile angle are recorded for each surface. Table 4.12 details the results of these tests. The complete set of results including individual measurements and vehicle dynamics can be seen in Tables 5 and 6 in Appendix .1.

The measured profile angle for the seventeen surfaces are plotted against the horizontal wall angle in Figure 4.13. In this figure, the manually measured profile angle is plotted against MIMIC's predicted values. The errors detailed in Table 4.12 can be identified in this figure. Figure 4.13 exhibits significant

Table 4.12: Profile Angle - MIMIC's Calculations Compared to Point Cloud Measurements for Angled Surfaces - XP1

No.	α_{targ}	β_{targ}	σ	Error
1	32.67^o	4.54^o	0.1983^o	5.925^o
2	54.61^o	3.51^o	0.4323^o	5.443^o
3	2.63^o	-0.29^o	0.1454^o	5.027^o
4	62.64^o	-4.9^o	0.1956^o	5.101^o
5	22.31^o	6.75^o	0.3335^o	0.704^o
6	-10.47^o	-1.3^o	0.3158^o	1.156^o
7	-7.12^o	-0.5^o	0.2095^o	0.646^o
8	8.16^o	-0.6^o	0.4089^o	0.592^o
9	65.87^o	-0.9^o	0.2257^o	2.215^o
10	-5.76^o	-4.1^o	0.3507^o	2.155^o
11	15.8^o	1.2^o	0.3063^o	4.258^o
12	-11.5^o	2.86^o	0.2667^o	3.395^o
13	8.15^o	2.54^o	0.1350^o	5.692^o
14	22.1^o	3.78^o	0.3859^o	2.932^o
15	84.16^o	-2.88^o	0.2319^o	0.271^o
16	87.73^o	0.22^o	0.2067^o	3.000^o
17	63.28^o	-0.1^o	0.1407^o	2.508^o

deviation in certain parts of the manually measured values from the predicted values. In each case the predicted value is greater than the measured values. This error is not constant, as the test areas were chosen at random intervals along the route. This resulted in a different road geometry and therefore different vehicle dynamics at each point. To assess the effect of the vehicle dynamics on the profile angle, the measured profile data was compared to navigation data for each point. Interestingly, the vehicle pitch displayed the most correlation with the profile angle errors which disagrees with the earlier assumption that roll would be the most common error source. Figure 4.14 illustrates the influence of vehicle pitch on the profile angle. This figure shows that when the pitch of the vehicle was highest, the error was lowest. This correlation is further demonstrated in Figure 4.15. This is unexpected and could be due to a number of factors:

- The XP1 mount is uneven, and a pitch of 2^o to 3^o counteracts this.
- As the vehicle was in motion the scanner mount may have dipped slightly due to the force of acceleration of the vehicle.
- The shock mountings of the laser scanner and INS may cause the mount to dip slightly under their own weight, and the forward motion of the vehicle or the gradient of the road surface may have counteracted this.
- The XP1 is not properly calibrated and a boresight alignment error exists between the scanner and the INS.

To investigate the effect of vehicle dynamics further, the Optech Lynx data is examined. Table 4.13 illustrates the sample data taken from a number of surfaces that are present in the Optech point cloud data. The full set of

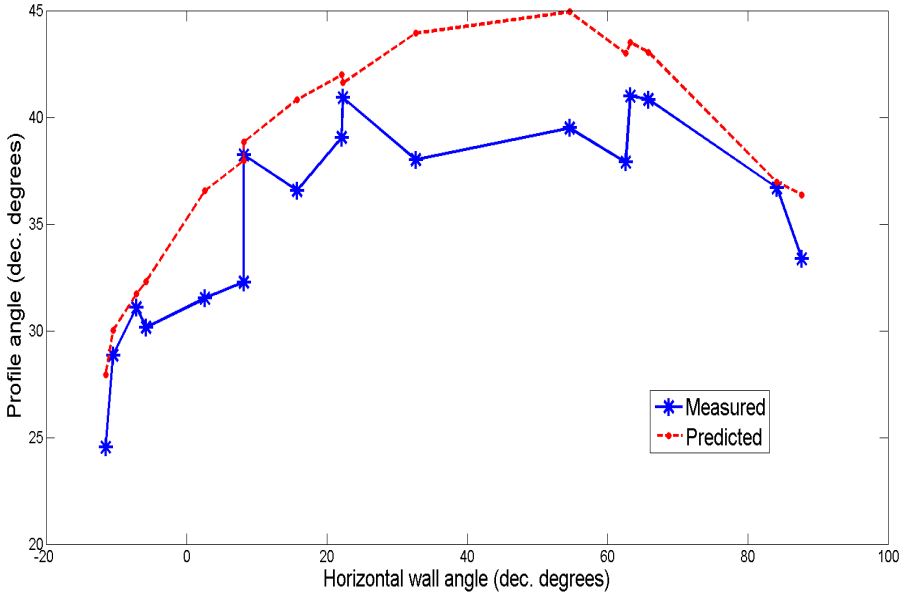

Figure 4.13: Plotting Manually Measured Versus Predicted Profile Angle for a Set of Point Cloud Angled Surfaces

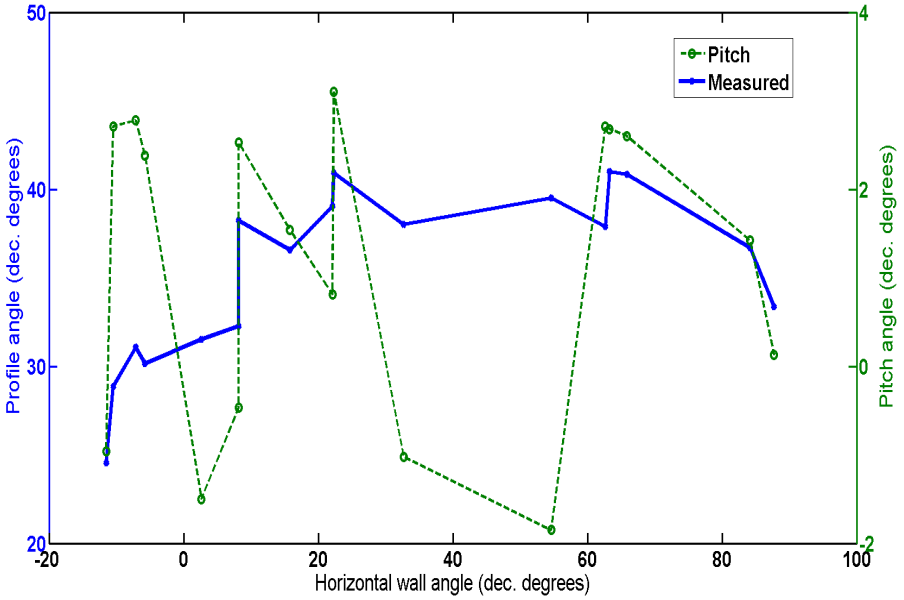

Figure 4.14: MIMIC's Predicted Profile Angle Plotted with Vehicle Pitch

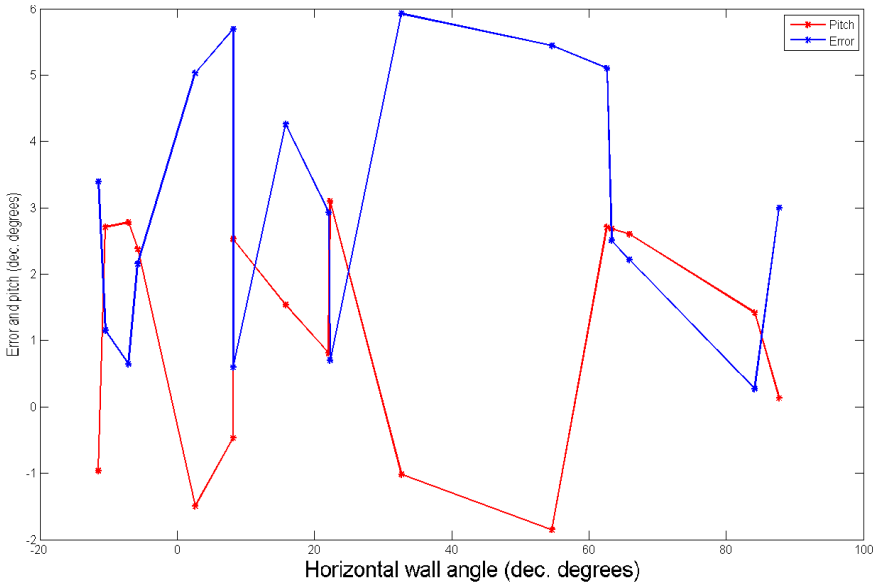

Figure 4.15: MIMIC's Profile Angle Error Plotted with Vehicle Pitch

results are available in Tables 7 and 8 in Appendix .1. The errors are lower for the Optech Lynx than the XP1, the largest error is approximately 1.5^o. This is a difference of approximately 4.4^o when compared to the maximum error in the XP1 data. There are four important differences between the Optech Lynx and the XP1 data that must be taken into consideration.

- Firstly, the Optech Lynx data is of a small test section around their office in Ontario. The size of the dataset limits the number of surfaces that are eligible as potential test areas. It is possible that a larger dataset may result in higher errors.

- Secondly, the Optech Lynx never left the carpark. There is a limit to the number of velocities available for testing. Therefore if acceleration is an issue, it is unlikely to be identified in the Optech Lynx data.

- Thirdly, because the data does not include any major roadways, the

vehicle dynamics experienced by the Optech Lynx during the survey are minimal when compared to the XP1 dataset. The largest value for vehicle dynamics in the profile angle tests from the Optech data is less than 1^o. The XP1 encountered roll and pitch of up to 4^o in the course of the survey.

- The final and possibly most important difference is that the Optech Lynx is a commercial system designed for high accuracy surveys. It has been rigorously calibrated whereas the XP1 is a research platform and has not been calibrated to the same standards. It is possible that some misalignment exists in the XP1's mounting.

Table 4.13: Profile Angle - MIMIC's Calculations Compared to Point Cloud Measurements for Angled Surfaces - Optech Lynx

No.	α_{targ}	β_{targ}	σ	Error
1	19.660^o	0^o	0.1452^o	0.2250^o
2	17.835^o	0^o	0.1953^o	0.3912^o
3	-0.750^o	0^o	0.4646^o	0.4600^o
4	-3.800^o	0^o	0.1083^o	1.5028^o
5	-11.050^o	0^o	0.1261^o	0.1546^o

4.4.1.5 Discussion and Error Sources

Assessing the error bounds must necessarily be carried out in Chapter 5 when applying each of the profile and point values in the final point density calculation. In Section 5.4.5 it will be possible to vary each of the inputs and then estimate what error significantly impacts on point density, allowing the errors to be assessed. This section summarises the errors for each of

the profile angle tests. In Table 4.14, the minimum, mean and maximum of MIMIC's errors are listed for each test conducted in this section. The errors from the CAD tests are consistently low, validating MIMICs profile angle calculations. The point cloud tests on angled surfaces result in larger errors than those recorded for the ground profile angle tests (a mean error of 0.091^o when compared to 3.007^o). It is unclear whether this is caused by vehicle dynamics or through manual interpretation of the profiles. Four potential error sources have been highlighted. The first is the manual process of measuring the profile angle of targets in real world point clouds. The second is the effect of vehicle dynamics. Vehicle dynamics have not been included as inputs into MIMIC. The third potential error source is encountered when dealing with real world point clouds. Accurate measurements of the orientation of the surface in the horizontal and vertical axes are required. This too is a manual process which potentially contributes to the profile angle errors. The final potential error source is system calibration. This was highlighted by the differences between the Optech Lynx and the XP1 for the profile angle results.

Although error bounds will be defined in Chapter 5, the largest errors for the ground and angled surfaces are highlighted to provide a preliminary estimate of these errors. The user inputs are varied until the predicted and measured values match. This is repeated for each input variable. Table 4.15 details the extent an input value has to individually change to eliminate the error. The largest profile angle error of the point cloud tests on the ground could potentially be caused by a mistake in the horizontal rotation of the scanner of 0.1^o. This is a plausible scenario if the XP1 system is incorrectly configured. For the point cloud tests on angled surfaces, the errors are higher.

The highest error would require a change in the scanner or target horizontal rotation of 11.3^o, or an error of 7.1^o or 20.1^o in vertical rotations of the scanner or target to compensate for it. To have an error of that size in any one value is unlikely, but if a small error is introduced into each of the inputs it could conceivably account for the 5.925^o and becomes even more likely when vehicle dynamics are considered.

Table 4.14: Profile Angle - Summary of MIMIC Errors

Test	Surface Type	Min	Mean	Max
CAD	Horizontal	0^o	0^o	0^o
Point Cloud	Ground	0.0790^o	0.0910^o	0.1020^o
CAD	Vertical	0.0075^o	0.0425^o	0.0755^o
CAD	Angled	0.0245^o	0.0489^o	0.0878^o
Point Cloud (XP1)	Angled	0.2710^o	3.0007^o	5.9250^o
Point Cloud (Optech)	Angled	0.2250^o	0.5467^o	1.5028^o

Table 4.15: Profile Angle - Variation in MIMIC Input that Corresponds to Errors on Point Cloud Surfaces

Surface	Max Error	α_{scan}	γ_{scan}	α_{targ}	β_{targ}
Ground	0.102^o	0.1^o	n/a	n/a	n/a
Wall	5.925^o	11.3^o	7.1^o	-11.3^o	20.1^o

4.4.2 Profile Spacing

In this section MIMIC's profile spacing calculations are validated. Similarly to Section 4.2.2 the methods for calculating profile spacing on a horizontal plane, on a vertical plane and on an angled plane are verified. Due to the difficulty in finding suitable surfaces, the point cloud tests are not applied

for parallel, vertical structures. Additionally, by employing the rotation of the surface to provide variations in the interaction between the scan plane and target, these tests are more rigorous than if they are limited to purely vertical structures. As explained in the previous section, MIMIC is validated through a series of CAD tests and point cloud tests using XP1 and Optech Lynx data.

4.4.2.1 Measuring Profile Spacing

By applying data from the XP1 and Optech Lynx, it is possible to choose scan profiles from different vehicle speeds and then measure the horizontal and vertical profile distance. The INS onboard each of the MMS provides high accuracy velocity information. Vehicle velocity is one of the inputs into MIMIC. As with the profile angle tests, the verification process involves manual interpretation of profiles. Figure 4.16 illustrates the difficulty in measuring profile spacing in point cloud data. Test data is selected in areas of even and uneven point distribution to assess the impact of manual interpretation of scan profiles when taking measurements to validate profile spacing. Five measurements are recorded for each profile spacing measurement. The standard deviation of these measurements (σ) is then calculated. Table 4.16 details the results of the profile spacing measurements. These results are then averaged and the measured profile spacing compared against the value from MIMIC. Table 4.17 displays these results and the corresponding error. Similarly to the profile angle measurements in Section 4.4.1.2 the measurements exhibiting the higher σ also exhibit the higher errors, 0.00316m as opposed to 0.00008m. These errors arise when manually approximating the scan profile is inhibited by non uniform point spacing along the scan profile

and it is a potential error source.

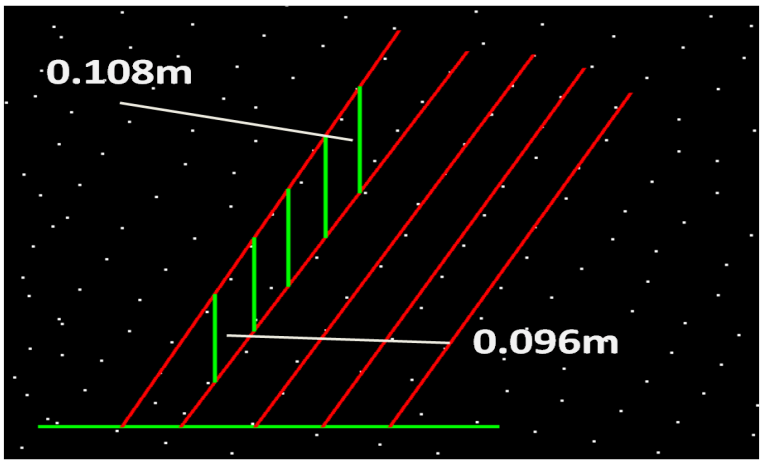

Figure 4.16: Manual Selection of Scan Profiles and the Impact on Profile Spacing

Table 4.16: Manually Measuring Profile Spacing in Point Clouds

No.	Profile Spacing 1 (m)	Profile Spacing 2 (m)
1	0.1185	0.0950
2	0.1139	0.0975
3	0.1089	0.0957
4	0.1043	0.0959
5	0.0991	0.0960
σ (m)	0.00765	0.00091

4.4.2.2 Horizontal Plane

In this section, MIMIC's profile spacing calculations for a horizontal plane are validated using CAD data. The CAD profile spacing tests involve intersecting a plane representing the scan plane with a horizontal plane representing the ground. Figure 4.12 illustrates the interaction for the three planes. The

Table 4.17: Profile Spacing - Manual Measurement and Error

Result	Profile Spacing 1 (m)	Profile Spacing 2 (m)
Measured (Average)	0.10894	0.09602
MIMIC	0.11210	0.09610
Error	0.00316	0.00008

scan plane is orientated in a series of configurations. The horizontal and vertical scanner rotations are decreased in turn by 15^o from 45^o to 15^o for each test. The distance between subsequent scan planes is measured. Changes in mirror speed and vehicle speed are modelled by increasing the offset distance between subsequent scan planes. These tests illustrate the performance of MIMIC at measuring profile spacing when compared to a series of CAD measurements. CAD measurements represent a hypothetical, ideal scenario where no errors or external forces impact on the data. Tables 4.18 and 4.19 detail the profile spacing measurements for vertical and horizontal profile spacing respectively on a horizontal plane. The values from MIMIC correspond exactly with those measured in the CAD environment.

Table 4.18: Vertical Profile Spacing on a Horizontal Plane in CAD tests for a Mirror Frequency of 100Hz

No.	α_{scan}	γ_{scan}	Velocity	MIMIC(m)	CAD(m)	Err.(m)
1	45^o	45^o	5m/s	0.050	0.050	0
2	45^o	30^o	10m/s	0.100	0.100	0
3	30^o	30^o	15m/s	0.150	0.150	0
4	30^o	15^o	20m/s	0.200	0.200	0
5	15^o	15^o	25m/s	0.250	0.250	0

Table 4.19: Horizontal Profile Spacing on a Horizontal Plane in CAD tests for a Mirror Frequency of 100Hz

No.	α_{scan}	γ_{scan}	Velocity	MIMIC(m)	CAD(m)	Err.(m)
1	45^o	45^o	5m/s	0.0500	0.0500	0
2	45^o	30^o	10m/s	0.1000	0.1000	0
3	30^o	30^o	15m/s	0.0866	0.0866	0
4	30^o	15^o	20m/s	0.1154	0.1154	0
5	15^o	15^o	25m/s	0.6690	0.6690	0

These CAD tests demonstrate MIMICs ability to predict profile spacing on a horizontal plane, but as MIMIC is designed to have real-world applications it must be assessed with real world data. Figure 4.17 illustrates a profile spacing measurement on point cloud data. Each scan profile is manually interpreted and then a measurement between the two is recorded. The Optech Lynx data provides the opportunity to test profile spacing for different mirror speeds. The results of these point cloud tests can be seen in Tables 4.20 and 4.21 for vertical and horizontal profile spacing respectively.

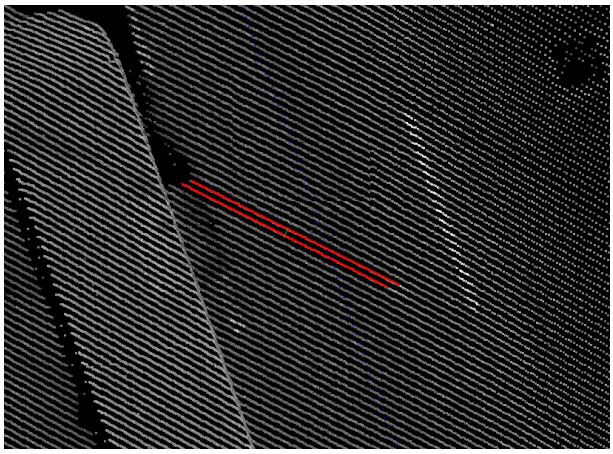

Figure 4.17: Profile Spacing Measurements on the Road Surface

Table 4.20: Vertical Profile Spacing - MIMIC Predictions Versus Manual Measurements of Optech Lynx Data for the Road Surface

No.	Vel (m/s)	M_f	$d_{P_r\mathrm{SV}}$ (m)	σ (m)	Err (m)
1	7.088	150 Hz	0.04680	0.000050	0.00040
2	7.53	150 Hz	0.04954	0.000171	0.00066
3	3.42	150 Hz	0.02352	0.000058	0.00072
4	5.802	150 Hz	0.03918	0.000000	0.00050
5	5.58	150 Hz	0.03696	0.000311	0.00024
6	6.86	200 Hz	0.03480	0.000299	0.00050
7	7.324	200 Hz	0.02846	0.000050	0.00039
8	3.35	200 Hz	0.01590	0.000129	0.00085
9	6.799	200 Hz	0.03578	0.000506	0.00178
10	5.6	200 Hz	0.02730	0.000294	0.00070

Table 4.21: Horizontal Profile Spacing - MIMIC Predictions Versus Manual Measurements of Optech Lynx Data for the Road Surface

No.	Vel (m/s)	M_f	$d_{P_r\mathrm{SH}}$(m)	σ (m)	Err (m)
1	7.088	150 Hz	0.0362	0.000045	0.00070
2	7.53	150 Hz	0.0385	0.000110	0.00022
3	3.42	150 Hz	0.0174	0.000023	0.00040
4	5.802	150 Hz	0.0296	0.000040	0.00040
5	5.58	150 Hz	0.0285	0.000191	0.00023
6	6.86	200 Hz	0.0263	0.000170	0.00015
7	7.324	200 Hz	0.0281	0.000324	0.00099
8	3.35	200 Hz	0.0128	0.000449	0.00075
9	6.799	200 Hz	0.0260	0.000216	0.00050
10	5.6	200 Hz	0.0214	0.000040	0.00070

The point cloud profile spacing tests for the ground highlight a number of issues. Firstly, σ is extremely low, less than 1mm in each case. A low σ indicates a reliable measurement. The profile spacing errors are also low, the highest error is 0.00178m. The correlation between less reliable measurements, identified by relatively high σ values, and high errors was reinforced

in these tests. The measurement with an associated error of 0.00178m also has the highest standard deviation, thus reinforcing the point that this scan profile was the most difficult to measure accurately. The full set of profile results, including vehicle dynamics are included in Tables 9 and 10 in Appendix .1. Upon closer examination, the vehicle dynamics recorded by the INS do not suggest that the MMS was experiencing significant roll, pitch or yaw at the time of that measurement (-0.1036^o, 1.5399^o and 0.004^o respectively). Therefore vehicle dynamics can be disregarded as an error source in this case. The reason for assuming that these values are not significant is that a number of other measurements were recorded with comparable values of roll, pitch and yaw and they did not exhibit similar errors. This suggests the error in this test is primarily due to the manual interpretation of the profile. Excluding this one error, MIMIC has in each case correctly predicted the profile spacing for different vehicle velocities and mirror speeds on the ground to less than 1mm.

4.4.2.3 Vertical Plane

Section 4.4.2 explained that due to the difficulty in finding parallel, vertical surfaces the tests for measuring profile spacing on parallel, vertical surfaces were limited to measurements in CAD models. These tests are carried out by intersecting a disc representing the scan plane with another plane representing the parallel, vertical surface as illustrated in Figure 4.12. For vertical surfaces the horizontal and vertical profile spacing are required for the point density calculation. Table 4.22 illustrates the predicted and measured vertical profile spacing and Table 4.23 illustrates the predicted and measured

horizontal profile spacing for a vertical surface. As with the previous CAD model tests, there is zero error. This result validates MIMIC calculations of horizontal and vertical profile spacing on vertical surfaces. The profile angle is required to calculate the vertical profile spacing and therefore any error in calculating profile angle is an intrinsic component of the vertical profile spacing calculation for a vertical surface.

Table 4.22: Horizontal Profile Spacing - MIMIC Predictions Versus CAD Tests for a Vertical Plane

No.	α_{scan}	γ_{scan}	Velocity	MIMIC (m)	CAD (m)	Error (m)
1	45^o	45^o	5m/s	0.05	0.05	0
2	45^o	30^o	10m/s	0.10	0.10	0
3	30^o	30^o	15m/s	0.15	0.15	0
4	30^o	15^o	20m/s	0.20	0.20	0
5	15^o	15^o	25m/s	0.25	0.25	0

Table 4.23: Vertical Profile Spacing - MIMIC Predictions Versus CAD Tests for a Vertical Plane

No.	α_{scan}	γ_{scan}	Velocity	MIMIC (m)	CAD (m)	Error (m)
1	45^o	45^o	5m/s	0.0500	0.0050	0
2	45^o	30^o	10m/s	0.1224	0.1224	0
3	30^o	30^o	15m/s	0.2250	0.2250	0
4	30^o	15^o	20m/s	0.6464	0.6464	0
5	15^o	15^o	25m/s	0.9012	0.9012	0

4.4.2.4 Angled Plane

Vertical surfaces rotated horizontally and vertically around the Y and Z axes respectively are used to validate MIMIC's calculations for angled planes.

In the initial CAD tests, in order to accommodate every type of rotation, the surface is rotated clockwise and anti-clockwise around the Z axis. This represents a horizontal rotation of the target. The same process is applied for rotations around the Y axis which represent vertical inclinations of the target. The axes for target rotation were illustrated in Figure 3.14(b). Rotations around two axes are applied and these represent horizontal and vertical rotations of the target. Table 4.24 illustrates the performance of MIMIC against these measured values for horizontal profile spacing on a vertical surface and Table 4.25 for vertical profile spacing. A constant vehicle velocity of 10m/s is applied and a horizontal/vertical scanner rotation of $45^o/45^o$ is applied respectively. The CAD profile spacing measurements return a zero error, validating MIMIC's calculations of profile spacing on angled surfaces.

Table 4.24: Horizontal Profile Spacing - MIMIC Calculations Compared to CAD Measurements for an Angled Plane

No.	α_{targ}	β_{targ}	MIMIC (m)	CAD (m)	Error (m)
1	15^o	0^o	0.0816	0.0816	0
2	0^o	15^o	0.1000	0.1000	0
3	15^o	15^o	0.0816	0.0816	0
4	-15^o	0^o	0.1414	0.1414	0
5	0^o	-15^o	0.1000	0.1000	0

The next test involves angled structures selected from the XP1 and Optech Lynx data to validate MIMIC using point cloud data. The Optech Lynx data is again used to provide a method for verifying different scanner rotations and mirror speeds. Using data from both MMSs allows more rigorous testing. Objects such as walls and building faces are chosen and the horizontal and

Table 4.25: Vertical Profile Spacing - MIMIC Calculations Compared to CAD Measurements for an Angled Plane

No.	α_{targ}	β_{targ}	MIMIC (m)	CAD (m)	Error (m)
1	15^o	0^o	0.0707	0.0707	0
2	0^o	15^o	0.0615	0.0615	0
3	15^o	15^o	0.0645	0.0645	0
4	-15^o	0^o	0.0707	0.0707	0
5	0^o	-15^o	0.0615	0.0615	0

vertical angles of these features are measured. Using software designed by researchers at the NCG [Lewis et al., 2010, Lewis et al., 2012, McElhinney et al., 2011], areas of interest are quickly identified and extracted from large survey files. As in previous tests, five measurements are recorded for each set of scan profiles and σ is calculated to provide an indication of the quality of each measurement. The results for horizontal and vertical profile spacing at two different mirror speeds and a selection of vehicle velocities are displayed in Tables 4.26 and 4.27.

The errors from the point cloud tests are higher than in the CAD tests but are still low, less than 1mm in all but four of the cases. Figure 4.18 illustrates the errors and plots them against standard deviation. This helps visualise the quality of each manual measurement used to validate the predicted values. In Figure 4.18 it can be seen that the majority of MIMIC's calculations have an error of less than 1mm and a σ of less than 2mm. The results for horizontal and vertical profile spacing are included in Tables 11, 12, 13 and 14 in Appendix .1. Interestingly, none of the measurements containing the larger errors were recorded when vehicle dynamics were high. This would

Table 4.26: Horizontal Profile Spacing - MIMIC Calculations Compared to Point Cloud Measurements for an Angled Vertical Surface at Different M_f and Vehicle Velocities

No.	α_{targ}	β_{targ}	Vel.(m/s)	σ(m)	Err. (m)	M_f (Hz)
1	1.930^o	0^o	4.80	0.0045	0.0016	100
2	0.156^o	15^o	5.00	0.0002	0.0004	100
3	2.810^o	30^o	4.97	0.0047	0.0005	100
4	-1.000^o	45^o	4.90	0.0004	0.0004	100
5	48.590^o	6.21^o	4.83	0.0005	0.0006	100
6	72.546^o	20^o	4.90	0.0005	0.0005	100
7	0.000^o	0^o	10.97	0.0005	0.0005	100
8	46.320^o	0^o	12.96	0.0017	0.0005	100
9	39.977^o	0^o	12.49	0.0012	0.0008	100
10	70.900^o	0^o	12.68	0.0015	0.0003	100
11	19.700^o	0^o	4.07	0.0002	0.0004	150
12	17.835^o	0^o	5.72	0.0009	0.0010	150
13	$- 0.750^o$	0^o	3.71	0.0001	0.0005	150
14	$- 3.800^o$	0^o	4.15	0.0005	0.0013	150
15	$- 11.050^o$	0^o	4.52	0.0002	0.0005	150

Table 4.27: Vertical Profile Spacing - MIMIC Predictions Compared to Point Cloud Measurements for an Angled Vertical Surface at Different M_f

No.	α_{targ}	β_{targ}	Vel.(m/s)	σ(m)	Err. (m)	$M_f(Hz)$
1	1.930^o	0^o	4.80	0.0013	0.0002	100
2	0.156^o	15^o	5.00	0.0005	0.0011	100
3	2.810^o	30^o	4.97	0.0006	0.0006	100
4	-1.000^o	45^o	4.90	0.0004	0.0007	100
5	48.590^o	6.21^o	4.83	0.0009	0.0010	100
6	72.546^o	20^o	4.90	0.0008	0.0002	100
7	0.000^o	0^o	10.97	0.0020	0.0015	100
8	46.320^o	0^o	12.96	0.0018	0.0005	100
9	39.977^o	0^o	12.49	0.0021	0.0004	100
10	70.900^o	0^o	12.68	0.0007	0.0008	100
11	19.700^o	0^o	4.07	0.0010	0.0007	150
12	17.835^o	0^o	5.72	0.0001	0.0005	150
13	-0.750^o	0^o	3.71	0.0005	0.0002	150
14	-3.800^o	0^o	4.15	0.0002	0.0007	150
15	-11.050^o	0^o	4.52	0.0003	0.0005	150

imply that, unlike profile angle, vehicle dynamics have no significant effect on profile spacing.

4.4.2.5 Discussion and Error Sources

Tests have been designed in Chapter 5 to assess the effect of errors in calculating profile spacing on the point density calculation. This section identifies and quantifies each of these errors. Table 4.28 summarises the errors for each of the tests. The largest errors are less than 2mm, whereas the mean errors are, in all cases, less then 1mm. This appears to be satisfactory, but for large targets with a low profile spacing an error of 1mm may impact on the point density due to the number of profiles. This will be discussed in Section 5.4.5. Table 4.29 has been collated to assist in visualising what

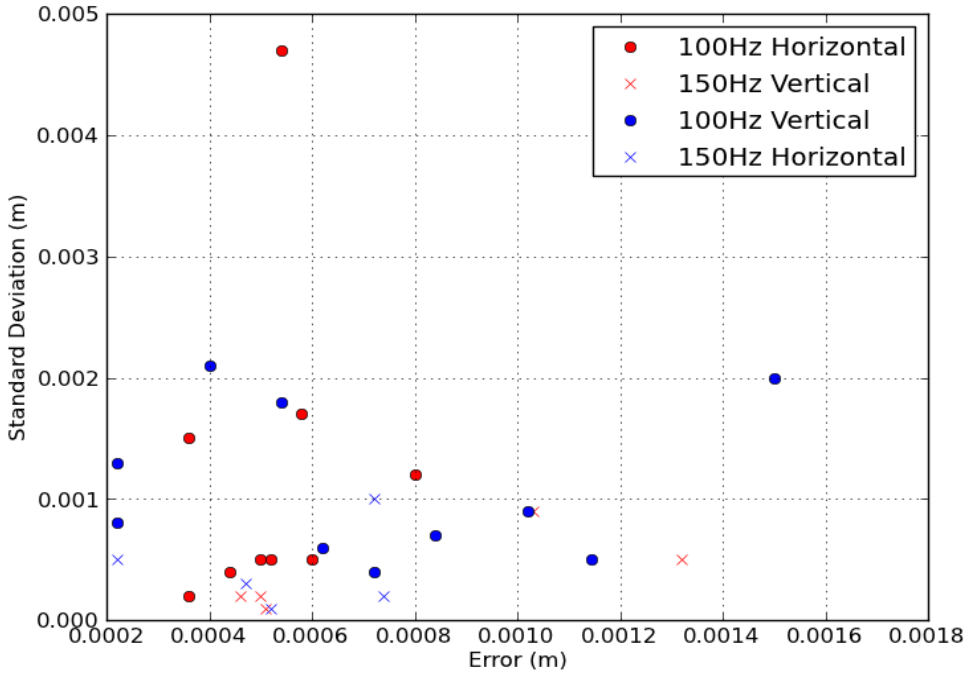

Figure 4.18: Horizontal and Vertical Profile Spacing on an Angled Surface for Different Mirror Frequencies - Error v Std Dev

may have contributed to MIMIC's calculation errors. As in Section 4.4.1.5, each of the input values is incremented individually until the predicted and measured values match. By examining Table 4.29, it is clear that even small discrepancies in the profile measurements or system settings could account for those errors. This demonstrates the accuracy of MIMIC for calculating profile spacing on an angled surface.

Table 4.28: Error Table - Profile Spacing

Test	$d_{P_r\text{S}}$	Min (m)	Mean (m)	Max (m)
CAD	Horizontal ($d_{P_r\text{SH}}$)	0.00000	0.00000	0.00000
CAD	Horizontal ($d_{P_r\text{SV}}$)	0.00000	0.00000	0.00000
Point Cloud	Ground ($d_{P_r\text{SV}}$)	0.00024	0.00067	0.00178
Point Cloud	Ground ($d_{P_r\text{SH}}$)	0.00015	0.00050	0.00099
CAD	Angled ($d_{P_r\text{SH}}$)	0.00000	0.00000	0.00000
CAD	Angled ($d_{P_r\text{SV}}$)	0.00000	0.00000	0.00000
Point Cloud	Angled ($d_{P_r\text{SH}}$)	0.00040	0.00070	0.00170
Point Cloud	Angled ($d_{P_r\text{SV}}$)	0.00020	0.00070	0.00150

Table 4.29: Error Quantification: Profile Spacing

Surface	Err(m)	α_{scan}	γ_{scan}	α_{targ}	β_{targ}	M_f	Vel(m/s)
Grnd (H)	0.0009	0.10^o	n/a	n/a	n/a	0.01Hz	0.002
Grnd (V)	0.0018	1.65^o	n/a	n/a	n/a	1.63Hz	0.200
Wall (H)	0.0017	1.50^o	n/a	1.93^o	n/a	4.00Hz	0.200
Wall (V)	0.0015	1.00^o	0.5^o	n/a	1^o	1.50Hz	0.130

4.4.3 Point Spacing

In this section, MIMIC's point spacing calculations are verified. These tests validate the geometric formulae used to calculate point spacing on the scan

plane. The formulae are verified using CAD models, an XP1 point cloud and an Optech Lynx point cloud. The Optech Lynx point cloud facilitates testing of the effect of different scanner rotations on point spacing on angled surfaces. The Optech Lynx data further enables robust testing because it has been supplied at different PRRs and mirror frequencies.

4.4.3.1 Horizontal Plane

For the CAD tests, a set of 3D lines are created in a CAD environment. These 3D lines represent laser pulses. The lines incorporate scanner rotations, scanner height, the ASW and a selection of specified horizontal target distances. These 3D lines are then extended to intersect with a planar surface as illustrated in Figure 4.19. The angle between each of the 3D lines is the ASW. The distance between the points of intersection on the plane is then measured and this value is the point spacing. The horizontal range to the intersection point is varied for each test. Table 4.30 details these measurements for a scanner height of 3.1m (the XP1's scanner height) and an ASW of 0.12^o (the XP1's ASW) for varying vertical scanner rotations and varying target ranges. The measurements recorded in the CAD environment are in agreement with the output from MIMIC. The predicted values correspond exactly with the measured values and therefore the CAD tests validate MIMIC's calculations for point spacing on a horizontal plane.

The point spacing calculation requires a planar surface. Therefore these point cloud tests require a surface with a constant elevation for testing. Planar road surfaces are not common. Due to the danger posed by water pooling on the road surface (skidding, ice) roads must be able to drain this water.

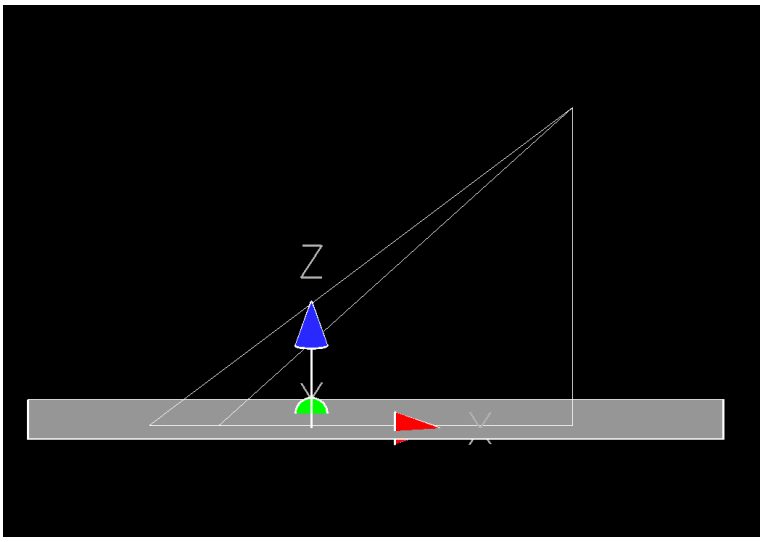

Figure 4.19: Point Spacing - CAD Measurements on a Planar Horizontal Surface

Table 4.30: Point Spacing - MIMIC Predictions Compared to CAD Measurements at a Scanner Height of 3.1m and an ASW of 0.12^o

No.	γ_{scan}	H_r (m)	MIMIC (m)	CAD (m)	Error (m)
1	45^o	2	0.0110	0.0110	0
2	45^o	4	0.0169	0.0169	0
3	45^o	6	0.0265	0.0265	0
4	30^o	1	0.0081	0.0081	0
5	30^o	3	0.0128	0.0128	0
6	30^o	5	0.0222	0.0222	0
7	15^o	7	0.0389	0.0389	0
8	15^o	8	0.0487	0.0487	0
9	15^o	9	0.0599	0.0599	0

Engineers design roads to facilitate good drainage [Schofield, 2007]. A result of these designs is that roads of constant elevation in cross section are almost non-existent in a real world setting. One potential surface of constant elevation for these tests is the road crest. On well constructed roads, the elevation of the road does not change over short distances in the direction of travel, except for traffic control measures such as speedbumps. For example, if the vehicle is turning at a junction a scan profile could be obtained which extends along the road crest. Figure 4.20(a) demonstrates this principle. Two scan profiles are manually selected to demonstrate this difference in elevation change. Figure 4.20(b) displays the variation in elevation of a scan profile crossing the road and of a scan profile running along the road crest. A significant deviation in the height of the points across the road (the red line) is apparent when compared to the points along the road crest (the blue line). The elevation remains relatively constant for a distance of approximately 10m on the road crest. A scan profile of constant elevation is manually selected from the data for the point cloud tests.

The 10m scan profile along the road crest consists of 366 points. The 2D Cartesian distance between subsequent points is calculated, using

$$\text{Cartesian Distance} = \sqrt{(x2 - x1)^2 + (y2 - y1)^2}. \tag{4.41}$$

This introduces two potential error sources. The first is the approximation of the scan profile. Figure 4.21 illustrates this issue. The Cartesian distance that is calculated for validation is the dashed red line. MIMIC assumes a constant scan profile, and the point spacing that it calculates is represented by the green and blue lines. An extreme case is highlighted in

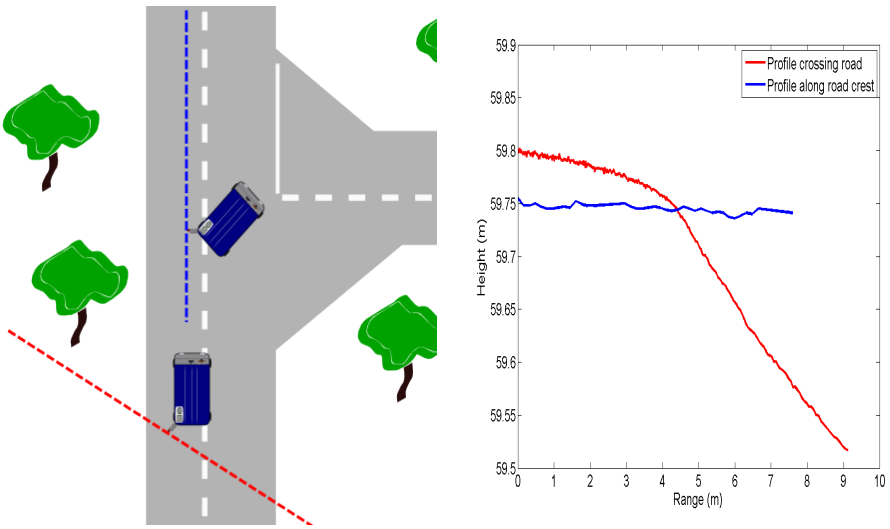

(a) (b)

Figure 4.20: Point Spacing (a) Standard Profile Crossing the Road / Profile on the Road crest (b) Elevation Change

Figure 4.21. The second potential error source relates to system calibration. The 2D Cartesian calculation assumes that the road surface is planar, but if orientation errors exist in the scanner calibration then this may not be the case. The measured distance between subsequent points is then compared against the point spacing MIMIC calculates for a point at that distance from the scanner.

To assess the importance of a minimum height deviation to the calculation, a non-planar surface is also included in these point spacing tests. Points from a profile along the road crest and a scan profile crossing the road are measured and both are plotted as a function of range. A curve is fitted to the data for comparison with the theoretical model as shown in Figure 4.22(a) for profiles crossing the road and 4.22(b) for the road crest. The variation in the point spacing measurements arising from the 2D Cartesian calculation can

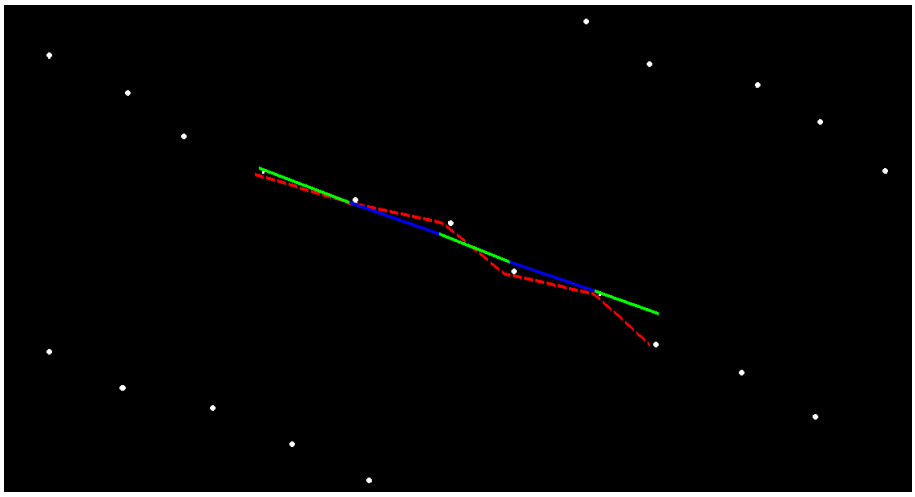

Figure 4.21: Ground Point Spacing - Measurement Innaccuracies Through Utilisiation of Cartesian Coordinate Formula

be seen in these images for both surfaces. The final plot of each quadratic fit is shown in Figure 4.23. The predicted and the measured point spacing for the planar road crest correspond, thus experimentally validating MIMIC for a planar surface with point cloud data. The point spacing for the scan profile that runs across the road gradient deviates from the predicted value. This is due to the change in elevation of the scan profile crossing the road. It is important to note that the deviation begins to become more pronounced at a range of approximately 5m. Figure 4.20(b) shows that the change in elevation of the scan profile crossing the road increases significantly at the 5m mark. The 5m mark is where the crest in the road lies and therefore the elevation changes. As the elevation changes, the road deviates from the plane used in MIMICs calculations and therefore errors accumulate accordingly. The ground point spacing tests could not be repeated for the Optech Lynx data as there are no right or left turns at a junction to provide an area of minimum height deviation as illustrated in Figure 4.20(a). If precise information on the road gradient is provided, MIMIC could be adapted to

calculate point spacing on scan profiles crossing the road. This will not be attempted in this thesis but will be discussed in greater detail in Chapter 8 as a potential topic for future work.

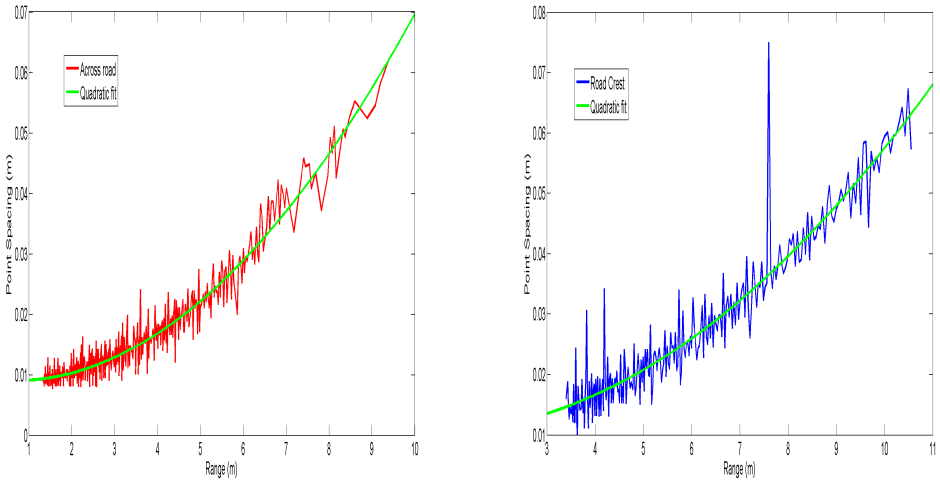

(a) (b)

Figure 4.22: Quadratic Fit (a) Across Road (b) Along Road Crest

4.4.3.2 Vertical Plane

Horizontal and vertical rotations of the scanner are incorporated to verify the point spacing calculations on a vertical surface. A set of 3D lines are created representing individual laser pulses. These lines are separated by the ASW. For the CAD tests both the horizontal and vertical rotations of the scanner are altered. These 3D lines are then extended to intersect with the vertical surface. The distance between the two points of intersection is the point spacing. Similarly to the previous CAD tests, a scanner height of 3.1m is applied and an ASW of 0.12^o. Table 4.31 illustrates the predicted point spacing against the measured point spacing for a vertical surface. A different

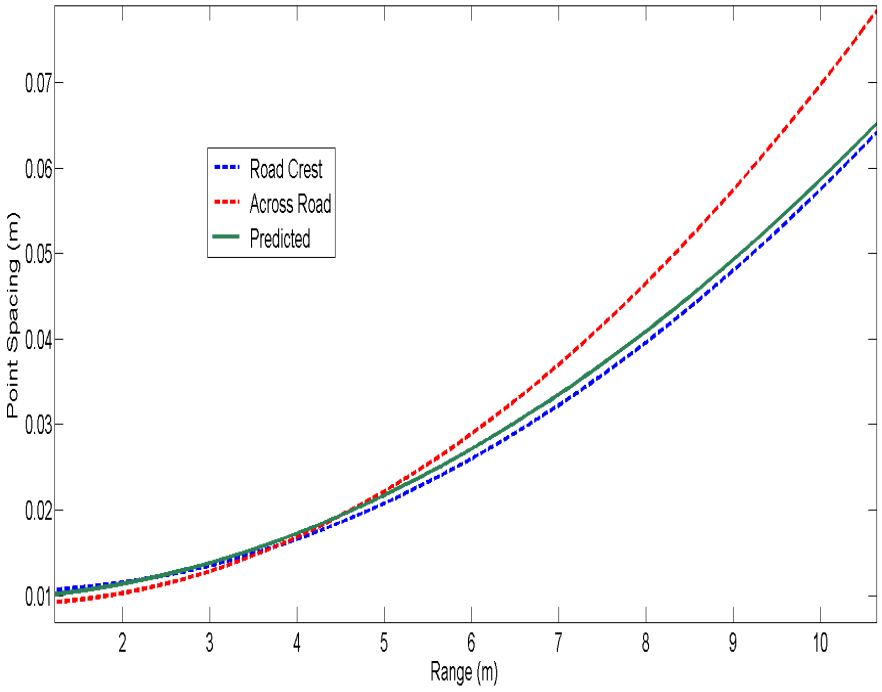

Figure 4.23: Comparing Measured and Calculated Point Spacing Along and Across the Road Crest as a Function of Range

target range is applied for each test. MIMIC has predicted the point spacing accurately and with zero error. Due to the difficulty in locating vertical, parallel surfaces, the point cloud tests are applied to angled surfaces only.

Table 4.31: Point Spacing - MIMIC Predictions Compared to CAD Measurements for a Vertical Plane at a Scanner Height of 3.1m and an ASW of 0.12^o

No.	α_{scan}	γ_{scan}	Range	MIMIC (m)	CAD (m)	Error (m)
1	45^o	45^o	2m	0.0072	0.0072	0
2	45^o	45^o	3m	0.0109	0.0109	0
3	45^o	30^o	3m	0.0099	0.0099	0
4	45^o	30^o	4m	0.0132	0.0132	0
5	30^o	30^o	5m	0.0126	0.0126	0
6	30^o	30^o	4m	0.0101	0.0101	0
7	30^o	15^o	6m	0.0147	0.0147	0
8	30^o	15^o	7m	0.0171	0.0171	0
9	15^o	15^o	8m	0.0174	0.0174	0
10	15^o	15^o	9m	0.0196	0.0196	0

4.4.3.3 Angled Planes

Horizontal and vertical scanner rotations are investigated for verification of MIMIC's point spacing calculations for an angled surface. The range from the scanner to the target is constant and only the target orientation is varied in these tests to assess the effect of target orientation on point spacing. For the initial CAD tests a vertical surface is placed in various orientations and a series of 3D lines representing laser pulses are created. The scanner is at an elevation of 3.1m, orientated at $45^o/45^o$ and placed at a range of 4m from the target, although the range changes depending on the rotation of the target. An ASW of 0.12^o is once again applied. The test set-up is illustrated

in Figure 4.24. The target is rotated in 15^o steps in horizontal and vertical and then a dual axis rotation. Anti-clockwise and clockwise rotations are included. The 3D lines are intersected with the rotated surface and distance between two points of intersection is measured. The results are displayed in Table 4.32. Once again, the CAD tests validate MIMICs method for calculating point spacing on angled surfaces, returning a zero error.

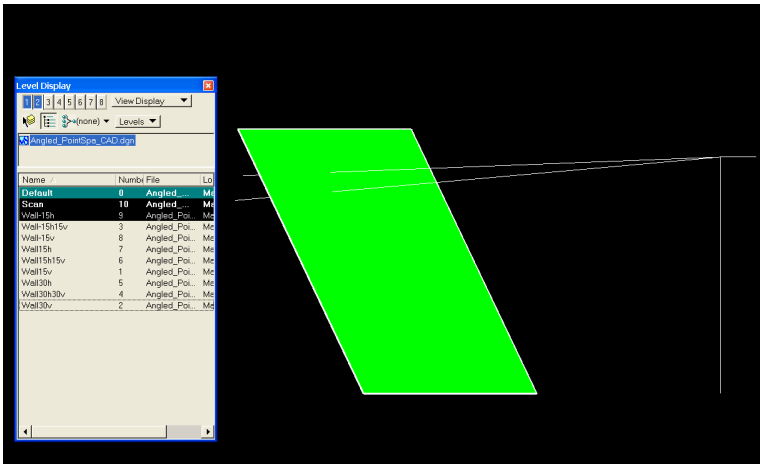

Figure 4.24: Point Spacing - CAD Measurements on an Angled Plane

To validate the point spacing calculation with point cloud data, a set of 16 surfaces from the XP1 and Optech Lynx datasets are selected. The selected surfaces have varying target heights, ranges to the scanner and surface orientations. The distance between subsequent points on the angled surface is measured manually. The results of these tests have been detailed in Tables 4.33, 4.34 and 4.35. The complete set of results are included in Tables 15 and 16 in Appendix .1. Tests 1 - 6 are from the XP1's Riegl VQ-250 operating at 300kHz with a mirror speed of 100Hz and the scanner rotated at 45^o/45^o, tests 7-11 are taken by the Optech scanner rotated at 37.48^o/29.6^o

Table 4.32: Point Spacing - MIMIC Predictions Compared to CAD Measurements for an Angled Plane at a Scanner Height of 3.1m and an ASW of 0.12^o

No.	α_{targ}	β_{targ}	MIMIC(m)	CAD(m)	Error(m)
1	15^o	0^o	0.0129	0.0129	0
2	0^o	15^o	0.0201	0.0201	0
3	15^o	15^o	0.0157	0.0157	0
4	30^o	0^o	0.0100	0.0100	0
5	0^o	30^o	0.0280	0.0280	0
6	30^o	30^o	0.0210	0.0210	0
7	-30^o	0^o	0.0339	0.0339	0
8	0^o	-30^o	0.0063	0.0063	0
9	-30^o	-30^o	0.0061	0.0061	0

operating at 125kHz and with a mirror speed of 100Hz, and tests 12 - 16 are recorded at the same scanner rotation but operating at 500kHz and a mirror speed of 200Hz. In each case the errors are low, with the largest error just under 2mm at a range of approximately 8m. By altering the target rotation for each point, the range to the target, the height difference between the scanner and target, the PRR and the mirror speed, MIMICs capabilities of predicting point spacing are tested robustly. Figure 4.25 graphically illustrates the error of the points plotted against the standard deviation. As with previous examples, the lower the standard deviation the more reliable the measurement and the lower the error the better the match between the predicted and measured values.

Table 4.33: Point Spacing - MIMIC Predictions Compared to Point Cloud Measurements for an Angled Surface. Surveyed with a Scanner Rotation of $45^o/45^o$, a PRR of 300kHz and a M_f of 100Hz on the XP1

No.	α_{targ}	β_{targ}	Z_{diff} (m)	Range(m)	σ(m)	Error(m)
1	1.93^o	0.00^o	1.492	5.367	0.0003	0.0009
2	0.15^o	15.00^o	1.476	5.947	0.0004	0.0017
3	2.81^o	30.00^o	1.479	7.796	0.0004	0.0009
4	-1.00^o	45.00^o	1.351	6.409	0.0013	0.0015
5	48.59^o	6.21^o	1.426	5.291	0.0008	0.0001
6	72.54^o	20.00^o	1.443	6.181	0.0005	0.0012

Table 4.34: Point Spacing - MIMIC Predictions Compared to Point Cloud Measurements for an Angled Surface. Surveyed with a Scanner Rotation of $37.48^o/29.6^o$, a PRR of 125kHz and a M_f of 100Hz on the Optech Lynx

No.	α_{targ}	β_{targ}	Z_{diff} (m)	Range(m)	σ(m)	Error(m)
7	19.67^o	0^o	2.647	16.840	0.0021	0.0008
8	16.74^o	0^o	2.531	7.580	0.0007	0.0018
9	-1.28^o	0^o	2.480	11.190	0.0009	0.0004
10	-10.80^o	0^o	2.795	10.010	0.0007	0.0016
11	30.81^o	0^o	2.392	12.940	0.0011	0.0011

Table 4.35: Point Spacing - MIMIC Predictions Compared to Point Cloud Measurements for an Angled Surface. Surveyed with a Scanner Rotation of $37.48^o/29.6^o$, a PRR of 500kHz and a M_f of 200Hz on the Optech Lynx

No.	α_{targ}	β_{targ}	Z_{diff} (m)	Range(m)	σ(m)	Error(m)
12	18.95^o	0^o	2.337	7.550	0.0005	0.0002
13	16.24^o	0^o	2.280	6.230	0.0007	0.0001
14	-2.18^o	0^o	2.348	7.760	0.0001	0.0012
15	-12.80^o	0^o	2.582	8.950	0.0011	0.0012
16	33.05^o	0^o	2.110	10.110	0.0002	0.0008

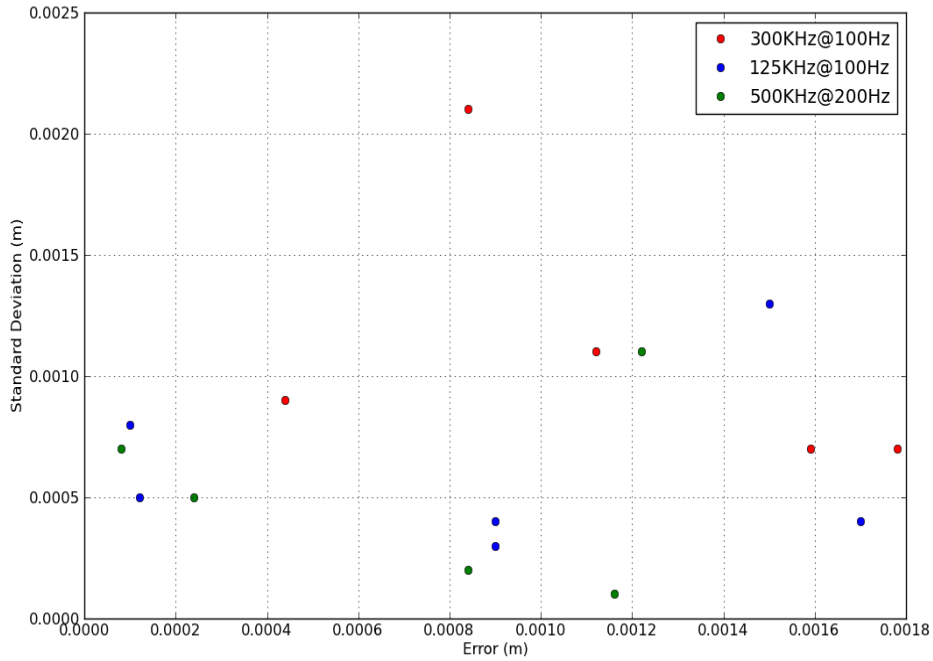

Figure 4.25: Point Spacing - Point Cloud Tests on an Angled Surface for Different Scanner and Mirror Frequencies - Error v Std Dev

4.4.3.4 Discussion and Error Sources

This section provides a summary of the errors and identifies the minimum, mean and maximum errors for each test, as displayed in Table 4.36. An examination of each error is included in Chapter 5 in the point density calculations. As the error in point spacing is a function of range and the target's attributes, it is not possible to quantify these errors in the same manner as the profile spacing and profile angle tests. For instance, a 2mm error at a range of 1m could be due to the same angular error as a 20mm error at a range of 20m. When analysing the errors, one trend that becomes apparent is that although the errors are low, the predictions for the 500kHz system exhibit the highest errors of the three tests. The reason for this is uncertain and it may be simply down to the choice of test sites. Overall the errors are low, but an examination of the effect of these errors in the point density calculation in Chapter 5 will provide a definitive answer on the accuracy of MIMIC's predictions.

Table 4.36: Point Spacing - Summary of MIMIC's Calculation Errors in Point Cloud Tests

Test	Min (m)	Mean (m)	Max (m)
Ground Point Spacing	0.00001	0.00200	0.037
Angled Point Spacing	0.00008	0.00097	0.018

4.5 Conclusions

This chapter presented the geometric formulae for calculating the profile angle, profile spacing and the point spacing on different target types. These

target types included horizontal planes and angled surfaces. The profile angle, profile spacing and point spacing calculations were then validated in a series of tests using constructed CAD models and point cloud data from the two test MMS introduced in earlier chapters. MIMIC requires three parameters to calculate point density on a target.

The first value calculated was the profile angle. A series of CAD tests were designed to verify the calculations. MIMIC's values were compared to the CAD measurements and the errors were quantified. The errors were low, and largely due to the manual element of the validation process. The point cloud tests exhibited higher errors, demonstrating the impact of vehicle dynamics and also highlighting a potential calibration issue with the XP1 data. The highest mean error for the profile angle tests was 3.0007^o. This error was encountered in the point cloud tests on an angled surface with the XP1. The Optech Lynx data exhibited lower errors, and would seem to reinforce the calibration issue with the XP1, however differences between the two datasets preclude a definitive answer on this. Dedicated calibration tests would be required to answer this question and this is outside the scope of this thesis.

The second output value from MIMIC was the profile spacing. A combination of CAD and point cloud tests were once again applied to validate MIMIC's calculations. There was no error in each of the CAD tests which validated the profile spacing calculations. The results from the point cloud tests were also promising, with all errors below 2mm. The highest mean error for the profile spacing tests was 0.0007m, this was encountered in the point cloud tests on an angled surface.

The final output from MIMIC was the point spacing. The CAD tests once again returned no error, validating MIMIC's point spacing calculations. The highest mean error for the point spacing tests was 0.002m, which was encountered in the point cloud tests on a horizontal surface. The reason for this error has been shown to be the measurement method for validating point spacing. By calculating a Cartesian distance between the points, the uneven point distribution introduced errors in the measured values.

Assessment of errors in the profile angle, profile spacing and point spacing claculations will be carried out in detail in the following chapter. Chapter 5 will introduce the methodology for calculating point density using these three outputs.

Chapter 5

Calculating Point Density

Three elements are required to calculate point density: profile angle, profile spacing and point spacing. Chapter 4 detailed and validated the process of calculating these three elements for a single location on an object. MIMIC accepts targets of varying dimensions and is designed to provide point spacing information at multiple locations on the target. These additional point spacing values are combined with the profile information in the point density calculation. The 2D planar procedure in MIMIC's calculation module (described in Chapter 4) is adapted for 3D real world objects. This chapter details the methods employed to calculate point density and validates these methods.

5.1 Introduction

The method for calculating point spacing and profile information was presented and validated in the previous chapter. It was demonstrated that point density could be accurately calculated on targets with varying rotations and elevations for scanners at different orientations and elevations. Existing point

density calculators [RIEGL, 2012a] do not take these factors into account. These calculators do not accept targets of varying elevation and rotation and ignore the variations in point spacing that are present on these targets. This leads to inaccuracies in their point density calculations. This chapter demonstrates the process that has been developed to calculate point density on targets of different dimensions and rotations. A grid structure is applied to the target and this allows for the calculation of point spacing at multiple locations on the target. Section 5.2 discusses the gridding process in more detail for different target types and also demonstrates how this is beneficial for targets of different dimensions and orientations. Section 5.2.3 explains how each output from the profile spacing, profile angle and point spacing calculations are combined in the point density calculation for different targets. Section 5.3 demonstrates how different 2D targets are combined to represent real world 3D features. The point density calculations are verified in Section 5.4.

5.2 Targets

Assuming constant vehicle velocity, zero course deviation and zero vehicle dynamics, the profile angle and the profile spacing do not vary across a planar target. Chapter 3 explained that profile angle and profile spacing are not affected by range. Therefore the point spacing is the only output from Chapter 4 that varies across the target. The orientation, dimensions of, and range to the target all influence point spacing. To calculate the point density of a target the point spacing is calculated at different locations on the target. MIMIC creates a grid structure over the target and calculates point spacing for each grid cell. The grid structure is user specified. This section details the

process involved in gridding a target. It also defines the valid target types.

5.2.1 Gridding Targets

The gridding process applies a MxM grid over a target, as shown in Figure 5.1(a). The MxM gridding approach is successful for large targets whose width and height are similar, as illustrated in Figure 5.1(a), however this grid structure is not optimised for narrow targets, as illustrated in Figure 5.1(b). Large areas of redundant measurements are visible in this figure, particularly on the horizontal axis of the target. If this grid structure is applied to a narrow, vertical target, eight measurements are recorded across the horizontal axis of the target. For a narrow vertical target, it is unlikely that any variation in point spacing would be evident between these eight measurements. Eight measurements would also be recorded for the vertical axis of the target where there is more potential for variation in point spacing and this may be insufficient for a tall target, particularly if the target is vertically rotated. On an vertically rotated target the variation in point density increases. Therefore a different grid structure is designed for narrow objects that are predominantly vertical. This structure is a single column of vertical grids. An example of the gridding structure for narrow targets is illustrated in Figure 5.2(a). This grid structure can be amended to include a second column if additional measurements are required across the horizontal axis of the target. The requirement for a second column depends on the width of the target.

The size of each grid cell is dependant on the size of the target and the grid structure selected by the user. For instance, if the target is 2m wide and

1m metre tall and the user selects 64 grids (8x8), the dimensions of each grid cell are 0.5m x 0.25m. If the user believes there is a significant point spacing variation across the target the number of grid cells can be increased. MIMIC is designed to apply a 4 (2x2), a 16 (4x4) and a 64 (8x8) grid structure. Section 5.4.1 demonstrates the effect of the different grid structures on the point density calculation.

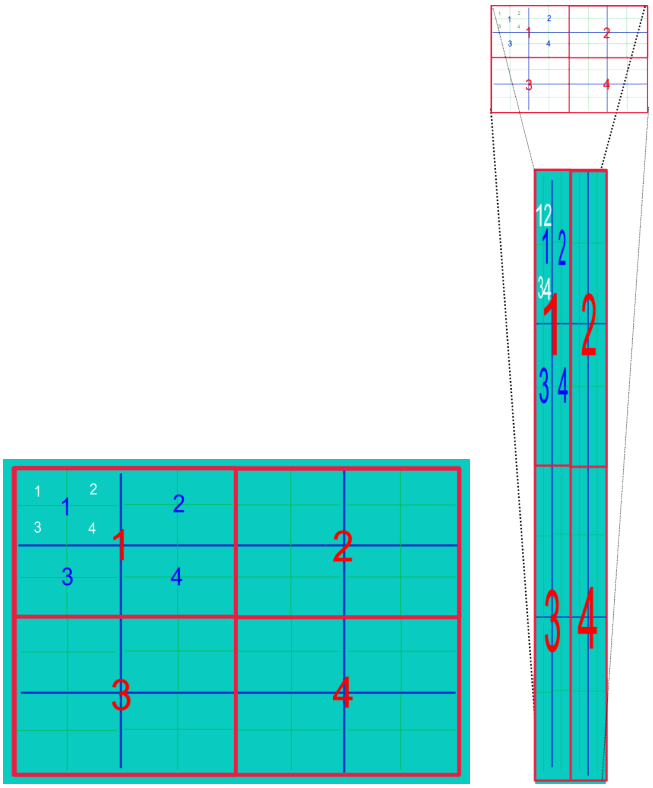

(a) (b)

Figure 5.1: Standard M x M Grid Structure Applied to (a) a Wide Target and (b) a Narrow Vertical Target

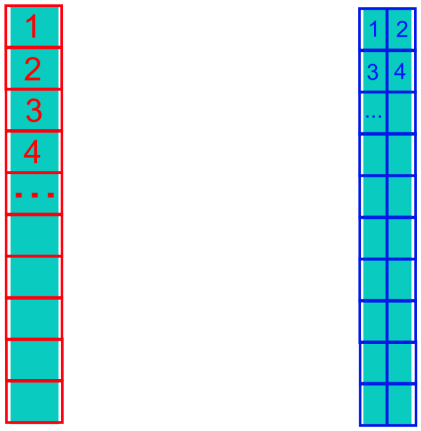

(a) (b)

Figure 5.2: Amended Grid Structure Designed for a Narrow Target (a) Single Column (b) Additional Horizontal Column

5.2.2 Position of Grid Cell Centre

The centre point of each grid cell requires the user specified target dimensions, range to the target and the grid structure for calculation. All grid cell centres are offsets to a pivot point, as illustrated in Figure 5.3. The pivot point is the fixed point on the target that MIMIC applies horizontal and vertical target rotations around. The center of the cell is assigned a (H Offset,V Offset) coordinate comprising the horizontal and vertical offset from this pivot point. Figure 5.3 illustrates this principle for one of the grid cell centres on the target. The horizontal offset can be positive or negative to identify whether it is on the left hand side or right hand side of the target relative to the pivot point.

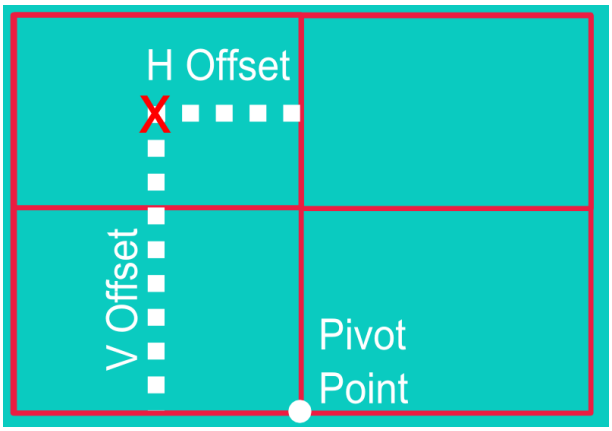

Figure 5.3: Horizontal and Vertical Offsets from the Pivot Point to the Grid Cell Centres

5.2.2.1 Range to Grid Cell Centre

The horizontal range (H_r) to the target is user specified in the input stage of MIMIC. The horizontal range to each grid cell does not change if no target rotations are applied. The true range to the grid cell centres from the scanner are calculated using the offsets to the grid cell centre and the information on the dimensions of the target. By applying the formulae and principles from Section 4.3.2, the grid cell centres are calculated. If target rotations are applied, then the range measurements vary per grid cell centre. An additional step is required for rotated targets.

5.2.2.2 Orientation of Target

A target is rotated around the pivot point. Rotations of the target alter the height of, and the range to, the grid cell centres. The effect of target rotations on these values varies depending on what target rotations are applied. Figure 5.4 displays the two axes of rotation for the target. In Figure 5.4(a) a horizontal rotation of the target is illustrated. Rotating around the pivot

point, a horizontal rotation results in a decrease and increase in range to alternate sides of the target. The elevation of the grid cell centres are not effected by a horizontal rotation of the target. Figure 5.4(b) illustrates a vertical rotation of the target. A target can incline away from or towards the MMS. If the target is inclined away from the MMS the elevation of the target decreases but the range to the target is increased. If the target is inclined towards the MMS the elevation decreases and the range to the target also decreases.

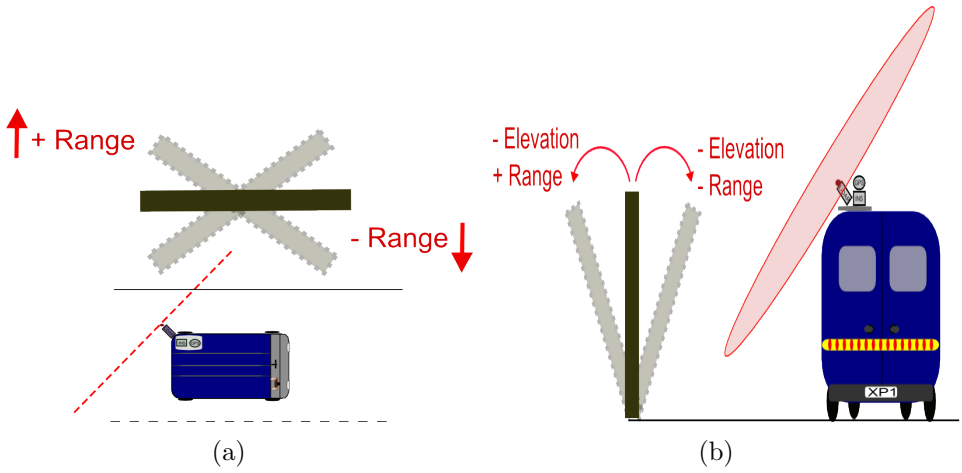

Figure 5.4: Changes in Range to and Elevation of Grid Cell Centres for (a) a Horizontal Target Rotation (b) a Vertical Target Rotation

The following principles are applied to calculate the change in range to, and elevation of, each grid cell centre resulting from a horizontal and vertical target rotation. MIMIC initially calculates the change in range resulting from a horizontal rotation of the target. A horizontal rotation (α_{targ}) is applied to the target at the pivot point, p, as illustrated in Figure 5.5. For each grid cell centre, the change in the horizontal range to the point, $r1$, can be calculated with

$$r1 = \text{H Offset} * \sin \alpha_{\text{targ}}. \tag{5.1}$$

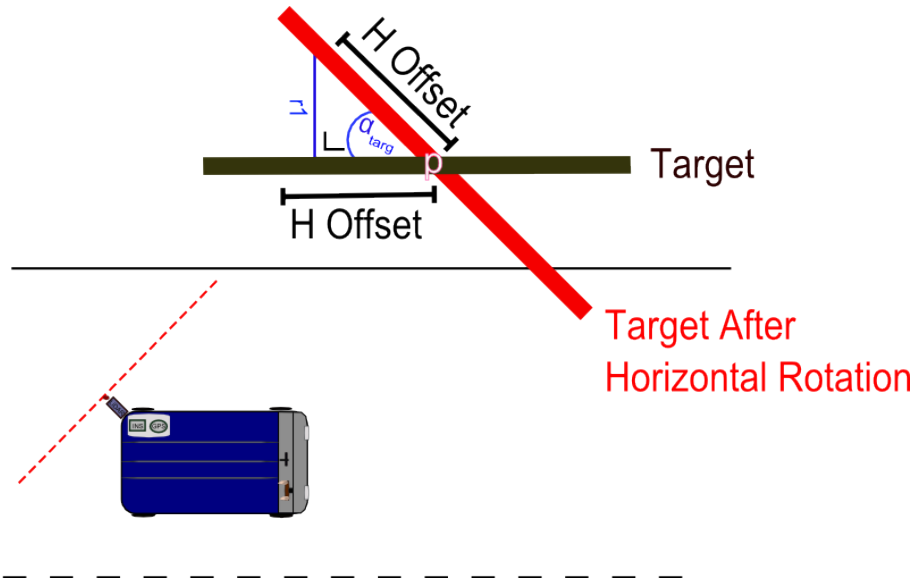

Figure 5.5: Calculating the Change in Horizontal Range, r1, from the Scanner to the Target as a Result of a Horizontal Target Rotation

$r1$ is added or subtracted automatically by MIMIC from the initial horizontal range (H_r) depending on whether it is a positive or negative horizontal offset and on the direction of the target rotation.

A vertical rotation of the target (β_{targ}) impacts on both the range to, and elevation of, the grid cell centres. Figure 5.6 illustrates the change in range, $r3$, resulting from a vertical target rotation. To calculate $r3$, $r2$ in Figure 5.7 is required. Figure 5.8 illustrates the rotated target in profile. $r2$ is calculated with

$$r2 = \text{V Offset} * \sin \beta_{\text{targ}}. \tag{5.2}$$

Once $r2$ is calculated, the change to H_r for each grid cell centre is calculated with

$$r3 = r2 * \sin(90 - \alpha_{\text{targ}}). \tag{5.3}$$

$r3$ is also automatically added to or subtracted from H_r depending on the direction of the rotation of the target. After this step, the range to each grid cell centre reflects the affects of horizontal and vertical target rotations.

Figure 5.8 also illustrates the variables required for calculating the elevation of each grid cell center after a vertical rotation of the target. The amended elevation for each grid cell centre, $v1$, is calculated using

$$v1 = V\ \ Offset * \sin(90 - \beta_{\text{targ}}). \tag{5.4}$$

The amended elevations of, and horizontal ranges to each grid cell centre are entered into the formulae in Section 4.3. The point spacing is then calculated for each grid cell centre.

5.2.3 Point Density

To compute the point density of each grid cell, the profile angle and profile spacing are combined with the point spacing that has been calculated for each grid cell centre. This is carried out by tracing each scan profile through the grid structure. Starting at the bottom left hand corner of the target (0,0), MIMIC records which grid cells each scan profile (starting at 0,0) intersects. The length of the scan profile within that cell is also recorded. Figure 5.9 illustrates this process along with the intersection points of the scan profile

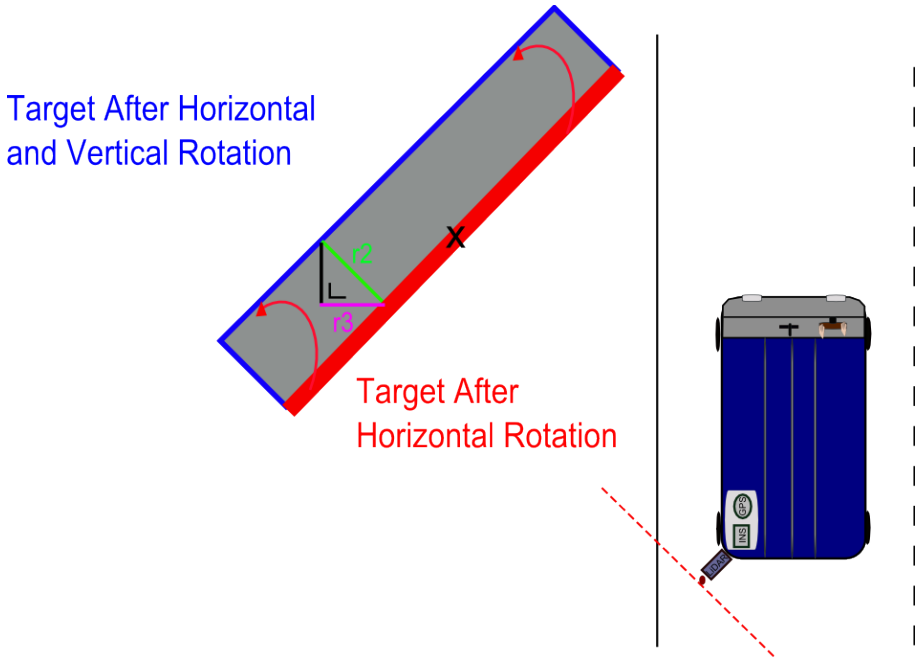

Figure 5.6: Calculating the Change in Horizontal Range, r3, from the Scanner to the Target as a Result of a Vertical Target Rotation for Each Grid Cell Centre - Top Down View

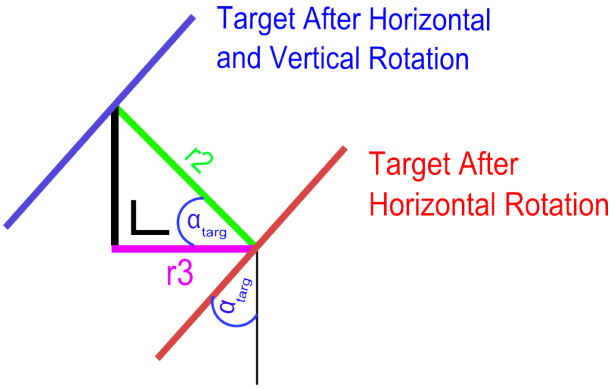

Figure 5.7: Calculating $r3$ for Each grid Cell Centre - Top Down View

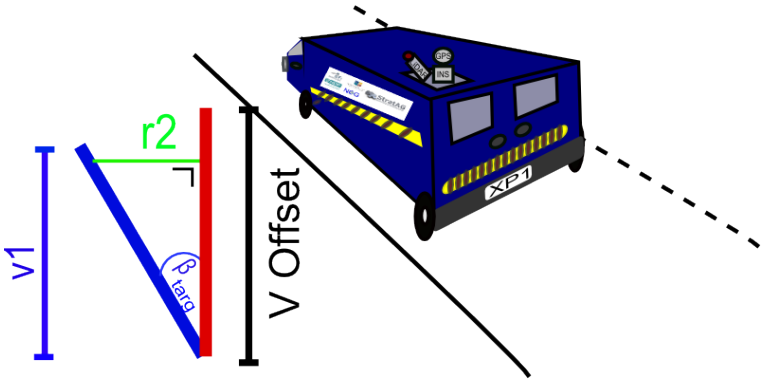

Figure 5.8: Calculating $r2$ and $v1$ for Each Grid Cell Centre- Profile View

and each grid cell. To calculate the number of points in that grid cell, the segment length is multiplied by the point spacing calculated for that grid cell.

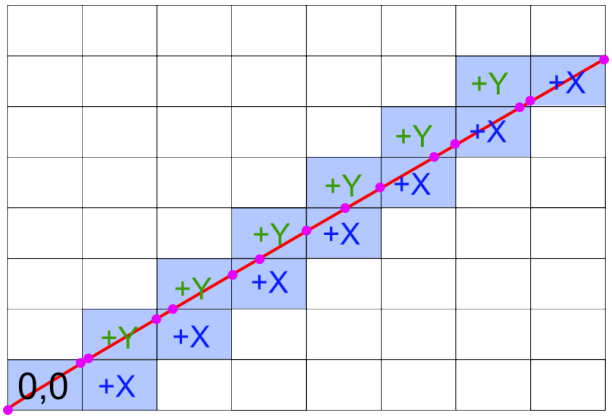

Figure 5.9: Calculating the Intersection Points of the Scan Profile and Individual Grid Cells

Using the computed horizontal and vertical profile spacing, each of the scan profiles that intersect the target can be calculated. The starting point (0,0) is incremented by the horizontal and vertical profile spacing. The X coordinate is incremented by the horizontal profile spacing until the X coordinate matches the width of the target. Starting again at (0,0) the Y value is incremented by the vertical profile spacing until the Y value matches the

height of the target. This method accounts for every profile that intersects the target. The number of points in each cell are calculated by multiplying the point spacing for that grid cell by the length of scan profile in that grid cell. These point density values are then summed for each grid cell and this calculation returns the point density of the target. When calculating point density in this way, one potential issue must be considered. MIMIC assumes that the first point on the target is exactly at the target edge, (0,0). In practice that is not the case as the first point could be any distance up to the point spacing inside the target as the previous pulse may have just missed the target. This error source is illustrated in Figure 5.10.

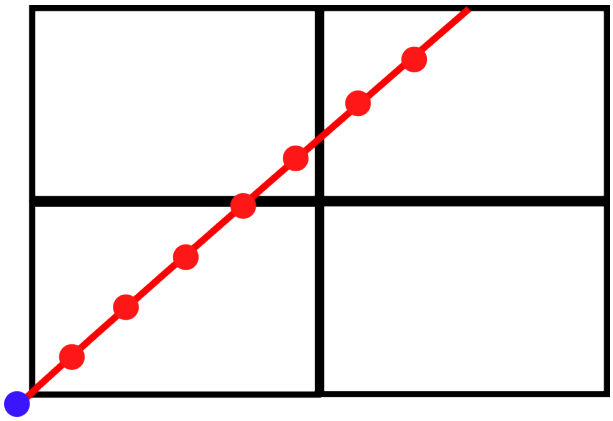

Figure 5.10: Potential Error Source: MIMIC Assumes the First Point is at the Target Boundary whereas the First Point may be Inside the Target.

5.3 Combining Surfaces

MIMIC operates by treating the component parts of 3D targets as a series of 2D planar surfaces. MIMIC then calculates the point spacing, profile angle and profile spacing for each plane, as Section 3.3.2.2 explained. This section describes the methodology developed to calculate point density for targets

consisting of multiple planes and also cylindrical targets.

5.3.1 Multi-Faced Targets

MIMIC only accepts individual 2D planes as valid target types. Multi-faced 3D targets are not a valid input. Therefore MIMIC requires user input to identify the 2D planes that comprise a 3D object. For example, a 3D building requires user input to identify each plane. The range to each plane, the target dimensions and its horizontal and vertical rotations are defined by the user. MIMIC then automatically calculates point density for each plane using the procedure presented in the previous sections. Automatically deconstructing 3D structures into a series of 2D planes is something that could be investigated in any future work.

5.3.2 Cylinders

Cylindrical targets are more complicated. MIMIC does not accept curved surfaces as a valid input. For MIMIC to calculate point density on a cylinder it is first converted into a series of planes. In Chapter 3 a hexagonal formation was introduced as a planar approximation of a cylinder that retains the basic cylindrical shape. Each plane is manually defined by the user. One potential error source that arises by approximating a cylinder with a hexagon is depicted in Figure 5.11. Depending on whether the planar surfaces are drawn inside (Figure 5.11(a)) or outside the cylinder (Figure 5.11(b)), the range to the plane changes accordingly. In Figure 5.11(a), the yellow area is incorrectly added to the true range to the target. In Figure 5.11(b), the area marked in yellow is incorrectly subtracted from the true range to the target. For large cylinders this may be an issue as it results in a change of point

spacing, however small objects like signposts will not exhibit any change in point spacing arising from this error source. For instance, a cylinder of diameter 0.2m (each face of the hexagon would be approximately 0.05m - 0.08m) would result in a change in the range to target of 0.015m. This small adjustment in range would not result in any noticeable impact on point spacing.

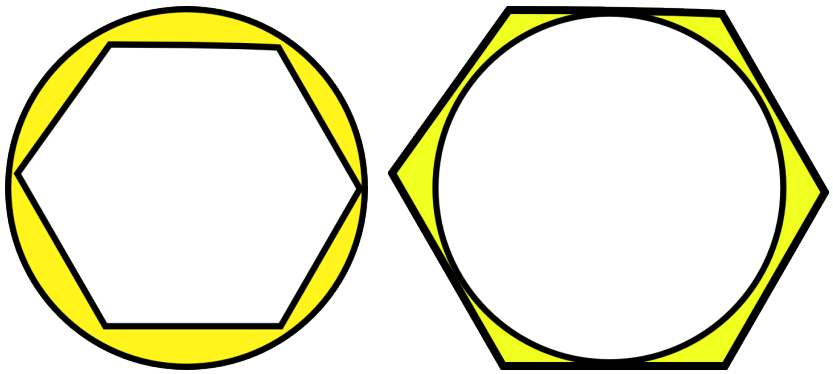

(a) (b)

Figure 5.11: Potential Error Source: A Hexagonal Approximation of a Cylindrical Target (a) Range to Target is Increased and (b) Range to Target is Decreased

MIMIC applies a hexagon to the cylinder using the method displayed in Figure 5.11(b). It applies this method because the tangent point between the cylinder and the face of each hexagon is the mid point of the horizontal axis of the plane. For a single column grid structure, the centre of the grid cell is also the mid point of the horizontal dimension of the plane. Therefore the point of intersection between the hexagon and the cylinder and the center of the grid cell are the same point. Section 5.4.3 assesses MIMICs point density calculations on cylindrical targets.

5.3.3 Line-of-Sight

As explained in Section 3.2.3.5, the line of sight to a target can vary depending on the position and orientation of the scanner. This is particularly relevant for dual scanner systems where one face of an object is only visible to one scanner. This is one of the main benefits of employing a second scanner as exhibited by the work of [Yoo et al., 2009] reviewed in Chapter 2. Dual scanners increase the coverage of a multi-faced target. Figure 5.12 illustrates the principle of line of sight for a dual scanner configuration similar to that on the Optech Lynx. This scanner configuration is common to most commercial systems. Only two faces of the object can be surveyed by a single scanner system. The addition of a second scanner enables a third face of the target to be surveyed and also provides an overlap on the face of the target closest to the MMS.

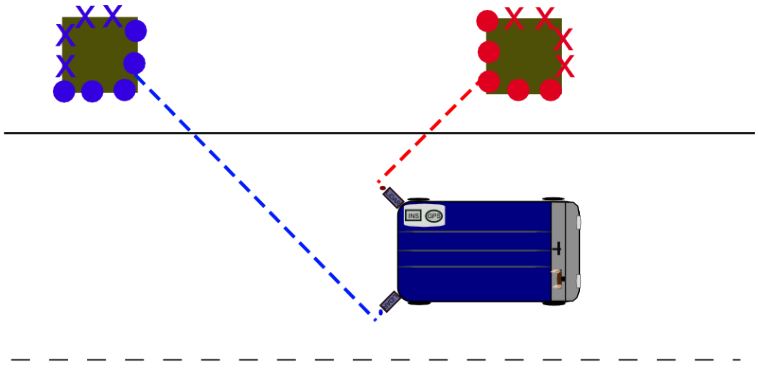

Figure 5.12: Scanner 1 and Scanner 2 Survey Different Faces of the Target. The Offset and Orientation of Scanner 2 Results in an Increased Range to Target

5.4 Results and Analysis

This section verifies that the methodology and formulae presented in the previous sections are capable of combining the point spacing, profile spacing and profile angle outputs from Chapter 4 into an overall accurate representation of the point density of a target. Verifying the point density calculations in a CAD environment would require each laser pulse to be drawn and would be extremely time consuming. Therefore for these tests MIMIC's capabilities are verified using the XP1 and Optech Lynx point cloud data only. The recommended grid structure is first identified in Section 5.4.1. Different mirror frequencies and PRRs are used to robustly test MIMIC's point density calculations for different scanners on angled and cylindrical targets. Section 5.4.4 details the tests facilitated by the Optech Lynx data for verifying the effect of incorporating a second scanner on point density. Finally, the impact that errors in the profile information and point spacing calculations have on the final point density calculation are assessed in Section 5.4.5.

5.4.1 Grid Structure

One factor that must be considered when assessing the quality of the point density calculation is the number of grids employed in the calculation. A 4x4 grid structure is applied for all of the standard target point density tests in this chapter. This is because a 4x4 grid structure provides a higher level of detail than a 1x1 or a 2x2 grid structure, but due to the manual nature of the measurements is less time consuming than an 8x8 grid structure. Increasing the number of grids increases the number of point spacing measurements on the surface. For example, a larger error in point density would arise if a 2x2 grid structure is applied to a large wide target than if a 4x4 grid

structure is applied. A 6x1 grid structure is applied for the narrow vertical targets. This grid structure is chosen for narrow vertical targets because the cylinders used in the testing are not large targets. Additionally none of the cylindrical targets were rotated vertically minimising point spacing variation.

To demonstrate the effect of different grid structures on the point density calculation, a large 5m x 2m target is selected. The target is rotated horizontally by 30^o. The range to the target is 6m and the scanner elevation is 3.1m. The scanner is orientated at 45^ox45^o, operating at a 300KHz PRR and a 100Hz mirror frequency. The vehicle is simulated at 50km/h. This target is chosen to illustrate the variation in point spacing on a large, rotated target and the resulting effect that different grid structures have on the point density calculations. Table 5.1 demonstrates the effect of sampling with five different grids structures. The first grid structure, a 1x1, represents existing point density calculators that calculate point spacing at a single central target location. The 2x2 is the smallest grid structure that MIMIC utilises. Both the 1x1 and 2x2 grid structures do not calculate the increased and decreased point spacing at the extents of the target and have therefore insufficiently described the target. By incrementally increasing the number of grids the change in point density for different grid structures is identified. For a large rotated target, a difference of almost 634 points exists between the 1x1 and 16x16 grid structures.

These tests are repeated for a smaller target using the same parameters, but varying the target dimensions. The target dimensions are 1m x 0.5m. The results are displayed for each grid structure in Table 5.2. The variation

Table 5.1: Calculating the Influence of Different Grid Structures on MIMIC's Point Density Calculations for a Rotated 5m x 2m Target

No. Grids	Point Density
1 (1x1)	8527pts
4 (2x2)	8901pts
16 (4x4)	9040pts
64 (8x8)	9104pts
256 (16x16)	9161pts

in point density is low, a variation of only 1 point for each grid structure, including the 1x1. However, it should be noted that in these tests on the 1x1 grid structure, MIMIC is used to calculate point spacing at the centre of the target. Unlike existing point density calculators, target orientation, target elevation, scanner orientation and scanner elevation have all been included in the calculation, therefore the point spacing calculation for the 1x1 grid structure gives a misleading indication of its accuracy. These results and the previous 5m x 2m target tests demonstrate that the 1x1 grid structure is only suitable for small targets. The 4x4 grid structure is chosen for the validation tests in this thesis because it provides additional point spacing measurements for large, rotated targets but because of the manual nature of the measurements in the validation tests it is less time consuming than the 8x8 or 16x16 grid structures.

5.4.2 Angled Surfaces

The quality of the point density calculations for angled surfaces are assessed in this section. The point density calculations are validated by gridding a target and comparing the number of points in each cell with MIMIC's calculated

Table 5.2: Calculating the Influence of Different Grid Structures on MIMIC's Point Density Calculations for a Rotated 1m x 0.5m Target

No. Grids	Point Density
1 (1x1)	442pts
4 (2x2)	441pts
16 (4x4)	441pts
64 (8x8)	441pts
256 (16x16)	441pts

value for that cell. Angled targets of different dimensions are first identified in the point cloud. The two target types are illustrated in Figure 5.13. The dimensions of the target outlined in red are 1m x 0.5m. The dimensions of the target outlined in blue are 0.5m x 0.5m. Targets of these dimensions are identified on four different angled surfaces and a 4x4 grid structure is applied to each. The dimensions, orientation and range to each target are defined in MIMIC. MIMIC calculates a total point density for the target and also calculates the point density for each grid cell. The point density is measured for the entire target and also for each individual grid cell. This is illustrated for a 0.5m x 0.5m target in Figure 5.14.

Table 5.3 displays the details of the point density tests for the 1m x 0.5m target at different PRRs and mirror frequencies. Table 5.4 displays the results of these tests. Table 5.5 displays the details of the point density tests for the 0.5m x 0.5m target at different PRRs and mirror frequencies. Table 5.6 displays the results of the tests for the 0.5m x 0.5m target. The complete set of results detailing all survey variables and vehicle dynamics can be seen in Tables 17 and 18 in Appendix .2.

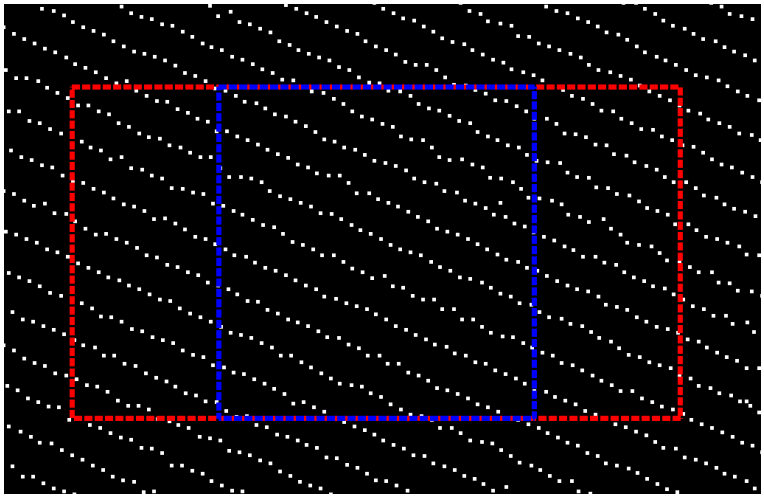

Figure 5.13: Validating MIMIC's Point Density Calculations on Two Angled Targets of Dimensions 1m x 0.5m (Red) and 0.5m x 0.5m (Blue)

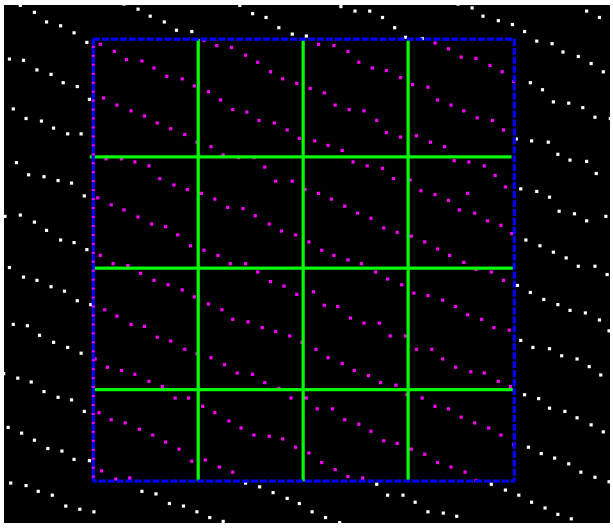

Figure 5.14: Validating MIMIC's Point Density Calculations by Measuring Point Density for Each Grid Cell on a 0.5m x 0.5m Target

Table 5.3: Test Parameters for Validating MIMIC's Point Density Calculations on an Angled Target of Dimensions 1m x 0.5m for the Optech Lynx

No.	H_r(m)	Vel(m/s)	Z_{diff}(m)	α_{targ}	PRR	M_f
1	7.665	5.813	1.218	17.33^o	125KHz	100Hz
2	11.796	7.224	1.953	-1.12^o	125KHz	100Hz
3	11.432	7.21	2.089	0.1^o	250KHz	150Hz
4	6.422	5.318	1.345	22.79^o	250KHz	150Hz

Table 5.4: Calculated and Measured Point Density for an Angled Target of Dimensions 1m x 0.5m

No.	MIMIC	Measured	%Error	Profiles	Error Per Profile
1	253pts	269pts	5.90%	27	0.59pts
2	117pts	122pts	4.09%	18	0.27pts
3	247pts	284pts	13.02%	28	1.32pts
4	675pts	741pts	8.90%	45	1.46pts

Table 5.5: Test Parameters for Validating MIMIC's Point Density Calculations on an Angled Target of Dimensions 0.5m x 0.5m

No.	H_r(m)	Vel(m/s)	Z_{diff}(m)	α_{targ}	PRR	M_f
5	7.665	5.813	1.218	17.33^o	125KHz	100Hz
6	11.796	7.224	1.953	-1.12^o	125KHz	100Hz
7	11.432	7.21	2.089	0.1^o	250KHz	150Hz
8	6.422	5.318	1.345	22.79^o	250KHz	150Hz

The results in Tables 5.4 and 5.6 demonstrate that MIMIC is capable of calculating the number of points for a specific target on an angled surface for different scanner settings and vehicle velocities. Although there are errors in each case and MIMIC consistently underestimates the number of points that are in the target area, the errors are justifiable for two reasons.

Table 5.6: Calculated and Measured Point Density for an Angled Target of Dimensions 0.5m x 0.5m

No.	MIMIC	Measured	%Error	Profiles	Error Per profile
5	127pts	137pts	7.29%	14	0.7pts
6	58pts	62pts	6.45%	9	0.4pts
7	124pts	147pts	15.64%	14	1.64pts
8	337pts	352pts	4.26%	22	0.68pts

- The point density of Target 4 in Table 5.4 is underestimated by 66 points. This is the largest error in the point density tests. However, the error is large because the total number of points is high. An error of 66 points for Target 4 corresponds to a percentage error of only 8.90% which is not the largest percentage error.

- The errors must be compared to the number of profiles. The 4th Target in Table 5.4 is underestimated by 66 points, but comprises 45 profiles. This equates to an error of approximately 1.46 points per profile.

To further investigate MIMIC's point density calculations, the individual grid cells are examined. The results for each individual grid cell for Targets 1 - 4 are visualised in Figures 5.15 and 5.16. In each image, the manually measured value is displayed in blue, MIMIC's predicted value is displayed in green and the discrepancy is displayed in red. A value of 0 indicates an accurate calculation of point density, a positive value indicates MIMIC predicted more than was measured in the real world data and a negative value means an underestimation for those grid cells. An underestimation of 4 points in one cell in Target 4 (Figure 5.16(b)) is the highest error. The total point density for this target is underestimated by 66 points, however target 4 also has the highest point density, with over five times as many points as Target

2. Although the errors were lower in Target 2, due to the low point density of Target 2, Target 4 is a higher quality calculation.

Targets 5 - 8 are the smaller, 0.5m x 0.5m target type and are illustrated in Figures 5.17(a) - 5.17(d). The greatest error on the 0.5m x 0.5 targets is -3 points on Target 8. This target exhibits the highest errors but it has approximately six times as many points per grid cell as Target 6 which is the most accurate prediction. The point density for Target 6 is correctly predicted for eight (50%) of the grid cells. The remaining grid cells are low overestimates or underestimates of 1 point. Overall, the errors are low, particularly when compared with the number of points per profile. The average error for all of the targets is 0.88 points per profile. An error of less than one point per profile is acceptable.

M: 17 P: 16 -1	M: 18 P: 16 -2	M: 16 P: 16 0	M: 16 P: 16 0
M: 17 P: 16 -1	M: 16 P: 16 0	M: 18 P: 16 -2	M: 17 P: 16 -1
M: 16 P: 16 0	M: 16 P: 16 0	M: 15 P: 16 +1	M: 17 P: 16 -1
M: 17 P: 16 -1	M: 18 P: 16 -2	M: 16 P: 16 0	M: 16 P: 16 0

(a)

M: 8 P: 7 -1	M: 7 P: 7 0	M: 8 P: 7 -1	M: 6 P: 7 +1
M: 6 P: 7 +1	M: 10 P: 8 -2	M: 6 P: 7 +1	M: 8 P:7 -1
M: 8 P: 7 -1	M: 6 P: 7 +1	M: 7 P: 7 0	M: 6 P: 8 +2
M: 7 P: 8 +1	M: 8 P: 7 -1	M: 8 P: 8 0	M: 8 P: 7 -1

(b)

Figure 5.15: Predicted and Measured Point Density for an Angled Target of Dimensions 1m x 0.5m. (a) Target Number 1 and (b) Target Number 2

M: 16 P: 15 -1	M: 17 P: 15 -2	M: 16 P: 15 -1	M: 16 P: 15 -1
M: 18 P: 15 -3	M: 16 P: 15 -1	M: 16 P: 15 -1	M: 17 P: 15 -2
M: 16 P: 15 -1	M: 16 P: 15 -1	M: 18 P: 15 -3	M: 16 P: 15 -1
M: 17 P: 16 -1	M: 18 P: 16 -2	M: 17 P: 16 -1	M: 16 P: 16 0

(a)

M: 44 P: 41 -3	M: 45 P: 42 -3	M: 45 P: 42 -3	M: 47 P: 43 -4
M: 44 P: 42 -2	M: 45 P: 42 -3	M: 45 P: 43 -2	M: 45 P: 43 -2
M: 44 P: 41 -3	M: 44 P: 42 -2	M: 44 P: 42 -2	M: 45 P: 43 -2
M: 44 P: 42 -2	M: 44 P: 41 -3	M: 45 P: 42 -3	M: 45 P: 43 -2

(b)

Figure 5.16: Predicted and Measured Point Density for an Angled Target of Dimensions 1m x 0.5m. (a) Target Number 3 and (b) Target Number 4

M: 9 P: 8 -1	M: 7 P: 8 +1	M: 9 P: 7 -2	M: 8 P: 8 0
M: 9 P: 8 -1	M: 8 P: 7 -1	M: 9 P: 8 -1	M: 8 P: 8 0
M: 8 P: 7 -1	M: 8 P: 8 0	M: 8 P: 8 0	M: 9 P: 8 -1
M: 8 P: 8 0	M: 8 P: 8 0	M: 10 P: 8 -2	M: 7 P: 8 +1

(a)

M: 4 P: 4 0	M: 4 P: 4 0	M: 4 P: 4 0	M: 4 P: 4 0
M: 4 P: 4 0	M: 4 P: 4 0	M: 3 P: 4 +1	M: 3 P: 4 +1
M: 3 P: 4 +1	M: 3 P: 4 +1	M: 2 P: 3 +1	M: 5 P: 4 -1
M: 4 P: 3 -1	M: 3 P: 4 +1	M: 4 P: 4 0	M: 4 P: 4 0

(b)

M: 9 P: 8 -1	M: 8 P: 8 0	M: 9 P: 8 -1	M: 8 P: 8 0
M: 9 P: 8 -1	M: 7 P: 8 +1	M: 10 P: 8 -2	M: 8 P: 8 0
M: 9 P: 8 -1	M: 8 P: 8 0	M: 10 P: 8 -2	M: 8 P: 8 0
M: 9 P: 8 -1	M: 9 P: 8 -1	M: 8 P: 8 0	M: 9 P: 8 -1

(c)

M: 22 P: 21 -1	M: 22 P: 21 -1	M: 24 P: 21 -3	M: 20 P: 21 +1
M: 23 P: 21 -2	M: 22 P: 21 -1	M: 20 P: 21 +1	M: 23 P: 21 -2
M: 21 P: 21 0	M: 22 P: 21 -1	M: 22 P: 21 -1	M: 22 P: 21 -1
M: 22 P: 21 -1	M: 22 P: 21 -1	M: 22 P: 21 -1	M: 22 P: 21 -1

(d)

Figure 5.17: Predicted and Measured Point Density for an Angled Target of Dimensions 0.5m x 0.5m. (a) Target Number 5 (b) Target Number 6 (c) Target Number 7 (d) Target Number 8

5.4.3 Cylinders

In MIMIC, 3D cylinders are converted into a series of narrow vertical 2D planes. This section assesses the process of representing a curved 3D object with 2D planes. Figure 5.18(a) displays a cylinder extracted from a point cloud when viewed from above and Figure 5.18(b) illustrates this cylinder in profile view. This cylinder was surveyed using a single scanner MMS. Therefore only 2 of the cylinder's 'faces' were surveyed. In these tests, each of the four cylindrical targets have been manually assigned two faces of the hexagonal approximation. These faces are denoted (i) and (ii) and correspond to a manual interpretation of the 'faces' of the cylinder. A 6x1 grid structure is applied to each face of the target. The points in each grid cell are manually counted. This point density value is then compared with the value from MIMIC. The target parameters are listed in Table 5.7. Each cylinder therefore consists of two planes, with different orientations. These orientations are listed in Table 5.8.

Table 5.7: Test and Target Parameters for Validating MIMIC's Point Density Calculations on a Cylindrical Target

Target	Width	Height	Z_{diff}(m)	Vel(m/s)	PRR	M_f
1(i + ii)	0.19m	0.74m	2.13	3.95	250KHz	150Hz
2(i + ii)	0.08m	1.59m	1.83	5.77	250KHz	150Hz
3(i + ii)	0.08m	1.10m	1.91	4.81	300KHz	100Hz
4(i + ii)	0.05m	1.10m	1.77	4.30	300KHz	100Hz

Figure 5.18 illustrates the process of applying the hexagonal planar shape to identify each face of the target from above and in side view. Figure 5.19(a) depicts a side view of the cylinder and displays the two sets of points from

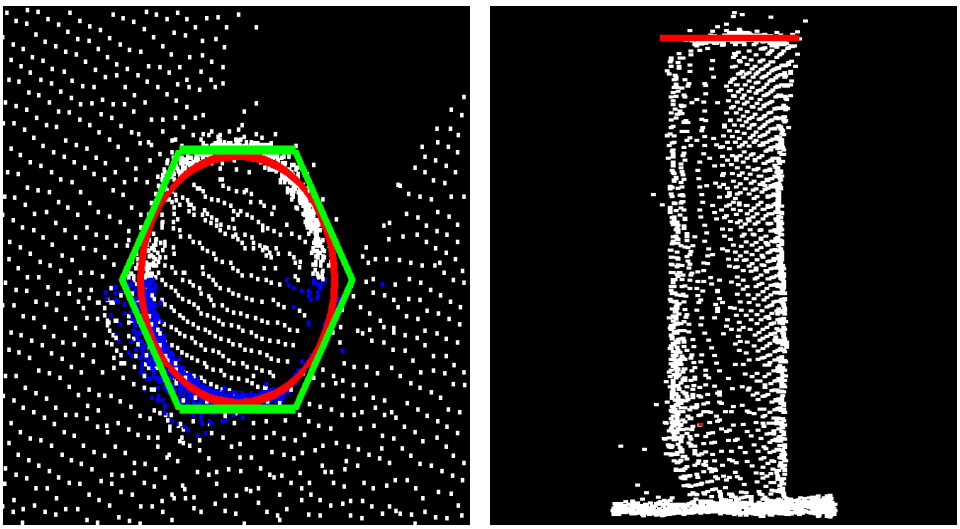

(a) (b)

Figure 5.18: Converting a Cylindrical Target into a Hexagonal Planar Target (a) Top Down View and (b) Side View

Faces (i) and (ii) after manual classification. The manual classification process can potentially introduce errors. Figure 5.19(b) illustrates the process of gridding a vertical target and measuring the points in that grid cell. Table 5.8 displays the point density for both manual measurements and MIMIC's calculations for each cylinder face. The complete results are available in Tables 19 and 20 in Appendix .2. The errors have increased for cylindrical targets. The manual interpretation of the cylinder could potentially result in points being incorrectly assigned to a face and the results in Table 5.8 reinforce this hypothesis. For each target, an underestimation of point density on one cylinder face is matched with an overestimation of point density on the other. The point density for the combined cylinder is calculated and the results are displayed in Table 5.9. For each cylinder as a whole, the point density errors are less than 10%. The error source identified in Section 5.3.2 is not an issue in these tests because the largest cylinder used in these tests has a diameter

of 0.19m. The cylinder used in the example in Section 5.3.2 has a diameter of 0.2m and the influence on range to that target was negligible.

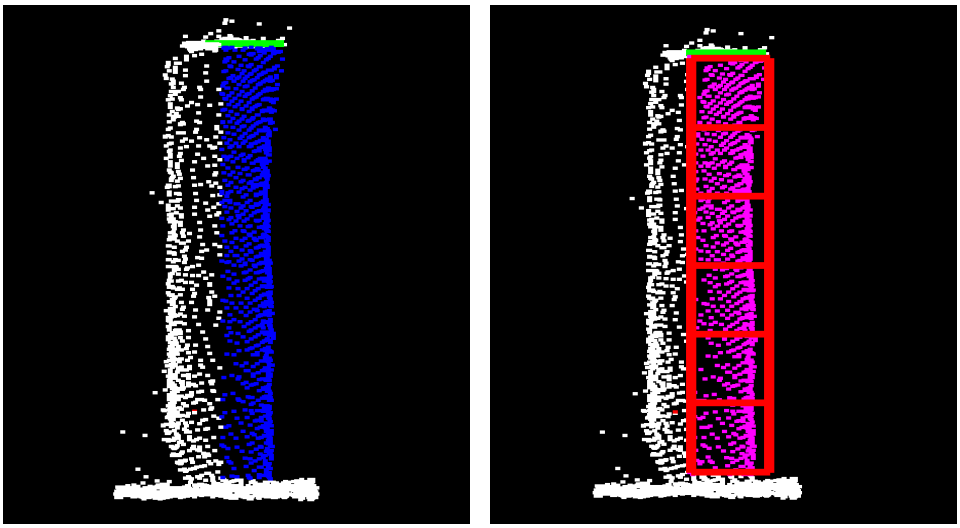

(a) (b)

Figure 5.19: Calculating Point Density on Cylindrical Targets - (a) Manual Identification and Classification of Cylinder Faces and (b) Applying a 6x1 Grid Structure to the Cylindrical Target

The predicted and measured values for each grid cell are displayed for both faces of all 4 cylinders in Figure 5.20. Cylinder 1, Face(ii) displays the highest errors. The percentage error for Cylinder 1, Face(ii) is 27.23%. The error for this entire cylinder is 8.0% as displayed in Table 5.9, and this reduction in error of 19% suggests an incorrect manual classification of the cylinder face. The base of Cylinder 3, Face(i) was covered by vegetation, and the magnitude of the error reflects this with MIMIC overestimating by 12 points in this grid cell alone. This cylinder is illustrated in Figure 5.19 and it can be seen that the bottom left hand side of the cylinder is incomplete. One of the research assumptions listed in Chapter 1 is that there are no obstructions between the scanner and the target and therefore MIMIC does

Table 5.8: Calculated and Measured Point Density for Each Face of a Cylindrical Target

Target (Face)	H_r(m)	α_{targ}	MIMIC	Measured	%Error
1(i)	5.118	0.814^o	301pts	322pts	-6.52%
1(ii)	5.118	49.35^o	313pts	246pts	+27.23%
2(i)	6.692	29.12^o	150pts	150pts	0%
2(ii)	6.692	77.228^o	108pts	112pts	-3.57%
3(i)	7.950	71.36^o	87pts	80pts	+8.75%
3(ii)	7.950	19.711^o	101pts	104pts	-2.8%
4(i)	7.438	66.8166^o	111pts	101pts	+9.90%
4(ii)	7.438	19.085^o	121pts	137pts	-11.67%

Table 5.9: Percentage Error for Both Faces on a Cylinder Combined

Target	MIMIC	Measured	%Error
1	614	568	+8.0%
2	258	262	-1.5%
3	188	205	-8.2%
4	232	238	-2.5%

not model this. Overall, the results are encouraging. Excluding Cylinder 1, Face (ii), the percentage errors in Table 5.8 for each target are comparable with the percentage error for the planar targets in Tables 5.4 and 5.6. Table 5.10 lists the error per profile for each target face. The highest error is 2.2 P_{pp} on Cylinder 1, Face(ii), however this has already been shown to contain large errors in point density. The average error per profile is 0.51 points P_{pp}. An error of less than one P_{pp} is acceptable. These tests validate MIMIC's method of approximating curved cylindrical targets with a combination of planar targets.

Table 5.10: Calculated and Measured Point Density. Error per Profile for each Cylinder Face

Target	Face	Profiles	Error	Error per profile
1	(i)	28	21pts	0.75pts
1	(ii)	30	67pts	2.2pts
2	(i)	32	0pts	0.00pts
2	(ii)	32	4pts	0.12pts
3	(i)	34	7pts	0.20pts
3	(ii)	34	3pts	0.08pts
4	(i)	38	10pts	0.26pts
4	(ii)	38	16pts	0.42pts

5.4.4 Calculating Point Density for Dual Scanner MMSs

This section validates the point density calculations for a Dual Scanner MMS. The dual scanner Optech Lynx enables MIMIC's calculations to be experimentally validated. There are a number of potential error sources when incorporating a second scanner in MIMIC's calculations. As explained in Section 1.7, MIMIC assumes zero course deviation between measurements

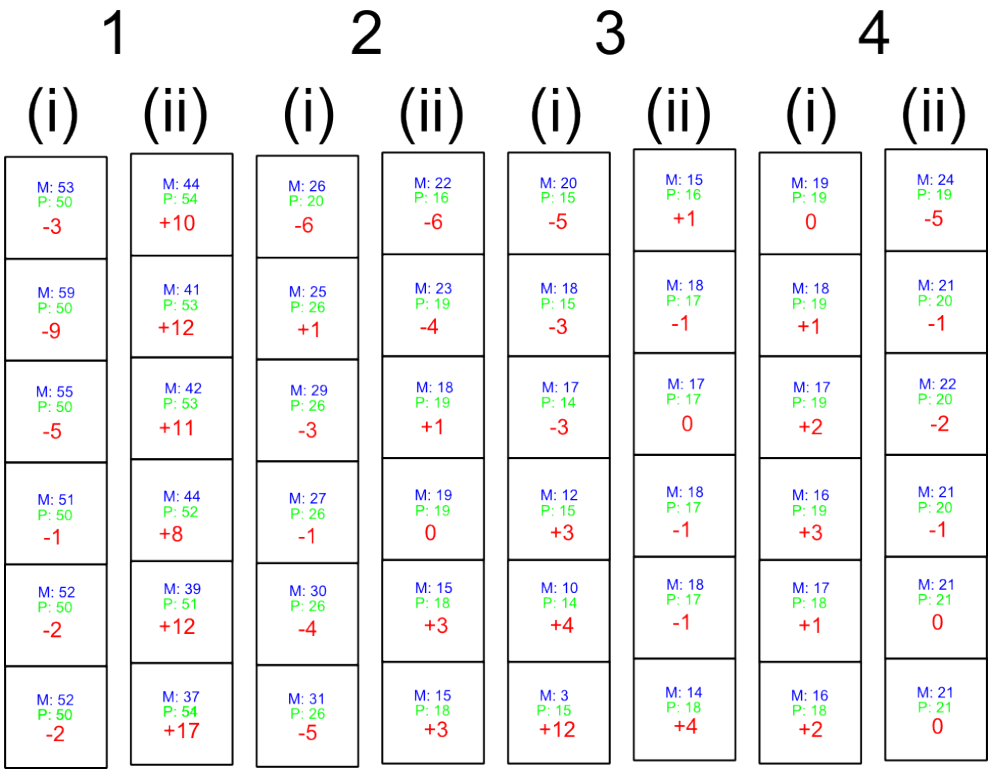

Figure 5.20: Calculated and Measured Point Density for Both Faces of Cylindrical Targets, Numbers 1 - 4

and therefore MIMIC does not calculate a separate target orientation in relation to Scanner 2. Figure 5.21 illustrates this potential error source. In this example, laser pulses from Scanner 1 first strike the target at 0:00 seconds. Due to its orientation, Scanner 2 can not survey the target at this time. Scanner 2 first encounters the object at 0:002 seconds, but by this time the heading of the vehicle has changed. This heading change has altered the orientation of the target in relation to Scanner 2, whereas MIMIC applies the original target orientation specified by the user. Figure 5.21 demonstrates an extreme case, however to minimise this potential error the test data is manually selected from areas of minimum course deviation. Any deviation in heading, orientation, scanner height or vehicle velocity between the two times of measurement will result in errors. For example, in the angled surface tests on Target 1 a difference of approximately 2 seconds exists between the measurements recorded on the target by Scanner 1 and those recorded by Scanner 2. The time is 139340.636 seconds for the first pulse striking the target from Scanner 1 and 139342.604 for the first pulse striking the target from Scanner 2. The point density calculation is influenced in a number of ways:

- There is a course deviation of 2.9956^o between the two measurements. This introduces errors into the profile angle, profile spacing and point spacing calculations for Scanner 2.

- The course deviation of 2.9956^o results in a change in horizontal range to the target of 0.4m. This introduces errors into the point spacing calculations.

- There is also a 0.18m height change in this time that is not factored

into the calculation. This introduces errors into the point spacing calculations.

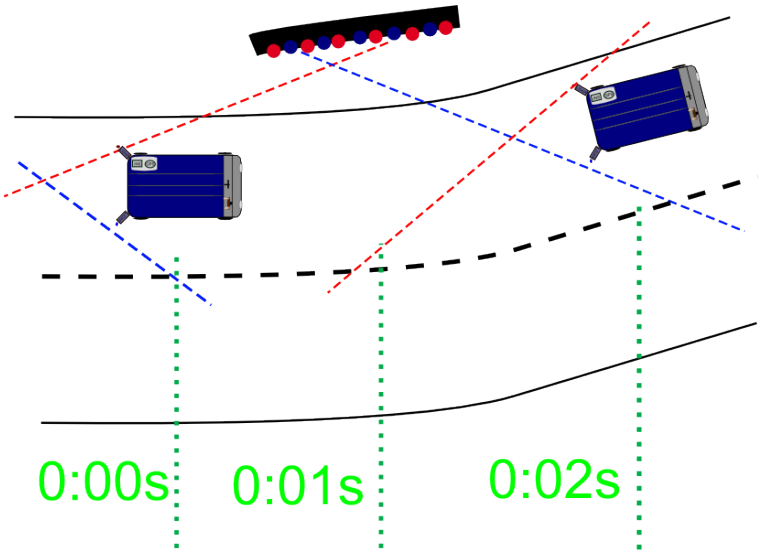

Figure 5.21: Potential Error Source : A Heading Change Between Measurements from Scanner 1 and Scanner 2 Alters the Orientation of the Target in Relation to the MMS

5.4.4.1 Dual Scanner MMSs on Angled Surfaces

The process of calculating point spacing, profile spacing and profile angle for the second scanner is identical to the methods illustrated in Chapter 4. The point density on each target is manually measured. The measured values and MIMIC's calculations are compared. The Optech Lynx data is used to verify these calculations. Scanner 2 is offset 1.389m from Scanner 1 on the Optech Lynx and this offset along with the horizontal and vertical rotations of each scanner are input in MIMIC. Table 5.11 provides details on the four targets. A comparison of the manually measured points and MIMIC's calculated values are detailed in Table 5.12. The complete set of results including

vehicle dynamics are provided in Table 21 in Appendix .2. In each case the percentage error for Scanner 1 is within 6% of Scanner 2. In each case except the last MIMIC underestimated the point density of the target. The largest errors exist for Target 2, however both scanners are displaying large errors which implies there is a problem with the cylinder in the point cloud. These results validate MIMIC's point density calculations for a second scanner on an angled surface.

Table 5.11: Test and Target Parameters for Validating MIMIC's Point Density Calculations for a Dual Scanner System on an Angled Target

Target	Width (m)	Height (m)	α_{targ}	H_r (m)	Z_{diff} (m)
1	1.0	0.5	16.532^o	8.736	0.859
2	0.5	0.5	16.532^o	8.736	0.859
3	1.0	0.5	-25.14^o	5.756	2.018
4	0.5	0.5	-25.14^o	5.756	2.018

Table 5.12: Calculated and Measured Point Density for an Angled Target for both Scanners on the Dual Scanner Optech Lynx

Target	Scanner	MIMIC	Measured	%Error
1	1	385pts	415pts	7.22%
1	2	190pts	219pts	13.24%
2	1	193pts	226pts	14.60%
2	2	96pts	116pts	17.24%
3	1	388pts	417pts	6.95%
3	2	432pts	444pts	2.70%
4	1	193pts	194pts	0.51%
4	2	216pts	207pts	4.34%

The scanner offset increases the horizontal range to the target from Scan-

ner 2. This results in a lower point density than for Scanner 1. For example, the predicted point density on Target 1 is over 100% higher for Scanner 1 than for Scanner 2. Additionally, the orientation of Scanner 2 also influences the point density on targets rotated towards the MMS. This is not a constant effect, as the opposite is the case for Targets 3 and 4 where the negative rotation of the target results in an increased point spacing and profile spacing for Scanner 1 but a decreased point spacing and profile spacing for Scanner 2. This results in an increase in point density for Scanner 2 relative to Scanner 1. Scanner 2 captures 6% more points than Scanner 1 for Target 4. Chapter 6 will investigate scanner orientation and location for a single scanner and dual scanner MMS. Potential course changes can be implemented as future work but for the current objectives of MIMIC the results have shown that MIMIC can perform satisfactorily without them. There is no significant difference in the percentage error when comparing the point density measurements from Scanner 1 with those from Scanner 2. This implies that MIMIC can robustly calculate point density when in situations where small course deviations are present

5.4.4.2 Dual Scanner MMSs on Cylindrical Targets

After successfully demonstrating MIMIC's ability to calculate point density for scanners at different locations and orientation for angled surfaces, these tests are repeated for cylindrical targets. Figure 5.22(a) illustrates the point distribution for Scanner 1 on a cylindrical target while Figure 5.22(b) illustrates the point distribution for Scanner 2. It is possible to see from this image that each scanner has captured a different face of the cylinder and that there is a degree of overlap in the centre of the cylinder (Face (ii)). Two

cylindrical targets are chosen and each cylinder consists of three faces. Each cylinder face is listed in Table 5.13 and are denoted (i), (ii) and (iii) for both cylindrical targets. Faces (i) and (ii) are captured by Scanner 1 while Faces (ii) and (iii) are captured by Scanner 2. Face (ii) is the area of overlap and is captured by both scanners. The rotations of each face and the dimensions, height difference and horizontal range to the target are also displayed in this table for both scanners. Table 5.14 displays a comparison between the measured point density and the value calculated by MIMIC. The complete set of results including vehicle dynamics are provided in Table 22 in Appendix .2. The greatest errors occurred for Scanner 1 on Face (ii) for both cylinders. This is potentially due to the difficulty in manually classifying the faces of that cylinder in the point cloud. Larger errors in the cylinder tests do not necessarily imply an error in the calculations but rather a problem with the manual classification of cylinder faces. By analysing the cylinder as a whole this can be verified. Table 5.15 lists the total point density for both targets from both scanners. The errors are lower than 5% for both cylinders and implies that overall MIMIC can calculate point density for a cylinder and that the manual verification process is the cause of the errors in the previous tests. The low errors further validate MIMIC's ability to calculate point density without incorporating course deviation.

5.4.5 Contribution of Errors

A series of tests are designed to demonstrate the effect that errors in the calculation of the output values: profile angle, profile spacing and point spacing

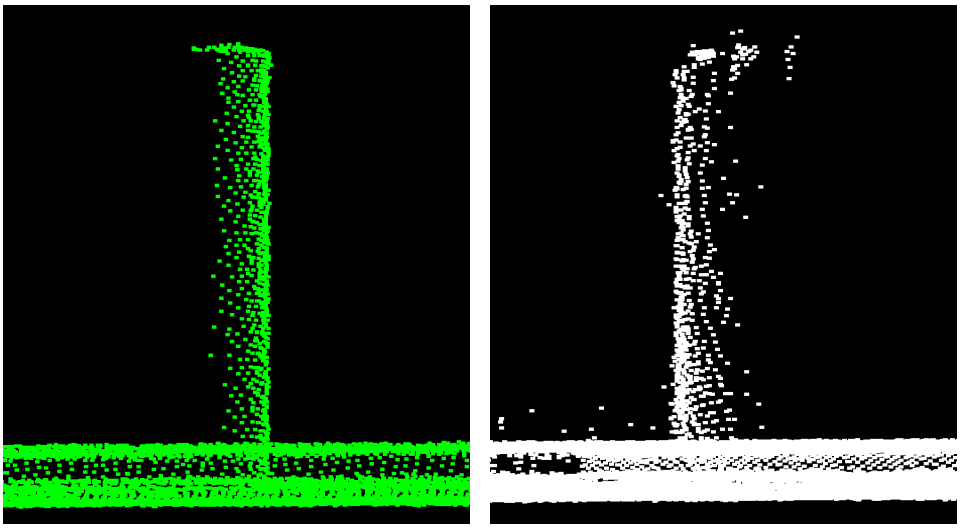

(a) (b)

Figure 5.22: Returns from Two Scanners on a Cylindrical Target - (a) Scanner 1 and (b) Scanner 2

Table 5.13: Test and Target Parameters MIMIC's Point Density Calculations on Each Face of a Cylindrical Target for the Dual Scanner Optech Lynx

Target	Face	Width (m)	Height (m)	α_{targ}	H_r	Z_{diff}
1	(i)	0.035	1.3	47.76^o	3.42m	1.76m
1	(ii)	0.035	1.3	-8^o	3.42	1.76m
1	(iii)	0.035	1.3	-83.26^o	3.42m	1.76m
2	(i)	0.035	1.3	61.73^o	4.85m	1.85m
2	(ii)	0.035	1.3	-22.32^o	4.85m	1.85m
2	(iii)	0.035	1.3	-81.65^o	4.85m	1.85m

Table 5.14: Calculated and Measured Point Density for Each Face of a Cylindrical Target for the Dual Scanner Optech Lynx

Target	Face	Scanner	MIMIC	Measured	%Error
1	(i)	1	113pts	103pts	9.70%
1	(ii)	1	98pts	111pts	11.71%
1	(ii)	2	60pts	60pts	0.00%
1	(iii)	2	57pts	64pts	10.94%
2	(i)	1	46pts	42pts	9.52%
2	(ii)	1	63pts	56pts	12.50%
2	(ii)	2	48pts	49pts	2.04%
2	(iii)	2	41pts	43pts	4.65%

Table 5.15: Percentage Error for Three Faces on a Cylinder Combined from the Dual Scanner Optech Lynx

Target	MIMIC	Measured	%Error
1	328	338	-2.9%
2	198	190	+4.0%

have on the point density calculation. The greatest error in the output values detailed in Section 4.4 was approximately 5% of the true value. Each output value is therefore modified by +/- 5% and the point density now calculated for a target. The effect of the +/- 5% error on the final point density calculation is then identified. A parallel, vertical target (1m x 0.5m) is specified, at a range of 6m from the scanner. The scanner defined in MIMIC is the XP1's VQ250, orientated at $45^o/45^o$ and operating at a 300KHz PRR and a 100Hz mirror frequency. The vehicle velocity is simulated at 50km/h.

Table 5.16 details the outputs of these tests. Errors in the profile angle calculation have the biggest impact on the point density calculation. A -5% error in the profile angle calculation results in a 12.23% error in the point

density calculation whereas a +5% results in a 8.9% error. The reason for this discrepancy will be discussed in greater detail in the next chapter when investigating the influence of vertical scanner rotation on profile angle and point density. Interestingly, a +/-5% error in the profile spacing calculation has very little effect on the point density calculation, less than 1%. Comparing these values with the previous results for point density angled vertical surfaces, cylinders and irregular surfaces it is possible to see how a small error in calculating profile angle, profile spacing or point spacing could explain the errors that are present.

Table 5.16: Influence of Errors in Calculating Profile Information and Point Spacing on the Point Density Calculation, +/-5% Variation

Input	%Variation	Amended	MIMIC	%Error
Profile Angle	+5%	691pts	759pts	8.95%
Profile Angle	-5%	852pts	759pts	12.23%
Profile Spacing	+5%	756pts	759pts	0.39%
Profile Spacing	-5%	763pts	759pts	0.52%
Point Spacing	+5%	723pts	759pts	4.74%
Point Spacing	-5%	799pts	759pts	5.27%

5.5 Conclusions

This chapter presented the methods for calculating point density using the outputs of profile angle, profile spacing and point spacing. A gridding approach was developed to accurately calculate point density on large or angled targets. A grid structure was applied to targets to increase the number of point spacing measurements per target. A 4x4 grid structure was chosen as the most suitable for these tests because it was capable of accurately calcu-

lating point density but minimised the manual component of the validation tests. These methods were validated using a combination of targets. Point density was calculated for vertical, angled and cylindrical targets. A hexagonal planar approximation of a cylinder was applied to facilitate point density calculations on a curved surface. Variations in the target dimensions, orientation, elevation and range robustly tested MIMIC's point density calculations for different scanner parameters. MIMIC's point density calculations were also validated for dual scanner MMSs.

The first target types investigated were angled and parallel vertical surfaces. Point density was calculated for large and small targets. The XP1 and Optech Lynx provided point clouds that were used for validation. An average error of less than one point per profile validated MIMIC's point density calculations for parallel and angled targets.

The second target type was a multi-faced cylindrical target. MIMIC approximates cylindrical targets with a hexagonal shape. The highest point density errors were returned when calculating point density for this target type. It was explained that this was potentially due the manual interpretation of each face on the cylinder or obstructions between the scanner and the target. An average error of less than one point per profile validated MIMIC's point density calculations for cylindrical targets.

Once the point density calculation for a single scanner system was validated, the ability of MIMIC to calculate point density resulting from a change in the scanner position and orientation was tested. MIMIC's point density

calculations were then validated using dual scanner systems on angled and cylindrical targets. Scanner 2 results in approximately 50% lower point density than Scanner 1 on a parallel vertical target. This value is dependant on target orientation, the offset to the target and the orientation of the target. MIMIC calculated point density on a cylindrical target, and although errors were represent when individual faces were examined, the total point density of the cylinder results in errors $\leq$ 4%, validating MIMICs methodology of calculating point density for dual scanner system on cylindrical targets. For both angled and cylindrical targets, similar point density percentage errors for Scanner 1 and Scanner 2 imply that MIMIC can calculate point density accurately without incorporating course deviation, justifying the research assumption in Chapter 1.

In the next chapter, MIMIC is applied in a series of tests assessing scanner configuration. After testing the effect of scanner orientation and position on point density, scanner hardware parameters will also be investigated.

Chapter 6

Assessing MMS Parameters

The second objective of this thesis is to identify the recommended MMS configuration and scanner hardware settings for surveying specific targets. The number, orientation and location of the laser scanners on a MMS impact point density. Hardware settings like the PRR, mirror frequency and FOV also influence point density. In this chapter MIMIC is applied in a series of tests to assess the influence of these MMS parameters on point density.

6.1 Introduction

This chapter investigates the impact of scanner configuration and scanner settings on point density. Section 6.2 assesses the effect of horizontal and vertical rotations of the scanner on point density. The importance of a vertical scanner rotation when surveying narrow targets is assessed. These tests are then repeated for dual scanner MMSs in Section 6.2.3. Section 6.3 identifies the impact of scanner position on point density. Scanner settings like the PRR, the mirror speed and the FOV are not included in the configuration tests as the configuration tests are designed to be hardware independant.

These scanner settings are investigated in Section 6.4 when assessing their importance for surveying small targets. Section 6.5 summarises the findings in this chapter.

6.2 Scanner Orientation

Horizontal rotations of the scanner increase the range to the target. Vertical rotations of the scanner increase the profile angle. Dual axis scanner rotations do both. This section quantifies the effect that horizontal, vertical and dual axis scanner rotations have on point density. Horizontal scanner rotations are explored in Section 6.2.1. In Section 6.2.2, the effect of vertical rotations on profile spacing are explored. A vertical scanner rotation is important when surveying narrow vertical targets and has been a recurring theme in this thesis. A combination of horizontal and vertical scanner rotations are explored in Section 6.2.3. The dimensions and orientation of the target influences point density, however as the tests in this section are designed to assess MMS parameters only the target orientation and dimensions remain constant for each test.

6.2.1 Horizontal Scanner Rotations

A horizontal rotation of the scanner ensures laser returns from surfaces perpendicular to the direction of travel. One result of this is that a horizontal rotation of the scanner increases the range to the target, as Figure 6.1 illustrates for subsequent 15^o increments. This section quantifies the impact of different horizontal rotations of the scanner on point density and also investigates this effect at different vehicle velocities.

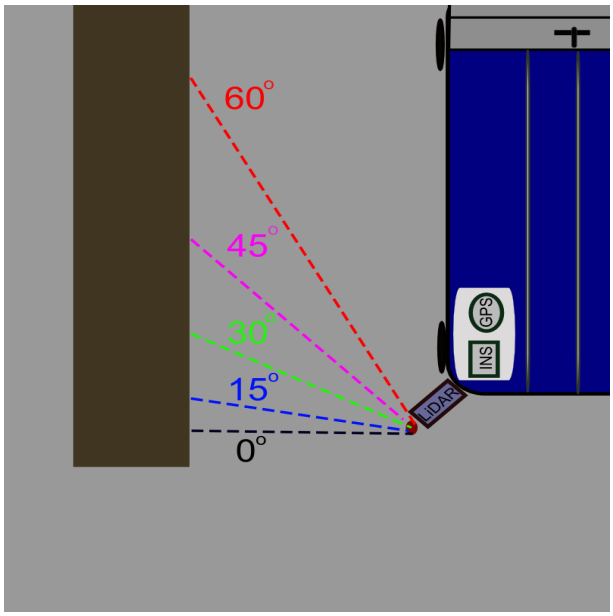

Figure 6.1: Variations in Range to Target Arising from a Horizontal Scanner Rotation

The scanner hardware defined in MIMIC operates at a 300kHz PRR and a 100Hz mirror frequency. The initial tests employ a constant vehicle velocity of 50km/h. The simulated target is 2m wide and 1m high and defined at a constant 5m range. Table 6.1 details the test and target parameters. The horizontal scanner rotation is increased in 15^o increments. The point density is calculated for the entire target after each scanner rotation change and the results of these tests are displayed in Table 6.2. Tests 1-4 demonstrate the effect that an increased measurement range arising from a horizontal rotation of the scanner has on the point density on a parallel vertical target. The higher the horizontal rotation of the scanner, the higher the point spacing and therefore the lower the point density. For example, the 60^o horizontal scanner rotation in Test 4 results in only 60% of the point density when compared with the 0^o horizontal scanner rotation in Test 1.

Table 6.1: Target and Test Parameters for Assessing the Impact of a Horizontal Scanner Rotation on Point Density

Target Width	Target Height	PRR	M_f	Velocity	H_r(m)
2m	1m	300kHz	100Hz	50km/h	5m

Table 6.2: Assessing the Impact of Horizontal Scanner Rotations on Point Density for a Parallel 2m x 1m target at a Horizontal Range of 5m

Test	α_{scan}	γ_{scan}	α_{targ}	β_{targ}	MIMIC
1	15^o	0^o	0^o	0^o	1103pts
2	30^o	0^o	0^o	0^o	1029pts
3	45^o	0^o	0^o	0^o	890pts
4	60^o	0^o	0^o	0^o	670pts

Investigating the effect of vehicle velocity and horizontal scanner rotation on point density requires the vehicle velocity to be varied. Five vehicle velocities are input ranging from 10km/h to 50km/h. The target parameters do not vary from the previous test. Point density is calculated for the four horizontal scanner rotations listed in Table 6.2 at five different vehicle velocities. Figure 6.2 illustrates the results of these tests, while Table 23 in Appendix .3 details the results. This figure illustrates the relationship between velocity and point density for a parallel target. The relationship between the velocity and the point density is not linear. As the vehicle velocity doubles, the point density halves. The 25% difference in point density between a 45^o horizontal scanner rotation and a 60^o horizontal scanner rotation at 10km/h is greater than the 20% difference between a 15^o horizontal scanner rotation and a 45^o horizontal scanner rotation. This implies that moving from a 45^o-60^o rotation results in a larger decrease in point density than moving from a 15^o-45^o

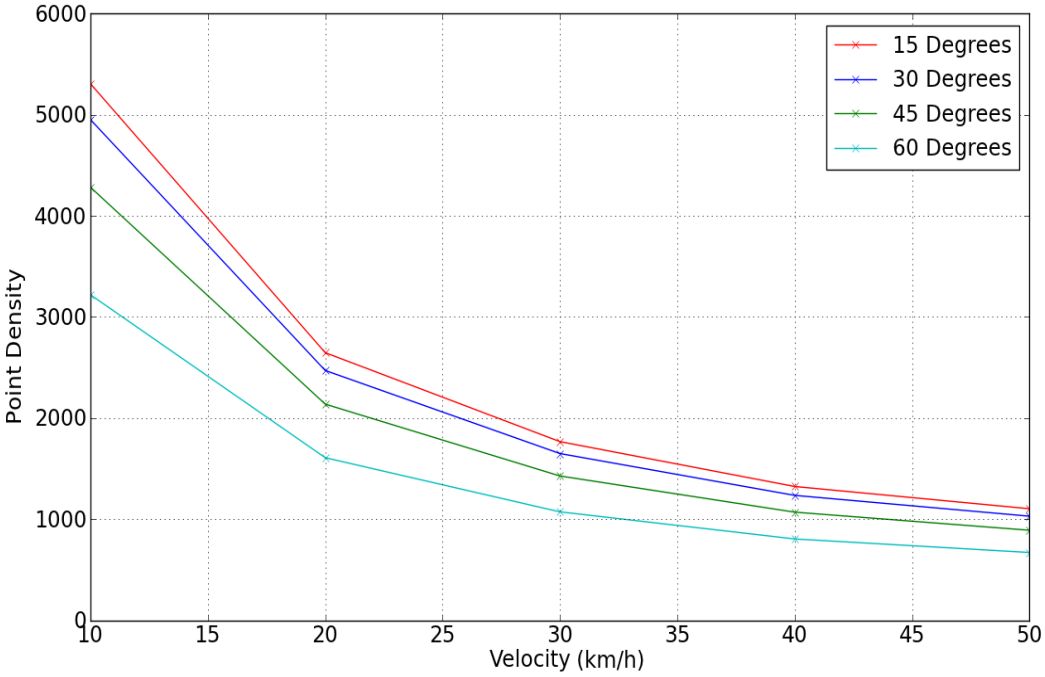

Figure 6.2: Calculating the Effect of Vehicle Velocity and a Horizontal Scanner Rotation on the Point Density on a Parallel Vertical Target. Target Range is 5m and Target Dimensions are 2m x 1m

rotation, despite this being twice the angular change. This effect is due to the orientation of the surface, which in these tests is parallel. The higher scanner rotations have increased the range to the target, as Figure 6.1 illustrated, and therefore increased point spacing . For rotated targets the lower scanner rotations are effected similarly, as Figure 6.3 illustrates. The aim of this section is to assess the effect of the system parameters on point density, not the target parameters. Therefore the target rotation is not altered.

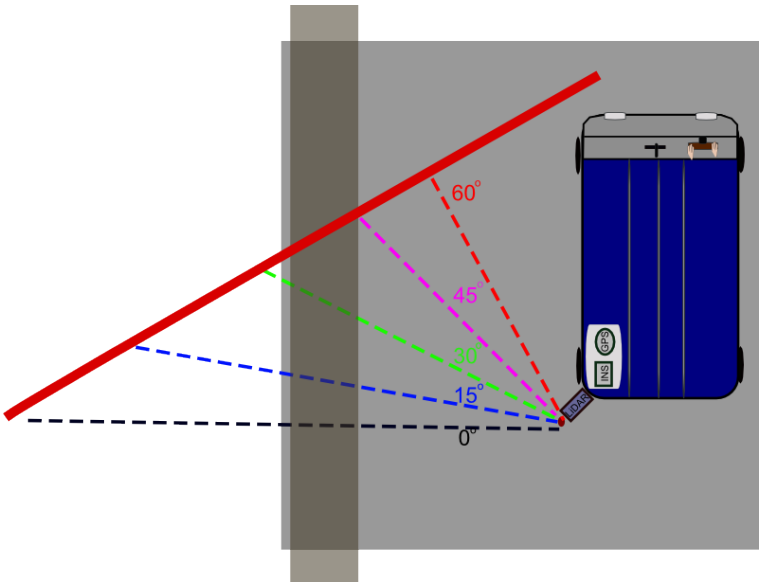

Figure 6.3: Point Density and Horizontal Scanner Rotations are Influenced by Horizontal Target Rotations

6.2.2 Vertical Scanner Rotation

Point density is also influenced by vertical scanner rotations. A vertical scanner rotation alters the profile angle on vertical surfaces and is important for increasing the number of profiles striking a narrow target. Automated algorithms described in Section 1.4.6 required a minimum profile spacing to recognise cylindrical objects. MMSs rely on vertical rotations of the scanner to achieve this. This section quantifies the effect of vertical scanner rotations on point density and on profile spacing.

6.2.2.1 Parallel Vertical Targets

Four vertical scanner rotations are implemented to assess their effect on point density. A parallel vertical target with dimensions of 2m x 1m and at 5m range from the scanner is defined. The scanner is rotated vertically in 15^o increments and the point density is measured on the target after each rotation.

The results of calculating point density for different vertical scanner rotations on this target are detailed in Table 6.3. Each of the vertical rotations result in an equal or higher point density for the target than the corresponding horizontal scanner rotation in the previous tests on the same target.

Table 6.3: Assessing the Impact of Vertical Scanner Rotations on Point Density for a Parallel 2m x 1m target at a Horizontal Range of 5m at 50km/h

Test	α_{scan}	γ_{scan}	α_{targ}	β_{targ}	MIMIC
1	0^o	15^o	0^o	0^o	1103pts
2	0^o	30^o	0^o	0^o	1168pts
3	0^o	45^o	0^o	0^o	1264pts
4	0^o	60^o	0^o	0^o	1328pts

The next test examines the impact of vertical scanner rotations and vehicle velocity on point density. Vehicle velocities from 10km/h to 50km/h are specified. The standard parallel vertical target with dimensions of 2m x 1m at 5m range from the scanner is defined. Employing this target in each experiment ensures consistency between the tests and facilitates comparison of the results. Point density is calculated for the four vertical scanner rotations listed in Table 6.3. Figure 6.4 illustrates the effect of vehicle velocity and vertical scanner rotations on point density, while Table 23 in Appendix .3 details the results. These tests demonstrate that increasing the vertical rotation of the scanner increases the point density, although the difference becomes less pronounced at higher velocities. For example, there is approximately 250 points in the difference between the 15^o and 60^o vertical rotations at 50km/h but a difference of over 1000 points at 10km/h.

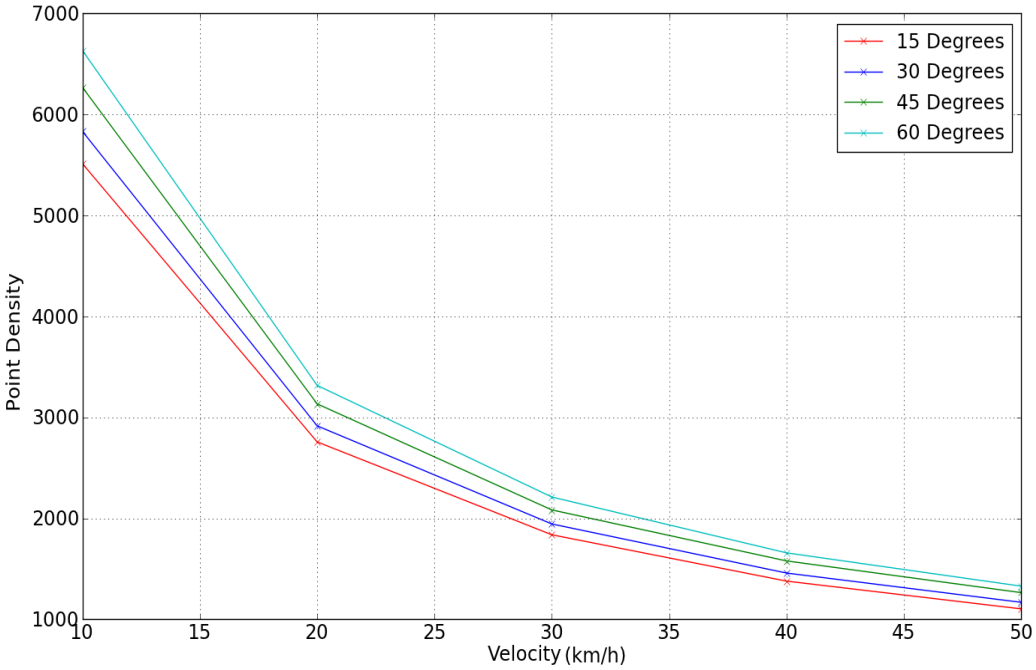

Figure 6.4: Calculating the Effect of Vehicle Velocity and a Vertical Scanner Rotation on the Point Density on a Parallel Vertical Target. Target Range is 5m and Target Dimensions are 2m x 1m

6.2.2.2 Narrow Objects

Narrow vertical targets are a common type of roadside infrastructure. MIMIC uses this target type to represent each face in the hexagonal approximation of a cylinder. It is important to minimise vertical profile spacing on these narrow, vertical features because profile spacing is a potential limiting factor to certain automated algorithms. The target parameters are altered for these tests and a target 0.1m x 2m is defined. A scanner operating at a 300kHz PRR and a 100Hz mirror frequency is simulated in MIMIC. The tests are designed with a constant vehicle velocity of 50km/h. Table 6.4 details the target and test parameters. The point density on the target is measured after each 15^o increase in the vertical scanner rotation. Table 6.5 displays the results for the point density tests. These tests demonstrate how the point density on a narrow vertical object increases as the vertical profile spacing decreases. The point density has increased by a factor of 33% between Test 1 and Test 4 after an additional 45^o vertical scanner rotation.

Table 6.4: Target and Test Parameters for Assessing the Impact of a Horizontal Scanner Rotation on Point Density

Target Width	Target Height	PRR	M_f	Velocity	H_r(m)
0.1m	2m	300kHz	100Hz	50km/h	5m

The number of profiles that strike a target are relevant for automated algorithms. The lowest vertical scanner rotation (15^o) results in just over 12% the number of scan profiles that the 60^o rotation does. Despite this under-performance, it is important to note that a high number of scan profiles does not guarantee a high number of points striking the target. For example, Test 1 results in only 8.33% the number of profiles that Test 4 does, yet

Table 6.5: Assessing the Impact of Vertical Scanner Rotations on Point Density and Profile Spacing for a Narrow Vertical Target 0.1m x 2m at a Horizontal Range of 5m

Test	α_{scan}	γ_{scan}	α_{targ}	β_{targ}	Profiles	MIMIC	P_{pp}
1	0^o	15^o	0^o	0^o	3	122pts	40.66
2	0^o	30^o	0^o	0^o	8	129pts	16.12
3	0^o	45^o	0^o	0^o	14	144pts	10.28
4	0^o	60^o	0^o	0^o	25	163pts	6.52

Test 1 is 74% of the point density of Test 4. Assuming an equal distribution of points per profile line, there is approximately 41 points per profile (P_{pp}) in Test 1. There is approximately 7 P_{pp} in Test 4. This demonstrates the trade-off between the number of scan profiles intersecting with a target and the number of P_{pp}. Short scan profiles crossing the target can lead to a point cloud that inadequately represents the target. This is particularly important if the target is at a range that results in a large point spacing. The significance of this will be demonstrated in Section 7.4.2.

6.2.3 Dual Axis Scanner Rotations

Dual axis scanner rotations are an important development for the current generation of MMSs. This scanner orientation provides the benefits of both a horizontal and a vertical scanner rotation. Features perpendicular to the direction of travel can be surveyed. Additionally, profile spacing is decreased on narrow targets. The tests in this section apply a series of horizontal and vertical rotations to a target. The point density is calculated at different vehicle velocities to assess the impact of vehicle velocity and dual axis scanner rotations on point density. These tests identify the recommended dual axis scanner orientation for different targets.

6.2.3.1 Parallel Vertical Targets

The first target type is a parallel target 2m wide x 1m high. The vehicle velocity is constant at 50km/h for these initial tests. A scanner operating at a 300kHz PRR and a 100Hz mirror frequency is defined. The test and target parameters are detailed in Table 6.6. The scanner rotation is simultaneously increased by 15^o for both horizontal and vertical scanner rotations after each test. Four dual axis scanner configurations are defined and the point density is calculated for the target. Table 6.7 details the results of these tests for the different scanner orientations. For every increase in horizontal and vertical rotation there is a corresponding increase in point density. The $60^o/60^o$ horizontal/vertical dual axis scanner rotation is capable of a higher point density than the other three scanner configurations. This would seem to conflict with the results in Section 6.2.1 where a 60^o horizontal scanner rotation results in a higher measurement range and therefore a larger point spacing and a reduced point density.

Table 6.6: Target and Test Parameters for Assessing the Impact of a Dual Axis Scanner Rotation on Point Density

Target Width	Target Height	PRR	M_f	Velocity	H_r(m)
2m	1m	300kHz	100Hz	50km/h	5m

To investigate this further, a test where the horizontal scanner rotation remains fixed but the vertical scanner rotation is varied is designed. In this test, the horizontal scanner rotation is set at 60^o but the vertical scanner rotation is increased by 15^o after each test. Table 6.8 details the results of these tests. As the vertical scanner rotation is increased the point density increases. This is because the vertical scanner rotation decreases profile

Table 6.7: Assessing the Impact of Dual Axis Scanner Rotations on Point Density for a Parallel 2m x 1m target at a Horizontal Range of 5m

Test	α_{scan}	γ_{scan}	α_{targ}	β_{targ}	MIMIC
1	15^o	15^o	0^o	0^o	1142pts
2	30^o	30^o	0^o	0^o	1380pts
3	45^o	45^o	0^o	0^o	2039pts
4	60^o	60^o	0^o	0^o	4196pts

spacing and therefore increases point density. These tests demonstrate that a high vertical scanner rotation is best for increasing point density on this target type.

Table 6.8: Assessing the Importance of Vertical Scanner Rotations in a Dual Axis Scanner Orientation for a Parallel 2m x 1m target at a Horizontal Range of 5m

Test	α_{scan}	γ_{scan}	α_{targ}	β_{targ}	MIMIC
1	60^o	15^o	0^o	0^o	842pts
2	60^o	30^o	0^o	0^o	1245pts
3	60^o	45^o	0^o	0^o	2214pts
4	60^o	60^o	0^o	0^o	4196pts

The next test examines the impact of dual axis scanner rotations and vehicle velocity on point density for a parallel vertical target. Vehicle velocities from 10km/h to 50km/h are specified in MIMIC. The point density is then measured for the target at each vehicle velocity and dual-axis scanner rotation. These measurements are illustrated in Figure 6.5, while the complete series of tests are available in Table 24 in Appendix .3. The results illustrate the importance of a vertical scanner rotation for increasing point density from parallel vertical targets. For example, at 10km/h the $60^o/60^o$ scanner orientation results in 10,793 returns more than the $45^o/45^o$ orientation. This

represents a 205% increase. At 40km/h, the $60^o/60^o$ scanner orientation is comparable with the $15^o/15^o$ at the lowest velocity of 10km/h. The $60^o/60^o$ orientation returns 5245 points while the $15^o/15^o$ orientation returns 5713. These results reinforces the importance of vertical scanner rotations for this target type.

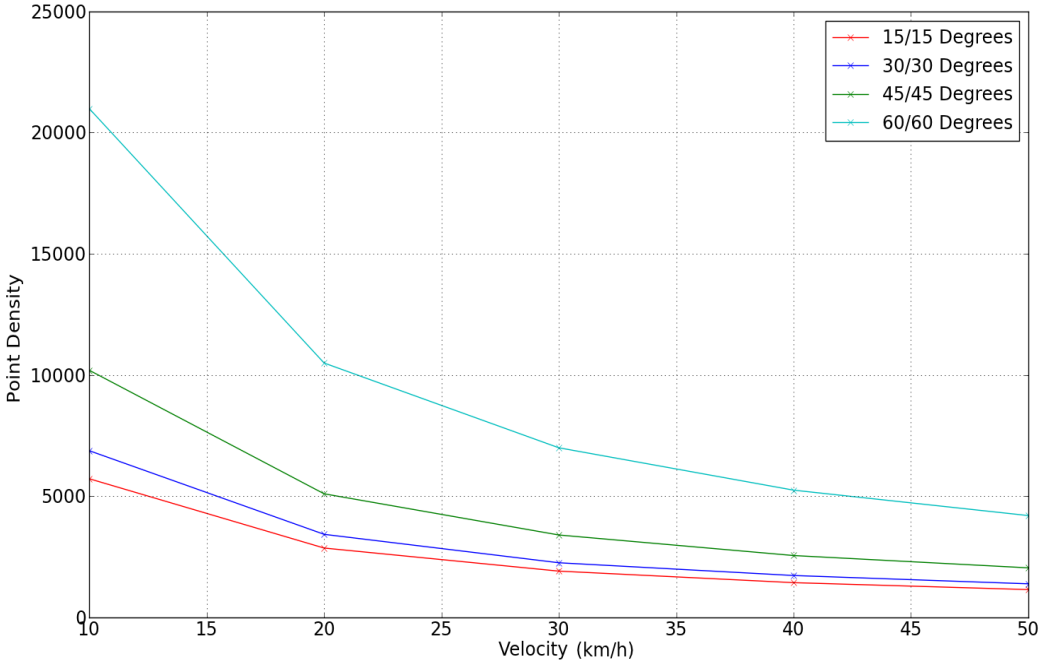

Figure 6.5: Calculating the Effect of Vehicle Velocity and a Dual Axis Scanner Rotation on the Point Density of a Parallel Vertical Target. Target Range is 5m and Target Dimensions are 2m x 1m

Despite the high point density arising from this configuration, a $60^o/60^o$ orientation is not suitable for all targets. For instance, a target rotated -30^o or higher relative to the parallel target would not intersect with the $60^o/60^o$ scan plane. This scenario would result in no laser returns from the target

and is an unacceptable risk for a single scanner MMS operating commercially as it could result in having to re-survey an area. One reason for avoiding a large horizontal rotation of the scanner is the increased measurement range to targets on the far side of the MMS. This influences point density on the road surface and on distant objects, as illustrated in Figure 6.6(a). Although the tests in this chapter focus on near side infrastructure, most MMS surveys drive the route multiple times in both directions. Capturing data from MMSs that drive the route in both directions results in an overlap between each survey, usually in the middle of the road. To avoid having to resurvey an area it is important to have this overlap between scans at the limit of the scanner range because the increased range leads to a reduced point density and the overlap introduces redundant measurements. A large horizontal rotation of the scanner would decrease point density in this area of overlap. Another issue is that a large vertical rotation of the scanner increases the range from the scanner to the ground and the range increase increases the point spacing on the ground. If applied in conjunction with a horizontal rotation of the scanner, the closest point on the ground to the scanner is offset from the road centre (marked with an 'x' in Figure 6.6(b)). On a planar surface the point spacing will increase from this point outwards along the scan profile and results in a lower point spacing on the road surface.

6.2.3.2 Narrow Targets

A vertical scanner rotation is important when surveying narrow objects, however the tests in Section 6.2.2.2 identified an issue with this. A compromise between the number of scan profiles intersecting a target and the P_{pp} is required. A target of dimensions 0.1m x 2m is defined. A scanner operating

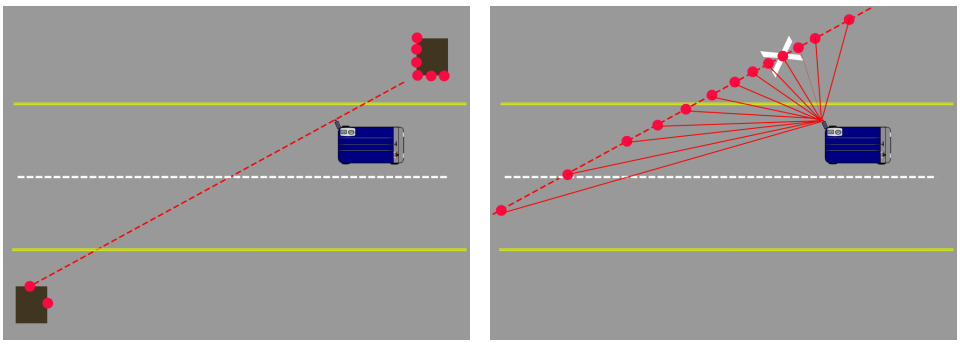

(a) (b)

Figure 6.6: Effect of Large Scanner Rotations on Point Density (a) Large Horizontal Scanner Rotation Results in an Increased range to Target on the Far Side of the MMS (b)Horizontal and Vertical Scanner Rotation Results in Decreased Point Spacing on the Road Center.

at a 300kHz PRR and a 100Hz mirror frequency is also defined. These tests are designed with a constant vehicle velocity of 50km/h. Unlike the tests in the previous sections, target parameters are varied in these tests. The range to the target is increased in 5m increments. The target range is varied in these tests to identify the effect of increased point spacing on the number of points per profile, as this is particularly important for surveying narrow targets. Table 6.9 lists the target and test parameters.

The horizontal scanner rotation is fixed at 60^o whereas the vertical scanner rotation is increased by 15^o after each test. The target is simulated at three different ranges, increased in 5m intervals. By examining Table 6.10 the effect of the increased point spacing on point density at longer ranges for vertical rotations can be seen. For example, at 15m range, the 8 profile lines resulting from the 15^o vertical scanner rotation will approximately have only three P_{pp}. This is not ideal, but three points may provide some idea of the dimensions of the object, or depending on the accuracy of the scanner and

navigation solution may show that it is a curved surface. For the 60^o vertical rotation this is not the case, as for the 50 profile lines this will result in just over 1 P_{pp}. One point per profile is not sufficient to define an object.

Table 6.9: Target and Test Parameters for Assessing the Impact of a Dual Axis Scanner Rotation on Point Density for a Narrow Target

Target Width	Target Height	PRR	M_f	Velocity
0.1m	2m	300kHz	100Hz	50km/h

Table 6.10: Assessing the Importance of Vertical Scanner Rotations in a Dual Axis Scanner Orientation for a Narrow Vertical 0.1m x 2m target at Different Horizontal Ranges

Test	$\alpha_{\text{scan}}/\gamma_{\text{scan}}$	Profiles	MIMIC 5m	MIMIC 10m	MIMIC 15m
1	$60^o/15^o$	8	85pts	40pts	26pts
2	$60^o/30^o$	17	117pts	49pts	30pts
3	$60^o/45^o$	29	197pts	71pts	41pts
4	$60^o/60^o$	50	393pts	136pts	72pts

The next test examines the impact of dual axis scanner rotations and vehicle velocity on point density for narrow targets. The vehicle velocity is increased in 10km/h increments and the point density is measured on the target defined in Table 6.9 for each velocity. The range to the target is constant at 5m for these tests. Figure 6.7 illustrates the results of the point density calculation and vehicle velocity on a narrow target for a selection of dual axis scanner rotations. The complete set of results are detailed in Table 25 in Appendix .3. The increased point density arising from a $60^o/60^o$ scanner orientation is approximately double the point density of the $45^o/45^o$ scanner orientation. As previously explained, this is due to the smaller vertical profile spacing arising from a high vertical scanner rotation. To verify

this, two different dual axis scanner rotations and their intersection with a parallel vertical surface is calculated by MIMIC. The profile spacing and profile angle are measured. The difference in profile angle between the two is 19.10^o, and this results in a difference in profile spacing of 0.058m which could be significant for smaller targets. Table 6.11 details the influence of smaller profile angles on vertical point spacing for two scanner configurations.

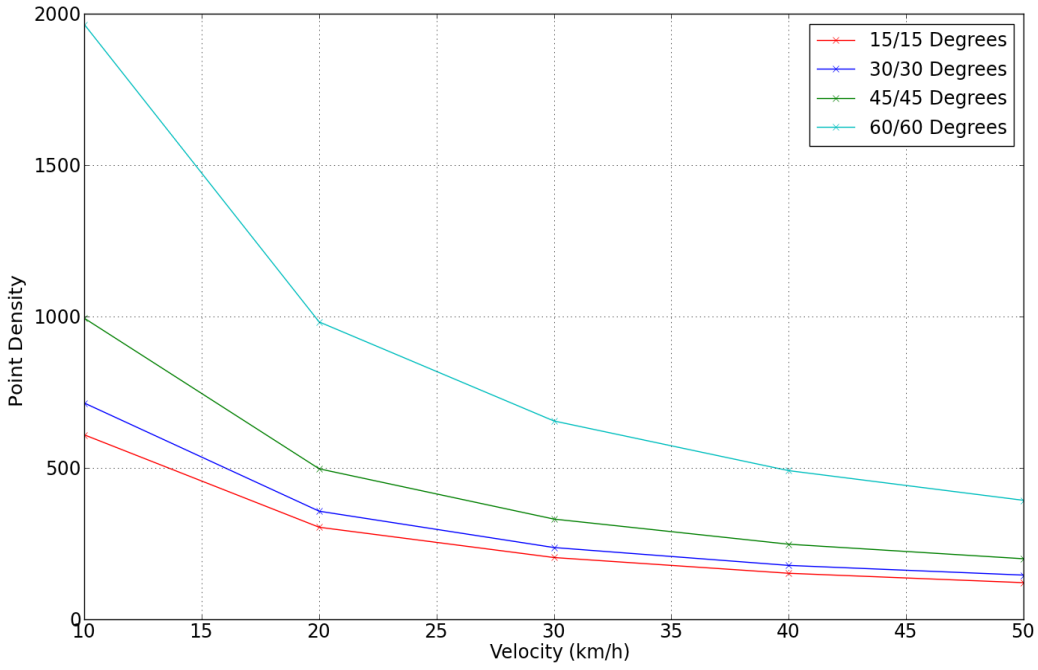

Figure 6.7: Calculating the Effect of Vehicle Velocity and a Dual Axis Scanner Rotation on the Point Density of a Narrow Vertical Target. Target Range is 5m and Target Dimensions are 0.1m x 2m

It is important to note that at shorter ranges, the reduction in P_{pp} may not be an issue. To demonstrate this, a test is designed to measure the P_{pp} for a narrow target using four different dual axis scanner rotations. A target

Table 6.11: Identifying the Relationship Between Profile Angle and Profile Spacing for Different Dual Axis Rotations

No.	α_{scan}	γ_{scan}	α_{targ}	β_{targ}	θ_{P_rA}	d_{P_rS}
1	45^o	45^o	0^o	0^o	35.26^o	0.098m
2	60^o	60^o	0^o	0^o	16.10^o	0.040m

range of 5m and a vehicle velocity of 50km/h is applied. Table 6.12 lists the number of P_{pp} for these tests. Six is the lowest number of P_{pp} occurring in these tests. This occurs in Test 4, which is the $60^o/60^o$ dual axis rotation and therefore has the highest number of profiles. Although the number of P_{pp} from the $15^o/15^o$ dual axis rotation is five times this amount, six points is sufficient for defining a narrow object only 0.1m wide. Conversely, the $15^o/15^o$ rotation provides the highest number of P_{pp}, but this must be offset against the number of scan profiles that may be required by an automated algorithm. Figure 6.8 illustrates the number of scan profiles on a target at different velocities for each scanner rotation. At all velocities the number of scan profiles for each dual-axis scanner rotation drops significantly, reinforcing the link between velocity and profile spacing.

Table 6.12: Calculating Points per Profile on a Narrow Vertical Target 0.1m x 2m for Different Dual Axis Scanner Rotations at 5m range and Velocity of 50km/h

No.	α_{scan}	γ_{scan}	α_{targ}	β_{targ}	P_{pp}
1	15^o	15^o	0^o	0^o	30
2	30^o	30^o	0^o	0^o	14
3	45^o	45^o	0^o	0^o	10
4	60^o	60^o	0^o	0^o	6

As has been demonstrated, when designing a system to maximise point

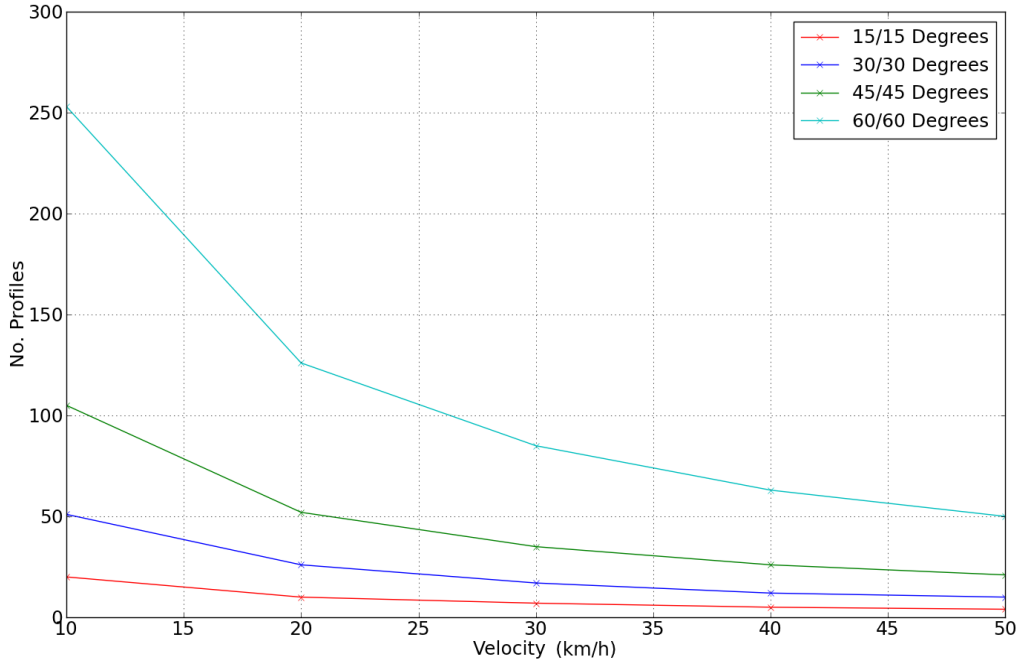

Figure 6.8: Calculating the Effect of Vehicle Velocity and a Dual Axis Scanner Rotation on the Number of Profiles Intersecting a Narrow Vertical Target. Target Range is 5m and Target Dimensions are 0.1m x 2m

density there is a trade off between the number of scan profiles intersecting a narrow target and also the number of P_{pp}. A high point density may not accurately define a target if the number of P_{pp} is too low, or if the profile spacing is too high. A number of factors influence point density; system parameters, target parameters and vehicle parameters. Consideration must also be given to target orientations that will return no points for specific scanner orientations. Therefore when designing a fixed scanner system, deciding on the scanner orientation is an extremely important decision. It is a decision that could cause manufacturers to err on the side of caution to ensure the MMS can be operated in the majority of scenarios. Alternatively, including a second scanner will largely negate these risks. A second scanner will also increase the number of returns from a target.

6.2.3.3 Recommended Orientation

Although the final choice of scanner orientation is largely target dependent, this section identifies the effect of combining higher vertical scanner rotations with lower horizontal scanner rotations. These tests investigate whether this is a more practical configuration for a dynamic real-world environment. A number of trends are apparent when investigating the results in Sections 6.2.3.1 and 6.2.3.2.

- As the dual scanner vertical and horizontal rotations are increased by 15^o (e.g. $15^o/15^o$ up to $30^o/30^o$) the point density approximately doubles.
- As the dual scanner vertical and horizontal rotations are increased by 15^o, the number of profiles approximately doubles.

- As the velocity doubles, the point density approximately halves.
- As the range doubles, the resulting point density is approximately half.

When selecting the horizontal scanner rotation for the tests in this section, two important factors must be considered. Firstly, higher horizontal rotations ($\geq 60^o$) of the scanner could potentially miss a surface that is angled away from the MMS ($\geq$ -30^o). Additionally, a low horizontal rotation (15^o) results in too few points striking a surface perpendicular to the direction of travel, which is the primary reason for introducing a horizontal rotation of the scanner. For these reasons, horizontal scanner rotations of 30^o and 45^o are selected while vertical scanner rotations of 30^o, 45^o and 60^o are selected. A 2m x 1m parallel vertical target is defined for these tests. The target range is fixed at 5m and the vehicle velocity is set at 50km/h. A scanner operating at a 300kHz PRR and a 100Hz mirror frequency is also defined in MIMIC. The target and test parameters are listed in Table 6.13.

Table 6.13: Target and Test Parameters for Assessing the Impact of a Dual Axis Scanner Rotation on Point Density for a Narrow Target

Target Width	Target Height	PRR	M_f	Velocity
2m	1m	300kHz	100Hz	50km/h

The point density for each scanner orientation is calculated. The point density results are then assessed to identify whether these configurations perform better than the 30^o/30^o and 45^o/45^o configurations employed in the previous sections. For each scanner rotation combination, the increased vertical rotation of the scanner leads to an increased point density. By combining a 45^o horizontal rotation with a 60^o vertical rotation the point density is

increased from 10,188 to 14,343 points on the target when compared to the $45^o/45^o$ orientation. This equates to a 40% increase in point density and also diminishes the risk of missing a negatively rotated target that would arise with a 60^o horizontal scanner rotation. Additionally it also decreases the distance to the target when compared with the 60^o horizontal scanner rotation and therefore decreases the point spacing on the target. Figure 6.9 illustrates the results of these tests, while Table 26 in Appendix .3 details each test.

These results are target dependant and system specific. For standard parallel targets, a $\alpha_{\text{scan}}/\gamma_{\text{scan}}$ of $45^o/60^o$ is the recommended orientation for near side infrastructure. This orientation is particularly relevant for maximising point density with single scanner MMSs. The 45^o α_{scan} increases the number of profiles intersecting with objects perpendicular to the direction of travel, yet does not constitute an excessive α_{scan} that could potentially result in zero returns on negatively rotated targets. The 60^o γ_{scan} decreases the vertical profile spacing and therefore increases point density. However, for the multiple possible angled targets, the recommended orientation may change. MIMIC allows for examination of multiple target orientations and dimensions. MIMIC can therefore provide the recommended configuration information for any valid user defined target.

6.3 Scanner Position

In this thesis, MIMIC has provided the capability to assess point density on targets for different system configurations. One potential variable is the horizontal position of the scanner on the MMS. This can be varied in the X

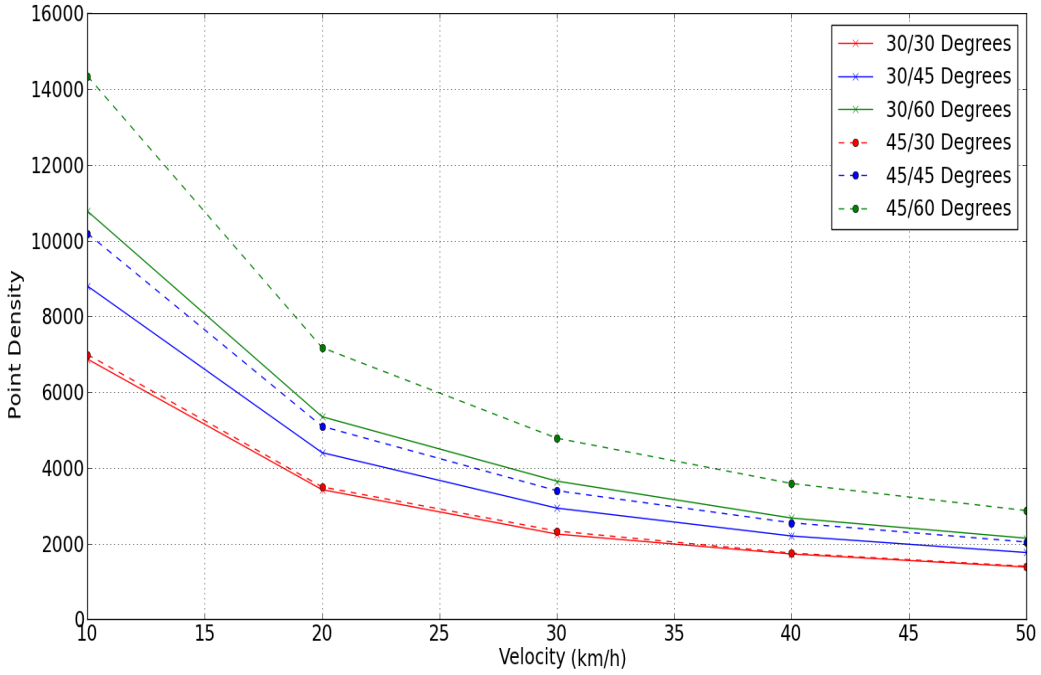

Figure 6.9: Calculated Point Density: Identifying the Recommended Dual Axis Scanner Rotation for Increasing Point Density on a Parallel Vertical Target at Different Vehicle Velocities. Target Range is 5m and Target Dimensions are 2m x 1m

or Y plane, as illustrated in Figure 6.10 with Scanners 1 - 4. Different MMSs may have different vehicle coordinate systems (X and Y are interchangeable) and so the axis labels may differ between MMSs. In these tests X refers to the horizontal axis (the width of the vehicle) and Y refers to the vertical axis (the length of the vehicle). The impact that changing the scanner location in either axis has on point density is examined in the following sections. It is important to note that changes in the location of the scanner assume no obstructions caused by the vehicle body or the navigation sensors. Scanners located near the extremities of the MMS should be able to avoid obstructions from the vehicle by introducing a vertical rotation of the scanner, although this could result in a situation similar to that displayed in Figure 6.6(b). In the previous sections in this chapter, only positive scanner rotations were explored. In this section, negative horizontal scanner rotations are also explored. Negative scanner rotations were not explored in the previous tests because the change in position on the MMS that facilitates a negative rotation of the scanner had not been investigated. The orientation of the target is even more influential on the point density when comparing a positively rotated scanner (Scanners 1,2 and 4) to a negatively rotated scanner (Scanner 3). Therefore, different target rotations are incorporated in these tests to identify the strengths and weaknesses of each scanner configuration.

6.3.1 Varying Scanner Position on X Axis

For Scanners 1 and 2, a change in the horizontal axis of the scanner, as illustrated in Figure 6.10, is analogous with an increase in the horizontal range to the target. These tests quantify the effect that altering the position of the scanner on the X axis of the MMS has on point density. The two scan-

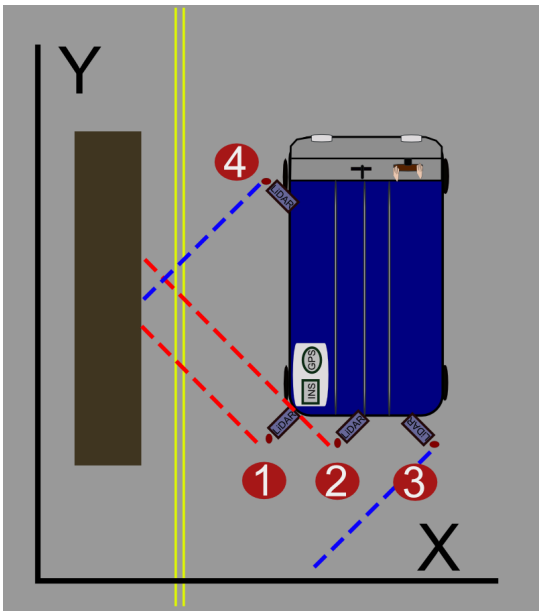

Figure 6.10: Horizontal Scanner Position - Scanners 1, 2, 3 and 4 Situated on the X/Y Axes

ners used in these tests are orientated at a 45^o horizontal and a 45^o vertical rotation matching the scanner orientation on the XP1. Table 6.14 details the scanner parameters. An offset of 1m is defined for Scanner 2. A 2m x 1m target and a vehicle velocity of 50km/h is defined. The target and test parameters are listed in Table 6.15.

Table 6.14: Scanner Parameters for Assessing the Impact of Horizontal Scanner Position in the X Axis on Point Density for an Angled Target - Scanners 1 and 2

Scanner	α_{scan}	γ_{scan}	PRR	M_f
1	45^o	45^o	300kHz	100Hz
2	45^o	45^o	300kHz	100Hz

Four different target orientations are applied in these tests. The first target is parallel to the direction of travel, whereas the second is rotated

Table 6.15: Test and Target Parameters for Assessing the Impact of Horizontal Scanner Position in the X Axis on Point Density for an Angled Target - Scanners 1 and 2

Target Width	Target Height	Offset	Velocity	H_r
2m	1m	1m	50km/h	5m

horizontally and the third vertically. The fourth target is a combination of both rotations. The point density is then measured for both scanners on the same target after each rotation. Table 6.16 details the results for each test in both scanner positions. For each target, Scanner 1 consistently outperforms Scanner 2. Scanner 1 returns 333 more points than Scanner 2 for a parallel target. The results in Table 6.16 show that although the percentage drop in point density varies depending on the orientation of the surface, a 1m change in horizontal scanner position in the X axis results in approximately an average 16% decrease in point density on each target.

Table 6.16: Calculating Point Density on Angled Targets Dimensions 2m x 1m for Two Different Scanner Positions at 5m Range and Velocity of 50km/h - Scanners 1 and 2

Target	Scanner	α_{targ}	β_{targ}	MIMIC	% Change
1	1	0^o	0^o	2039	17%
1	2	0^o	0^o	1706	
2	1	15^o	0^o	2107	14%
2	2	15^o	0^o	1818	
3	1	0^o	15^o	2185	18%
3	2	0^o	15^o	1797	
4	1	15^o	15^o	2257	16%
4	2	15^o	15^o	1906	

A potential configuration for a dual scanner MMS is for the second scanner to be orientated at -45^o horizontal and offset from Scanner 1 in the X

axis. This configuration is illustrated in Figure 6.10 as Scanner 3 and is similar to the scanner arrangement on the Optech Lynx. To assess the effect of this configuration on point density the same tests are repeated. However, to eliminate the effect of two different H_r on the point density, a 0m scanner offset is applied to Scanner 3. Therefore Scanner 3 is placed at the same location as Scanner 1, but retains its -45^o horizontal rotation. Table 6.17 details the scanner parameters. The target is a 2m x 1m target at 5m range from the scanner and the vehicle velocity is defined at 50km/h. Table 6.18 details these test and target parameters.

Table 6.17: Scanner Parameters for Assessing the Impact of Horizontal Scanner Position on the X Axis on Point Density for an Angled Target - Scanners 1 and 3

Scanner	α_{scan}	γ_{scan}	PRR	M_f
1	45^o	45^o	300kHz	100Hz
3	-45^o	45^o	300kHz	100Hz

Table 6.18: Test and Target Parameters for Assessing the Impact of Horizontal Scanner Position on the X Axis on Point Density for an Angled Target - Scanners 1 and 3

Target Width	Target Height	Offset	Velocity	H_r
2m	1m	0m	50km/h	5m

Four positive target rotations and one negative target rotation are applied. The point density is calculated for both scanners on each target after every rotation. Table 6.19 details the results of these tests. Scanner 1 has outperformed Scanner 3. For a parallel target, a negatively rotated scanner such as Scanner 3 results in a 68% drop in point density when compared to a

positively rotated scanner. The underlying reason for the lower point density for Scanner 3 in these tests is the increased point spacing resulting from a different angle of intersection, θ_{scan}, between the scan pulse and the surface. It is important to note that although the values for Scanner 3 are lower than for Scanner 1, obtaining an equivalent point density with both scanners is not the primary reason for incorporating a second scanner. A second scanner is installed and orientated in this manner to eliminate data shadows in the survey by capturing information in areas that the first scanner has no line of sight to, as the work by [Yoo et al., 2009] has demonstrated. Additionally, negatively rotated scanners result in an improved point density for negatively rotated targets. The test on Target 5 displays this. This target is orientated at -30^0 horizontally, and the % drop in point density for Scanner 3 when compared to Scanner 1 has now decreased to 26%.

Table 6.19: Calculating Point Density on Angled Targets Dimensions 2m x 1m for Two Different Scanner Orientations at 5m Range and Velocity of 50km/h - Scanners 1 and 3

Target	Scanner	α_{targ}	β_{targ}	MIMIC	% Change
1	1	0^o	0^o	2039	68%
1	3	0^o	0^o	643	
2	1	15^o	0^o	2107	84%
2	3	15^o	0^o	332	
3	1	0^o	15^o	2185	68%
3	3	0^o	15^o	696	
4	1	15^o	15^o	2257	82%
4	3	15^o	15^o	402	
5	1	-30^o	0^o	1504	26%
5	3	-30^o	0^o	1115	

6.3.2 Varying Scanner Position on Y Axis

This section explores the effect that changing the scanner position in the Y axis has on point density. Changing the scanner's position in the Y axis but keeping the same rotation has no effect on the point density. This is because the range to the target and the angle of intersection between the scan plane and target would not vary between the two scanners. An identical orientation for both scanners would also negate the primary advantage arising from installation of a second scanner, elimination of data shadows. To assess the possibility of utilising the Y axis for a second scanner, Scanner 4 is defined, as shown in Figure 6.10. Scanner 4 is rotated horizontally to 135^o and vertically to 45^o. Table 6.20 details the scanner parameters in these tests. Table 6.21 details the test and target parameters.

Table 6.20: Scanner Parameters for Assessing the Impact of Horizontal Position in the Y Axis on Point Density for an Angled Target - Scanners 1 and 4

Scanner	α_{scan}	γ_{scan}	PRR	M_f
1	45^o	45^o	300kHz	100Hz
3	135^o	45^o	300kHz	100Hz

Table 6.21: Test and Target Parameters for Assessing the Impact of Horizontal Scanner Position in the Y Axis on Point Density for an Angled Target - Scanners 1 and 4

Target Width	Target Height	Offset	Velocity	H_r
2m	1m	0m	50km/h	5m

One potential benefit of placing a scanner in this position is that it eliminates scanner offset. This decreases the measurement range to near side

objects but requires a suitable vertical rotation of the scanner to ensure the scanners FOV is not obstructed by the vehicle body or other MMS sensors. It is important to note that this scanner configuration increases the range to objects on the far side of the vehicle and is therefore more suitable when surveying near side targets. The point density is calculated for both scanners on the target after each target rotation. Table 6.22 details the results of these tests. Scanner 4 displays a comparable point density with Scanner 1 for parallel targets. On Target 2, as the target orientation changes by 15%, the point density is reduced for Scanner 4, resulting in a 13% drop in point density. As in the previous tests, a negative horizontal target rotation has the opposite effect. On Target 5, a negative target rotation results in a 13% drop in point density for Scanner 1 and a corresponding rise for Scanner 4. Each scanner orientation exhibits higher point density on targets that face towards that scanner. Positive target rotations result in an increased point density for positive scanner rotations. Negative target rotations result in an increased point density for negative scanner rotations.

An additional benefit of Scanner 4 is that this scanner is able to survey the face of an object that Scanner 1 is incapable of surveying due to the objects orientation (a negative target rotation $\geq$ -45^o). This is one of the primary benefits of a dual scanner system. A drawback of the Scanner 1 and 4 configuration is that it results in a decrease in point density on targets on the other side of the MMS. In a vehicle with a fixed configuration, this would lead to difficulties in countries where vehicles drive on a different side of the road.

Table 6.22: Calculating Point Density on Angled Targets Dimensions 2m x 1m for Two Different Scanner Orientations at 5m Range and Velocity of 50km/h - Scanners 1 and 4

Target	Scanner	α_{targ}	β_{targ}	Points	% Change
1	1	0^o	0^o	2039	0%
1	4	0^o	0^o	2039	
2	1	15^o	0^o	2107	13%
2	4	15^o	0^o	1832	
3	1	0^o	15^o	2185	0%
3	4	0^o	15^o	2185	
4	1	15^o	15^o	2257	25%
4	4	15^o	15^o	1986	
5	1	-15^o	0^o	1832	-13%
5	4	-15^o	0^o	2107	

6.4 Scanner Settings

The previous sections have investigated the effect that scanner position and orientation have on point density. Although scanner settings are largely hardware dependant, three scanner settings are investigated in this section to identify their effect on point spacing and profile spacing. These are the M_f, the PRR and the FOV. The M_f impacts on profile spacing, whereas the PRR and FOV impact on point spacing. The point and profile spacing that a MMS will display for different target and survey parameters is important when surveying for small targets of specific dimensions.

6.4.1 Mirror Frequency and Profile Spacing

The scanner hardware settings and configuration of the XP1 were simulated in the previous tests. This section simulates the hardware settings and configuration of the Optech Lynx because it is capable of a higher M_f. A series

of tests are designed to assess the effect of the M_f on vertical profile spacing on a parallel vertical target for multiple vehicle velocities. The target and test parameters are listed in Table 6.23. The Optech Lynx $\alpha_{\text{scan}}/\gamma_{\text{scan}}$ are $37.49^o/29.6^o$. The maximum M_f for the Optech Scanner is 200HZ. The point density is calculated for the target at four different 50Hz increments of the M_f. The vehicle velocity is increased in 10km/h increments and the results of these tests are displayed in Figure 6.11. These complete results are detailed in Table 27 in Appendix .3.

The 50Hz mirror frequency exhibits significantly higher profile spacing at all velocities than the other three mirror frequencies. For users of MIMIC, the profile spacing information can be applied to ascertain whether the vertical profile spacing is sufficient for the required target. The vertical profile spacing displayed by the 200Hz M_f at 40km/h (0.074m) is comparable with the 50Hz M_f at 10km/h (0.077). The performance of the 50Hz M_f in relation to the 200Hz M_f demonstrates the importance of M_f in reducing profile spacing. For instance, at 50Km/h, profiles are 40cm apart and no data in between these would be captured by a scanner operating at 50Hz. However, a high M_f will result in less points per profile, and therefore a target-dependant compromise must be reached.

Table 6.23: Target and Test Parameters for Examining the Correlation Between Mirror Frequency and Vertical Profile Spacing on a Parallel Vertical Target at Different Vehicle Velocities

Target Width	Target Height	PRR	M_f	Velocity
2m	1m	200kHz	200Hz	50km/h

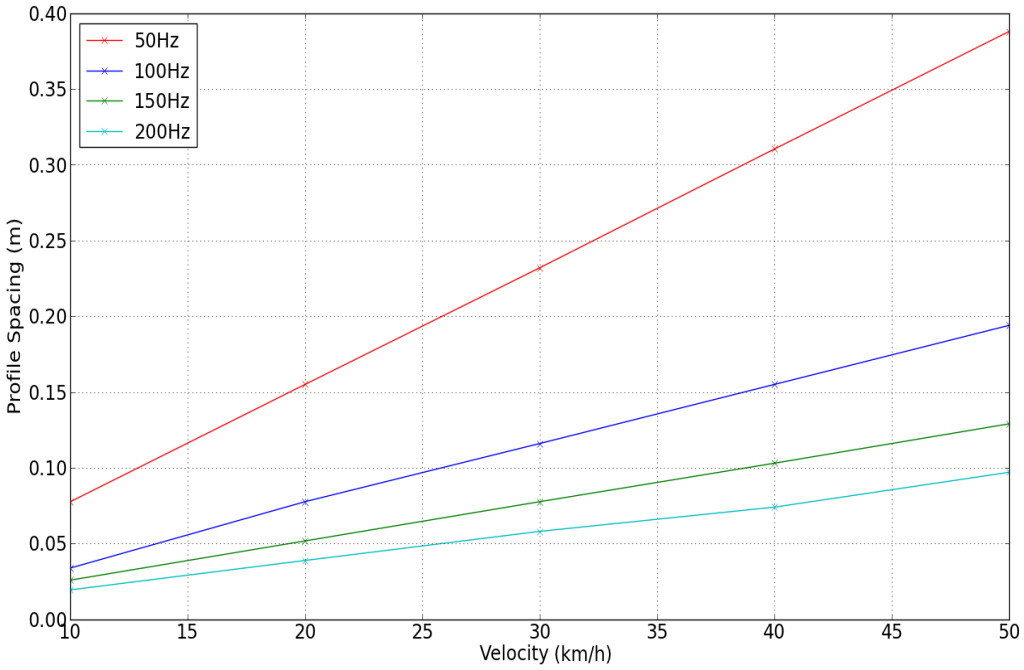

Figure 6.11: Calculated Profile Spacing: Examining the Correlation Between Mirror Frequency and Vertical Profile Spacing on a Parallel Vertical Target at Different Vehicle Velocities. Target Range is 5m and Target Dimensions are 2m x 1m

6.4.2 PRR and Point Spacing

PRR is one of the primary factors influencing point spacing. A series of tests are defined to measure the impact of range and PRR on the point spacing on a target. The target is a parallel vertical target, of dimensions 2m x 1m. The scanner that is defined for the point spacing tests is a Riegl VQ-250 operating at a 100Hz mirror speed. The Riegl VQ-250 is defined in MIMIC for these tests because it has a higher PRR than the Optech V200. The PRR is increased by 50kHz after each measurement and the horizontal distance is increased by 5m increments for each PRR test. Table 6.24 lists the target and test parameters for these tests. Table 28 in Appendix .3 details the tests.

Table 6.24: Target and Test Parameters for Examining the Influence of PRR and Target Range on Point Spacing on a Parallel Vertical Target

Target Width	Target Height	PRR	M_f	Velocity
2m	1m	300kHz	100Hz	50km/h

Figure 6.12 displays the results of the tests carried out to identify the correlation between PRR and H_r on a parallel vertical target. For the majority of near side infrastructure a 25m H_r is excessive, but it has been included to provide information on point spacing at long ranges. MIMIC can be used to generate information similar to this to ascertain whether a specific configuration is suitable for surveying a specific target. For example, with a 100kHz PRR, objects that are at 10m range from the MMS cannot be smaller than 0.1m. If a specific number of returns are required to define the 0.1m object at 10m range for an automated object recognition algorithm, then a higher PRR is required.

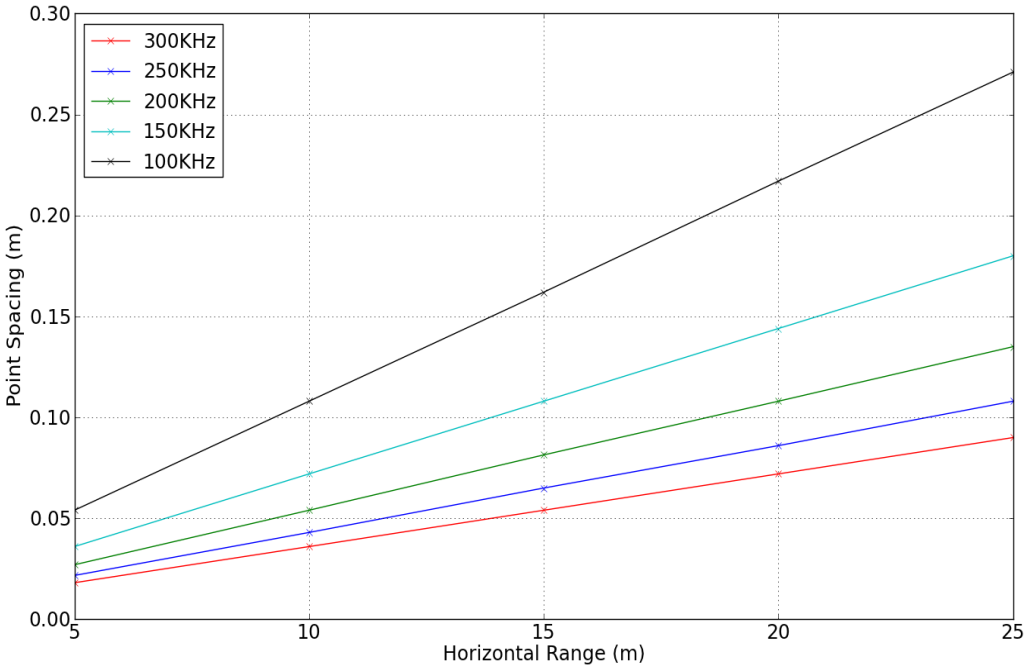

Figure 6.12: Calculated Point Spacing: Examining the Correlation Between PRR and Horizontal Range for Point Spacing on a Parallel Vertical Target. Target Dimensions are 2m x 1m

6.4.3 Field of View

The FOV of a scanner is a user selectable setting. The FOV can be set to limit a survey to a particular area around the MMS. By decreasing the FOV it is possible to achieve a smaller ASW. A smaller ASW will decrease point spacing in this area and therefore increase point density. A series of tests are designed to identify the correlation between FOV, PRR and point spacing. These tests are carried out on a parallel vertical target of dimensions 2m x 1m for a 2D scanner operating a full-circle 360^o FOV. Table 6.25 lists the target and test parameters. Table 29 in Appendix .3 details these tests in their entirety.

Table 6.25: Target and Test Parameters for Examining the Influence of PRR and Target Range on Point Spacing on a Parallel Vertical Target

Target Width	Target Height	PRR	M_f	Velocity
2m	1m	300kHz	100Hz	50km/h

The PRR is increased in 50Hz increments. The FOV is then decreased in 45^o increments for each PRR. The point density is calculated for the target after each decrease. The FOV is not decreased below 180^o for two reasons.

- Limiting the FOV could result in incomplete scan coverage of an area. In the example illustrated in Figure 6.13 the scanner is assigned a dual axis rotation and the FOV is limited to 180^o. With this configuration, the road under the vehicle is not surveyed.

- A low FOV could also potentially decrease the ASW below the smallest selectable ASW for that piece of hardware. For example, if a FOV of 180^o were applied to the VQ-250 it would result in an ASW of 0.06^o.

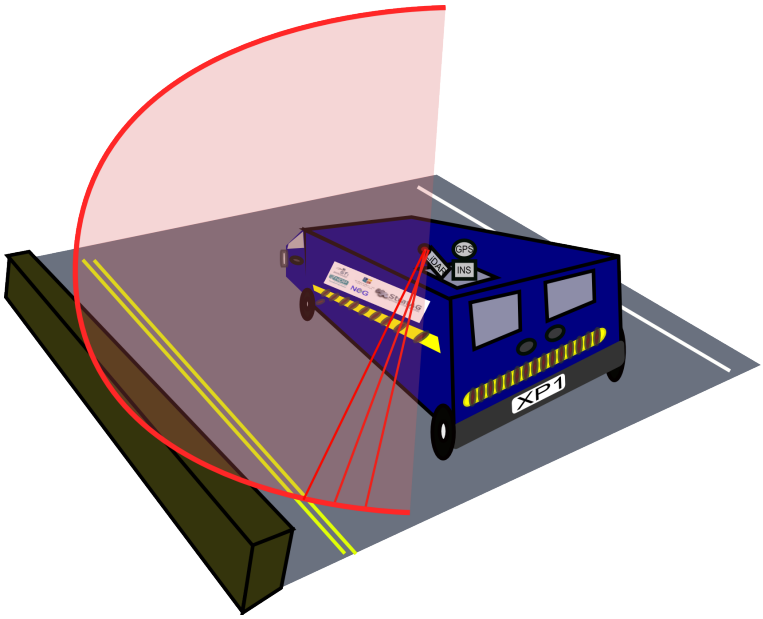

Figure 6.13: The effect of Decreasing the Scanner FOV on the Coverage of the Environment

> The minimum possible ASW setting for this scanner is 0.018^o and therefore a 180^o FOV is valid as it does not result in an ASW of lower than the minimum allowable by the hardware. This may become an issue at lower FOVs and for this reason 180^o is the cut-off for these tests.

A M_f of 100Hz is defined in these tests and a constant H_r of 5m is applied. Figure 6.14 illustrates the results for the FOV tests and the effect of decreasing FOV for increased point spacing, while the full table is available in Table 29 in Appendix .3. The impact of a higher FOV on point spacing is linear. For specific targets the point density can be increased if the area of interest in relation to the MMS is defined beforehand. If the Surveyor is certain that no extra features or redundancy from different scanner viewpoints is required, this is an acceptable solution. Examples of potential targets could be road-side crash barriers or kerb stones. By Minimising the FOV the area

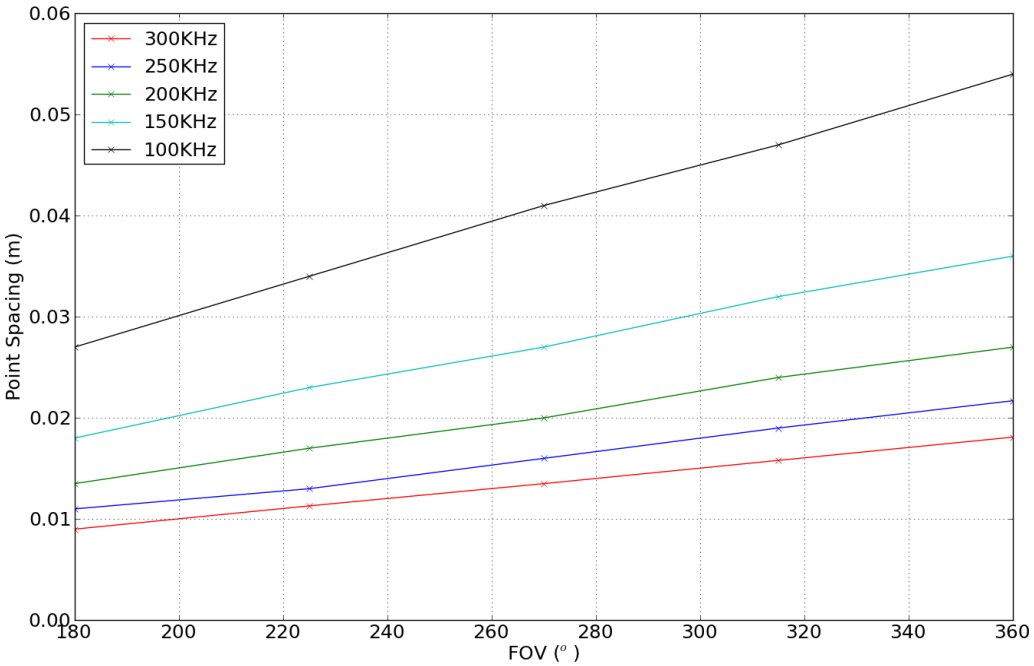

Figure 6.14: Calculated Point Spacing: Examining the Correlation Between PRR and FOV for Point Spacing on a Parallel Vertical Target. Target Dimensions are 2m x 1m

of interest could be surveyed with a higher point density.

6.5 Conclusion

In this chapter, the scanner configuration and hardware settings were varied to measure their influence on point density, profile spacing and point spacing. Three areas were investigated and a series of tests designed for each to assess their impact on point density. The first area that was investigated was the orientation of the scanner. These tests encompassed horizontal, vertical and dual axis scanner rotations. The second area that was investigated was the position of the scanner. These tests investigated the impact of positioning the scanner at different points on the X and Y axis of the MMS. The final area investigated was the impact of scanner settings on point density. Changes to the scanner's pulse repetition rate, mirror frequency and field of view were examined. A number of important findings were made in these three areas.

The scanner orientation tests identified and verified four important points. Firstly, in general horizontal rotations of the scanner increase point spacing and therefore decrease point density. Secondly, in general vertical rotations of the scanner decrease profile spacing and therefore increase point density. Thirdly, a trade off between profile spacing and the number of points per profile is required, particularly for narrow targets. Finally, the recommended orientation for a scanner on a MMS was identified as a $\alpha_{\text{scan}}/\gamma_{\text{scan}}$ of $45^o/60^o$. This recommended orientation has been optimised to maximise point density on near side infrastructure while minimising the possibility of zero returns from negatively rotated target with a single scanner MMS.

The scanner position tests identified and verified two important points.

Firstly, a change in scanner position on the X axis is analogous with a change in the horizontal range to the target. Secondly, utilising the Y axis of the MMS for the second scanner results in an increased performance on near side infrastructure and also provides the benefits of traditional dual scanner systems. Dual scanner systems potentially eliminate data shadows and increase point density on targets rotated away from the first scanner. The recommended scanner position when surveying near side infrastructure was identified as scanner positions 1 and 4. This scanner set-up increases point density while minimising data shadows.

The tests on scanner hardware settings identified and verified three important points. Firstly, while increasing mirror frequency is important for decreasing profile spacing, these tests reinforced the issue of a trade-off between points per profile and profile spacing. Secondly, a high PRR is important when surveying small or narrow targets. If the PRR can not be increased, the range to target must be decreased or the FOV decreased. The FOV can be tailored for specific surveys. Halving the FOV has the same effect as halving the point spacing.

In the next chapter MIMIC is applied in a series of tests benchmarking MMS point density. The performance of one commercial and two hypothetical MMSs will be calculated for a combination of target parameters.

Chapter 7

Benchmarking MMS Point Density

This chapter details the methods and tests employed to benchmark the performance of three different MMSs in terms of their point density. This is the third and final objective of this thesis. One real-world and two theoretical MMSs are included in this benchmarking process. Each of the MMSs are dual scanner systems. In this chapter a series of tests are applied to compare the two theoretical systems against a commercial system. Both theoretical systems are a modified and improved version of the XP1 and the commercial system is the Optech Lynx. The first theoretical system is designed using the recommended scanner orientation and position identified in Chapter 6 for near side infrastructure. The second theoretical system is a dual scanner version of the XP1.

7.1 Introduction

The three MMSs have been selected for these tests because of specific scanner hardware and configuration differences. These MMSs therefore provide a range of systems suitable for benchmarking. Point density is measured on a selection of targets under different test parameters. The point density tests for large planar targets are detailed in Section 7.3 and for multi-faced targets in Section 7.4. Section 7.5 summarises all of the findings in this chapter.

7.2 Test Systems

Three MMSs are assessed in these tests. The hardware and configuration of the two theoretical versions of the XP1 are described in this section. These MMSs are called the XP1+ and XP2. The scanner configuration of the Optech Lynx is also detailed in this section. MIMIC enables benchmarking of multiple scanner configurations in terms of their point density. Scanner elevations are standardised for each system at the height of the scanner on the XP1, which is 3.1m. This ensures the results are dependant on the hardware configuration only and not influenced by the dimensions of the platform.

7.2.1 XP1 + Configuration

The XP1 is a single scanner system employing a single VQ-250, whereas the XP1+ is a dual scanner system. Incorporating another high specification scanner can be very costly and increases data throughput on the MMS. The XP1+ incorporates a cheaper, limited FOV, low PRR, SICK LMS. Table 7.1 lists the relevant parameters of the two scanners on the XP1+. The PRR of

the SICK is only 9% that of the Riegl. This shortcoming is partially offset by the lower FOV of the SICK which decreases the ASW. The two scanners are orientated and positioned in accordance with the recommended configuration identified in the previous chapter. Figure 7.1 illustrates the scanner position and configuration on the XP1+ while Table 7.2 details this configuration. The SICK LMS is situated at the same position on the vehicles X axis as the Riegl VQ-250 but is offset in the Y axis by 2m. This offset does not influence point density in any way but is assigned merely to reinforce the difference in the Y axis of the two scanners. A 60^o vertical rotation is applied to both scanners to maximise point density. Horizontal scanner rotations of 45^o and 135^o respectively are introduced to minimise the range change resulting from a large horizontal rotation of the scanner and minimise the risk of zero returns from angled surfaces.

Table 7.1: XP1 + Scanner Parameters

Scanner	M_f	PRR	FOV	ASW
Riegl VQ-250	100Hz	300kHz	360^o	0.12^o
SICK LMS 221	75Hz	27.075kHz	180^o	0.99^o

Table 7.2: XP1+ Scanner Configuration

Scanner	α_{scan}	γ_{scan}	XY Position (m)
Riegl VQ-250	45^o	60^o	0,0
SICK LMS 221	135^o	60^o	0,2

7.2.2 XP2 Configuration

The XP2 incorporates a second VQ-250 scanner and has retained the XP1s $45^o/45^o$ $\alpha_{\text{scan}}/\gamma_{\text{scan}}$ scanner orientation. The second scanner is negatively

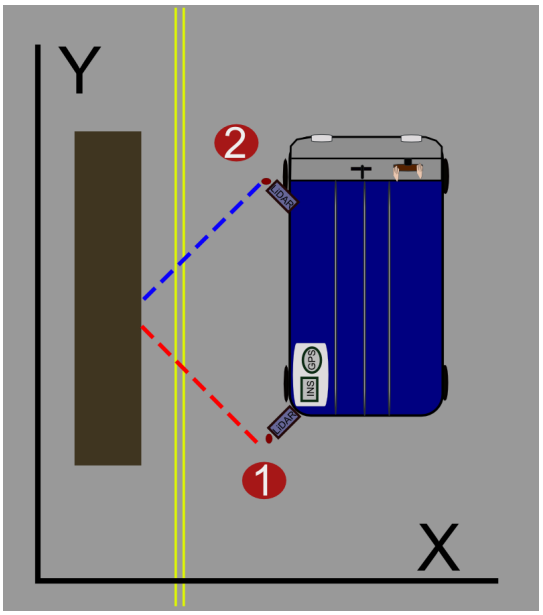

Figure 7.1: XP1+ Scanner Locations

rotated to -45^o/45^o. In Table 7.3 the parameters for both scanners are listed. Figure 7.2 illustrates the scanner location and configuration on the XP2. This scanner configuration is detailed in Table 7.4. The second scanner is offset by 1.389m in the X axis, assigning it the same X,Y coordinates as the second scanner on the Optech Lynx. A standard offset is assigned to enable a comparison between the XP2 and the Optech Lynx.

Table 7.3: XP2 Scanner Parameters

Scanner	M_f	PRR	FOV	ASW
Riegl VQ-250 (1)	100Hz	300kHz	360^o	0.12^o
Riegl VQ-250 (2)	100Hz	300kHz	360^o	0.12^o

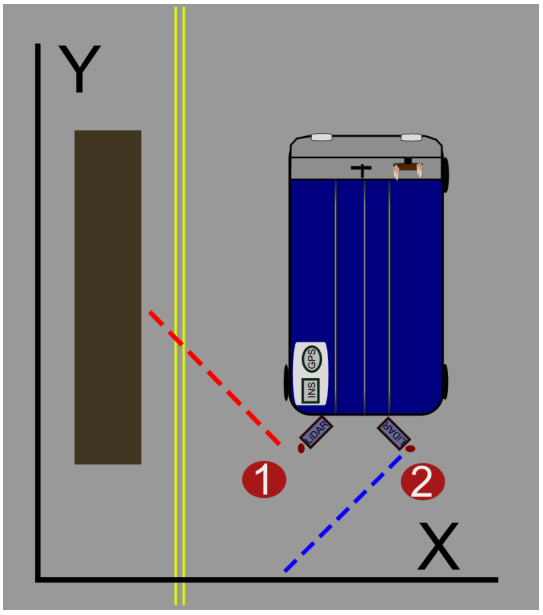

Figure 7.2: XP2 Scanner Locations

Table 7.4: XP2 Scanner Configuration

Scanner	α_{scan}	γ_{scan}	XY Position (m)
Riegl VQ-250 (1)	45^o	45^o	0,0
Riegl VQ-250 (2)	-45^o	45^o	1.389,0

7.2.3 Optech Lynx Configuration

The Optech Lynx is an existing commercial MMS and data from this system has been used in the validation tests in the preceding chapters. Two V200 scanners are defined in these benchmarking tests. The parameters of the two V200 scanners are listed in Table 7.5. The Optech V200 is included in these tests because it is similar in performance to the Riegl VQ-250 onboard the XP1. Figure 7.3 illustrates the scanner location and configuration on the Optech Lynx while Table 7.6 details each scanners position and orientation. The V200 is capable of a higher mirror frequency than the VQ-250 (200Hz as opposed to 100Hz) but a lower PRR (200kHz as opposed to 300kHz). Therefore, the profile spacing from the Optech V200 is lower than the Riegl VQ-250, but the point spacing is higher for the V200.

Table 7.5: Optech Lynx Scanner Parameters

Scanner	M_f	PRR	FOV	ASW
V200 (1)	200Hz	200kHz	360^o	0.36^o
V200 (2)	200Hz	200kHz	360^o	0.36^o

Table 7.6: Optech Lynx Scanner Configuration

Scanner	α_{scan}	γ_{scan}	XY Position (m)
V200 (1)	37.48^o	29.6^o	0,0
V200 (2)	-37.53^o	29.95^o	1.389,0

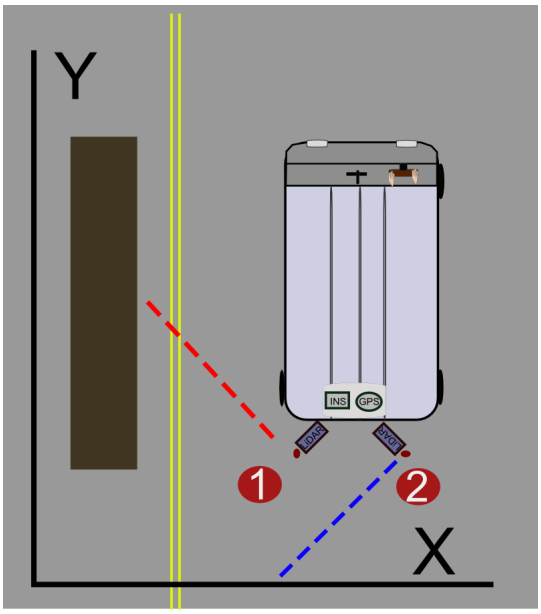

Figure 7.3: Optech Lynx Scanner Locations

7.3 Benchmarking MMS Point Density on 2D Targets

The initial benchmarking tests are performed on parallel vertical targets of two different sizes. Point density is calculated for both target types for all three systems. The target range and vehicle velocity is varied in these tests and this facilitates a robust comparison of the three systems.

7.3.1 2D Large Targets

A parallel vertical target 2m wide x 1m high is selected as the first target. The target range is defined as 5m. This test involves calculating point density for five vehicle velocities ranging from 10km/h to 50km/h in 10km/h increments. Point density is calculated for all three MMSs and the results are detailed in Table 7.7. In Figure 7.4 the point density results are plotted

as a function of velocity for all three MMSs. These tests identify that the Riegl Scanners are capable of a higher point density than the Optech scanners on a planar surface. This is primarily due the lower PRR of the Optech scanner and because the M_f, PRR and FOV of the Optech scanners result in an angular step width of 0.36^o. This ASW is three times greater than that of the Riegl, which is 0.12^o.

Although the higher M_f results in twice the number of profiles on a target for the Optech V200 than the Riegl VQ-250, the higher vertical rotation of the Riegl scanners negates this advantage for a parallel target by decreasing the vertical profile spacing. Figure 7.4 illustrates that the XP1+ is capable of a higher point density than the XP2 and Optech Lynx which both operate high grade second scanners. The higher point density demonstrates the positive effect of implementing the recommended scanner configuration identified in this thesis.

The results for a large parallel vertical target demonstrate an additional advantage of the recommended configuration. Table 7.7 shows that the single VQ-250 in the $45^o/60^o$ orientation is capable of a higher point density than the both Riegl VQ-250s in the $45^o/45^o$ orientation combined. For instance, at 10km/h, Scanner 1 on board the XP1+ is capable of capturing 4,155 points more than the same scanner on the XP2. Applying the recommended configuration to the SICK LMS has also improved its performance. By eliminating the scanner offset and introducing a 60^o vertical scanner rotation its performance is comparable with the more expensive, second Riegl VQ-250 on the XP2 and outperforms the second V200 on the Optech Lynx. At 10km/h the

Table 7.7: Calculating Point Density on Parallel Vertical Targets of Dimensions 2m x 1m for Three Dual Scanner MMSs at 5m Range and Varying Vehicle Velocities

MMS	Velocity	Scanner1	Scanner2	Combined
XP1+	10km/h	14343pts	2581pts	16924pts
XP1+	20km/h	7171pts	1290pts	8461pts
XP1+	30km/h	4781pts	860pts	5641pts
XP1+	40km/h	3585pts	646pts	4231pts
XP1+	50km/h	2870pts	516pts	3386pts
XP2	10km/h	10188pts	2949pts	13137pts
XP2	20km/h	5094pts	1474pts	6568pts
XP2	30km/h	3395pts	982pts	4377pts
XP2	40km/h	2547pts	737pts	3284pts
XP2	50km/h	2039pts	590pts	2629pts
Lynx	10km/h	4635pts	2262pts	6897pts
Lynx	20km/h	2317pts	1131pts	3448pts
Lynx	30km/h	1544pts	754pts	2298pts
Lynx	40km/h	1158pts	565pts	1723pts
Lynx	50km/h	927pts	452pts	1379pts

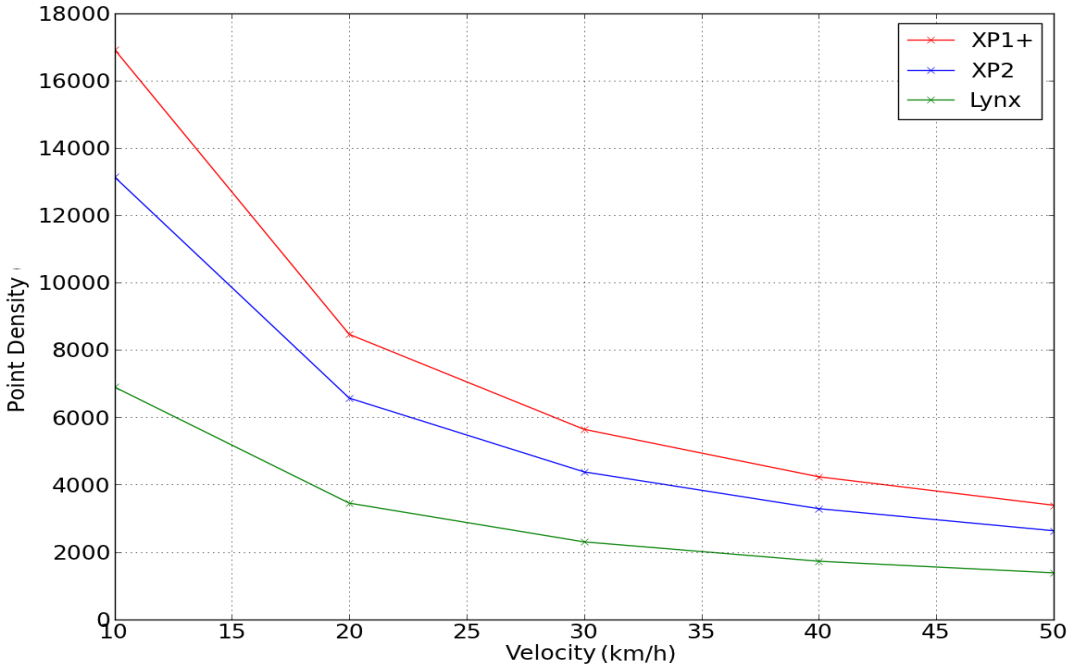

Figure 7.4: Calculated Point Density: Benchmarking Dual Scanner MMS Performance on a Parallel Vertical Target at Different Vehicle Velocities. Target Range is 5m and Target Dimensions are 2m x 1m

SICK LMS captured only 368 points less than Scanner 2 on the XP2 but 319 more than Scanner 2 on the Optech Lynx. Figure 7.5 shows the number of points for each of the second scanners at different velocities. The XP2 is capable of the highest point density at all vehicle velocities. However, the XP1+ with only one high grade scanner is capable of a higher point density than the Optech Lynx.

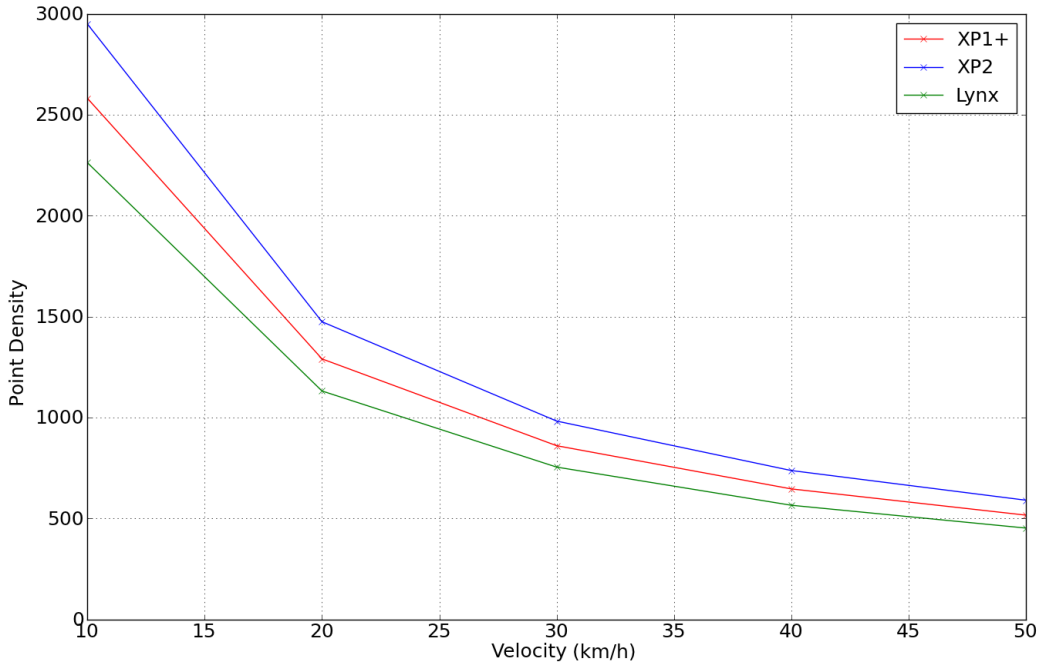

Figure 7.5: Calculated Point Density: Benchmarking the Performance of the Second Scanner on a MMS on a Parallel Vertical Target at Different Vehicle Velocities. Target Range is 5m and Target Dimensions are 2m x 1m

In the second set of tests, the vehicle velocity is fixed at 50km/h while the target range is varied from 5m to 25m in 5m increments. Table 7.8 displays the results for these benchmarking tests and Figure 7.6 plots these results.

The XP1+ has again returned a higher number of points than the other two MMSs. The XP1+ is capable of a higher point density than the XP2 and Optech Lynx even before Scanner 2 is included in the combined point density figure. For example, at 25m range, Scanner 1 on the XP2 captures only 63% of the points that Scanner 1 on the XP1+ is capable of, despite being the same type of scanner, a Riegl VQ-250. This underlines the importance of a vertical scanner rotation for increasing point density.

Table 7.8: Calculating Point Density on Parallel Vertical Targets of Dimensions 2m x 1m for Three Dual Scanner MMSs at 50km/h and Varying Target Ranges

MMS	H_r	Scanner 1	Scanner 2	Combined
XP1+	5m	2870pts	516pts	3386pts
XP1+	10m	1616pts	292pts	1908pts
XP1+	15m	953pts	172pts	1125pts
XP1+	20m	657pts	119pts	776pts
XP1+	25m	497pts	90pts	587pts
XP2	5m	2039pts	590pts	2629pts
XP2	10m	937pts	430pts	1367pts
XP2	15m	573pts	332pts	905pts
XP2	20m	409pts	268pts	677pts
XP2	25m	317pts	225pts	542pts
Lynx	5m	927pts	452pts	1379pts
Lynx	10m	472pts	303pts	775pts
Lynx	15m	306pts	224pts	530pts
Lynx	20m	225pts	177pts	402pts
Lynx	25m	178pts	146pts	324pts

For large targets, the Riegl VQ-250 outperforms the Optech V200 scanner at all target ranges. Although the SICK LMS outperforms the Optech at close range (5m), the low ASW results in a decreased point spacing at long ranges. The Optech V200 performs better at ranges over 5m. A number of factors should be considered when interpreting these results. Firstly, the

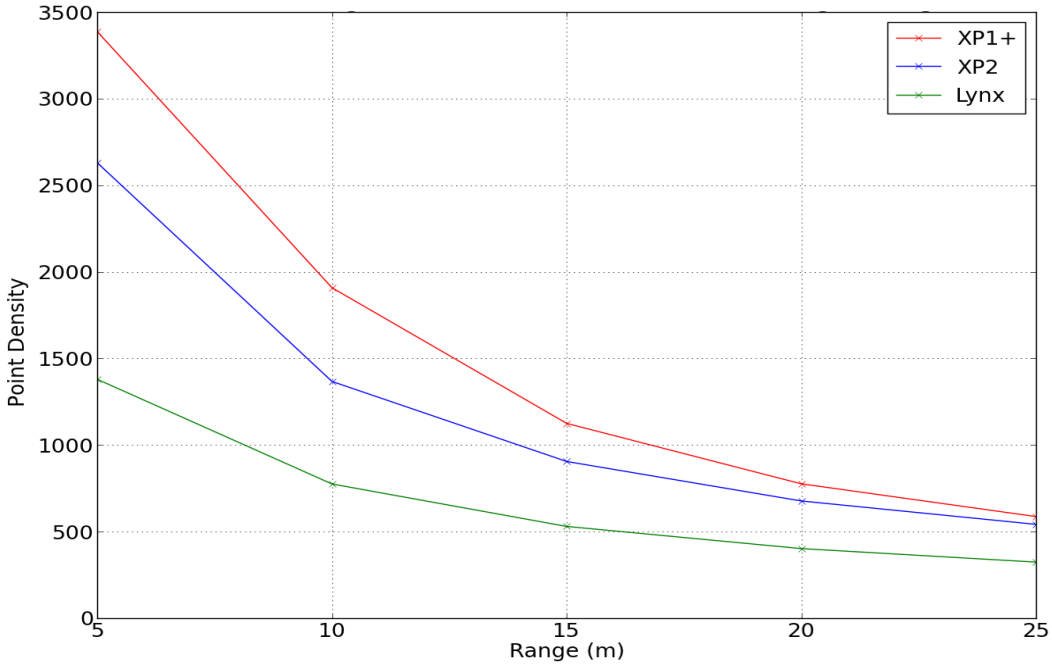

Figure 7.6: Calculated Point Density: Benchmarking Dual Scanner MMS Performance on a Parallel Vertical Target at Different Target Ranges. Vehicle Velocity is 50km/h and Target Dimensions are 2m x 1m

primary reason for the predominance of the Riegl scanner in these tests is its high PRR. Secondly, the SICK has outperformed the second Optech V200 scanner at short ranges, but it is also 1.389m closer to the target than the second Optech V200 due to the configuration on the XP1+. This influences the SICK's performance for all targets.

7.3.2 Small Targets

The tests in the previous section identified that the recommended scanner orientation positively influences the XP1+ in terms of maximising point density. However, the Optech Lynx has been designed to maximise point density 360 ^{o} around the vehicle, whereas the XP1+ has been designed to maximise it on near side infrastructure only. For this reason, the XP2 is a fairer comparison with the Optech Lynx. The XP2 achieves a higher point density with a single scanner on a large planar target than the Optech Lynx does with dual scanners. The main advantage of the Optech V200 is the 200Hz M_f which minimises profile spacing when compared to the 100Hz M_f on the Riegl VQ-250. To assess the benefit of a scanner with a higher mirror speed, the profile spacing and point spacing are tested at different vehicle velocities and target ranges for each MMS. These tests identify what size target could potentially be missed by a specific profile spacing or by a specific point spacing.

7.3.2.1 Profile Spacing

The horizontal and vertical profile spacing for each MMS are measured on a parallel vertical target of dimensions 2m x 1m. The target range is defined at

5m and the vehicle velocity is increased from 10km/h to 50km/h in 10km/h increments. Profile spacing is not influenced by target range and therefore a constant range to target of 5m is applied throughout these tests. The results of the horizontal profile spacing tests on a parallel vertical target are detailed in Table 7.9. Figure 7.7 plots the horizontal profile spacing exhibited by each MMS on a parallel target at varied vehicle velocities. The XP1+ incorporates two different scanners and therefore the profile spacing is different for each. For this reason, both scanners are plotted in this figure. Scanner 1 and Scanner 2 on the XP2 and Optech Lynx are identical. Profile spacing does not differ for these scanners on a parallel target and therefore only one scanner is plotted. These tests demonstrate the impact of the higher M_f on profile spacing as the Optech Lynx is capable of a smaller profile spacing than the other systems. At 10km/h the Riegl profile spacing of 0.027m is almost double the profile spacing of the Optech which is 0.014m. The profile spacing of the SICK LMS is not comparable with the Riegl or Optech scanners, for example at 10km/h the profile spacing of 0.037m for the SICK LMS is almost three times that of the Optech. The Optech profile spacing of 0.694m at 50km/h is similar to the 0.074m profile spacing of the SICK LMS at 20km/h.

The results of the vertical profile spacing tests on a parallel vertical target are detailed in Table 7.10 and Figure 7.8 illustrates these results. The improved vertical rotation of the scanners on the XP1+ outperforms the other systems in terms of vertical profile spacing, despite the low M_F of the SICK LMS. The vertical profile spacing of 0.011m for Scanner 1 on the XP1+ is almost double that of the Optech Lynx(0.019m), a reversal of the results in the horizontal profile spacing tests. The SICK LMS outperforms the Optech

Table 7.9: Calculating Horizontal Profile Spacing on Parallel Vertical Targets of Dimensions 2m x 1m for Three Dual Scanner MMSs at 5m Target Range and Varying Vehicle Velocities

MMS	Velocity	Scanner 1 (m)	Scanner 2 (m)
XP1+	10km/h	0.027m	0.037m
XP1+	20km/h	0.055m	0.074m
XP1+	30km/h	0.083m	0.110m
XP1+	40km/h	0.110m	0.148m
XP1+	50km/h	0.138m	0.185m
XP2	10km/h	0.027m	0.027m
XP2	20km/h	0.055m	0.055m
XP2	30km/h	0.083m	0.083m
XP2	40km/h	0.111m	0.111m
XP2	50km/h	0.138m	0.138m
Lynx	10km/h	0.014m	0.014m
Lynx	20km/h	0.028m	0.028m
Lynx	30km/h	0.042m	0.042m
Lynx	40km/h	0.055m	0.055m
Lynx	50km/h	0.070m	0.070m

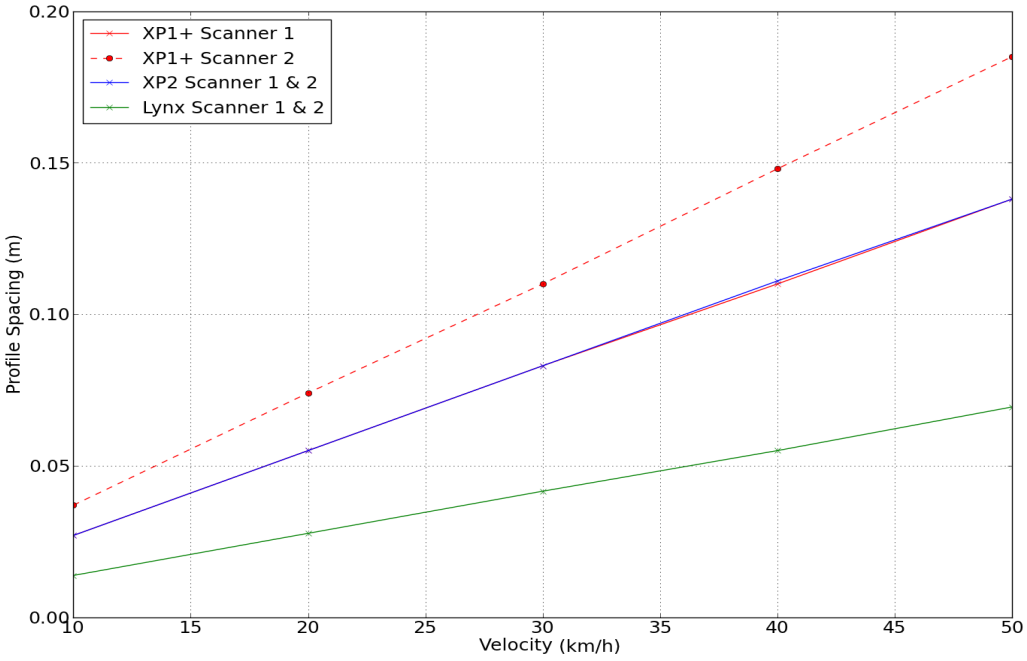

Figure 7.7: Calculated Horizontal Profile Spacing: Benchmarking Dual Scanner MMS Performance on a Parallel Vertical Target at Different Vehicle Velocities. Target Range is 5m and Target Dimensions are 2m x 1m

V200 scanner in terms of vertical profile spacing. The vertical profile spacing exhibited by the SICK LMS is 22% shorter than the Optech V200. This is due to the 60^o vertical scanner rotation on the XP1+ compared to 29.95^o vertical scanner rotation on the Optech Lynx. The XP2 and Lynx performed almost identically. In this case, the larger vertical and horizontal rotations of the VQ-250s offset the higher mirror speed of the Lynx.

Table 7.10: Calculating Vertical Profile Spacing on Parallel Vertical Targets of Dimensions 2m x 1m for Three Dual Scanner MMSs at 5m Target Range and Varying Vehicle Velocities

MMS	Velocity	Scanner 1	Scanner 2
XP1+	10km/h	0.011m	0.015m
XP1+	20km/h	0.022m	0.030m
XP1+	30km/h	0.034m	0.045m
XP1+	40km/h	0.045m	0.060m
XP1+	50km/h	0.056m	0.075m
XP2	10km/h	0.019m	0.019m
XP2	20km/h	0.039m	0.039m
XP2	30km/h	0.058m	0.058m
XP2	40km/h	0.078m	0.078m
XP2	50km/h	0.098m	0.098m
Lynx	10km/h	0.019m	0.019m
Lynx	20km/h	0.038m	0.038m
Lynx	30km/h	0.057m	0.057m
Lynx	40km/h	0.077m	0.077m
Lynx	50km/h	0.096m	0.096m

These tests highlight the effect of M_f on horizontal profile spacing. They demonstrate that for vertical profile spacing, certain scanner orientations can offset the disadvantage of a lower mirror speed by increasing profile angle, reducing vertical profile spacing and thereby increasing point density. A MMS benefiting from the recommended configuration identified in this

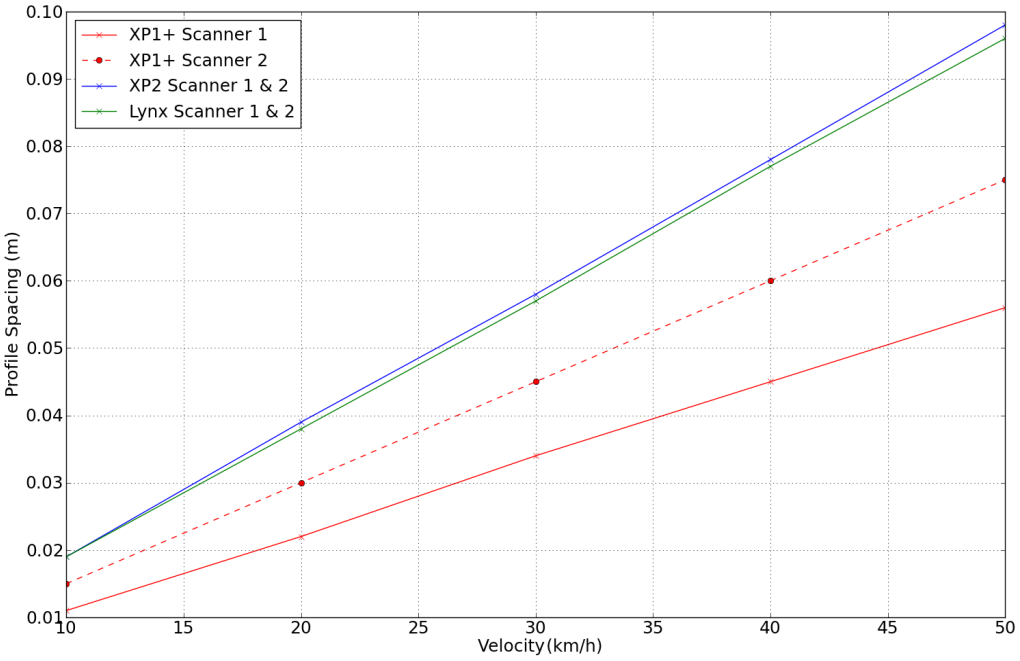

Figure 7.8: Calculated Vertical Profile Spacing: Benchmarking Dual Scanner MMS Performance on a Parallel Vertical Target at Different Vehicle Velocities. Target Range is 5m and Target Dimensions are 2m x 1m

thesis is then able to capture data on targets that may otherwise have been too small for that system at that vehicle velocity.

7.3.2.2 Point Spacing

The second important system output that must be considered for small targets is point spacing. If the point spacing is high, it is possible that there will be zero returns from a small target regardless of the horizontal and vertical profile spacing. To quantify this for the three MMSs under investigation in this chapter, point spacing is calculated for each scanner on a parallel vertical target at different target ranges. The target range is varied from 5m to 25m in 5m increments. Point spacing is not influenced by vehicle velocity and therefore a constant velocity of 50km/h is applied throughout these tests.

Table 7.11 lists the results of these tests for each MMS and Figure 7.9 plots the results of these tests for point spacing and target range. In each test, the Riegl scanner has the lowest point spacing due to it's high PRR. At all target ranges, the point spacing of the Riegl is over twice as small (43%) as the point spacing of the Optech scanner. The SICK LMS results in a higher point spacing in these tests because of it's low PRR. At a range of 25m, the SICK LMS is exhibiting a point spacing that is over four times (419%) the point spacing of Scanner 2 on the XP2. These results reinforce the significance in selecting the correct scanner configuration for increasing point density. Due to the XP1+'s application of the recommended scanner configuration identified in the previous chapter, the SICK LMS produced comparable point density with Optech and Riegl scanners in the earlier tests on larger targets. However, these results demonstrate that the SICK LMS

is not suitable for surveying narrow targets at long ranges. For instance, for a target like a circular road sign of radius 0.5m at 10m horizontal range the SICK's point spacing of 0.25m would return an insufficient number of points to distinguish that object in the point cloud. For this target, it could result in two and possibly only one point hitting the target per scan profile. In this scenario, the Optech scanner would perform better with approximately five to six points on each scan profile whereas the Riegl scanners would perform best with over ten points per scan profile.

Table 7.11: Calculating Point Spacing on Parallel Vertical Targets of Dimensions 2m x 1m for Three Dual Scanner MMSs at 50km/h and Varying Target Ranges

MMS	Range	Scanner 1	Scanner 2
XP1+	5m	0.019m	0.080m
XP1+	10m	0.039m	0.161m
XP1+	15m	0.050m	0.242m
XP1+	20m	0.078m	0.323m
XP1+	25m	0.097m	0.403m
XP2	5m	0.018m	0.023m
XP2	10m	0.036m	0.041m
XP2	15m	0.054m	0.060m
XP2	20m	0.072m	0.078m
XP2	25m	0.091m	0.096m
Lynx	5m	0.042m	0.054m
Lynx	10m	0.085m	0.097m
Lynx	15m	0.127m	0.139m
Lynx	20m	0.169m	0.182m
Lynx	25m	0.211m	0.224m

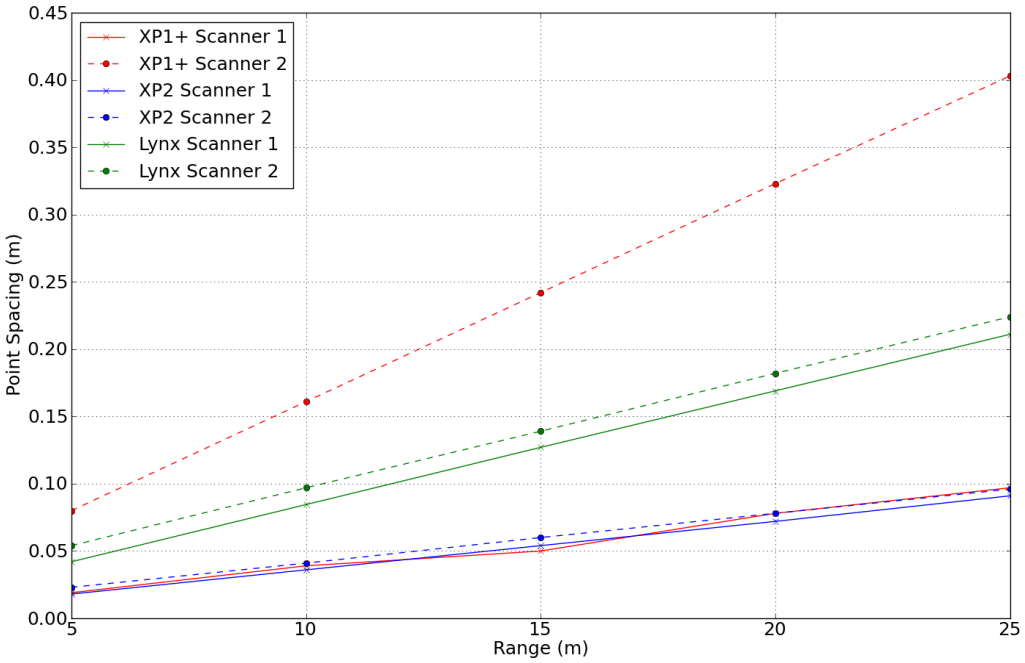

Figure 7.9: Calculated Point Spacing: Benchmarking Dual Scanner MMS Performance on a Parallel Vertical Target at Different Target Ranges. Vehicle Velocity is 50km/h and Target Dimensions are 2m x 1m

7.4 Multi-Faced Targets

The preceding tests have all dealt with parallel, planar targets. However, the majority of roadside infrastructure are angled targets or have multiple faces. In this section a number of benchmarking tests are conducted to examine the performance of each MMS configuration for multi-faced targets. In this section MIMIC calculates point density on the angled surfaces of two multi-faced structures. The first structure is represented by three large vertical planes and the second structure, a cylinder, is represented by three narrow vertical planes.

7.4.1 Structures

The first structure that is used in these tests is composed of three planar faces, one facing the road and two angled away from the road. Figure 7.10 illustrates the 3D structure from a front and top-down view. The top down view in Figure 7.10(b) displays the angular rotation for each face of the target. A 125^o rotation corresponds to a 55^o rotation towards and away from the target for the two faces respectively. This target rotation is chosen to ensure the scan plane resulting from the horizontal scanner rotation of Scanner 1 on each of the MMSs does not intersect with the third plane of the target, and therefore the coverage of Face (iii) depends on Scanner 2 only. Similarly, Face (i) is not visible to Scanner 2. Face (ii) is the only face that will exhibit an overlap from both Scanner 1 and Scanner 2. Each of the faces is a 2m x 2m square target and Table 7.12 lists the parameters of each face, including the increased range to the centre of the Face (i) and Face (iii) along with their orientation. The point density on each face is measured to benchmark the performance of each MMS on this structure for different vehicle velocities.

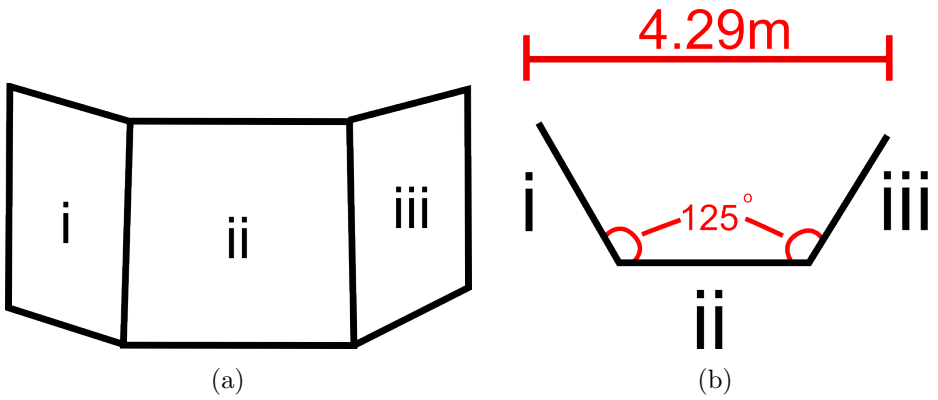

Figure 7.10: Target Representing a Structure (a) Front View (b) Top-Down View

Table 7.12: Multi-Faced Targets : 3D Structure Parameters

Face	H_r	α_{targ}
i	5.819m	55^o
ii	5.000m	0^o
iii	5.819m	-55^o

The point density for each face is measured at different vehicle velocities. The vehicle velocity is increased in 10km/h increments from 10km/h to 50km/h. The target range is not varied in these tests. This is because the effect of increased range on point spacing is more relevant for a narrow object. A high point spacing decreases the number of P_{pp} and therefore potentially results in an insufficient number of returns to define narrow targets in the point cloud. The target range is varied in the tests on cylindrical structures. Face (i) can only be surveyed by Scanner 1 on each of the MMS and therefore there is no return from Scanner 2. Due to the target rotation and position, the H_r is 5.819m. Table 7.13 lists the point density calculated for Face (i). The point density is illustrated in Figure 7.11 and plotted against

vehicle velocity. Due to their higher PRR, the Riegl scanners display the highest point density. Scanner 1 on the XP1+ is capable of 11% more points than the same scanner on the XP2 because of its application of the recommended configuration identified in the previous chapter. The Riegl scanners are both capable of over twice the number of points than the Optech scanner.

Table 7.13: Calculated Point Density: Benchmarking Dual Scanner MMS Performance on Face (i) of a Multi-Faced Structure at Different Vehicle Velocities. Target Range is 5.819m. Target Dimensions are 2m x 2m

MMS	Velocity	Scanner 1	Scanner 2
XP1+	10km/h	18353pts	0
XP1+	20km/h	9181pts	0
XP1+	30km/h	6121pts	0
XP1+	40km/h	4590pts	0
XP1+	50km/h	3672pts	0
XP2	10km/h	16415pts	0
XP2	20km/h	8207pts	0
XP2	30km/h	5471pts	0
XP2	40km/h	4103pts	0
XP2	50km/h	3283pts	0
Lynx	10km/h	8050pts	0
Lynx	20km/h	4025pts	0
Lynx	30km/h	2683pts	0
Lynx	40km/h	2012pts	0
Lynx	50km/h	1610pts	0

This process is repeated for Face (ii) of the multi-faced structure. The point density for the target is calculated at five different vehicle velocities. The vehicle velocity is increased in 10km/h increments from 10km/h to 50km/h. Table 7.14 lists the point density calculated for each MMS on Face (ii). Due to the target rotation and position, the H_r is now 5m. For each MMS, the point density is higher for this face of the target because it

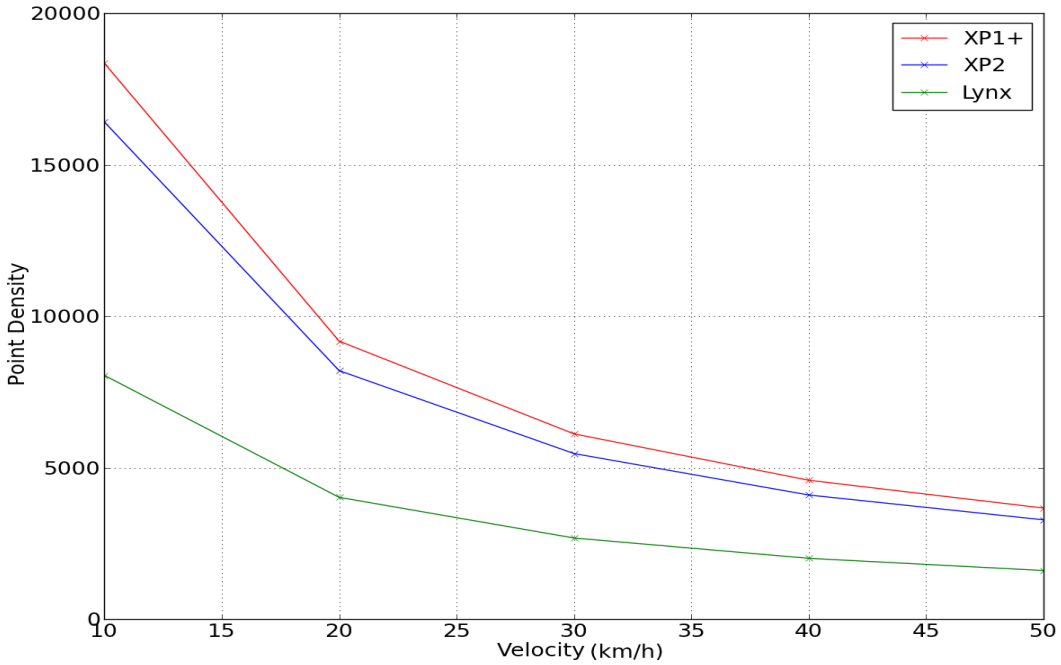

Figure 7.11: Calculated Point Density: Benchmarking Dual Scanner MMS Performance on Face (i) of a Multi-Faced Structure at Different Vehicle Velocities. Range to Target is 5.819m and Target Dimensions are 2m x 2m

is visible to both scanners and it also has a lower H_r. Figure 7.12 illustrates the point density for different vehicle velocities for each MMS. It demonstrates that the XP1+ has again outperformed the other two systems. For the XP1+, the point density on Face (ii) is approximately double the number on Face (i). The XP1+ is capable of returning 37% more points than the XP2 for Face (ii). This is due to implementation of the recommended scanner configuration for both scanners on the XP1+.

Table 7.14: Calculated Point Density: Benchmarking Dual Scanner MMS Performance on Face (ii) of a Multi-Faced Structure at Different Vehicle Velocities. Target Range is 5m. Target Dimensions are 2m x 2m

MMS	Velocity	Scanner 1	Scanner 2	Combined
XP1+	10km/h	31041pts	5597pts	36638pts
XP1+	20km/h	15520pts	2798pts	18318pts
XP1+	30km/h	10347pts	1865pts	12212pts
XP1+	40km/h	7760pts	1399pts	9159pts
XP1+	50km/h	6210pts	1119pts	7329pts
XP2	10km/h	19970pts	6661pts	26631pts
XP2	20km/h	9985pts	3330pts	13315pts
XP2	30km/h	6656pts	2220pts	8876pts
XP2	40km/h	4992pts	1665pts	6657pts
XP2	50km/h	3997pts	1333pts	5330pts
Lynx	10km/h	9404pts	4908pts	14312pts
Lynx	20km/h	4702pts	2453pts	7155pts
Lynx	30km/h	3134pts	1635pts	4769pts
Lynx	40km/h	2351pts	1226pts	3577pts
Lynx	50km/h	1881pts	981pts	2862pts

The H_r to Face (iii) is 5.819m. Face (iii) is only visible to Scanner 2 on each of the MMSs. The point density is measured for each MMS on Face (iii) at five different vehicle velocities ranging from 10km/h to 50km/h. Table 7.15 lists the point density for Face (iii). Figure 7.13 plots the point density in relation to vehicle velocity for each MMS. The point density on Face (iii)

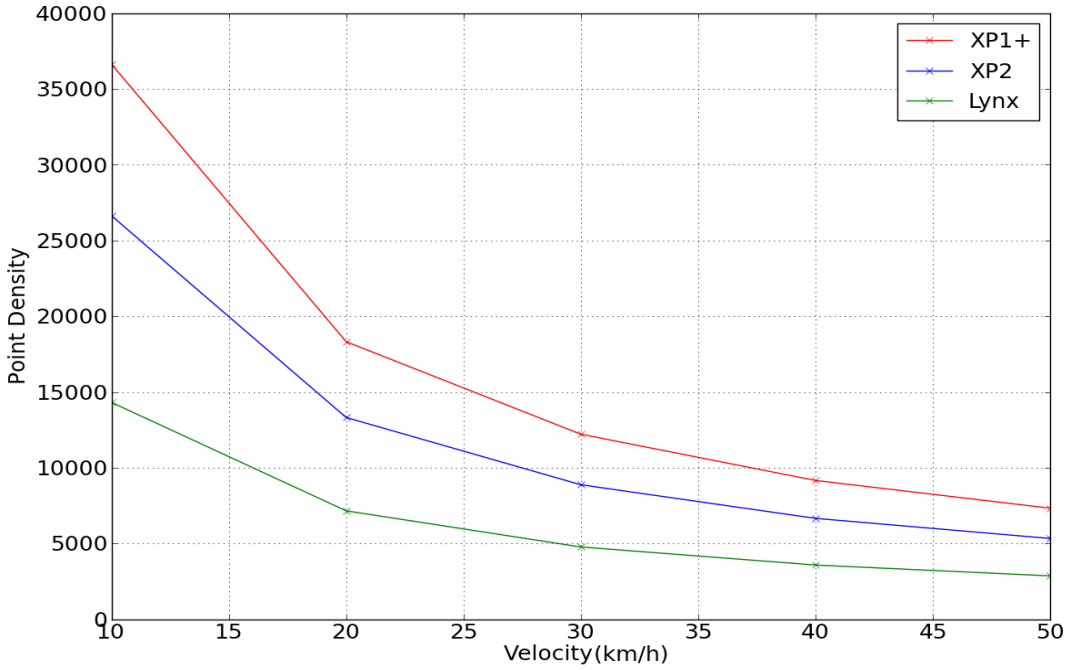

Figure 7.12: Calculated Point Density: Benchmarking Dual Scanner MMS Performance on Face (ii) of a Multi-Faced Structure at Different Vehicle Velocities. Range to Target is 5m and Target Dimensions are 2m x 2m

is lower than for the previous two faces. The low point density is due to the negative horizontal scanner rotation of Scanner 2 on the XP2 and the Optech Lynx and the scanner offset. In these tests, Scanner 2 on the XP2 exhibits a higher point density than Scanner 2 on the other systems because of the higher PRR. The Riegl VQ-250 returns over 3 times (327%) the point density of the SICK LMS. The Optech Scanner 2 also exhibits a higher point density than the SICK LMS on the XP1+, with the V200 returning almost 89% more points than the SICK LMS. Despite the decreased H_r arising from the recommended scanner position on the XP1+, the SICK has underperformed in these tests in relation to Scanner 2 on the Optech Lynx. This differs to the findings from the parallel vertical target tests. Table 7.16 lists the point density measurements for Scanner 2 on each MMS on both a parallel vertical target of dimensions 2m x 1m and Face (iii) of a multi-faced structure at 10km/h. Scanner 2 performance is comparable for the parallel target, but for Face (iii) of the multi-faced, the XP+ returns approximately 30% of the points when compared with the XP2 and approximately 52% of the points when compared with the Optech Lynx. This is due to the increased measurement range to Face (iii) (5.819m). The tests in the previous section identified that the point density of the SICK decreased in relation to the Optech at distances over 5m. Additionally, the recommended orientation of Scanner 2 on the XP1+ is not optimal for targets rotated by -55^o. This reinforces the link between target orientation and the recommended scanner orientation.

Table 7.15: Calculated Point Density: Benchmarking Dual Scanner MMS Performance on Face (iii) of a Multi-Faced Structure at Different Vehicle Velocities. Target Range is 5.819m. Target Dimensions are 2m x 2m

System	Velocity	Scanner 1	Scanner 2
XP1+	10km/h	0	3286pts
XP1+	20km/h	0	1643pts
XP1+	30km/h	0	1095pts
XP1+	40km/h	0	821pts
XP1+	50km/h	0	657pts
XP2	10km/h	0	10757pts
XP2	20km/h	0	5378pts
XP2	30km/h	0	3585pts
XP2	40km/h	0	2689pts
XP2	50km/h	0	2151pts
Lynx	10km/h	0	6232pts
Lynx	20km/h	0	3116pts
Lynx	30km/h	0	2077pts
Lynx	40km/h	0	1558pts
Lynx	50km/h	0	1246pts

Table 7.16: Calculated Point Density: Comparison of Scanner 2 Point Density for each MMS on Rotated and Parallel Targets

Target	Dimensions	XP1+	XP2	Optech Lynx
Face (iii)	2m x 2m	3286pts	10757pts	6232pts
Parallel Vertical	2m x 1m	2581pts	2949pts	2262pts

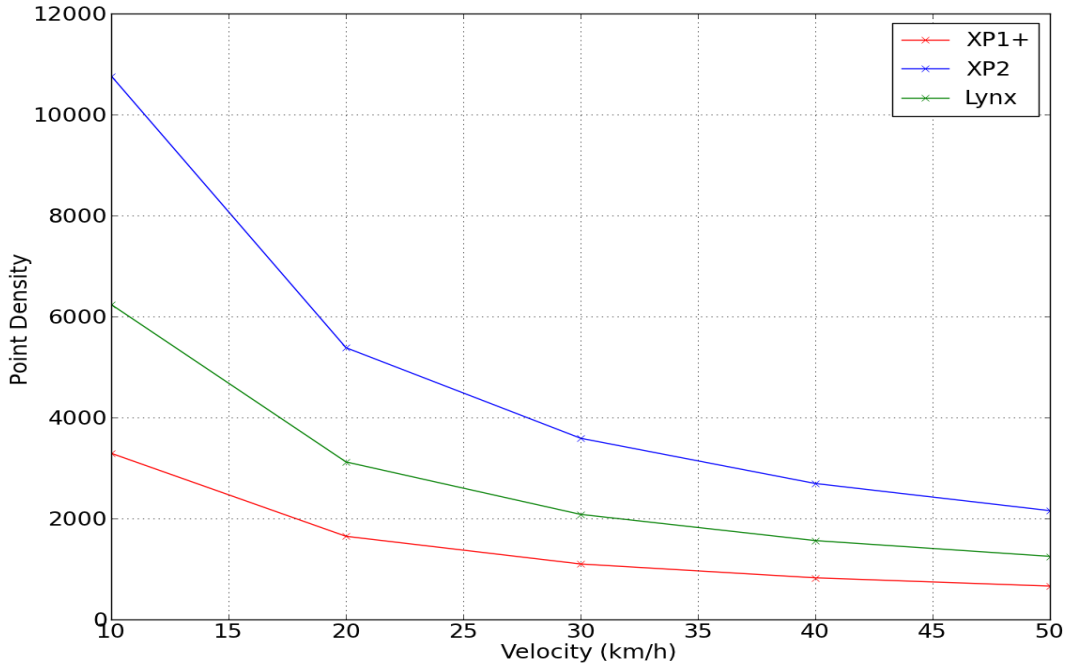

Figure 7.13: Calculated Point Density: Benchmarking Dual Scanner MMS Performance on Face (iii) of a Multi-Faced Structure at Different Vehicle Velocities. Range to Target is 5.819m and Target Dimensions are 2m x 2m

7.4.2 Cylinders

The second structure that is used in these tests is also composed of three planar faces, one facing the road and two angled away from the road. This is a hexagonal approximation of a cylindrical target. Figure 7.14 illustrates the cylinder that is used in the benchmarking tests. The proportions and shape of this hexagonal structure are identical to the multi-faced structure used in the previous tests. However, the target dimensions have changed. The cylinder is 0.214m in diameter, and each face of the cylinder is 0.1m wide and 2m high. The point density is calculated on each face of the cylinder for each MMS at different vehicle velocities. The velocity is increased in 10km/h increments from 10km/h to 50km/h. The point density is also calculated for each face at different target ranges. This is to assess the performance of each MMS when surveying narrow targets at increasing H_r. Similarly to the multi-faced structure in the previous tests, the scanners on-board the MMSs are incapable of surveying all faces of the target. Faces (i) and (ii) are visible to Scanner 1. Faces (ii) and (iii) are visible to Scanner 2. The scanners overlap and increase point density on Face (ii). Table 7.17 lists the parameters for the three planar faces of the cylinder involved in the calculation.

Table 7.17: 3D Cylinder - Target Parameters

Face	Range (m)	α_{targ}
i	5.04	55^o
ii	5	0^o
iii	5.04	-55^o

These results have been plotted against vehicle velocity in Figures 7.15 to 7.17 respectively. The point density measurements for each vehicle velocity

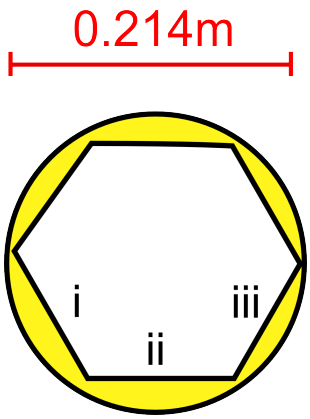

Figure 7.14: Planar Faces for the Cylindrical Target

on each target face for each MMS are detailed in Tables 30, 31 and 32 in Appendix .4. Figure 7.15 illustrates the point density from Scanner 1 for Face (i). The Riegl scanner outperforms the Optech in terms of point density. The Riegl VQ-250 on the XP2 returns 2.003 times the point density of the Optech V200. The Riegl scanner on the XP1+ and XP2 perform similarly, despite their different orientation. This is due to the rotation of the target. The rotation of the target alters the profile angle and this results in a closer match between the number of points from the Riegl Scanner 1 on the XP1+ and those from the Riegl Scanner 1 on the XP2. In Figure 7.16, the higher vertical scanner rotation has resulted in a higher point density for the Riegl scanners when compared to the Optech scanners. The Riegl VQ-250 on the XP1+ returns 1.55 times the point density when compared to the VQ-250 on the XP2. The difference is due to its application of the recommended configuration. Face (iii) is only visible to Scanner 2 on each of the MMSs. Figure 7.17 highlights how the narrow width of the target and the low ASW of the SICK LMS has resulted in very few points on the target on Face (iii) for that scanner. The high PRR VQ250 on the XP2 has performed best for narrow targets at short ranges over different vehicle velocities.

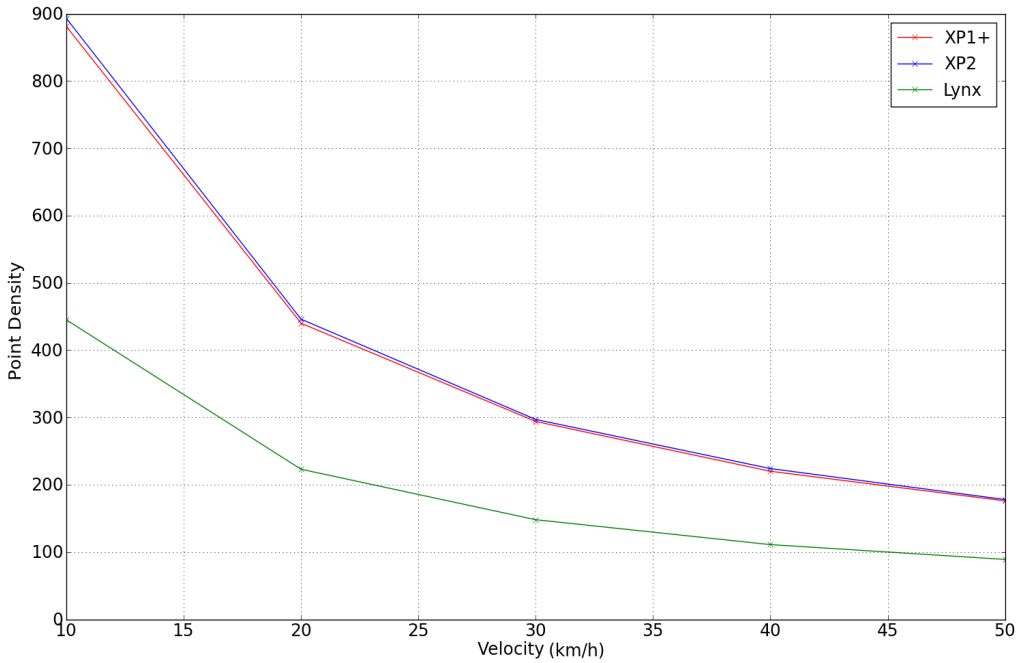

Figure 7.15: Calculated Point Density: Benchmarking Dual Scanner MMS Performance on Face (i) of a Narrow Structure at Different Vehicle Velocities. Range to Target is 5.04m and Target Dimensions are 0.1m x 2m

A high number of points striking the target does not necessarily define a target if these points result from a large number of profiles intersecting the target. A high number of profiles implies a lower P_{pp}. This effect is increased at different target ranges because the point spacing increases. Tables 33, 34 and 35 in Appendix .4 list the full set of point density calculations for different target ranges, however a representative subset of this table is included Table 7.18. The minimum number of points required to define a fixed radius curve is 3, as illustrated in Figure 7.18(a). Figure 7.18(b) illustrates a cylinder with the three required points marked on it. These three points are at the

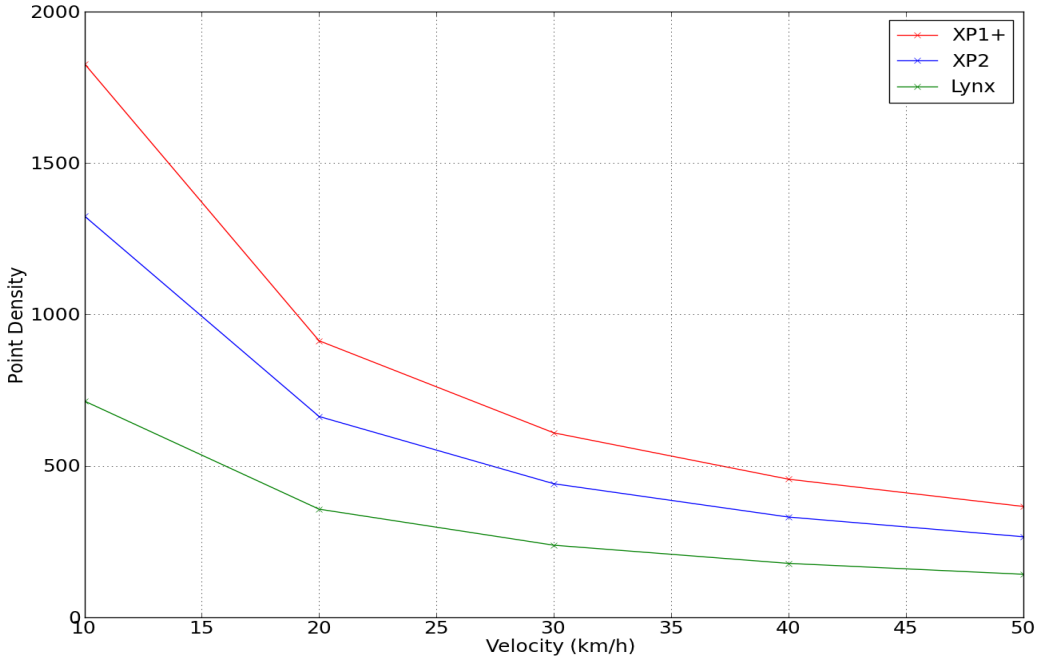

Figure 7.16: Calculated Point Density: Benchmarking Dual Scanner MMS Performance on Face (ii) of a Narrow Structure at Different Vehicle Velocities. Range to Target is 5m and Target Dimensions are 0.1m x 2m

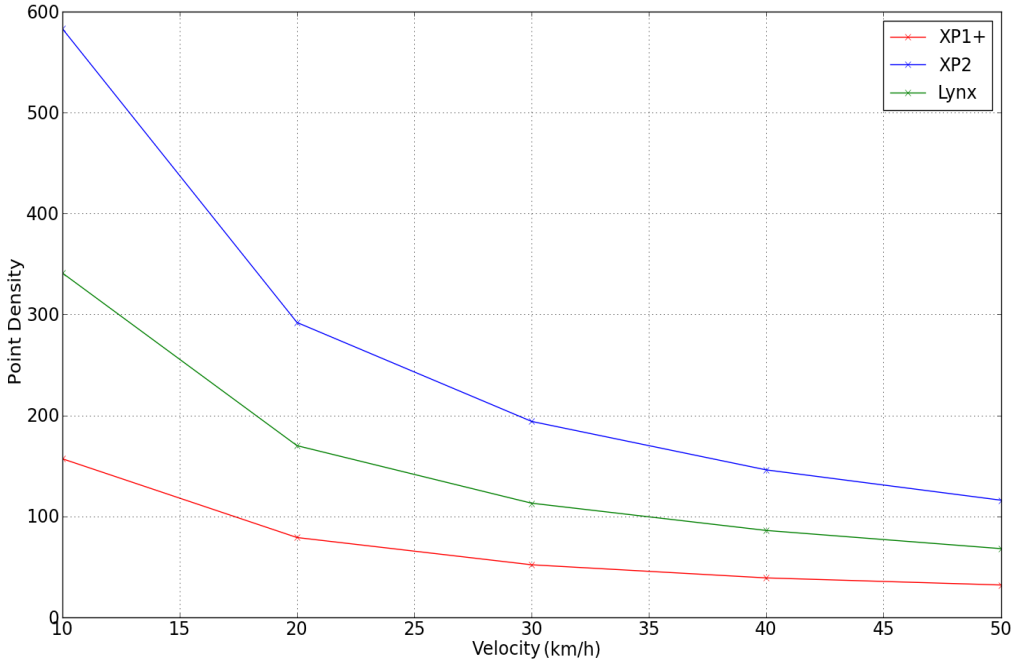

Figure 7.17: Calculated Point Density: Benchmarking Dual Scanner MMS Performance on Face (iii) of a Narrow Structure at Different Vehicle Velocities. Range to Target is 5.04m and Target Dimensions are 0.1m x 2m

same elevation on the target. Scanner orientations alter this scenario. Figure 7.18(c) illustrates a scan profile crossing one face of a cylindrical target with 3 P_{pp}. In this scenario the 3 P_{pp} are at different elevations. However, it is reasonable to assume that for a narrow target the 3 P_{pp} do not deviate significantly in elevation. For example, a profile angle of 45^o results in a height deviation between the first and third point of only 0.085m for a target face 0.1m wide. A change in radius of the cylinder is unlikely over that short distance. Therefore assuming that a minimum of 3 P_{pp} are required from angled scan profiles on cylindrical targets is justifiable. These tests demonstrate that for varying target parameters and system configurations, only a number of the scan profiles meet this criteria for a narrow cylinder. Table 7.18 lists each of the scan profiles that have 3 or more points and Figure 7.19 plots point density as a function of range for a narrow vertical target. This image also also highlights the 3 P_{pp} cut-off. In practice 3 P_{pp} would not be a sufficient number due to accuracy errors in the LiDAR data as the points may not represent the true curve. Additional measurements would be required. Certain configurations do not return any points at different ranges. These are represented in Figure 7.19 as a zero return.

These results highlighted a number of issues. Firstly, except for one instance with the XP2 on Face (i), none of the MMSs used in these benchmarking tests can return the required number of P_{pp} on a target at 15m horizontal range. The XP2 returned 3 P_{pp} on Face (ii) at 15m H_r. Performance in terms of P_{pp} drops significantly between 5m and 10m horizontal range for narrow vertical targets. The number of P_{pp} approximately halves as the range doubles. The XP2 returned the most points for each cylinder face in these tests,

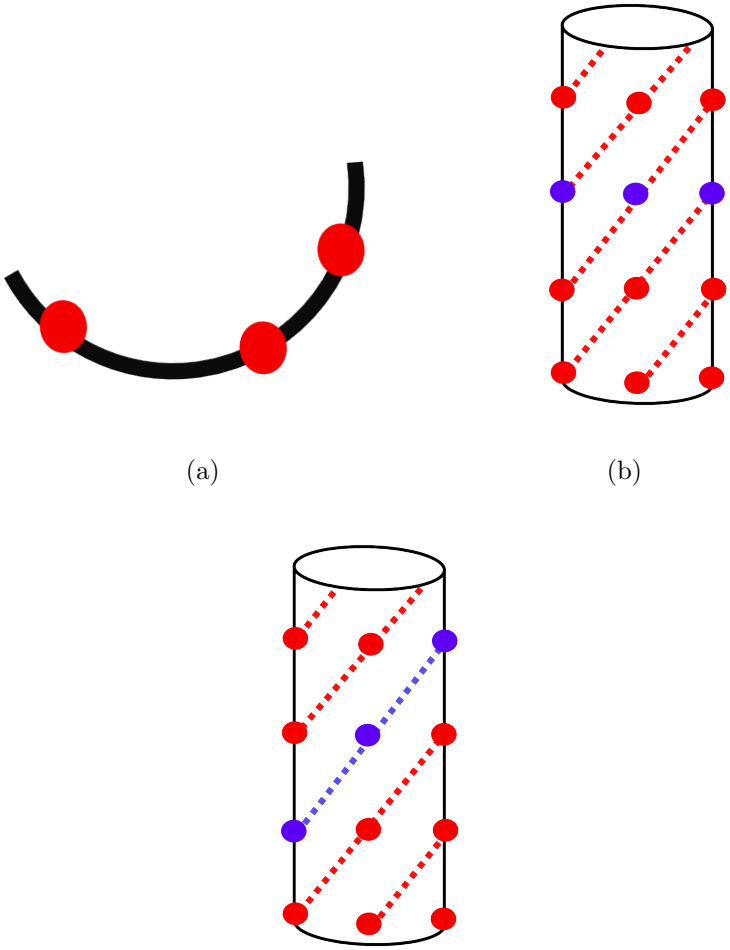

Figure 7.18: Quantifying the Number of P_{pp} Required. (a) Defining a Fixed Radius Curve using 3 Points (b) 3 Points at the Same Elevation (c) 3 points at Different Elevations

but only returns a maximum of 5 P_{pp} at 10m range. The Optech scanner returns a lower point density and lower P_{pp} on each surface. The Riegl scanner is capable of capturing more points than the Optech scanner. At the shortest measurement range, 5m, the Optech returns 4 P_{pp}, whereas the XP2 returns 8. 8 P_{pp} potentially provide a better definition of the object in the point cloud. The SICK LMS on the XP1+ fails this test. It is not able to return a minimum of three points on the scan profile for Face (iii). The SICK LMS is the only scanner on the XP1+ MMS able to survey that face and therefore XP1+ could potentially be unable to define the surface and this MMS is not suitable for narrow objects without employing multiple passes.

Table 7.18: Calculated Points per Profile: Benchmarking Dual Scanner MMS Performance on a Narrow Multi-Faced Structure at Different Target Ranges. Vehicle Velocity is 50km/h. Target Dimensions are 0.1m x 2m

MMS	Face	H_r (m)	P_{pp}
XP1+	i	5	5
XP1+	i	10	4
XP1+	ii	5	9
XP1+	ii	10	4
XP2	i	5	8
XP2	i	10	5
XP2	i	15	3
XP2	ii	5	10
XP2	ii	10	4
XP2	iii	5	5
XP2	iii	10	3
Lynx	i	5	4
Lynx	i	5	4
Lynx	iii	5	3

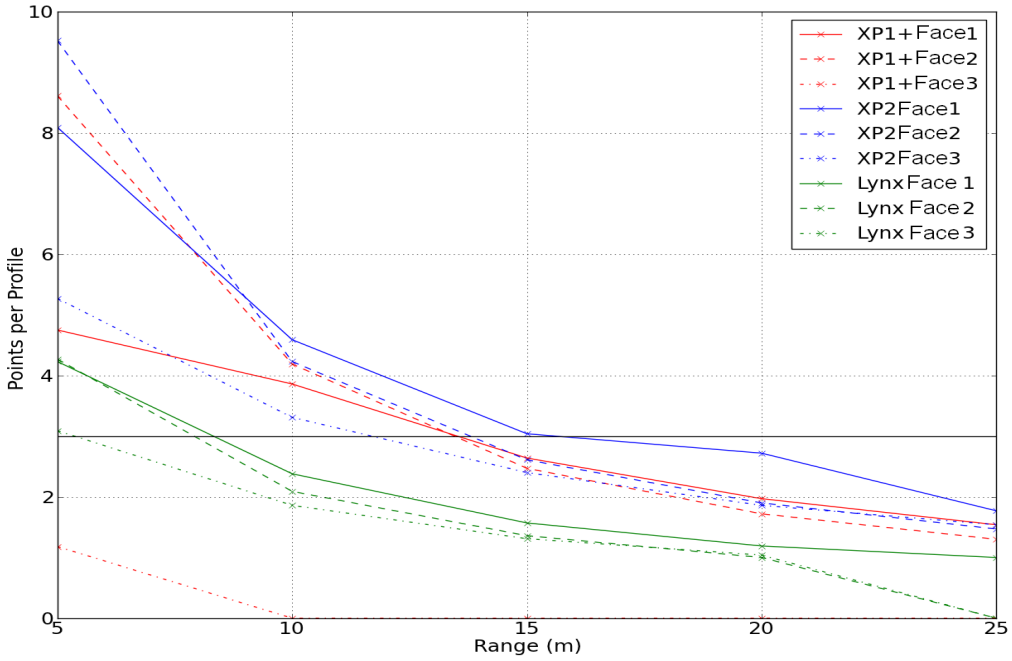

Figure 7.19: No. of Points Per Profile at Different Target Ranges

7.5 Conclusion

A point density benchmarking process was applied to three MMSs in this chapter. The point density on various targets was measured in MIMIC for one commercial and two theoretical MMSs. Each of these MMSs operated dual scanners. These MMSs displayed hardware and configuration differences and facilitated point density benchmarking in a number of key areas. 2D and 3D targets of different dimensions were defined for these tests.

A combination of large and small 2D vertical parallel targets were employed in the first stage of the benchmarking tests. The Riegl VQ-250 emerged as the scanner capable of the highest point density on the large targets. This was primarily due to it's high PRR. Through application of the recommended scanner configuration identified in the previous chapter, the VQ-250 on the XP1+ was capable of outperforming the same piece of hardware on the XP2. The recommended configuration also allowed the SICK LMS to outperform the Optech V200 for the large target. The Optech V200 outperformed the other two scanner types in terms of horizontal profile spacing due to its higher M_f. However, through application of the recommended configuration, this advantage was negated for the scanners on the XP1+. This highlights the importance of identifying the correct scanner orientation for a specific target. The Riegl VQ-250 was capable of the smallest point spacing, and this is an important factor in a MMS survey.

Two 3D, multi-faced structures were designed to assess MMS point density for this target type. The Riegl VQ-250 performed best in these tests for each face of the 3D structure. The second multi-faced structure was a

narrow vertical target, approximating a cylinder. A requirement of three P_{pp} was set as sufficient for defining a fixed radius curve. These tests identified that at ranges over 10m MMS performance is unreliable and only one MMS, the XP2, was capable of obtaining three P_{pp} at 15m range. The SICK LMS was wholly unsuitable for this target type, failing to return 3 P_{pp} on Face (iii) of the target. As this scanner is the only one on the XP1+ capable of surveying Face (iii), this implies that the XP1+ is not suitable for surveying narrow targets without multiple passes.

The Optech scanner has been outperformed by the Riegl scanner in these tests in terms of point density, however these results once again raise the issue of how many points are sufficient to define an object in a a point cloud manually or using an automated algorithm. This thesis will not answer this question. The required point density is dependant on the use of the data, or the automated algorithm being applied for feature extraction. MIMIC can only calculate the resultant point density.

The final chapter of this thesis will summarise the work completed, introduce work in progress, identify potential future work and answer the research questions posed in this thesis. It concludes with some final remarks.

Chapter 8

Conclusions and Additional Work

The main goal of this thesis is to investigate MMS point density. Achieving this goal first required a method to calculate point density to be designed. This method, MIMIC, facilitated assessment of MMS configuration and hardware and also a series of tests benchmarking MMSs. The core contributions of this thesis included: a wide ranging study on the factors influencing point density, development of a system to calculate point density, identification of the importance of a vertical scanner rotation for increasing point density, a definition of the recommended MMS configuration when surveying near side infrastructure and identification that a high PRR is preferable to a high mirror frequency for the majority of targets.

This chapter discusses the main conclusions of the research presented in this thesis, summarises the results from this doctoral research in Section 8.1 and presents the chief novel contributions to the area of MMS performance.

The main contributions to the area of MMS performance are outlined in Section 8.2. An introduction to the work in progress is provided in Section 8.3. Potential improvements to MIMIC's algorithm are detailed in Section 8.4. This chapter concludes with some final remarks on the work in this thesis in Section 8.5.

8.1 Thesis Summary

This thesis investigated the area of MMS performance and this investigation incorporated four distinct stages. These stages included an introduction to the topic, literature review and investigation of the factors influencing point density, the point density calculations, MMS configuration assessment and MMS benchmarking.

In stage one, the requirement for improving understanding of the performance of MMSs was identified. The area of MMS performance was investigated in Chapters 1 and 2 and was divided into three sub-topics. These sub-topics were: absolute and relative accuracy, repeat survey accuracy and point density. Contemporary research in this field was identified and reviewed. A review of contemporary research in the field of MMS performance illustrated that research in this area was limited. Understanding the relationships between laser scanners, the survey vehicle and the survey environment is crucial to ensuring a more effective outcome from a MMS survey. It was the lack of understanding of these relationships that provided the motivation for this thesis. Point density was introduced as the focus of this thesis and discussed in Chapters 2 and 3.

The methodology designed to complete this objective involved designing algorithms capable of calculating point density for MMS surveys and stage two detailed and validated the methodology employed to complete this Objective. These point density calculation algorithms were combined into a system named MIMIC, and detailed in Chapter 3. MIMIC outputs three values: the profile angle, the profile spacing and the point spacing. The profile angle, profile spacing and point spacing calculations were validated in Chapter 4. Point density was calculated through the combination of these three outputs and this process was validated in Chapter 5.

The methodology designed to complete the second objective involved developing a set of tests capable of assessing the configuration of a MMS in terms of laser scanner orientation, position and hardware settings. The application of these tests and the analysis of the results constituted the third stage of this thesis and was detailed in Chapter 6.

The fourth stage of this thesis was the implementation of a series of tests designed to complete the third and final objective. The objective was to benchmark the performance of three MMSs in terms of their point density. In these benchmarking tests, the impact of multiple system configurations on the point density of a selection of targets was examined. Chapter 7 detailed the benchmarking tests.

8.2 Main Contributions to the Field of MMS Performance

The work carried out to complete the three objectives of this thesis contribute to the field of MMS performance. In the following sections, the methodology designed to complete each objective is briefly assessed in terms of it's contribution to the body of knowledge in the field of MMS performance.

8.2.1 Calculating Point Density

Although each of the existing methods for calculating profile information, point spacing and point density had their strengths, Chapter 2 identified shortcomings in each of these existing methods. In this chapter, three factors were identified as impacting on point density, these were: the scanner parameters, the vehicle parameters and the target parameters. Existing studies employed manual measurements, geometric formulae and LiDAR simulations to assess the point density of a target although these methods were only capable of providing limited information. None of these methods provided specific values for profile angle, profile spacing or point spacing and none investigated their contribution to the point density calculation. The manual measurements were a labour intensive process and do not provide a method for calculating point density. The LiDAR simulations required additional manual measurements after rendering to identify profile information, point spacing and point density and do not provide a method for calculating point density. The limited geometric formulae employed to-date did not incorporate scanner parameters, such as scanner elevation, position or orientation. Target parameters such as dimension and orientation were also excluded.

These parameters influence the uniformity of the point spacing and therefore the point density.

The system for calculating point density designed in this thesis, MIMIC, addressed the shortcomings of each of the existing methods by incorporating additional parameters for all three identified factors. Horizontal and vertical scanner rotations were included. Target rotations were applied and the target dimensions were altered. Point spacing was calculated at multiple locations across a target rather than at a single central location. Multiple point spacing measurements on the target are important when calculating point density for angled surfaces or large targets. Target dimensions can be varied and narrow targets and planar approximations of 3D features like cylinders are acceptable inputs. A series of tests have validated MIMIC's ability to calculate profile angle, profile spacing, point spacing and ultimately point density. Potential error sources have been identified as vehicle dynamics and incorrect system calibration. MIMIC has been validated as an accurate and efficient method for calculating point density for generic MMSs.

8.2.2 Assessing MMS Configuration

The number, position and orientation of the scanner(s) on a MMS influence point density. Scanner hardware settings such as the field of view, pulse repetition rate and mirror frequency also influence point density. Only one existing study focussed on assessing system configuration and it employed a simulator to project laser pulses from a MMS onto surrounding structures. However, different scanner hardware were not investigated. The effect of

system configurations on specific targets were also not investigated. The system for calculating point density designed in this thesis facilitated these tests enabling MMS configuration to be assessed for multiple target types. The effect of different hardware settings on point density was quantified. The importance of vertical rotations of the scanner for large targets was identified and the importance of a high PRR for narrow targets at different ranges was also investigated.

These tests identified the recommended scanner location and scanner orientation when surveying near side infrastructure. The importance of a vertical rotation of the scanner when attempting to increase point density was identified and investigated. By utilising the Y axis of the vehicle for the second scanner position the scanner offset was eliminated while simultaneously minimising data shadows. This contradicts current thinking in that both scanners are generally placed at the rear of the vehicle. MIMIC can be used to provide definitive information on a specific target type and a MMS can be configured accordingly to maximise point density. The recommended configuration varies depending on the target type, but the tests in this section provide a useful guideline for generic targets.

8.2.3 Benchmarking MMS

The final topic of this thesis was the benchmarking of MMSs in terms of their point density. Existing studies have been limited to tables listing MMS hardware components. Benchmarking has been applied to MMSs in terms of their planimetric and elevation accuracy but not in terms of their point density. MIMIC facilitated benchmarking of the system configuration and

hardware settings of one commercial and two hypothetical MMSs in terms of point density. The two hypothetical MMSs were designed from the guidelines of the system configuration tests. Through the calculation of point density on a set of targets, these theoretical MMSs were compared to a commercial MMS. The application of the recommended configuration identified in the previous objective resulted in an increase in performance of the low specification scanner when compared to higher specification scanners. Lower specification scanners were demonstrated not to be suitable for longer ranges. An additional finding in these tests is that a higher PRR was more important when surveying for small or narrow objects, particularly at long ranges.

8.3 Current Work

This section details work that is ongoing on MIMIC. The next version of MIMIC will incorporate a visualisation component and will accept circular and irregular shapes as valid target types.

8.3.1 Visualisation Module

The visualisation module will enable the presentation of the information on profile angle, profile spacing, point spacing and point density to the user in a clear and easily understandable format depending on their requirements. Using a form of interpolation known as Inverse Distance Weighting (IDW) [Shepard, 1968], point spacing can be displayed. An example of this is illustrated in Figure 8.1 where point spacing has been calculated for a target 5m wide x 4m high on a planar surface for a single scanner system. The target

range was 5m and the target was rotated 30^o in the horizontal plane. An 8x8 grid structure has been applied. Each grid cell represents a planar surface 0.625m wide x 0.5m high. This method effectively visualises the point spacing on the target and demonstrates the non-uniform distribution of point spacing on the target. Additional work is required to expand the IDW from the grid cells out to the extremities of the target. Visualisation methds for point density and profiles are required. These visualisation methods also require validation.

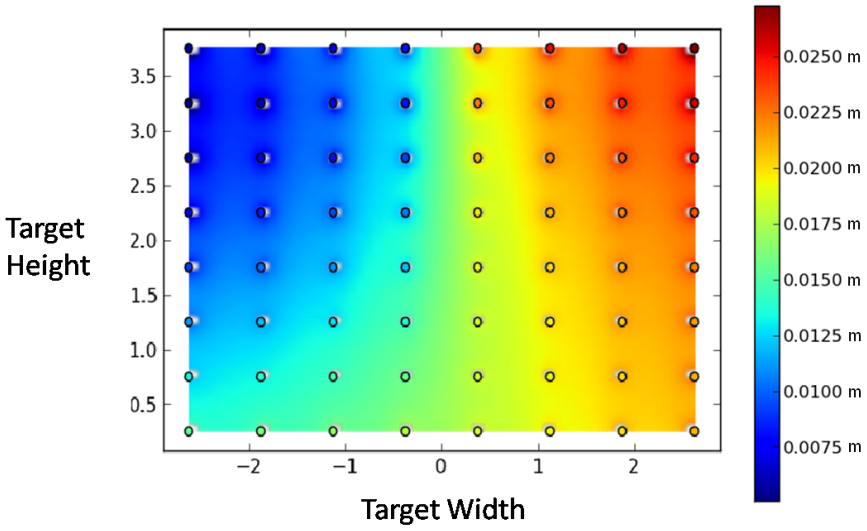

Figure 8.1: IDW Displaying Point Spacing on an Angled Target. Dimensions 5m x 4m and Range 5m

8.3.2 Circular Targets

To calculate point density for circular targets such as circular road signs the next version of MIMIC will develop the point density calculation. When calculating the path of each profile line through the grid structure, MIMIC will assign limits to the line segment calculations for each grid cell. These

limits are the points of intersection of the circle and the line as illustrated in Figure 8.2.

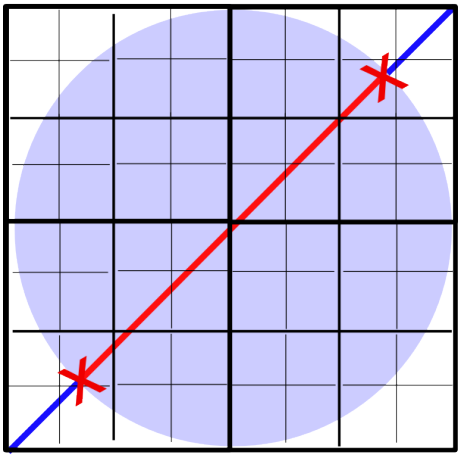

Figure 8.2: Intersections of Scan Profile and Circular Target

By substituting the equation of the circle where x1, y1 are the center points of the target and r is the radius

$$\text{Circle} = (x - x1)^2 + (y - y1)^2 = r^2, \tag{8.1}$$

into the equation of the line

$$\text{Line} = y - y1 = m(x - x1), \tag{8.2}$$

and then by finding the determinant using

$$\text{Determinant} = \frac{-b \pm \sqrt{(b^2 - 4ac)}}{2a}, \tag{8.3}$$

these points of intersection will be calculated. These points will then be specified by MIMIC as the start and end points of the scan profile and will

be calculated for each scan profile. No line segments outside of these points will be included in the point density calculation. This will enable calculation of point density for circular targets. Additional work is required to code this algorithm and to validate the point density calculations for this target type robustly.

8.3.3 Irregular Shapes

Not all roadside infrastructure conforms to a regular shape like rectangles or circles. A method is required to enable MIMIC to calculate point density for irregular shapes. One potential method for irregular shapes is the ray casting principle. Ray casting operates by counting the number of boundaries that a line crosses. In the case of MIMIC, each scan profile is a ray, set at a specific profile angle and separated by the profile spacing. The theory behind ray casting is that any ray that is cast from the inside of a polygon will cross an uneven number of boundaries, whereas any ray cast from the outside of a polygon will cross an even number of boundaries. Figure 8.3(a) illustrates this for a circular target. The ray originating from the centre of the circular target only crosses one boundary (an uneven number) whereas the ray originating outside the circular target crosses two boundaries (an even number). This is also valid for more complex targets like the one illustrated in Figure 8.3(b). The ray originating from inside the polygon crosses three boundaries whereas the ray originating outside crosses four boundaries. For MIMIC to apply this principle would require the inside/outside polygon check to be carried out for each line segment start and end point and would result in a significant increase in processing. Additional work is required to code this algorithm and to validate the point density calculations for this target type robustly

and to assess the efficiency of the algorithm.

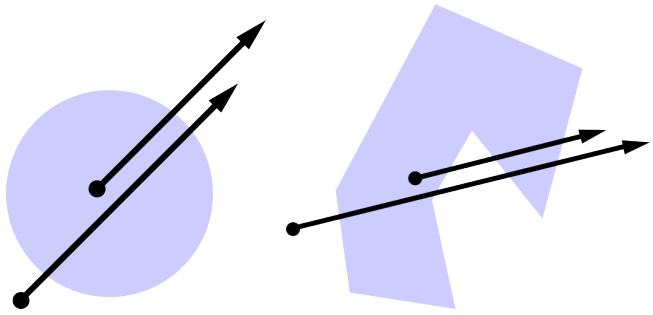

Figure 8.3: Ray Casting (a) Simple Target - Circle (b) Complex Target

8.4 Algorithm Improvements

In the course of this research, five avenues where MIMIC can be improved have been identified.

- Vehicle Dynamics 1. The first of these is the inclusion of vehicle roll and pitch as inputs to MIMIC. Roll and pitch can alter the profile angle and profile spacing on a target which influences point density. Their inclusion would enable MIMIC to calculate point density for roads with a gradient or cross-fall.

- Vehicle Dynamics 2. The second potential improvement would be to incorporate yaw in MIMIC. This would allow for point density to be calculated on infrastructure along curved sections of road.

- The third improvement would be the automated generation of valid system configurations for specific targets. The reverse of this could also be applied. Given a system configuration, MIMIC would automatically

identify what targets can not be surveyed by it. This would also aid researchers developing automated algorithms as the point density and distribution on targets can be clearly defined and quantified.

- MIMIC requires the user to manually identify the individual faces of a multi-faced structure. Future versions of MIMIC would accept these structures as valid target types and would automatically deconstruct these 3D objects into 2D planar targets and calculate the point density.

- Finally, point density calculations in MIMIC have been limited to near side infrastructure. The next version of MIMIC will include targets on both sides of the vehicle. This will enable further testing of dual scanner systems.

8.5 Final Remarks

MIMIC's capabilities for calculating point density have been experimentally validated. Although vehicle dynamics impact on the accuracy of the calculation, MIMIC is not a tool capable of predicting point density in every scenario at every stage in a survey. It is designed to be a tool to assist with system design, system configuration and automated algorithm design. MIMIC enables a user to identify the capabilities of their current MMS configuration, or to identify the recommended configuration for a specific target type.

The system configuration and benchmarking tests recommended large vertical rotations of the scanner. However, these tests compared a theoretical MMS configuration that was specifically configured for near side infrastructure with the Optech Lynx, a MMS that was designed for both near side

and far side infrastructure. It is the authors opinion that the Optech Lynx is the more practical for real world surveys. However, the increase in point density that arises from vertical rotations of the scanner demonstrate that improvements can be made to the current commercial MMS. Also, following on the trend of adjustable survey mounts as explained in Section 2.3.4, these findings will be of use for specific survey scenarios. MIMIC can then be applied to identify the recommended configurations and the MMS can be dynamically configured at the start of the survey.

Appendices

.1 Chapter 4 - Calculating Profile Information and Point Spacing

Table 1: Road Surface Profile Angle Tests - XP1 and Optech Lynx Data. Part 1

Test	α_{scan}	γ_{scan}	$\theta_{P_r\text{A}}1$	$\theta_{P_r\text{A}}2$	$\theta_{P_r\text{A}}3$	$\theta_{P_r\text{A}}4$	$\theta_{P_r\text{A}}5$
1	37.48^o	29.6^o	37.6^o	37.43^o	36.993^o	37.86^o	37.12^o
2	37.48^o	29.6^o	37.77^o	37.36^o	37.42^o	37.47^o	37.24^o
3	37.48^o	29.6^o	37.69^o	37.69^o	37.65^o	37.46^o	37.22^o
4	45^o	45^o	44.88^o	44.45^o	44.48^o	45.78^o	44.9^o
5	45^o	45^o	44.59^o	45.11^o	45.23^o	45.02^o	44.7^o
6	45^o	45^o	44.86^o	44.79^o	45.14^o	45.14^o	45.11^o

Table 2: Road Surface Profile Angle Tests - XP1 and Optech Lynx Data. Part 2

Test	Average $\theta_{P_r\text{A}}$	MIMIC	Roll	Pitch	Yaw	Error
1	37.401^o	37.48^o	-0.4194^o	-0.3436^o	0.003^o	0.0794^o
2	37.452^o	37.48^o	-0.4573^o	-0.3426^o	0.001^o	0.028^o
3	37.542^o	37.48^o	-0.4191^o	$-0.3337\ ^o$	0.004^o	0.062^o
4	44.898^o	45^o	-2.6641^o	1.2214^o	0.0315^o	0.102^o
5	44.93^o	45^o	-2.5781^o	1.0149^o	0.0015^o	0.07^o
6	45.008^o	45^o	-2.5747^o	1.1013^o	0.0415^o	0.008^o

Table 3: Profile Angle CAD Tests on an Angled Plane - Horizontal Target Rotation

α_{scan}	γ_{scan}	α_{targ}	$\theta_{P_r\text{A}}$	MIMIC
45^o	45^o	0^o	35.272^o	35.264^o
45^o	45^o	15^o	40.840^o	40.893^o
45^o	45^o	30^o	43.858^o	44.007^o
45^o	45^o	45^o	45.000^o	45.000^o
45^o	45^o	60^o	44.092^o	44.007^o
45^o	30^o	0^o	50.784^o	50.769^o
45^o	30^o	15^o	56.235^o	56.310^o
45^o	30^o	30^o	59.108^o	59.133^o
45^o	30^o	45^o	60.000^o	60.000^o
45^o	30^o	60^o	59.050^o	59.133^o
30^o	30^o	0^o	56.243^o	56.310^o
30^o	30^o	15^o	59.172^o	59.133^o
30^o	30^o	30^o	60.000^o	60.000^o
30^o	30^o	45^o	59.097^o	59.133^o
30^o	30^o	60^o	56.052^o	56.310^o
30^o	15^o	0^o	72.811^o	72.808^o
30^o	15^o	15^o	74.412^o	74.496^o
30^o	15^o	30^o	75.000^o	75.000^o
30^o	15^o	45^o	74.438^o	74.496^o
30^o	15^o	60^o	72.720^o	72.808^o
15^o	15^o	0^o	74.461^o	74.496^o
15^o	15^o	15^o	75.000^o	75.000^o
15^o	15^o	30^o	74.379^o	74.496^o
15^o	15^o	45^o	72.641^o	72.808^o
15^o	15^o	60^o	68.900^o	69.246^o

Table 4: Profile Angle CAD Tests on an Angled Plane - Vertical Target Rotation

α_{scan}	γ_{scan}	β_{targ}	$\theta_{P_r\text{A}}$	MIMIC
45^o	45^o	0^o	35.272^o	35.260^o
45^o	45^o	15^o	31.270^o	31.610^o
45^o	45^o	30^o	29.992^o	30.105^o
45^o	45^o	45^o	30.850^o	30.361^o
45^o	45^o	60^o	32.718^o	32.443^o
45^o	30^o	0^o	50.784^o	50.768^o
45^o	30^o	15^o	43.650^o	43.671^o
45^o	30^o	30^o	39.650^o	39.639^o
45^o	30^o	45^o	37.866^o	37.902^o
45^o	30^o	60^o	38.080^o	38.123^o
30^o	30^o	0^o	56.243^o	56.310^o
30^o	30^o	15^o	51.580^o	51.572^o
30^o	30^o	30^o	49.040^o	49.107^o
30^o	30^o	45^o	49.020^o	48.663^o
30^o	30^o	60^o	50.500^o	50.194^o
30^o	15^o	0^o	72.810^o	72.808^o
30^o	15^o	15^o	65.680^o	65.854^o
30^o	15^o	30^o	60.830^o	60.899^o
30^o	15^o	45^o	57.820^o	57.911^o
30^o	15^o	60^o	56.910^o	56.787^o
15^o	15^o	0^o	74.460^o	74.496^o
15^o	15^o	15^o	71.200^o	71.361^o
15^o	15^o	30^o	69.480^o	69.484^o
15^o	15^o	45^o	68.850^o	68.912^o
15^o	15^o	60^o	69.670^o	69.658^o

Table 5: Profile Angle - MIMIC's Calculations Compared to Point Cloud Measurements for Angled Surfaces - XP1. Part 1

Test	α_{targ}	β_{targ}	$\theta_{Pr\text{A}}1$	$\theta_{Pr\text{A}}2$	$\theta_{Pr\text{A}}3$	$\theta_{Pr\text{A}}4$	$\theta_{Pr\text{A}}5$	$\theta_{Pr\text{A}}6$	$\theta_{Pr\text{A}}7$	$\theta_{Pr\text{A}}8$	$\theta_{Pr\text{A}}9$	$\theta_{Pr\text{A}}10$
1	32.67^o	4.54^o	38.16^o	37.7^o	37.99^o	38.03^o	37.82^o	38.13^o	37.73^o	38.22^o	38.1^o7	38.2^o
2	54.61^o	3.51^o	39.66^o	39.04^o	39.03^o	39.37^o	39.07^o	39.72^o	39.65^o	39.78^o	40.4^o	39.25^o
3	2.63^o	-0.29^o	31.37^o	31.5^o	31.59^o	31.45^o	31.4^o	31.5^o	31.36^o	31.68^o	31.82^o	31.56^o
4	62.64^o	-4.9^o	37.8^o	37.92^o	37.59^o	37.85^o	37.89^o	38.03^o	37.76^o	37.89^o	38.34^o	37.82^o
5	22.31^o	6.75^o	41.31^o	41.48^o	41.08^o	40.7^o	40.82^o	40.99^o	40.63^o	40.88^o	40.95^o	40.32^o
6	-10.47^o	-1.3^o	28.86^o	28.35^o	28.87^o	29.1^o	28.91^o	28.93^o	29.34^o	28.72^o	28.35^o	29.11^o
7	-7.12^o	-0.5^o	30.8^o	31.32^o	31.19^o	30.81^o	31.25^o	31.15^o	31.21^o	31.06^o	30.75^o	31.2^o
8	8.16^o	-0.6^o	37.19^o	38.58^o	38.02^o	38.32^o	38.51^o	38.2^o	38.22^o	38.46^o	38.56^o	38.32^o
9	65.87^o	-0.9^o	40.55^o	41.05^o	40.99^o	40.37^o	40.74^o	41.03^o	40.77^o	40.95^o	40.95^o	40.95^o
10	-5.76^o	-4.1^o	30.97^o	30.1^o	30.16^o	30.11^o	29.99^o	29.55^o	30.31^o	30.02^o	30.14^o	30.2^o
11	15.8^o	1.2^o	36.44^o	36.75^o	36.9^o	36.72^o	36.21^o	36.19^o	36.26^o	36.6^o	36.54^o	37.11^o
12	-11.5^o	2.86^o	24.79^o	24.95^o	24.97^o	24.32^o	24.37^o	24.32^o	24.56^o	24.25^o	24.43^o	24.49^o
13	8.15^o	2.54^o	32.26^o	32.17^o	32.12^o	32.25^o	32.53^o	32.41^o	32.31^o	32.22^o	32.33^o	32.08^o
14	22.1^o	3.78^o	38.62^o	38.89^o	38.71^o	38.51^o	38.94^o	39.2^o	39.76^o	39.22^o	39.23^o	39.4^o
15	84.16^o	-2.88^o	36.52^o	36.97^o	36.63^o	36.39^o	36.72^o	36.44^o	36.58^o	36.84^o	37.12^o	36.68^o
16	87.73^o	0.22^o	33.1^o	33.24^o	33.05^o	33.43^o	33.26^o	33.66^o	33.54^o	33.49^o	33.59^o	33.34^o
17	63.28^o	-0.1^o	40.84^o	41.25^o	41.13^o	40.93^o	40.87^o	40.89^o	41.15^o	41.01^o	40.87^o	40.98^o

Table 6: Profile Angle - MIMIC's Calculations Compared to Point Cloud Measurements for Angled Surfaces - XP. Part 2

Test	σ	Average d_{P_rS}	MIMIC	Error	Roll	Pitch
1	0.198^o	38.015^o	43.94^o	5.925^o	0.62^o	-1.02^o
2	0.432^o	39.497^o	44.94^o	5.443^o	-1.89^o	-1.85^o
3	0.145^o	31.523^o	36.55^o	5.027^o	-1.78^o	-1.50^o
4	0.195^o	37.889^o	42.99^o	5.101^o	1.52^o	2.71^o
5	0.333^o	40.916^o	41.62^o	0.704^o	-1.98^o	3.10^o
6	0.315^o	28.854^o	30.01^o	1.156^o	-2.36^o	2.71^o
7	0.209^o	31.074^o	31.72^o	0.646^o	-2.54^o	2.78^o
8	0.408^o	38.238^o	38.83^o	0.592^o	-3.02^o	2.53^o
9	0.225^o	40.835^o	43.05^o	2.215^o	-0.85^o	2.60^o
10	0.350^o	30.155^o	32.31^o	2.155^o	-2.61^o	2.38^o
11	0.306^o	36.572^o	40.83^o	4.258^o	-1.38^o	1.54^o
12	0.266^o	24.545^o	27.94^o	3.395^o	2.08^o	-0.96^o
13	0.134^o	32.268^o	37.96^o	5.692^o	2.98^o	-0.47^o
14	0.385^o	39.048^o	41.98^o	2.932^o	-1.63^o	0.81^o
15	0.231^o	36.689^o	36.96^o	0.271^o	-3.96^o	1.42^o
16	0.206^o	33.370^o	36.37^o	3.000^o	-1.97^o	0.13^o
17	0.140^o	40.992^o	43.50^o	2.508^o	-1.00^o	2.68^o

Table 7: Angled Surface, Profile Angle - Real World Tests - Part 3, Optech Lynx2

Test	α_{targ}	β_{targ}	MIMIC	$\theta_{P_r\text{A}}1$	$\theta_{P_r\text{A}}2$	$\theta_{P_r\text{A}}3$	$\theta_{P_r\text{A}}4$	$\theta_{P_r\text{A}}5$
1	19.66^o	0^o	59.175^o	59.41^o	59.57^o	59.51^o	59.25^o	59.25^o
2	17.83^o	0^o	58.902^o	59.45^o	59.52^o	59.12^o	59.09^o	59.27^o
3	-0.75^o	0^o	54.126^o	55.15^o	54.44^o	54.32^o	54.98^o	54.04^o
4	-3.80^o	0^o	52.913^o	54.35^o	54.41^o	54.57^o	54.46^o	54.28^o
5	-11.05^o	0^o	49.376^o	49.10^o	49.32^o	49.37^o	49.21^o	49.1^o

Table 8: Angled Surface, Profile Angle - Real World Tests - Part 4, Optech Lynx2

Test	Average θ_{P_rA}	σ	Roll	Pitch	Yaw	Error
1	59.400^o	0.145^o	-0.848^o	-0.019^o	0.0028^o	0.225^o
2	59.293^o	0.195^o	-0.786^o	-0.163^o	0.008^o	0.391^o
3	54.586^o	0.464^o	-0.193^o	-0.478^o	0.006^o	0.460^o
4	54.416^o	0.108^o	0.005^o	0.965^o	0.006^o	1.503^o
5	49.221^o	0.126^o	-0.473^o	-0.136^o	0.006^o	0.155^o

Table 9: Road Surface Profile Spacing Tests - Real World Tests - Part 1

Test	Vel(m/s)	$d_{P_rS}1$	$d_{P_rS}2$	$d_{P_rS}3$	$d_{P_rS}4$	$d_{P_rS}5$	M_f(Hz)
1	7.088	0.047m	0.047m	0.047m	0.047m	0.047m	150
2	7.53	0.050m	0.050m	0.050m	0.049m	0.049m	150
3	3.42	0.023m	0.023m	0.023m	0.024m	0.024m	150
4	5.80	0.039m	0.039m	0.039m	0.039m	0.039m	150
5	5.58	0.037m	0.037m	0.037m	0.037m	0.036m	150
6	6.86	0.035m	0.035m	0.035m	0.035m	0.034m	200
7	7.32	0.028m	0.028m	0.028m	0.028m	0.028m	200
8	3.35	0.016m	0.016m	0.016m	0.016m	0.016m	200
9	6.80	0.035m	0.035m	0.036m	0.036m	0.036m	200
10	5.60	0.027m	0.027m	0.027m	0.027m	0.027m	200

Table 10: Road Surface Profile Spacing Tests - Real World Tests - Part 2

Test	Average d_{P_rS}	MIMIC	Error	Roll	Pitch	Yaw
1	0.047m	0.047m	0.000m	-0.839^o	-0.105^o	-0.005^o
2	0.049m	0.050m	0.001m	-0.659^o	-0.119^o	0.012^o
3	0.023m	0.023m	0.000m	0.621^o	1.569^o	0.0053^o
4	0.039m	0.039m	0.000m	0.759^o	0.880^o	-0.031^o
5	0.037m	0.037m	0.000m	-0.821^o	-0.21^o	0.009^o
6	0.035m	0.034m	0.001m	0.733^o	0.383^o	0.003^o
7	0.028m	0.028m	0.000m	0.497^o	1.163^o	0.001^o
8	0.016m	0.017m	0.001m	-0.493^o	-0.572^o	0.002^o
9	0.036m	0.034m	0.002m	-0.104^o	1.54^o	0.004^o
10	0.027m	0.028m	0.001m	-0.481^o	-0.252^o	0.004^o

Table 11: Horizontal Profile Spacing - MIMIC Predictions Compared to Point Cloud Measurements for an Angled Vertical Surface at Different M_f. Part 1

Test	α_{targ}	β_{targ}	Vel (m/s)	$d_{P_rSH}1$	$d_{P_rSH}2$	$d_{P_rSH}3$	$d_{P_rSH}4$	$d_{P_rSH}5$	M_f(Hz)
1	1.93^o	0^o	4.81	0.053m	0.051m	0.041m	0.048m	0.048m	100
2	0.16^o	15^o	5.00	0.049m	0.049m	0.049m	0.049m	0.048m	100
3	2.81^o	30^o	4.97	0.047m	0.047m	0.048m	0.046m	0.047m	100
4	-1.00^o	45^o	4.90	0.050m	0.051m	0.050m	0.049m	0.050m	100
5	48.59^o	6.21^o	4.84	0.034m	0.036m	0.034m	0.035m	0.035m	100
6	72.55^o	20^o	4.90	0.039m	0.040m	0.038m	0.038m	0.038m	100
7	0.00^o	0^o	10.97	0.109m	0.110m	0.110m	0.109m	0.109m	100
8	46.32^o	0^o	12.96	0.093m	0.093m	0.090m	0.090m	0.089m	100
9	39.98^o	0^o	12.49	0.090m	0.090m	0.090m	0.089m	0.092m	100
10	70.90^o	0^o	12.68	0.100m	0.102m	0.099m	0.098m	0.097m	100
11	19.70^o	0^o	4.079	0.028m	0.022m	0.023m	0.022m	0.022m	150
12	17.84^o	0^o	5.72	0.033m	0.034m	0.032m	0.033m	0.032m	150
13	-0.75^o	0^o	3.71	0.025m	0.024m	0.024m	0.024m	0.024m	150
14	-3.80^o	0^o	4.15	0.031m	0.030m	0.030m	0.030m	0.031m	150
15	-11.05^o	0^o	4.52	0.037m	0.037m	0.037m	0.036m	0.036m	150

Table 12: Horizontal Profile Spacing - MIMIC Predictions Compared to Point Cloud Measurements for an Angled Vertical Surface at Different M_f. Part 2

No.	σ	Average d_{P_rSH}	MIMIC	Error	Roll	Pitch	Yaw	M_f (Hz)
1	0.004m	0.048m	0.046m	0.002m	-1.402^o	1.195^o	0.002^o	100
2	0.000m	0.048m	0.049m	0.001m	-1.6273^o	1.21^o	0.002^o	100
3	0.000m	0.046m	0.047m	0.002m	-1.601^o	1.460^o	0.001^o	100
4	0.000m	0.050m	0.049m	0.001m	-1.362^o	1.276^o	0.006^o	100
5	0.000m	0.034m	0.034m	0.001m	-1.330^o	1.220^o	0.002^o	100
6	0.000m	0.038m	0.039m	0.001m	-1.560^o	1.172^o	0.005^o	100
7	0.000m	0.109m	0.109m	0.000m	-4.510^o	2.442^o	0.010^o	100
8	0.002m	0.091m	0.091m	0.000m	-3.142^o	1.979^o	0.002^o	100
9	0.001m	0.090m	0.090m	0.000m	-3.502^o	0.911^o	0.003^o	100
10	0.002m	0.099m	0.099m	0.000m	-3.034^o	1.281^o	0.004^o	100
11	0.000m	0.022m	0.023m	0.001m	-0.848^o	-0.020^o	0.003^o	150
12	0.001m	0.033m	0.032m	0.001m	-0.786^o	-0.163^o	0.008^o	150
13	0.000m	0.024m	0.024m	0.000m	-0.193^o	-0.478^o	0.006^o	150
14	0.001m	0.030m	0.029m	0.001m	0.005^o	0.965^o	0.006^o	150
15	0.000m	0.036m	0.036m	0.000m	-0.473^o	-0.136^o	0.006^o	150

Table 13: Vertical Profile Spacing - MIMIC Predictions Compared to Point Cloud Measurements for an Angled Vertical Surface at Different M_f. Part 1

Test	α_{targ}	β_{targ}	Vel(m/s)	$d_{P_rSV}1$ (m)	$d_{P_rSV}2$ (m)	$d_{P_rSV}3$ (m)	$d_{P_rSV}4$ (m)	$d_{P_rSV}5$ (m)	M_f (Hz)
1	1.93	0	4.8083	0.0345	0.0356	0.0338	0.032	0.0347	100
2	0.156	15	5	0.029	0.028	0.029	0.02888	0.0294	100
3	2.81	30	4.972	0.028	0.029	0.0289	0.0279	0.0291	100
4	-1	45	4.9041	0.027	0.0281	0.028	0.028	0.0278	100
5	48.59	6.21	4.838	0.0341	0.0333	0.0327	0.033	0.0348	100
6	72.546	20	4.9041	0.043	0.0451	0.044	0.0436	0.0447	100
7	0	0	10.97	0.077	0.0759	0.0793	0.0804	0.0799	100
8	46.32	0	12.96	0.0888	0.0931	0.0925	0.0899	0.0912	100
9	58.92	0	12.49	0.091	0.087	0.0879	0.0859	0.0862	100
10	70.9	0	12.68	0.0896	0.0889	0.0879	0.0882	0.0892	100
11	19.66	0	4.079	0.0356	0.0367	0.0369	0.0382	0.0375	150
12	17.835	0	5.72	0.0538	0.0538	0.0537	0.0537	0.0536	150
13	-0.75	0	3.712	0.034	0.034	0.0344	0.0342	0.0351	150
14	-3.8	0	4.15	0.0396	0.0392	0.0394	0.0393	0.0392	150
15	-11.05	0	3.324	0.042	0.0426	0.0427	0.0429	0.0426	150

Table 14: Vertical Profile Spacing - MIMIC Predictions Compared to Point Cloud Measurements for an Angled Vertical Surface at Different M_f. Part 2

Test	σ	Average $d_{Pr,SV}$	MIMIC	Error	Roll	Pitch	Yaw	M_f (Hz)
1	0.001m	0.034m	0.033m	0.001m	-1.402^o	1.195^o	0.002^o	100
2	0.000m	0.029m	0.030m	0.001m	-1.627^o	1.218^o	0.002^o	100
3	0.000m	0.028m	0.029m	0.001m	-1.601^o	1.460^o	0.000^o	100
4	0.000m	0.028m	0.028m	0.000m	-1.362^o	1.276^o	0.006^o	100
5	0.001m	0.033m	0.035m	0.002m	-1.330^o	1.220^o	0.002^o	100
6	0.001m	0.044m	0.044m	0.000m	-1.559^o	1.172^o	0.006^o	100
7	0.002m	0.078m	0.077m	0.001m	-4.510^o	2.442^o	0.010^o	100
8	0.002m	0.091m	0.092m	0.001m	-3.142^o	1.979^o	0.002^o	100
9	0.002m	0.088m	0.088m	0.000m	-3.503^o	0.911^o	0.003^o	100
10	0.001m	0.089m	0.090m	0.001m	-3.034^o	1.281^o	0.004^o	100
11	0.001m	0.037m	0.038m	0.001m	-0.848^o	-0.019^o	0.002^o	150
12	0.000m	0.054m	0.053m	0.001m	-0.786^o	-0.163^o	0.008^o	150
13	0.000m	0.034m	0.034m	0.000m	-0.193^o	-0.478^o	0.006^o	150
14	0.000m	0.039m	0.039m	0.000m	0.005^o	0.965^o	0.006^o	150
15	0.000m	0.043m	0.042m	0.001m	-0.473^o	-0.136^o	0.006^o	150

Table 15: Point Spacing - MIMIC Predictions Compared to Point Cloud Measurements for an Angled Surface, XP1 and Optech Lynx Data. Part 1

Test	α_{targ}	β_{targ}	Z_{diff}	H_r	$d_{PS}1$	$d_{PS}2$	$d_{PS}3$	$d_{PS}4$	$d_{PS}5$	PRR(kHz)
1	1.930^o	0^o	1.492m	5.367m	0.013m	0.013m	0.012m	0.013m	0.013m	300
2	0.156^o	15^o	1.476m	5.947m	0.016m	0.017m	0.016m	0.016m	0.016m	300
3	2.810^o	30^o	1.479m	7.796m	0.026m	0.026m	0.026m	0.027m	0.026m	300
4	-1.000^o	45^o	1.351m	6.409m	0.020m	0.023m	0.023m	0.024m	0.023m	300
5	48.590^o	6.21^o	1.426m	5.291m	0.015m	0.014m	0.013m	0.013m	0.015m	300
6	72.546^o	20^o	1.443m	6.181m	0.018m	0.019m	0.018m	0.019m	0.019m	300
7	19.670^o	0^o	2.647m	16.840m	0.104m	0.109m	0.104m	0.105m	0.106m	125
8	16.744^o	0^o	2.531m	7.580m	0.048m	0.050m	0.049m	0.050m	0.048m	125
9	-1.280^o	0^o	2.48m	11.190m	0.072m	0.072m	0.073m	0.074m	0.072m	125
10	-10.800^o	0^o	2.795m	10.010m	0.067m	0.068m	0.0689m	0.069m	0.068m	125
11	30.810^o	0^o	2.392m	12.940m	0.082m	0.082m	0.083m	0.080m	0.081m	125
12	18.950^o	0^o	2.337m	7.550m	0.023m	0.023m	0.024m	0.023m	0.023m	500
13	16.240^o	0^o	2.280m	6.230m	0.020m	0.019m	0.019m	0.018m	0.018m	500
14	-2.180^o	0^o	2.348m	7.760m	0.026m	0.026m	0.025m	0.026m	0.026m	500
15	-12.800^o	0^o	2.582m	8.950m	0.033m	0.030m	0.032m	0.032m	0.032m	500
16	33.050^o	0^o	2.110m	10.110m	0.032m	0.032m	0.032m	0.032m	0.032m	500

Table 16: Point Spacing - MIMIC Predictions Compared to Point Cloud Measurements for an Angled Surface, XP1 and Optech Lynx Data. Part 2

Test	σ	Average d_{PS}	MIMIC	Error	Roll	Pitch	Yaw	PRR (kHz)
1	0.000m	0.013m	0.014m	0.000m	-1.402^o	1.195^o	0.002^o	300
2	0.000m	0.016m	0.018m	0.002m	-1.627^o	1.218^o	0.002^o	300
3	0.000m	0.026m	0.027m	0.001m	-1.601^o	1.460^o	0.000^o	300
4	0.001m	0.022m	0.024m	0.002m	-1.362^o	1.276^o	0.005^o	300
5	0.001m	0.014m	0.014m	0.000m	-1.330^o	1.220^o	0.002^o	300
6	0.000m	0.019m	0.017m	0.002m	-1.559^o	1.172^o	0.005^o	300
7	0.002m	0.105m	0.106m	0.001m	-1.301^o	1.425^o	0.007^o	125
8	0.001m	0.049m	0.047m	0.002m	-0.806^o	-0.162^o	0.001^o	125
9	0.001m	0.073m	0.072m	0.001m	-0.254^o	-0.432^o	0.002^o	125
10	0.001m	0.068m	0.070m	0.002m	0.342^o	0.223^o	0.000^o	125
11	0.001m	0.082m	0.080m	0.002m	-1.453^o	1.165^o	0.005^o	125
12	0.000m	0.023m	0.023m	0.000m	-1.333^o	1.112^o	0.000^o	500
13	0.001m	0.019m	0.019m	0.000m	-0.041^o	0.220^o	0.001^o	500
14	0.000m	0.026m	0.024m	0.002m	-0.549^o	1.290^o	0.004^o	500
15	0.001m	0.032m	0.031m	0.001m	-1.290^o	0.270^o	0.000^o	500
16	0.000m	0.032m	0.031m	0.001m	-1.010^o	1.291^o	0.001^o	500

.2 Chapter 5 - Calculating Point Density

Table 17: Calculated and Measured Point Density for an Angled Target of Dimensions 1m x 0.5m. Part 1

Test	H_r	Width	Height	Z_{diff}	α_{targ}	β_{targ}
1	7.665m	1m	0.5m	1.218m	17.338^o	0^o
2	7.665m	0.5m	0.5m	1.218m	17.338^o	0^o
3	11.796m	1m	0.5m	1.953m	-1.120^o	0^o
4	11.796m	0.5m	0.5m	1.953m	-1.120^o	0^o
5	11.432m	1m	0.5m	2.089m	0.100^o	0^o
6	11.432m	0.5m	0.5m	2.089m	0.100^o	0^o
7	6.422m	1m	0.5m	1.345m	22.790^o	0^o
8	6.422m	0.5m	0.5m	1.345 m	22.790^o	0^o

Table 18: Calculated and Measured Point Density for an Angled Target of Dimensions 1m x 0.5m. Part 2

Test	Vel(m/s)	PRR (kHz)	M_f (Hz)	Roll	Pitch	Yaw
1	5.813	125	100	-0.892^o	0.037^o	-0.002^o
2	5.813	125	100	-0.892^o	0.037^o	-0.002^o
3	7.224	125	100	-0.249^o	-0.440^o	0.002^o
4	7.224	125	100	-0.249^o	-0.440^o	0.002^o
5	7.21	250	150	-0.313^o	-0.400^o	0.002^o
6	7.21	250	150	-0.313^o	-0.400^o	0.002^o
7	5.318	250	150	-0.121^o	-0.170^o	0.001^o
8	5.318	250	150	-0.121^o	-0.170^o	0.001^o

Table 19: Calculated and Measured Point Density for each Face of a Cylindrical Target. Part 1

Test	Width	Height	Z_{diff}	α_{targ}	β_{targ}	H_r	Face
1	0.197m	0.741m	2.130m	0.814^o	0.0^o	5.118m	i
2	0.197m	0.741m	2.130m	49.350^o	0.0^o	5.118m	ii
3	0.080mm	1.590m	1.834m	29.120^o	0.0^o	6.69m	i
4	0.080m	1.590m	1.834m	77.228^o	0.0^o	6.692m	ii
5	0.050m	1.100m	1.906m	71.360^o	-3.4^o	7.95m	i
6	0.050m	1.100m	1.906m	19.711^o	-3.4^o	7.95m	ii
7	0.050m	1.100m	1.773m	66.816^o	0.0^o	7.438m	i
8	0.050m	1.100m	1.773m	19.085^o	0.0^o	7.438m	ii

Table 20: Calculated and Measured Point Density for each Face of a Cylindrical Target. Part 2

Test	Vel(m/s)	α_{scan}	γ_{scan}	M_f	PRR	Roll	Pitch	Yaw
1	3.95	37.49^o	29.6^o	150	250	0.202^o	1.158^o	0.011^o
2	3.95	37.49^o	29.6^o	150	250	0.198^o	1.162^o	0.012^o
3	5.77	37.49^o	29.6^o	150	250	0.176^o	1.164^o	0.011^o
4	5.77	37.49^o	29.6^o	150	250	0.174^o	1.15^o	0.012^o
5	4.808	45^o	45^o	100	300	0.212^o	1.158^o	0.024^o
6	4.808	45^o	45^o	100	300	0.216^o	1.157^o	0.024^o
7	4.301	45^o	45^o	100	300	0.209^o	1.154^o	0.032^o
8	4.301	45^o	45^o	100	300	0.209^o	1.152^o	0.032^o

Table 21: Calculated and Measured Point Density for an Angled Target for both Scanners on the Dual Scanner Optech Lynx

Test	Scanner	α_{targ}	H_r	Z_{diff}	Width	Height	Vel(m/s)	MIMIC	Measured	Roll	Pitch	Yaw
1	1	16.532^o	8.736m	0.859m	1.0m	0.5m	6.54	385pts	415pts	0.222^o	1.178^o	0.0187^o
2	2	16.532^o	8.736m	0.859m	1.0m	0.5m	6.54	190pts	219pts	0.25^o	1.175^o	0.0186^o
3	1	16.532^o	8.736m	0.859m	0.5m	0.5m	6.54	193pts	226pts	0.194^o	1.197^o	0.0195^o
4	2	16.532^o	8.736m	0.859m	0.5m	0.5m	6.54	96pts	116pts	0.194^o	1.199^o	0.0198^o
5	1	-25.140^o	5.756m	2.018m	1.0m	0.5m	6.25	388pts	417pts	0.106^o	1.227^o	0.022^o
6	2	-25.140^o	5.756m	2.018m	1.0m	0.5m	6.25	432pts	444pts	0.115^o	1.223^o	0.024^o
7	1	-25.140^o	5.756m	2.018m	0.5m	0.5m	6.25	193pts	194pts	0.124^o	1.228^o	0.027^o
8	2	-25.140^o	5.756m	2.018m	0.5m	0.5m	6.25	216pts	207pts	0.122^o	1.169^o	0.022^o

Table 22: Calculated and Measured Point Density for each Face of a Cylindrical Target for both Scanners on the Dual Scanner Optech Lynx

Test	Scanner	α_{targ}	H_r	Z_{diff}	Vel(m/s)	MIMIC	Measured	Roll	Pitch	Yaw
1(i)	1	47.76^o	3.42m	1.76m	5.09	113pts	103pts	0.395^o	0.350^o	0.017^o
1(ii)	1	-8.00^o	3.42m	1.76m	5.09	98pts	111pts	0.395^o	0.351^o	0.017^o
1(ii)	2	-8.00^o	3.42m	1.76m	5.09	60pts	60pts	0.377^o	0.355^o	0.016^o
1(iii)	2	-83.26^o	3.42m	1.76m	5.09	57pts	64pts	0.366^o	0.349^o	0.014^o
2(i)	1	-22.32^o	4.85m	1.85m	5.74	46pts	42pts	0.245^o	0.352^o	0.012^o
2(ii)	1	61.73^o	4.85m	1.85m	5.74	63pts	56pts	0.224^o	0.346^o	0.012^o
2(ii)	2	-22.32^o	4.85m	1.85m	5.74	48pts	49pts	0.312^o	0.379^o	0.013^o
2(iii)	2	-81.65^o	4.85m	1.85m	5.74	41pts	43pts	0.311^o	0.395^o	0.015^o

.3 Chapter 6 - Assessing MMS Parameters

Table 23: Assessing the Impact of Horizontal an Vertical Scanner Rotations on Point Density for a Parallel 2m x 1m Target at a Horizontal Range of 5m and Varied Vehicle Velocities

Velocity(km/h)	α_{scan}	MIMIC α_{scan}	γ_{scan}	MIMIC γ_{scan}
10	15^o	5308pts	15^o	5513pts
20	15^o	2647pts	15^o	2757pts
30	15^o	1767pts	15^o	1837pts
40	15^o	1323pts	15^o	1378pts
50	15^o	1103pts	15^o	1103pts
10	30^o	4953pts	30^o	5833pts
20	30^o	2471pts	30^o	2916pts
30	30^o	1649pts	30^o	1944pts
40	30^o	1235pts	30^o	1458pts
50	30^o	1029pts	30^o	1168pts
10	45^o	4284pts	45^o	6269pts
20	45^o	2138pts	45^o	3134pts
30	45^o	1427pts	45^o	2083pts
40	45^o	1069pts	45^o	1578pts
50	45^o	890pts	45^o	1264pts
10	60^o	3220pts	60^o	6634pts
20	60^o	1608pts	60^o	3317pts
30	60^o	1072pts	60^o	2211pts
40	60^o	804pts	60^o	1658pts
50	60^o	937pts	60^o	1328pts

Table 24: Calculating the Effect of Vehicle Velocity and a Dual Axis Scanner Rotation on the Point Density of a Large Parallel Vertical Target. Target Range is 5m and Target Dimensions are 2m x 1m

Velocity (km/h)	α_{scan}	γ_{scan}	MIMIC
10	15^o	15^o	5713pts
20	15^o	15^o	2856pts
30	15^o	15^o	1904pts
40	15^o	15^o	1428pts
50	15^o	15^o	1142pts
10	30^o	30^o	6870pts
20	30^o	30^o	3422pts
30	30^o	30^o	2249pts
40	30^o	30^o	1723pts
50	30^o	30^o	1380pts
10	45^o	45^o	10188pts
20	45^o	45^o	5094pts
30	45^o	45^o	3395pts
40	45^o	45^o	2547pts
50	45^o	45^o	2039pts
10	60^o	60^o	20981pts
20	60^o	60^o	10490pts
30	60^o	60^o	6993pts
40	60^o	60^o	5245pts
50	60^o	60^o	4196pts

Table 25: Calculating the Effect of Vehicle Velocity and a Dual Axis Scanner Rotation on the Point Density of a Narrow Vertical Target. Target Range is 5m and Target Dimensions are 0.1m x 2m

Velocity (km/h)	α_{scan}	γ_{scan}	MIMIC	Profiles	P_{pp}
10	15^o	15^o	609pts	20	30
20	15^o	15^o	304pts	10	30
30	15^o	15^o	204pts	7	29
40	15^o	15^o	152pts	5	30
50	15^o	15^o	121pts	4	30
10	30^o	30^o	714pts	51	14
20	30^o	30^o	357pts	26	14
30	30^o	30^o	237pts	17	14
40	30^o	30^o	178pts	12	15
50	30^o	30^o	146pts	10	15
10	45^o	45^o	994pts	105	9
20	45^o	45^o	497pts	52	10
30	45^o	45^o	331pts	35	9
40	45^o	45^o	248pts	26	10
50	45^o	45^o	200pts	21	10
10	60^o	60^o	1964pts	253	8
20	60^o	60^o	982pts	126	8
30	60^o	60^o	655pts	85	8
40	60^o	60^o	491pts	63	8
50	60^o	60^o	393pts	50	8

Table 26: Calculated Point Density: Identifying the Recommended Dual Axis Scanner Rotation for Increasing Point Density on a Parallel Vertical Target at Different Vehicle Velocities. Target Range is 5m and Target Dimensions are 2m x 1m

Velocity (km/h)	α_{scan}	γ_{scan}	MIMIC
10	30^o	30^o	6870pts
20	30^o	30^o	3422pts
30	30^o	30^o	2249pts
40	30^o	30^o	1723pts
50	30^o	30^o	1380pts
10	30^o	45^o	8798pts
20	30^o	45^o	4399pts
30	30^o	45^o	2932pts
40	30^o	45^o	2199pts
50	30^o	45^o	1762pts
10	30^o	60^o	10776pts
20	30^o	60^o	5347pts
30	30^o	60^o	3647pts
40	30^o	60^o	2673pts
50	30^o	60^o	2141pts
10	45^o	30^o	6991pts
20	45^o	30^o	3495pts
30	45^o	30^o	2330pts
40	45^o	30^o	1747pts
50	45^o	30^o	1399pts
10	45^o	45^o	10188pts
20	45^o	45^o	5094pts
30	45^o	45^o	3395pts
40	45^o	45^o	2547pts
50	45^o	45^o	2039pts
10	45^o	60^o	14343pts
20	45^o	60^o	7171pts
30	45^o	60^o	4781pts
40	45^o	60^o	3585pts
50	45^o	60^o	2870pts

Table 27: Calculated Profile Spacing: Examining the Correlation Between Mirror Frequency and Vertical Profile Spacing on a Parallel Vertical Target at Different Vehicle Velocities. Target Range is 5m and Target Dimensions are 2m x 1m

Test	M_f(Hz)	Velocity (km/h)	d_{P_rSV}
1	200	10	0.019m
2	200	20	0.039m
3	200	30	0.058m
4	200	40	0.074m
5	200	50	0.097m
6	150	10	0.026m
7	150	20	0.052m
8	150	30	0.078m
9	150	40	0.103m
10	150	50	0.129m
11	100	10	0.034m
12	100	20	0.078m
13	100	30	0.116m
14	100	40	0.155m
15	100	50	0.194m
16	50	10	0.078m
17	50	20	0.155m
18	50	30	0.232m
19	50	40	0.310m
20	50	50	0.388m

Table 28: Calculated Point Spacing: Examining the Correlation Between PRR and Horizontal Range for Point Spacing on a Parallel Vertical Target. Target Dimensions are 2m x 1m

Test	PRR (kHz)	H_r	d_{PS}
1	300	5m	0.018m
2	300	10m	0.036m
3	300	15m	0.054m
4	300	20m	0.072m
5	300	25m	0.090m
6	250	5m	0.022m
7	250	10m	0.043m
8	250	15m	0.065m
9	250	20m	0.086m
10	250	25m	0.108m
11	200	5m	0.027m
12	200	10m	0.054m
13	200	15m	0.814m
14	200	20m	0.108m
15	200	25m	0.135m
16	150	5m	0.036m
17	150	10m	0.072m
18	150	15m	0.108m
19	150	20m	0.144m
20	150	25m	0.180m
21	100	5m	0.054m
22	100	10m	0.108m
23	100	15m	0.162m
24	100	20m	0.217m
25	100	25m	0.271m

Table 29: Calculated Point Spacing: Examining the Correlation Between PRR and FOV for Point Spacing on a Parallel Vertical Target. Target Dimensions are 2m x 1m

Test	PRR	FOV	d_{PS}
1	300^o	360^o	0.018m
2	300^o	315^o	0.016m
3	300^o	270^o	0.014m
4	300^o	225^o	0.011m
5	300^o	180^o	0.009m
6	250^o	360^o	0.022m
7	250^o	315^o	0.019m
8	250^o	270^o	0.016m
9	250^o	225^o	0.013m
10	250^o	180^o	0.011m
11	200^o	360^o	0.027m
12	200^o	315^o	0.024m
13	200^o	270^o	0.020m
14	200^o	225^o	0.017m
15	200^o	180^o	0.014m
16	150^o	360^o	0.036m
17	150^o	315^o	0.032m
18	150^o	270^o	0.027m
19	150^o	225^o	0.023m
20	150^o	180^o	0.018m
21	100^o	360^o	0.054m
22	100^o	315^o	0.047m
23	100^o	270^o	0.041m
24	100^o	225^o	0.034m
25	100^o	180^o	0.027m

.4 Chapter 7 - Benchmarking MMS Point Density

Table 30: Calculated Point Density for the XP1+: Benchmarking Dual Scanner MMS Performance on Narrow Structure at Different Vehicle Velocities. Range to Target is 5.04m and Target Dimensions are 0.1m x 2m

Face	Vel(km/h)	Scanner 1	Scanner 2	Combined	Profiles Scanner 1	Profiles Scanner 2
i	10	881pts	0pts	881pts	182	0
i	20	440pts	0pts	440pts	91	0
i	30	294pts	0pts	294pts	60	0
i	40	220pts	0pts	220pts	46	0
i	50	176pts	0pts	176pts	37	0
ii	10	1549pts	279pts	1828pts	180	135
ii	20	774pts	139pts	913pts	90	68
ii	30	516pts	93pts	609pts	60	45
ii	40	387pts	69pts	456pts	45	34
ii	50	310pts	56pts	366pts	36	27
iii	10	0pts	157pts	157pts	0	136
iii	20	0pts	79pts	79pts	0	68
iii	30	0pts	52pts	52pts	0	46
iii	40	0pts	39pts	39pts	0	34
iii	50	0pts	32pts	32pts	0	27

Table 31: Calculated Point Density for the XP2: Benchmarking Dual Scanner MMS Performance on Narrow Structure at Different Vehicle Velocities. Range to Target is 5.04m and Target Dimensions are 0.1m x 2m

Face	Vel(km/h)	Scanner 1	Scanner 2	Combined	Profiles Scanner 1	Profiles Scanner 2
i	10	893pts	0pts	893pts	107	0
i	20	446pts	0pts	446pts	53	0
i	30	297pts	0pts	297pts	35	0
i	40	224pts	0pts	224pts	27	0
i	50	178pts	0pts	178pts	22	0
ii	10	994pts	331pts	1325pts	105	105
ii	20	497pts	166pts	663pts	52	52
ii	30	331pts	110pts	441pts	52	52
ii	40	248pts	83pts	331pts	26	26
ii	50	200pts	66pts	266pts	21	21
iii	10	0pts	583pts	583pts	0	107
iii	20	0pts	292pts	292pts	0	53
iii	30	0pts	194pts	194pts	0	35
iii	40	0pts	146pts	146pts	0	27
iii	50	0pts	116pts	116pts	0	22

Table 32: Calculated Point Density for the Optech Lynx: Benchmarking Dual Scanner MMS Performance on Narrow Structure at Different Vehicle Velocities. Range to Target is 5.04m and Target Dimensions are 0.1m x 2m

Face	Velocity (km/h)	Scanner 1	Scanner 2	Combined	Profiles Scanner 1	Profiles Scanner 2
i	10	445pts	0pts	445pts	112	0
i	20	223pts	0pts	223pts	56	0
i	30	148pts	0pts	148pts	37	0
i	40	111pts	0pts	111pts	28	0
i	50	89pts	0pts	89pts	21	0
ii	10	470pts	244pts	714pts	111	111
ii	20	235pts	122pts	357pts	55	55
ii	30	157pts	81pts	238pts	37	37
ii	40	117pts	61pts	178pts	27	27
ii	50	94pts	48pts	142pts	22	22
iii	10	0pts	341pts	341pts	0	113
iii	20	0pts	170pts	170pts	0	57
iii	30	0pts	113pts	113pts	0	37
iii	40	0pts	86pts	86pts	0	29
iii	50	0pts	68pts	68pts	0	22

Table 33: No. of Points Per Profile at Different Target Ranges XP1+

Face	H_r	Scanner 1	Scanner 2	Combined	P_{pp}
i	5.04m	176pts	0pts	176pts	5
i	10.04m	143pts	0pts	143pts	4
i	15.04m	98pts	0pts	98pts	3
i	20.04m	73pts	0pts	73pts	2
i	25.04m	57pts	0pts	57pts	2
ii	5m	310pts	56pts	366pts	9
ii	10m	151pts	27pts	178pts	4
ii	15m	89pts	n/a	89pts	2
ii	20m	62pts	n/a	62pts	2
ii	25m	47pts	n/a	47pts	1
iii	5.04m	0pts	32pts	32pts	1
iii	10.04m	0pts	26pts	26pts	1
iii	15.04m	0pts	0pts	0pts	0
iii	20.04m	0pts	0pts	0pts	0
iii	25.04m	0pts	0pts	0pts	0

Table 34: No. of Points Per Profile at Different Target Ranges XP2

Face	H_r	Scanner 1	Scanner 2	Combined	P_{pp}
i	5.04m	178pts	0pts	178pts	8
i	10.04m	101pts	0pts	101pts	5
i	15.04m	67pts	0pts	67pts	3
i	20.04m	50pts	0pts	50pts	2
i	25.04m	39pts	0pts	39pts	2
ii	5m	200pts	66pts	266pts	10
ii	10m	89pts	46pts	135pts	4
ii	15m	55pts	34pts	89pts	3
ii	20m	40pts	27pts	67pts	2
ii	25m	31pts	23pts	54pts	1
iii	5.04mm	0pts	116pts	116pts	5
iii	10.04m	0pts	73pts	73pts	3
iii	15.04m	0pts	53pts	53pts	2
iii	20.04m	0pts	41pts	41pts	2
iii	25.04m	0pts	34pts	34pts	2

Table 35: No. of Points Per Profile at Different Target Ranges Optech Lynx

Face	H_r	Scanner 1	Scanner 2	Combined	P_{pp}
i	5.04m	89pts	0pts	89pts	4
i	10.04m	50pts	0pts	50pts	2
i	15.04m	33pts	0pts	33pts	2
i	20.04m	25pts	0pts	25pts	1
i	25.04m	21pts	0pts	21pts	1
ii	5m	94pts	48pts	142pts	4
ii	10m	46pts	31pts	77pts	2
ii	15m	30pts	23pts	53pts	1
ii	20m	22pts	0pts	22pts	1
ii	25m	0pts	0pts	0pts	0
iii	5.04m	0pts	68pts	68pts	3
iii	10.04m	0pts	41pts	41pts	2
iii	15.04m	0pts	29pts	29pts	1
iii	20.04m	0pts	23pts	23pts	1
iii	25.04m	0pts	0pts	0pts	0

Bibliography

[Aggarwal et al., 2009] Aggarwal, P., Syed, Z., and El-Sheimy, N. (2009). Hybrid extended particle filter (HEPF) for integrated inertial navigation and global positioning systems. *Measurement Science and Technology*, 20(5):055203 (9pp).

[Alamús et al., 2004] Alamús, R., Baron, A., Bosch, E., Casacuberta, J., Miranda, J., Pla, M., Sànchez, S., Serra, A., and Talaya, J. (2004). On the accuracy and performance of the geomobil system. *International Archives of Photogrammetry and Remote Sensing, Istambul, Turkey*, (Icc).

[Barber et al., 2008] Barber, D., Mills, J., and Smith-Voysey, S. (2008). Geometric validation of a ground-based mobile laser scanning system. *ISPRS Journal of Photogrammetry and Remote Sensing*, 63(1):128–141.

[Becker and Haala, 2009] Becker, S. and Haala, N. (2009). Grammar Supported Facade Reconstruction from Mobile LiDAR Mapping. *International Archive of Photogrammetry and Remote Sensing*, XXXVIII(2009):229–234.

[Betaille et al., 2007] Betaille, D., Chapelon, A., Lusetti, B., Kais, M., and Millescamps, D. (2007). High Integrity Reference Trajectory for Bench-

marking Land Navigation Data Fusion Methods. *2007 IEEE Intelligent Vehicles Symposium*, pages 346–351.

[Bevley and Cobb, 2010] Bevley, D. and Cobb, S. (2010). *GNSS for Vehicle Control*. Artech House, Boston, US, 1st edition.

[Boehler et al., 2003] Boehler, W., Bordas Vicent, M., and Marbs, A. (2003). Investigating laser scanner accuracy. *The International Archives of Photogrammetry, Remote Sensing and Spatial Information Sciences*, 34(Part 5):696–701.

[Brenner, 2009] Brenner, C. (2009). Global localization of vehicles using local pole patterns. In Denzler, J., Notni, G., and Se, H., editors, *Pattern Recognition*, volume 5748 of *Lecture Notes in Computer Science*, pages 61–70. Springer Berlin Heidelberg.

[Brun and Deschaud, 2007] Brun, X. and Deschaud, J.-E. (2007). On the way city mobile mapping user laser range scanner and fisheye camera. In *The 5th International Symposium on Mobile Mapping Technology MMT '07*, volume XXXVI-5/C55, Padua, Italy.

[Cahalane et al., 2010a] Cahalane, C., McCarthy, T., and McElhinney, C. (2010a). Mobile mapping system performance : An initial investigation into the effect of vehicle speed on laser scan lines. In *Remote Sensing & Photogrammety Society Annual Conference - 'From the sea-bed to the cloudtops'*, September 2010, Cork, Ireland.

[Cahalane et al., 2012] Cahalane, C., McCarthy, T., and McElhinney, C. P. (2012). Mimic: Mobile mapping point density calculator. In *Proceedings of the 3rd International Conference on Computing for Geospatial Research*

and Applications, COM.Geo '12, pages 15:1–15:9, Washington, D.C., USA. ACM.

[Cahalane et al., 2010b] Cahalane, C., McElhinney, C., and McCarthy, T. (2010b). Mobile mapping system performance : An analysis of the effect of laser scanner configuration and vehicle velocity on scan profiles. In *European laser Mapping Forum - 'ELMF 2010'*, Novermber 2010, The Hague, Holland.

[Cahalane et al., 2011] Cahalane, C., McElhinney, C., and McCarthy, T. (2011). Calculating the Effect of Dual-Axis Scanner Rotations and Surface Orientation on Scan Profiles. In *MMT11, The 7th International Symposium on Mobile Mapping Technology*, June 2011, Krakaw, Poland.

[California Department of Transport, 2012] California Department of Transport (2012). Caltrans District 4 - Interim Mobile Terrestrial Laser Scanning Guidelines. http://www.dot.ca.gov/newtech/newdriinternet/3d4dfiles/. Date Accessed: 5-10-2012.

[Chiang and Huang, 2008] Chiang, K.-W. and Huang, Y.-W. (2008). An intelligent navigator for seamless INS/GPS integrated land vehicle navigation applications. *Applied Soft Computing*, 8(1):722–733.

[Ellum and El-Sheimy, 2002] Ellum, C. and El-Sheimy, N. (2002). Land-based mobile mapping systems. *Photogrammetric Engineering & Remote Sensing*, (January).

[Faro, 2012] Faro (2012). Faro Focus Phase Based Scanner. http://www.faro.com. Date Accessed: 09-10-2012.

[Florida Department of Transport, 2012] Florida Department of Transport (2012). Terrestrial Mobile LiDAR Surveying and Mapping Guidelines. http://www.dot.state.fl.us/surveyingandmapping/regulations.shtm. Date Accessed: 5-10-2012.

[Foley et al., 1995] Foley, J. D., van Dam, A., Feiner, S. K., and Hughes, J. F. (1995). *Computer Graphics: Principles and Practice in C.* Addison-Wesley Professional.

[Geng et al., 2006] Geng, X., Li, Q., and Shi, Z. (2006). GPS/IMU/DMI integrated high-precision positioning approach. In *Proceedings of SPIE*, volume 6418, pages 1–8.

[Glennie, 2007] Glennie, C. (2007). Rigorous 3D error analysis of kinematic scanning LIDAR systems. *Journal of Applied Geodesy*, 1:147–157.

[Glennie, 2008] Glennie, C. (2008). A Kinematic Terrestrial LIDAR Scanning System. *Transporation Research Board of the National Academies*, (281):1–12.

[Glennie and Lichti, 2010] Glennie, C. and Lichti, D. D. (2010). Static Calibration and Analysis of the Velodyne HDL-64E S2 for High Accuracy Mobile Scanning. *Remote Sensing*, 2(6):1610–1624.

[Goad, 1991] Goad, C. C. (1991). The Ohio state university highway mapping project : the positioning component. In *47th Annual Meeting. The Institute of Navigation (ION)*, pages 117–120, Williamsburg, VA. The Institute of Navigation.

[Gonzlez-Jorge et al., 2011] Gonzlez-Jorge, H., Riveiro, B., Armesto, J., and Arias, P. (2011). Standard artifact for the geometric verification of terres-

trial laser scanning systems. *Optics and Laser Technology*, 43(7):1249 – 1256.

[Goulette et al., 2006] Goulette, F., Nashashibi, F., Abuhadrous, I., Ammoun, S., and Laurgeau, C. (2006). An integrated on-board laser range sensing system for on-the-way city and road modelling. In *Proceedings of the ISPRS Commission I Symposium,'From Sensors to Imagery'*, volume 61, Paris, France.

[GPS.gov, 2012] GPS.gov (2012). Details of the Global Positioning System Constellation. http://www.gps.gov/multimedia/images/constellation.jpg. Date Accessed: 11-10-2012.

[Graefe, 2007a] Graefe, G. (2007a). Kinematic surveying with static accuracy. In Grun, A. and Kahmen, H., editors, *8th Conference on Optical 3-D Measurement Techniques*, pages 142–149, Zurich, Switzerland.

[Graefe, 2007b] Graefe, G. (2007b). Quality management in kinematic laser scanning applications. *International Archives of Photogrammetry, Remote Sensing and Spatial Information Sciences*, 36(5/C55):6.

[Graefe et al., 2001] Graefe, G., Caspary, W., Heister, H., Klemm, J., and Sever, M. (2001). The road data acquisition system MoSES. Determination and accuracy of trajectory data gained with the Applanix POS/LV. In *Proceedings, The Third International Mobile Mapping Symposium, Cairo, Egypt, January*, pages 3–5.

[Grewal et al., 2007] Grewal, M. S., Weill, L. R., and Andrews, A. P. (2007). *Global Positioning Systems, Inertial Navigation and Integration*. John Wiley & Sons, New Jersey, US, 6th edition.

[Haala et al., 2008] Haala, N., Peter, M., Kremer, J., and Hunter, G. (2008). Mobile LiDAR mapping for 3D point cloud collection in urban areas: a performance test. *Proceedings of the 21st International Archives of the Photogrammetry, Remote Sensing and Spatial Information Sciences (ISPRS08*, 37.

[Hammoudi et al., 2009] Hammoudi, K., Dornaika, F., and Paparoditis, N. (2009). Extracting building footprints from 3D point clouds using terrestrial laser scanning at street level. *International Archive of Photogrammetry and Remote Sensing*, XXXVIII Pa(2009):65–70.

[Hesse and Kutterer, 2007] Hesse, C. and Kutterer, H. (2007). A mobile mapping system using kinematic terrestrial laser scanning (KTLS) for image acquisition. In Grun, A. and Kahmen, H., editors, *8th Conference on Optical 3-D Measurement Techniques*, pages 134–141, Zurich, Switzerland.

[Hofmann and Brenner, 2009] Hofmann, S. and Brenner, C. (2009). Quality assessment of automatically generated feature maps for future driver assistance systems. In *Proceedings of the 17th ACM SIGSPATIAL International Conference on Advances in Geographic Information Systems - GIS '09*, number 2009, pages 500–503, New York, New York, USA. ACM Press.

[Hong et al., 2006] Hong, S., Lee, M., Chun, H.-H., Kwon, S.-H., and Speyer, J. (2006). Experimental Study on the Estimation of Lever Arm in GPS/INS. *IEEE Transactions on Vehicular Technology*, 55(2):431–448.

[Huang et al., 2008] Huang, H., Chen, C., Jia, Y., and Tang, S. (2008). Automatic detection and recognition of circular road sign. In *Mechtronic and*

Embedded Systems and Applications, 2008. MESA 2008. IEEE/ASME International Conference on, pages 626 –630.

[Hunter and Cox, 2010] Hunter, G. and Cox, C. (2010). StreetMapper Brochure. Technical report, 3D Laser Mapping, Nottingham, UK.

[Hunter et al., 2006] Hunter, G., Cox, C., and Kremer, J. (2006). Development of a Commercial Laser Scanning Mobile Mapping System StreetMapper. In *Second International Workshop The Future of Remote Sensing, Antwerp*, pages 3–6.

[Hyyppä et al., 2009] Hyyppä, J., Jaakkola, A., Hyyppä, H., Kaartinen, H., Kukko, A., Holopainen, M., Zhu, L., Vastaranta, M., Kaasalainen, S., Krooks, A., Litkey, P., Lyytikainen-Saarenmaa, P., Matikainen, L., Ronnholm, P., Chen, R., Chen, Y., Kivilahti, A., and Kosonen, I. (2009). Map updating and change detection using vehicle-based laser scanning. *2009 Joint Urban Remote Sensing Event*, pages 1–6.

[IXSEA, 2009] IXSEA (2009). LANDINS user guide: introduction. Technical report, IXSEA.

[Jaakkola et al., 2008] Jaakkola, A., Hyyppä, J., Hyyppä, H., and Kukko, A. (2008). Retrieval algorithms for road surface modelling using laser-based mobile mapping. *Sensors*, 8(9):5238.

[Kaartinen et al., 2005] Kaartinen, H., Hyyppä, J., Gülch, E., Vosselman, G., Hyyppä, H., Matikainen, L., Hofmann, A. D., Mäder, U., and Persson, A. (2005). Accuracy of 3D City Models : EuroSDR comparison. In *International Archives of Photogrammetry, Remote Sensing and Spatial Information Sciences 36 (Part 3/W19)*, pages 227–232.

[Kaartinen et al., 2012] Kaartinen, H., Hyyppä, J., Kukko, A., Jaakkola, A., and Hyyppä, H. (2012). Benchmarking the Performance of Mobile Laser Scanning Systems Using a Permanent Test Field. *Sensors*, 12(9):12814–12835.

[Kaasalainen et al., 2011] Kaasalainen, S., Jaakkola, A., Kaasalainen, M., Krooks, A., and Kukko, A. (2011). Analysis of incidence angle and distance effects on terrestrial laser scanner intensity: Search for correction methods. *Remote Sensing*, 3(10):2207–2221.

[Kim et al., 2006] Kim, G., Sohn, H., and Song, Y. (2006). Road infrastructure data acquisition using a vehicle-based mobile mapping system. *Computer Aided Civil and Infrastructure Engineering*, 21(5):346.

[Kim et al., 2011] Kim, S., Hwang, S., Son, M., and Lee, I. (2011). Comprehensive high-speed simulation software for ladar systems. In *Proceedings of SPIE Volume 8181, Earth Resources and Environmental Remote Sensing/GIS Applications*.

[Konica, 2012] Konica (2012). Konica Minolta VI9i Triangulation Based Laser Scanner. http://www.konicaminolta.com/instruments/products/3d/non-contact/vivid910/index.html. Date Accessed: 11-10-2012.

[Kremer and Hunter, 2007] Kremer, J. and Hunter, G. (2007). Performance of the StreetMapper Mobile LIDAR Mapping System in "Real World" Projects. In *Photogrammetric Week*, volume 07, pages 215–225, Stuttgart, Germany.

[Kukko et al., 2007] Kukko, A., Andrei, C., Salminen, V., Kaartinen, H., Chen, Y., Rönnholm, P., Hyyppä, H., Hyyppä, J., Chen, R., Haggrén, H., and Others (2007). Road Environment Mapping System of the Finnish Geodetic Institute-FGI Roamer. In Ronnolm, P., Hyyppä, H., and Hyyppä, J., editors, *Proceedings of the ISPRS Workshop Laser Scanning 2007 and SilviLaser 2007, Espoo, Finland, 12-14 Sept. 2007*, volume XXXVI, pages 241–247, Espoo, Finland.

[Kukko and Hyyppä, 2009] Kukko, A. and Hyyppä, J. (2009). Small-footprint laser scanning simulator for system validation, error assessment and algorithm development. *Photogrammetric Engineering and Remote Sensing*, 75(9):11771189.

[Kukko et al., 2009] Kukko, A., Jaakkola, A., Lehtomaki, M., Kaartinen, H., and Chen, Y. (2009). Mobile mapping system and computing methods for modelling of road environment. In *2009 Joint Urban Remote Sensing Event*, Shanghai, China. Ieee.

[Kukko et al., 2012] Kukko, A., Kaartinen, H., Hyypp, J., and Chen, Y. (2012). Multiplatform mobile laser scanning: Usability and performance. *Sensors*, 12(9):11712–11733.

[Kumar, 2012] Kumar, P. (2012). *Road features extraction using terrestrial mobile laser scanning system.* PhD thesis, National University of Ireland Maynooth.

[Kumar et al., 2010] Kumar, P., McCarthy, T., and McElhinney, C. (2010). Automated road extraction from terrestrial based mobile laser scanning system using the gvf snake model. In *European laser Mapping Forum - 'ELMF 2010'*, November 2010, The Hague, Holland.

[Kumar et al., 2011] Kumar, P., McElhinney, C., and T, M. (2011). Utilizing terrestrial mobile laser scanning data attributes for road edge extraction with the GVF snake model. In *MMT11,The 7th International Symposium on Mobile Mapping Technology*, June 2011, Krakaw, Poland.

[Lehtomäki et al., 2010] Lehtomäki, M., Jaakkola, A., Hyyppä, J., Kukko, A., and Kaartinen, H. (2010). Detection of Vertical Pole-Like Objects in a Road Environment Using Vehicle-Based Laser Scanning Data. *Remote Sensing*, 2(3):641–664.

[Leica, 2012] Leica (2012). Leica HDS7000 Phase Based Laser Scanner. http://www.leica-geosystems.com/en/HDS700090337.htm. Date Accessed: 11-10-2012.

[Lewis et al., 2012] Lewis, P., Mc Elhinney, C. P., and McCarthy, T. (2012). Lidar data management pipeline; from spatial database population to web-application visualization. In *Proceedings of the 3rd International Conference on Computing for Geospatial Research and Applications*, COM.Geo '12, pages 16:1–16:10, Washington, D.C., USA. ACM.

[Lewis et al., 2010] Lewis, P., McElhinney, C., Schön, B., and Mccarthy, T. (2010). Mobile Mapping System LiDAR Data Framework. *International Archives of the Photogrammetry, Remote Sensing and Spatial Information Sciences*, XXXVIII-4/W15:135–138.

[Lichti, 2004] Lichti, D. (2004). A resolution measure for terrestrial laser scanners. *The International Archives of the Photogrammetry, Remote Sensing and Spatial Information Sciences*, 34(Part XXX).

[Lichti and Jamtsho, 2006] Lichti, D. and Jamtsho, S. (2006). Angular resolution of terrestrial laser scanners. *The Photogrammetric Record*, 21(114):141–160.

[Lillesand et al., 2008] Lillesand, T., Kiefer, R., and Chipman, J. (2008). In *Remote Sensing and Image Interpretation*, pages 626–726. John Wiley and Sons, Maryland, US, 6th edition.

[Lin et al., 2012] Lin, Y., Hyyppä, J., Kukko, A., Jaakkola, A., and Kaartinen, H. (2012). Tree height growth measurement with single-scan airborne, static terrestrial and mobile laser scanning. *Sensors*, 12(9):12798–12813.

[Lohani and Mishra, 2007] Lohani, B. and Mishra, R. (2007). Generating LiDAR data in laboratory: LiDAR simulator. In *International Archive of Photogrammetry, and Remote Sensing XXXVI (3)*, volume 52, pages 12–14.

[Madeira et al., 2012] Madeira, S., Gonalves, J. A., and Bastos, L. (2012). Sensor integration in a low cost land mobile mapping system. *Sensors*, 12(3):2935–2953.

[McElhinney et al., 2011] McElhinney, C., lewis, P., T, M., and McCarthy, T. (2011). Mobile terrestrial LiDAR data-sets in a Spatial Database Framework. In *MMT11,The 7th International Symposium on Mobile Mapping Technology*, June 2011, Krakaw, Poland.

[McElhinney et al., 2010] McElhinney, C. P., Kumar, P., Cahalane, C., and McCarthy, T. (2010). Initial results from European Road Safety Inspection (EURSI) mobile mapping project. In *ISPRS Commission V Technical Symposium*, volume 2007.

[Miller and Mills, 2008] Miller, P. and Mills, J. (2008). Terrestrial laser scanning for assessing the risk of slope instability along transport corridors. *International Archives of Photogrammetry, Remote Sensing and Spatial Information Sciences*, 37(B5):495–500.

[O Cathain, 2011] O Cathain, E. (2011). M1 Lane Improvement Scheme, Phase 2. Drinan Junction to Lissenhall Junction. Detailed Topographical Survey Survey Specification. http://www.nra.ie/Publications/. Ref: 08.234.108.08. Date Accessed:5-12-2011.

[Ohio Land Surveys, 2012] Ohio Land Surveys (2012). Survey Crew Image. http://www.ohiolandsurveys.com/. Date Accessed: 09-10-2012.

[Optech, 2012] Optech (2012). Optech Lynx M1 and V200 System Specifications. http://www.optech.ca/lynx.htm. Date Accessed: 09-10-2012.

[Ordnance Survey Ireland, 2012] Ordnance Survey Ireland (2012). OSi Active GPS Station Data. http://www.osi.ie/Services/GPS-Services/Active-GPS-Station-Data.aspx. Date Accessed: 11-10-2012.

[Petrie and Toth, 2009] Petrie, G. and Toth, C. K. (2009). Terrestrial Laser Scanners. In Shan, J. and Toth, C. K., editors, *Topographic Laser Ranging and Scanning: Principles and Processing*. Taylor & Francis Group, Boca Raton, US.

[Pothoua et al., 2006] Pothoua, A., Tothc, C., Karamitsosb, S., and Georgopoulosa, A. (2006). ON USING QA/QC TECHNIQUES FOR LIDAR-IMU BORESIGHT MISALIGNMENT. In *MMT07,The 5th International Symposium on Mobile Mapping Technology*.

[Prendergast, 2004] Prendergast, W. (2004). Best Practice Guidelines for Precise Surveying In Ireland. Irish Institution of Surveyors.

[Prendergast et al., 2008] Prendergast, W., Flynn, M., Corrigan, P., Sweeny, B., Martin, A., and Moran, P. (2008). Green Paper Proposing Reform of Boundary Surveys in Ireland. Irish Institution of Surveyors.

[Pu and Vosselman, 2007] Pu, S. and Vosselman, G. (2007). Extracting windows from terrestrial laser scanning. In *International Archives of Photogrammetry, Remote Sensing and Spatial Information Sciences Voll XXXVI, (Part 3/W52)*, volume 36, pages 320–325, Espoo, Finland. ISPRS.

[RIEGL, 2009a] RIEGL (2009a). Dual Scanner Data sheet Riegl VMX-250. http://www.riegl.com/nc/products/mobile-scanning/produktdetail/product/scannersystem/6/. Date Accessed: 09-10-2012.

[RIEGL, 2009b] RIEGL (2009b). Scanner Data Sheet Riegl VQ-250. pages 1–4, http://www.riegl.com/nc/products/mobile-scanning/produktdetail/product/scanner/22/. Date Accessed: 09-10-2012.

[RIEGL, 2011a] RIEGL (2011a). Dual Scanner Data sheet Riegl VMX-450. http://www.riegl.com/nc/products/mobile-scanning/produktdetail/product/scannersystem/10/. Date Accessed: 09-10-2012.

[RIEGL, 2011b] RIEGL (2011b). Scanner Data Sheet Riegl VQ-450. http://www.riegl.com/nc/products/mobile-

scanning/produktdetail/product/scanner/31/. Date Accessed: 09-10-2012.

[RIEGL, 2012a] RIEGL (2012a). RiACQUIRE Software Datasheet. http://products.rieglusa.com/item/software-packages/riacquire-data-acquisition-software/item-1011. Date Accessed: 11-10-2012.

[RIEGL, 2012b] RIEGL (2012b). Riegl VZ-6000 Time of Flight Terrestrial Laser Scanner. http://www.riegl.com/nc/products/terrestrial-scanning/produktdetail/product/scanner/33/. Date Accessed: 11-10-2012.

[Schaer et al., 2007] Schaer, P., Skaloud, J., Landtwing, S., and Legat, K. (2007). Accuracy estimation for laser point cloud including scanning geometry. In *5th International Symposium on Mobile Mapping Technology (MMT2007), Padua, Italy*.

[Schofield, 2007] Schofield, W. (2007). In *Engineering Surveying*. Butterworth-Heinemann, Oxford, UK, 6th edition.

[Schwarz and El-Sheimy, 2004] Schwarz, K. and El-Sheimy, N. (2004). MOBILE MAPPING SYSTEMS - STATE OF THE ART AND FUTURE TRENDS. In *International Archives of Photogrammetry, Remote Sensing and Spatial Information Sciences*, page 10, Istanbul, Turkey.

[Schwarz et al., 1993] Schwarz, K. P., Martell, H. E., El-Sheimy, N., Li, R., Chapman, M. A., and Cosandier, D. (1993). VISAT - A mobile highway survey system of high accuracy. In *Vehicle Navigation and Information Systems*, pages 476–481, Ottawa, Canada. IEEE.

[Seo et al., 2005] Seo, J., Member, S., Lee, J. G., and Park, C. G. (2005). Leverarm compensation for integrated navigation system of land vehicles. *Proceedings of 2005 IEEE Conference on Control Applications, 2005. CCA 2005.*, pages 523–528.

[Shepard, 1968] Shepard, D. (1968). A two-dimensional interpolation function for irregularly-spaced data. In *Proceedings of the 23rd National Conference ACM*, pages 517–524. ACM Press.

[Shi et al., 2008] Shi, Y., Shibasaki, R., and Shi, Z. (2008). An efficient method for extracting road lane mark by fusing vehicle-based stereo image and laser range data. In *Earth Observation and Remote Sensing Applications, 2008. EORSA 2008. International Workshop on*, pages 1 –5.

[SICK, 2010] SICK (2010). SICK LMS221 Scanner Specifications. https://www.mysick.com/saqqara/im0012759.pdf. Date Accessed: 09-10-2012.

[Soudarissanane et al., 2011] Soudarissanane, S., Lindenburgh, R., Menenti, M., and Teunissen, P. (2011). Scanning geometry: Influencing factor on the quality of terrestrial laser scanning points. *ISPRS Journal of Photogrammetry and Remote Sensing*, 66(4):389–399.

[Stratag, 2012] Stratag (2012). Strategic Research into Advanced Geotechnologies (StratAG) Webpage. http://www.stratag.ie/.

[Talaya et al., 2000] Talaya, J., Bosch, E., Alamús, R., Serra, A., and Baron, A. (2000). GEOVAN: The Mobile Mapping System from the ICC. In *Proceedings of the 4th International Symposium on Mobile Mapping Technology (MMT2004), Kunming, 2004.*

[Tao, 2000] Tao, C. (2000). Mobile mapping technology for road network data acquisition. *Journal of Geospatial Engineering*, 2(2):1–14.

[TerraSolid, 2012a] TerraSolid (2012a). TerraMatch User Guide. http://www.terrasolid.fi/en/products/terramatch. Date Accessed: 11-10-2012.

[TerraSolid, 2012b] TerraSolid (2012b). TerraScan User Guide. http://www.terrasolid.fi/en/products/terrascan. Date Accessed: 11-10-2012.

[Titterton and Weston, 2004] Titterton, D. H. and Weston, J. L. (2004). *Strapdown Inertial Navigation Technology*. Peter Peregrinus, London, UK, 2nd edition.

[Toth and Grejner-Brzezinska, 2001] Toth, C. and Grejner-Brzezinska, D. (2001). Modern mobile mapping: On-the-fly image processing. In *Proc. of the 3rd International symposium on mobile mapping*, pages 3–5.

[Toth and Grejner-brzezinska, 2004] Toth, C. and Grejner-brzezinska, D. (2004). Redefining the Paradigm of Modern Mobile Mapping : An Automated High-Precision Road Centerline Mapping System. *Photogrammetric Engineering & Remote Sensing*, 70(6):685–694.

[Trimble, 2010] Trimble (2010). Trimble MX8 Mobile Mapping System. http://www.trimble.com/geospatial/Trimble-MX8.aspx?dtID=overview. Date Accessed: 09-10-2012.

[Trimble, 2012] Trimble (2012). Survey Pro Data Logger User Guide. http://www.trimble.com/tsptsxtn.asp. Date Accessed: 11-10-2012.

[Tuck et al., 2012] Tuck, B., Young, J., and Guy, C. (2012). Airborne Installation and Integration of ALS Systems. In Renslow, M., editor, *Manual of Airborne Topographic LiDAR*. ASPRS, Maryland, US.

[Vosselman and Maas, 2010] Vosselman, G. and Maas, H. (2010). *Airborne and Terrestrial Laser Scanning*. Whittles Publishing.

[Yen and T.A., 2011] Yen, W., R. B. and T.A., L. (2011). LiDAR for Data Efficiency. http://www.wsdot.wa.gov/Research/Reports/700/778.1.htm. Date Accessed:5-10-2011.

[Yoo et al., 2009] Yoo, H., Goulette, F., Senpauroca, J., and Lepere, G. (2009). Simulation based comparative analysis for the design of laser terresttrial mobile mapping. In *Proceedings of the 6th International Symposium on Mobile Mapping Technology*, pages 839–854, Sao Paolo, Brazil.